

Understanding telomere dynamics with G-quadruplex secondary structures in *S. cerevisiae*

Doctoral thesis

to obtain a doctorate (PhD)

from the Faculty of Medicine

of the University of Bonn

Mona Hajikazemi

from Babol, Iran

2022

Written with authorization of
the Faculty of Medicine of the University of Bonn

First reviewer: Prof. Dr. Katrin Paeschke

Second reviewer: Prof. Dr. Oliver Gruss

Day of oral examination: 03.03.2022

For the clinic and polyclinic for Translationale Onkologie, Medizinische Klinik III,
Director: Prof. Dr. Peter Brossart

Table of Contents

Table of Contents.....	3
List of abbreviations	6
1. Introduction	8
1.1 Telomeres.....	8
1.1.1 Discovery of chromosomes termini.....	8
1.1.2 Structure of <i>Saccharomyces cerevisiae</i> telomeres.....	9
1.1.3 Telomere binding proteins in <i>S. cerevisiae</i>	10
1.1.4 Telomere associated helicases	15
1.1.5 Telomere replication and telomerase	15
1.1.6 Telomeric repeat-containing RNA (TERRA)	18
1.1.7 Telomere maintenance and regulation	18
1.2 G-quadruplex structures.....	20
1.2.1 First observation and structure of G-quadruplexes.....	20
1.2.2 Characterization of G-quadruplexes	21
1.2.3 Potential functions of G-quadruplexes at telomeres	24
1.3 Aim of the study	27
2. Material and methods	28
2.1 Strains, constructs, and media.....	28
2.2 Chromatin Immunoprecipitation (ChIP).....	28
2.2.1 Myc- tagged ChIP.....	28
2.2.2 BG4 ChIP	29
2.3 Cell cycle synchrony and confirmation of DNA content with fluorescence-activated cell sorting (FACS)	31
2.4 BG4 purification and validation	32
2.5 Telomere healing assay	32

2.6	Southern blot telomeres	33
2.7	Spot assay	34
2.8	Co-Immunoprecipitation	34
2.9	Hi-C.....	35
3.	Results.....	37
3.1	Identification of Non Telomeric Binding Sites (NTBS).....	37
3.1.1	Telomerase catalytic subunit (Est2) binds to endogenous regions.....	37
3.1.2	Like telomeres, Est2 binding to NTBS is regulated during the cell cycle	38
3.1.3	Est2 is not recruited to NTBS via canonical telomerase recruitment proteins 40	
3.1.4	3D organization of chromatin involved in Est2 and NTBS interaction.....	42
3.2	Telomeric G-overhang as the means of telomere maintenance.....	43
3.2.1	Oligonucleotides simulating telomeric G-overhang with different length form G4s with diverse topologies	43
3.2.2	Telomeric DNA secondary structures, impede Cdc13 binding	44
3.2.3	Folding kinetics of G-tails impact Cdc13 association to telomeres	46
3.2.4	G4 occupancy differs through the cell cycle at the telomeric region and is in accordance with the length of the G-overhang.....	49
3.2.5	Characterization of G4s at short and long telomeres in <i>S. cerevisiae</i>	51
3.2.6	G4 motif adjacent to a DSB does not induce telomere addition	52
3.3	Characterization of Zuo1 as a telomeric G4 binding protein	54
3.3.1	Zuo1 binds to <i>S. cerevisiae</i> telomeres without affecting telomere length ...	54
3.3.2	Zuo1 binds more to short telomeres.....	55
3.3.3	Zuo1 binds to a population of long telomeres.....	57
3.3.4	Zuo1 binds more to telomeres when the natural capping is compromised .	58
4.	Discussion.....	61

4.1	Non Telomeric Binding Sites (NTBS) as parking spots for telomerase catalytic subunit Est2.....	61
4.2	Telomeric G-overhang as the means of telomere maintenance.....	63
4.3	Zuo1 as a G-quadruplex binding protein.....	67
4.4	Future perspectives	71
5.	Abstract.....	72
6.	Supplementary figures	74
6.1	NTBS supplementary figures	74
6.2	Telomeric G-overhang supplementary figures	77
7.	List of figures and tables	80
8.	Tables	82
9.	References.....	121
10.	Acknowledgements	150
11.	Supplementary papers	151
11.1	Publications with PhD candidate as co-author, containing data presented in the thesis	151

List of abbreviations

ALT	Alternative lengthening of telomeres
ARS	Autonomously replicating sequence
ATM	Ataxia-telangiectasia mutated
ATR	Ataxia telangiectasia and Rad3 related
BSA	Bovine serum albumin
CD	Circular dichroism
ChIP	Chromatin immunoprecipitation
CST	Cdc13-Stn1-Ten1
DIG	Digoxigenin
DNA	Deoxyribonucleic acid
DSB	Double-strand breaks
EDTA	Ethylenediamine tetraacetic acid
EMSA	electrophoretic mobility shift assay
EMSA	Electrophoretic mobility shift assay
FACS	Fluorescence-activated cell sorting
G4	G-quadruplex
GCR	Gross chromosomal rearrangement
HDR	Homology directed repair
HEPES	4-(2-hydroxyethyl)-1-piperazineethanesulfonic acid
HR	Homologous recombination
HU	Hydroxyurea
IR	Ionizing gamma radiation

MRX	Mre11-Rad50-Xrs2
NER	Nucleotide excision repair
NHEJ	Non-homologous end joining
NMM	N-Methylmesoporphyrin IX
NMR	Nuclear magnetic resonance
NTBS	Non-telomeric binding sites
OD	Optical density
ORF	Open reading frames
PDS	Pyridostatin
POT1	Protection of telomere 1
PQS	Putative quadruplex-forming sequence
PTM	Post translational modifications
RNA	Ribonucleic acid
RPA	Replication protein A
SDS	Sodium dodecyl sulphate
SEM	Standard error mean
SIR	silent information regulator
SiRTAs	Sites of repair-associated telomere addition
TE	Tris-EDTA
TEBP	Telomere End Binding Protein
TERRA	Telomeric repeat-containing RNA
TERT	Telomerase Reverse Transcriptase
TPE	Telomere position effect

1. Introduction

1.1 Telomeres

1.1.1 Discovery of chromosomes termini

The discovery of the chromosomes end relies on the groundbreaking research of Barbara McClintock in the first half of the 20th century. She created a system with X-ray induced rearrangement to examine breakage-fusion-bridge cycle in maize chromosomes (McClintock, 1939). The chromosome breakage occurring in the gametophytes would behave like the natural chromosome ends in the embryos, if the resulting mutants were viable. This phenomenon was called “chromosome healing”. Around the same time, Hermann Muller observed for the first time that the ends of X-ray irradiated chromosomes differ from remaining parts of the genome in *Drosophila* chromosomes. The ends did not present alterations such as insertions or deletions due to the presence of a protective cap (Muller, H. J., 1938). McClintock and Muller called the chromosomes end “telomere”. Years later, in 1953, Watson and Crick proposed the double helix structure of DNA in their landmark paper (WATSON and CRICK, 1953) followed by the innovative discovery of semi-conservative DNA replication by Meselson and Stahl (Meselson and Stahl, 1958). New scientific challenges had been created regarding the discontinuous DNA replication. To draw a timeline for telomeric research, Hayflick’s finding on finite proliferation of somatic cells, known as senescence, was the next critical achievement to better understand chromosomal ends and their function. He proposed that normal cells can only divide for a finite number of divisions before they break down by programmed cell death (L and PS, 1961). To address the fundamental problem caused by shortening of lagging strand with each round of cell division, Watson and Olovnikov hypothesized that semi-conservative and discontinuous DNA replication would create a gap at the end of chromosomes (JD, 1972; Olovnikov, 1973). This phenomenon is known as the “end replication problem”. It seemed reasonable that the progressive shortening of chromosomes ends might explain the “Hayflick limit”. In 1970s, Elizabeth Blackburn initiated her memorable work on *Tetrahymena thermophila* which led to the discovery of telomeric sequences. Together with Joseph Gal, they observed that *Tetrahymena* chromosome ends contains 20-70 times of repetitive TTGGGG sequence (EH and JG, 1978). Together with Jack Szostak, Blackburn they transferred these observations to *Saccharomyces cerevisiae*, revealing that telomeric function is preserved among

organisms. Soon after that, Greider and Blackburn identified the reverse transcriptase enzyme termed telomerase, responsible for telomere extension (Greider and Blackburn, 1985). Blackburn, Szostak and Greider received the Nobel Prize in Medicine in 2009 for their remarkable discoveries. Nowadays it is known that telomeres are nucleoprotein structures at the end of eukaryotic chromosomes. They are responsible to maintain genome integrity and protect the ends from being recognized as double strand breaks, degraded by nucleases, end to end fusion and shortening because of incomplete replication (Förstemann and Lingner, 2001). The telomeric sequence in human carries up to 15 kb of double stranded TTAGGG followed by a 3' G-overhang. In human, the length of the G-overhang is variable from 100 to 280 nucleotides. The G rich nature of telomeres and the presence of G-tail is a general feature of eukaryotic chromosomes, which is almost conserved. The telomerase reverse transcriptase is responsible for extending telomeres (Greider and Blackburn, 1985). Telomerase consists of proteins for enzymatic reaction and RNA component, essential as template for adding the TG repeats to the 3' DNA end. Telomerase activity is absent in somatic cells and present in germline and immortalized cells like many cancer cell types. One of the basic steps in oncogenesis (for 80% of human cancer) is reactivation of the telomerase reverse transcriptase. Despite the vast research in the past years, there are lots of open questions regarding telomeres functions, correlation of telomere length and the life span of species, and the underlying molecular mechanisms regarding aging and cancer.

1.1.2 Structure of *Saccharomyces cerevisiae* telomeres

Due to the functional and structural conservation of telomeres and telomerase, fundamental research on telomeres has been performed using *S. cerevisiae*. Active telomerase is a feature of *S. cerevisiae*, which made it an ideal model organism for extensive telomere studies (e.g. mimicking a cancer phenotype). Like most organisms, *S. cerevisiae* contains two classes of telomere-associated sub telomeric regions known as X and Y' elements (Chan et al., 1983). All telomeres contain the X element, which is very heterogenous and varies in size. The Y' element is only present in 0 to 4 tandem repeats in long (6.7 kb) and short (5.2 kb) sizes, located immediately internal to half of the telomeres (Horowitz et al., 1984; Zakian et al., 1986). When both elements are present, X is proximal to Y' and centromere. Because of their variable sequence, different proteins bind to sub telomeric regions which can lead to distinct behaviors in individual telomeres.

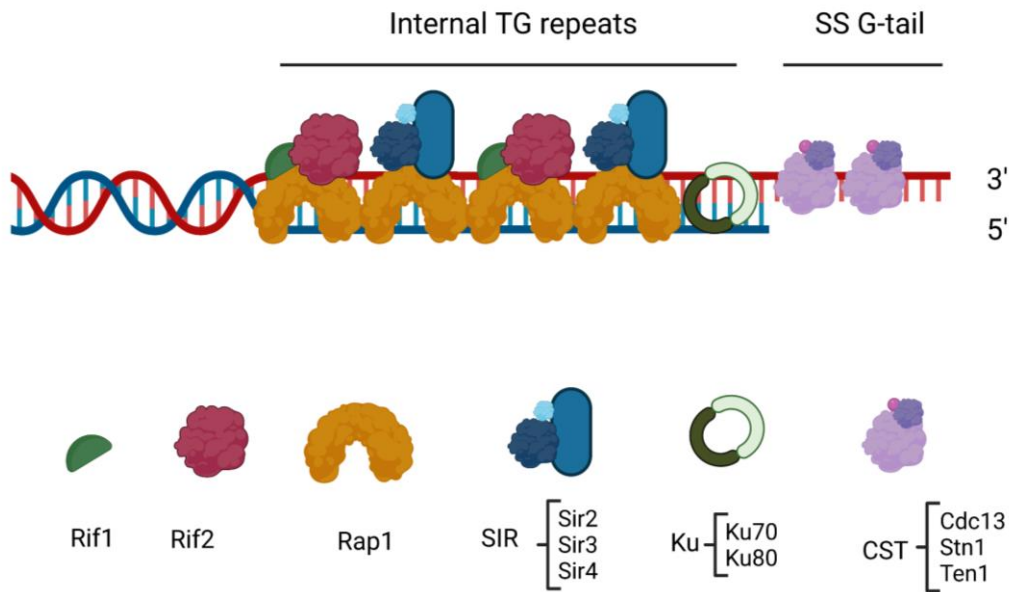


Figure 1.1. *Saccharomyces cerevisiae* telomere.

Schematic description of *S. cerevisiae* telomere consisting of the internal TG repeats and the overhangs. Rap1 protein interacts with Rif1, Rif2, and the SIR complex bind to Rap1. The Ku complex binds to telomeric DNA, and the CST complex (Cdc13, Stn1, Ten1) binds the ssDNA overhang (designed by biorender).

The core of telomere consists of 300 ± 75 base pair heterogeneous C1-3A/TG1-3 repeats, followed by 12-15 nucleotide single-stranded G-overhang at the 3' end (Fig. 1.1) (Förstemann and Lingner, 2001). In *S. cerevisiae* the telomerase holoenzyme consists of three proteins Est1, Est2 (the catalytic subunit), Est3 and the RNA component TLC1, which serves as template for reverse transcription (Joachim Lingner et al., 1997; Singer and Gottschling, 1994). The length of telomeric overhang changes during the cell cycle. In late S/G2 phase, when telomere extension is taking place, the telomeric G-tails reach ≥ 30 nucleotides in length. Long G-tails are result of cell cycle regulated C-strand degradation (Wellinger and Zakian, 2012). There are specific protein complexes that bind to the double stranded and single stranded part of the telomere. They all differ in their function and relevance for telomere maintenance which will be discussed in detail further.

1.1.3 Telomere binding proteins in *S. cerevisiae*

1.1.3.1 Rap1, Rif1 and Rif2

The key double stranded DNA binding complex involved in maintaining telomere length consists of Rap1, Rif1 and Rif2 proteins. Rap1 (repressor activator protein 1) consists of three conserved domains : a C-terminal domain called RCT, a centrally located DNA

binding domain (DBD) with two Myb-like folds and a BRCT domain at the N-terminal (P and D, 2001; Wotton and Shore, 1997). Rap1 binds every 18 nucleotide in telomeric repeats. Given the 300bp average telomere length, each individual telomere should be covered with 15-20 Rap1 molecules (Gilson et al., 1993; Wright and Zakian, 1995). Rap1 has multiple effects on telomeres, it protects the end of chromosomes, inhibits telomere-telomere fusions (Marcand et al., 2008; Pardo and Marcand, 2005) and cooperates to silencing of telomeres (Hardy et al., 1992). Telomeric Rap1 interacts with two other proteins through its C-terminal domain, Rif1 and Rif2 (Rap1 interacting factors 1 and 2). Measuring telomere elongation at nucleotide resolution has revealed telomerase does not act on every telomere in each cell cycle. It has more preference for shorter telomeric sequences and they are in extendible state (Teixeira et al., 2004). Inhibition of telomerase action at long ends has been shown to require Rap1, Rif1 and Rif2 interactions. To simplify studying heterogenous telomere length regulations, a system has been created to induce double strand breaks adjacent to varying length of telomeric tracts or Rap1 binding sites. It has been shown that short TG tracts were rapidly extended by telomerase followed by endonuclease cut, whereas TG tracts similar to native length were intact (Negrini et al., 2007). Depending on telomeres length (>120 bp), Rap1 binding inhibits telomerase action in *cis* (Marcand et al., 1999; Teixeira et al., 2004). Telomere binding by the Rap1-Rif1/2 complex are essential for maintaining its length as they negatively regulate telomerase and inhibit homologous recombination (Vega et al., 2003). Telomeres lose Rap1 binding sites as they shorten, therefore differences in Rif1 and Rif2 occupancy might be the key explanation about how the cells distinguish short telomeres from wild type length (McGee et al., 2010).

Differential distribution of Rif2 on wild type length and short telomeres is required for the activation of checkpoint kinase Tel1 and directing telomerase to short telomeres (McGee et al., 2010). Rif2 dependent modulation of telomere length requires binding of both Myb-like domains of Rap1 to DNA. Single Myb-like domain induces the formation of more complex Rap1-DNA folding that acts independently of Rif2 (Bonetti et al., 2020). Despite their distinct functions, deletion of either Rif1 or Rif2 induces the long telomere, however the effect is more strong in the absence of Rif1 (Wotton and Shore, 1997). Recruitment of Rif2 via Rap1 is essential in G1 and early S phase to prevent end resection and Tel1 activation. Rif1 deletion increases the temperature sensitivity of the cell. Rif1 is important

for capping the telomeres when the natural capping via CST (CDC13-Stn1-Ten1) complex is compromised (Anbalagan et al., 2011). Because the viability of cells with defective CST complex was impaired in the absence of Rif1, but not Rif2, it highlights their distinct functions (Anbalagan et al., 2011).

Rap1 also recruits the Sir complex (silent information regulator) which are responsible for the transcriptionally quiescence state of telomere proximal regions, known as telomere position effect (TPE) (Aparicio et al., 1991; Liu et al., 1994). The C-terminus of Rap1 interacts with Sir3/4 directly and Sir2 is recruited via Sir4 (IR et al., 1999; Wotton and Shore, 1997). The heterochromatic nature of the subtelomeric regions represses promoter activity and transcription of the genes close to telomeres, promoting TPE. SIR complex interacts with histones and spreads among the chromatin fiber to generate the silencing machinery. The Ku complex is also involved in driving the silencing mechanism (Fourel et al., 1999; M et al., 2011; S et al., 2004). This effect correlates with telomeres location, because they are clustered around the nuclear periphery and enriched in SIR proteins and mutations in Ku or SIR partially affects their position (F et al., 2002; M and SM, 1996; Palladino et al., 1993).

1.1.3.2 Ku complex (Yku70-Yku80)

The conserved Ku complex is a heterodimer which consists of two proteins: Yku70 and Yku80 in yeast. The Ku complex is double strand DNA binding protein which is an essential factor for Non-homologous end joining (NHEJ) (Hirano and Sugimoto, 2007; MD and RJ, 2007). The Ku complex is responsible for recruiting RNA template of telomerase, TLC1, to telomeres. Deletion of YKU70 or YKU80 results in extremely short telomeres with longer heterogeneous G-tails (Boulton and Jackson, 1998). The Ku proteins together with the small protein modifier SUMO play a role in anchoring the telomeres to the perinuclear space (Marvin et al., 2009).

1.1.3.3 CST complex (Cdc13, Stn1, Ten1)

The single stranded telomeric binding complex, consists of Cdc13, Stn1 and Ten1 (CST) proteins. The CST complex binds to ss telomeric DNA and caps the telomeres, which is vital particularly in G2/M (MD and RJ, 2006). The CST complex plays an essential role in protection of chromosomal ends by capping telomeres and preventing degradation by nucleases. Mutation in the proteins of the CST complex leads to accumulation of ss DNA

and C-strand resection (Garvik et al., 1995; Grandin et al., 2001). Altogether, the CST components are important for telomere capping, telomerase recruitment and synthesis of the C-strand.

In more detail, Cdc13 is a highly conserved telomere binding protein is mainly involved in telomerase recruitment and telomere protection. Cdc13 interacts with telomerase subunit Est1 through its OB fold domains which stimulates telomerase recruitment to telomeres (E et al., 2001; Nugent et al., 1996; Qi and Zakian, 2000). The temperature sensitive *cdc13-1* strain, carrying a point mutation in the OB2 domain of Cdc13, leads to disrupted nuclear localisation signal. The mutant has elongated G-rich ss DNA and the telomeres are unprotected (Mersaoui et al., 2018). Furthermore, there are *in vitro* data indicating that impaired Cdc13 capping function can be counterbalanced by alternative telomere structure conformations (Smith et al., 2011).

Cdc13 can be recruited to DSB to promote *de novo* telomere addition at endogenous regions (Mandell et al., 2011). This process is regulated with an interplay between SUMOylation and phosphorylation of Cdc13 (Zhang and Durocher, 2010). Cdc13 is SUMOylated in early-mid S phase which antagonizes telomerase function. It gets phosphorylated in a Cdk1-mediated manner and is involved in recruiting telomerase to the break sites (LE et al., 2011). Cdc13 has been reported to surpass Replication protein A (RPA) at telomeres and both can be found at telomeres during replication, meaning they are connected to the telomere replication mechanism (Luciano et al., 2012; V et al., 2004). It also interacts with Pol1, the catalytic subunit of Pol α , through its N-terminal domain and promotes C-strand synthesis (J et al., 2011; Qi and Zakian, 2000).

Stn1 interacts with Ten1 through its N-terminal domain which is essential for its capping function (Grandin et al., 2001; Puglisi et al., 2008). Stn1 also interacts through its C-terminal with Cdc13 and Pol12 (Grandin et al., 1997; Puglisi et al., 2008) and is involved in lagging strand DNA replication. Ten1 has been shown to interact with both Cdc13 and Stn1. Ten1 and Stn1 overexpression rescues the telomere defects of *cdc13-1* mutant (Grandin et al., 2001; RC et al., 2007). Some temperature sensitive mutants of *ten1* accumulate ss DNA in telomeres and some mutants show longer telomeres (Grandin et al., 2001; Qian et al., 2009). The CST complex and predominantly Cdc13 has an important role for keeping the telomeres intact and preventing fusions (Wu et al., 2020).

1.1.3.4 MRX complex (Mre11, Rad50, Xrs2)

Another key component of telomeres is the heterotrimeric MRX (Mre11, Rad50, Xrs2) complex which has a role in DSB recognition and regulation of telomere length via checkpoint activation (Boulton and Jackson, 1998; CI and V, 1998; D'Amours and Jackson, 2001; G. M et al., 2001; Ritchie and Petes, 2000). When telomeres are getting short and competent for elongation, they are bound by MRX complex and activate checkpoint kinases which trigger telomere elongation (Viscardi et al., 2007). The MRX complex is involved in C-strand resection which is essential for generating the ss DNA and telomeric G-overhang (Bonetti et al., 2009; M et al., 2004). Deletion of MRX complex components results in stable short telomeres (Boulton and Jackson, 1998). Some MRX mutants have been shown to have no telomere length effect (Y et al., 2001). Telomere elongation has been shown to occur in the absence of MRX if Tel1 has constitutive catalytic activity (Keener et al., 2019). This suggests that nucleolytic end processing via MRX complex might not be required for telomerase mediated elongation (Keener et al., 2019). The Xrs2 subunit of the MRX complex interacts with Tel1 checkpoint kinase which is the homologue of ATM (ataxia-telangiectasia mutated) in human. Docking model prediction showed that at normal length telomeres Rad50 interacts with Rif1 and this interaction antagonizes MRX transition to a DNA binding state, preventing the kinase activation and consequent telomere elongation (Roisné-Hamelin et al., 2021)

1.3.5 Telomere associated kinases

The cell cycle checkpoint machinery coordinates regulation of telomere length via two protein kinases Tel1 and Mec1. Tel1 has a preference for short telomeres and is involved in recruiting telomerase (McGee et al., 2010; RE et al., 2007; Sabourin et al., 2007). The preferential extension of short telomeres by telomerase is lost when Tel1 is deleted (Teixeira et al., 2004) Mec1, the other check point kinase is the homologue of ATR (ATM-Rad3-related) in human and binds more to DSB than to short telomeres (McGee et al., 2010). It has been proposed that Mec1 inhibits telomere addition on accidental DSB by inhibiting Cdc13 recruitment (Zhang and Durocher, 2010). Mec1 is an essential protein and binds to RPA-covered ssDNA after resection of a DSB (Zou et al., 2003). Furthermore, Cdc13 prevents Mec1 binding at telomeres to maintain genome integrity, but it does not affect Tel1 (Hirano and Sugimoto, 2007).

1.1.4 Telomere associated helicases

Helicases are motor proteins capable of unwinding protein-DNA structures as well as secondary DNA and RNA structures. Different lines of evidence demonstrate that different helicases act on telomeres. For instance, the Pif1 DNA helicase family is conserved from bacteria to mammals (Boulé and Zakian, 2006; ML et al., 2011). In *S. cerevisiae*, two members of the family have been identified. First, Pif1 the founding member and second, the ribosomal DNA recombination mutation 3 (Rrm3) (EJ and L, 2008; RL and AD, 1993). Both helicases are multifunctional and bind to specific regions in the genome including telomeres. Pif1 has two isoforms, a mitochondrial and an nuclear form. They originate from the same open-reading frame but use different start codons. The *pif1-m2* mutants lack the nuclear isoform. In *pif1-m2* cells, among other molecular changes, elongated telomeres are observed (Schulz and Zakian, 1994). Pif1 negatively regulates telomere extension by inhibiting telomerase through its helicase activity at DSB and telomeres (Myung et al., 2001; Zhou et al., 2000). Pif1 has been shown to segregate the RNA subunit of telomerase, TLC1 to the nucleus and regulates telomere extension by affecting the spatial distribution of telomerase components (Ouenzar et al., 2017). Pif1 is important to inhibit *de novo* telomere addition at DSBs through Mec1 dependent phosphorylation and telomere addition has been shown to increase in the absence of Pif1 (Ivessa et al., 2002; Makovets and Blackburn, 2009). Telomerase has preference for binding to short telomeres and its processivity is reduced in the absence of Pif1 (Phillips et al., 2015). Rrm3 has been shown to be more involved in replication of telomeres rather than telomerase activity and its mutants have only slightly longer telomeres (Ivessa et al., 2002).

1.1.5 Telomere replication and telomerase

Extension of telomeric sequences occurs mid to late S phase of the cell cycle. Short telomeres have been shown to get extended earlier in S phase (Bianchi and Shore, 2007). The newly synthesized leading strand has a blunt end and the lagging strand is left with a small gap at the 5' end after the removal of the template RNA (I and RJ, 1998; Wellinger et al., 1993) (Fig. 1.2). To solve the end replication problem and generate the G-overhangs, semiconservative replication is a prerequisite and telomeres need to go through extension as well as post replication C-strand dissection (RJ et al., 1996). The C-strand resection entails the same proteins that resect DSB to generate single stranded

tails for homologous recombination. Sgs1, a 3' to 5' RecQ family DNA helicase and Sae2 endonuclease are the critical factors for initiating the C-strand resection and generation of the G-overhang (Fig.1.2). The MRX complex acts similar to Sae2 for generating the G-tail but is not as important as Sae2 (M et al., 2004). Unlike a DSB, where extensive C-strand resection occurs with Exo1 or Dna2, Cdc13 together with the Ku complex seems to inhibit this function at telomeres. Telomere regulated resection is limited to ~30-100 nucleotide, therefore no DNA damage checkpoint or cell cycle arrest mechanisms gets activated (Bonetti et al., 2010; Vodenicharov et al., 2010). The CST components which interact with DNA polymerase alpha/primase and the Est1 subunit of telomerase seem to be an excellent coordinator between replication machinery and telomerase (Fig. 1.2). (Grossi et al., 2004; J et al., 2011; Qi and Zakian, 2000). Because telomerase cannot function on blunt ended DNA, post replication C-strand degradation is essential for its activity. Cdc13, together with the MRX complex which has preference for short telomeres have been shown to recruit telomerase. Recruitment of telomerase to telomeres is cell cycle dependant. On one hand recruitment of Est2 in G1 needs an interaction between yKu80 and the stem loop structure of TLC1 RNA, on the other hand, the recruitment in late S is dependent on the interaction of Cdc13 and Est3 (Chan et al., 2008; Fisher et al., 2004). Telomerase adds the TG repeats to the G strand and the CST complex interaction with DNA polymerase may promote the extension of the CA-rich strand (D and A, 2009; Diede and Gottschling, 1999). De novo telomere addition at DSB by telomerase can cause loss of genetic information distal to telomeres and induce genome instability (Bonaglia et al., 2011; Pennaneach et al., 2006; Putnam et al., 2004; Wilkie et al., 1990) It has been proposed that telomerase subunits are not connected to telomere during the cell cycle and the catalytic subunit of telomerase might have function at endogenous regions (Davé et al., 2020; Epum et al., 2020; Gallardo et al., 2008; Matmati et al., 2020; Obodo et al., 2016; Ouenzar et al., 2017; R et al., 2020; Schmidt et al., 2016; Strecker et al., 2017). A three dimensional diffusion model has been proposed wherein telomerase makes different contacts with telomere during cell cycle (Gallardo et al., 2008; Schmidt et al., 2016).

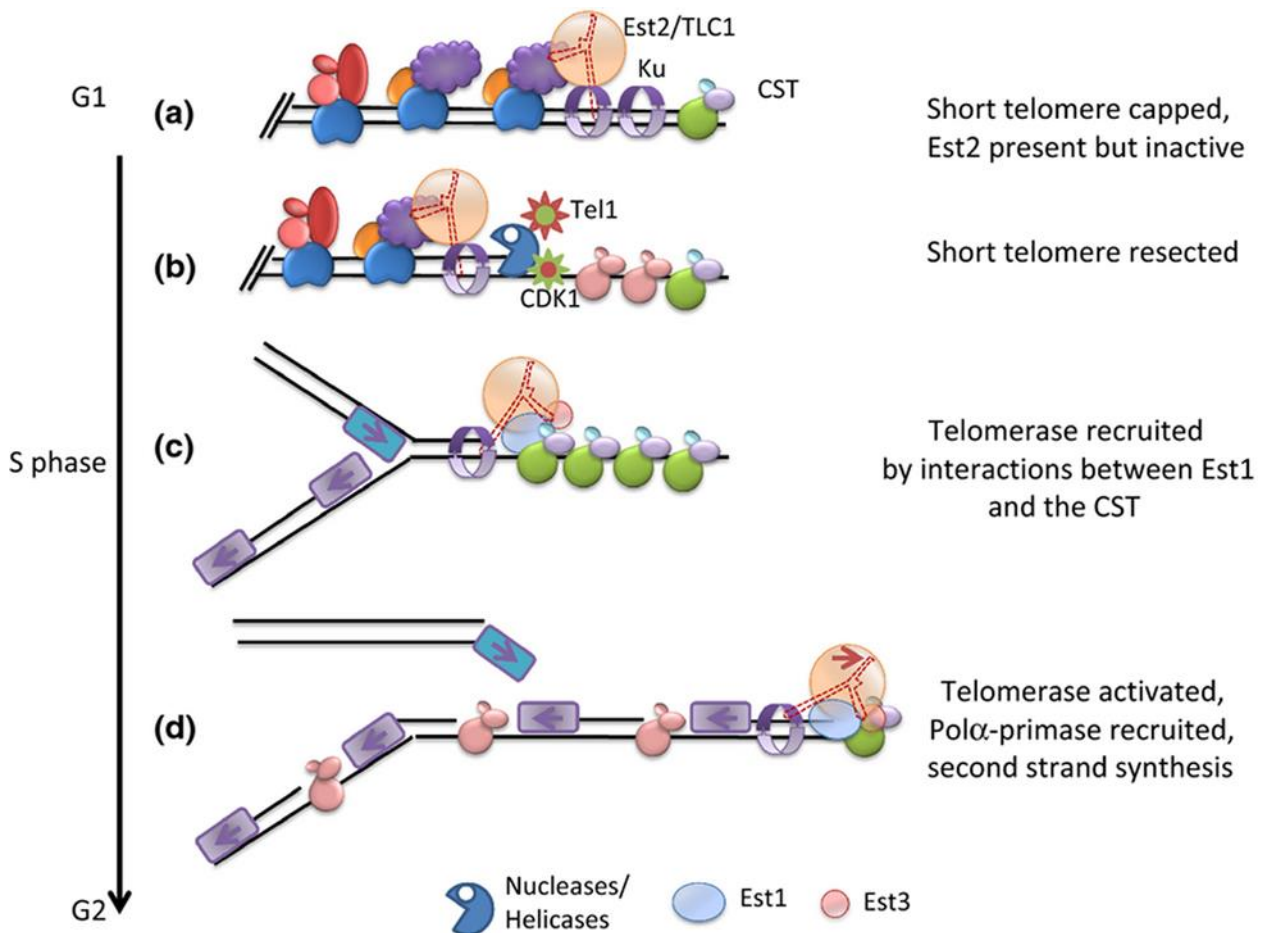


Figure 1.2. Telomere replication

A. Telomeres are capped by proteins and not available for extension in G1. **B.** Under the control of the kinases Tel1 and CDK1, end resection is done. **C.** CST recruits telomerase to telomeres through its interaction with Est1 and the CST. **D.** Telomerase extends the TG-rich strand and Pol α -primase, completes lagging-strand replication (adapted from Kupiec, 2014).

One of the proposed models to inhibit de novo telomere addition in yeast is TLC segregation to different cellular regions during cell cycle (Ouenzar et al., 2017). Different proteins like Pif1, SUMO ligase Siz1 are involved in moderating telomerase action at DSB (Boule et al., 2005; Obodo et al., 2016; Ouenzar et al., 2017; Phillips et al., 2015; Strecker et al., 2017; Zhang and Durocher, 2010; Zhou et al., 2000). Recently a subset of genomic sequences have been recognized where de novo telomere addition occurs upon DSB (Obodo et al., 2016). These sequences are termed as sites of repair-associated telomere addition (SiRTAs). De novo telomere addition at these sites has been associated to Cdc13 and Rap1 protein (Obodo et al., 2016). Despite these findings it is still not clear where telomerase localizes to specific endogenous sites and what's the possible outcome on genome stability.

1.1.6 Telomeric repeat-containing RNA (TERRA)

Despite the transcriptional repression, it is possible to detect noncoding telomeric repeat-containing RNA (TERRA) which is conserved from yeast to humans. TERRA is a long non-coding RNA transcribed from the subtelomeric regions towards the telomere (Feuerhahn et al., 2010; Luke et al., 2008). TERRA is transcribed by RNA polymerase II and is heterogeneous in size (0.2 – 10 kb) (Feuerhahn et al., 2010). The TERRA transcripts harbour the subtelomeric the Y' elements and are capable to encode a helicase which is expressed in cells in response to stress or loss of telomerase function (M et al., 1998). The current model is that TERRA forms physiologically relevant RNA-DNA hybrids at telomeres (Arora et al., 2014; Balk et al., 2013). In *S. cerevisiae*, TERRA is rapidly degraded by the Rat1 exonuclease, which is responsible for degrading all mRNAs (Luke et al., 2008). TERRA inhibits telomerase function *in vitro* (Redon et al., 2010) and it has been shown that high levels of TERRA accumulate at short telomeres, indicating a role of TERRA in telomerase activity (Cusanelli et al., 2013; Moravec et al., 2016). In humans, TERRA levels and localization are regulated throughout the cell cycle. The localization is perturbed in cancer cell lines that employ ALT to maintain telomere length (Flynn et al., 2015; Graf et al., 2017). In both human ALT cells and in the yeast equivalent (type II survivors), TERRA levels and DNA-RNA hybrid abundance at telomere, are elevated (Arora et al., 2014). Recent studies showed that TERRA levels are increased in yeast type II survivors in order to bypass replicative senescence and achieve immortality by promoting homology directed repair (HDR) at chromosome ends to maintain telomere length (Graf et al., 2017; Misino et al., 2018) .

1.1.7 Telomere maintenance and regulation

Because telomeres are the biological clock of the cells, their maintenance is tightly regulated and involves an equilibrium between shortening and lengthening mechanisms to maintain telomere homeostasis. There are two mechanisms to maintain telomere length: telomerase based telomere extension or recombination driven extension by HR also known as alternative lengthening of telomeres (ALT) (Li and Lustig, 1996; B. M et al., 2001). Telomerase mediated extension is regulated during the cell cycle and telomeres with short TG tract tend to be preferentially selected for extension (Teixeira et al., 2004). Different models have been proposed for telomerase mediated extension. The protein counting model suggests that depending on telomere length, more Rap1 and Rif1/2 are

bound to telomeres which negatively regulates telomerase recruitment (Levy and Blackburn, 2004; S et al., 1997). Another possible model is that telomerase moves along the DNA with replisome and has a longer way to reach the end of the longer telomeres and a higher chance to fall off from the replisome (Greider, 2016). Extensive resection of the C-strand in short TG tracts generates longer G-overhangs, capped with more CST, which promotes telomerase recruitment (Negrini et al., 2007). Another possibility is if telomerase becomes activated by short TG tracts (Meier et al., 2001). The last possibility is that the length of TG sequence, confirms the association of more telomerase to the telomeric region (Bianchi and Shore, 2007; Sabourin et al., 2007).

The cells deficient of telomerase activity, shorten their telomeres with each cell division and show ever shortening telomere (EST) phenotype, which enters the cells in the senescence state (Lundblad and Szostak, 1989). In *S. cerevisiae* it is enough to have a single short telomere that is not elongated by telomerase to start the growth arrest (Abdallah et al., 2009; B et al., 2009). A small population of senescing cells can overcome the short telomere length through ALT which results in two types of survivors. Type I survivors Y' elements are amplified via recombination and have very short TG1–3 repeat tracts on the ends (Chen et al., 2001). Type II survivors have long and heterogenous tracts of TG1–3 and grows faster than type I survivor (SC et al., 2000). The long and heterogenous nature of type II survivor is similar to immortal human tumor cell lines that maintain telomere length in the absence of telomerase (SC et al., 2000). Type I survivors amplify the subtelomeric Y' repeats and type two survivors have amplified terminal TG repeats (Lundblad and Blackburn, 1993; Teng and Zakian, 1999). Type I survivors grow slower in liquid culture but they are more common and overgrown by type II survivors (N and M, 2007; Teng and Zakian, 1999). Type I survivors show massive extension of Y' elements and maintain short telomeres with normal G-overhang. Type II survivors have increased telomeric TG repeats and show variable telomere length from very short to 10 kb long (Larrivé and Wellinger, 2006).

In summary, telomere homeostasis is regulated with multiple mechanisms during the cell cycle. On one hand maintaining telomere length is critical for the cells, on the other hand *de novo* telomere addition at endogenous regions should be avoided to maintain genome

stability. Understanding where telomerase is located during cell cycle would shed light on how the cells avoid of *de novo* telomere addition at genomic regions.

1.2 G-quadruplex structures

1.2.1 First observation and structure of G-quadruplexes

The first observation of higher-ordered genetic structures goes back to over 100 years ago in 1910. Bang reported that concentrated solutions of guanylic acid could form a gel (Bang, 1910). In 1962, Geller observed a phenomenon in dried fibers of guanylic acid gels, which he suggested may be due to helix formation (M et al., 1962). The structure became known as G-quartet, square arrangements of four guanines held together by Hoogsteen hydrogen bonding and stabilized by monovalent cations. First biological relevance of G-quartets was revealed with Sen and Gilberts discovery in 1988. They reported that single stranded short guanine-rich motifs can form four- stranded structures in promoters, telomeric and immunoglobulin switch regions (Sen and Gilbert, 1988). Studying telomeric sequences of *Oxytricha* and *Tetrahymena* lead to the model of DNA four-stranded helixes known as G-quadruplexes (JR et al., 1989; Sundquist and Klug, 1989). Stacking of G-quartets is the core element in the formation of higher-ordered G-quadruplex (G4) structures (Sundquist and Klug, 1989; Williamson et al., 1989) (Fig. 1.3). G4 structures require a specific sequence motif, which normally contains three or more consecutive guanines and a variable loop region (1-25 nt long). The *putative quadruplex-forming sequence* (PQS) is $G_{\geq 3}N_xG_{\geq 3}N_xG_{\geq 3}N_xG_{\geq 3}$, which includes four G-tracts is found in most eukaryotic telomeres (AK et al., 2005; JL and S, 2005; Rhodes and Lipps, 2015). G-quadruplexes can form diverse conformations depending on single (intramolecular) or multiple (intermolecular) strands, orientation of the strand (parallel, antiparallel, hybrid) or the bridging loop (propeller, lateral, diagonal) (and and Patel, 2003; Kang et al., 1992; M et al., 2002; Phan et al., 2006; Qin et al., 2015; Sen and Gilbert, 1988; Smith et al., 1994; Smith and Feigon, 1992; Sundquist and Klug, 1989) (Fig. 1.3). The stability of the G-quadruplex depends on the composition of the sequence (the more abundant Guanines on the G-tracts, more stable) and length of the bridging G-tracts shorter loops. The more

stable or the smaller the cation, the closer the G-quartets are making the structure more stable (Bochman et al., 2012).

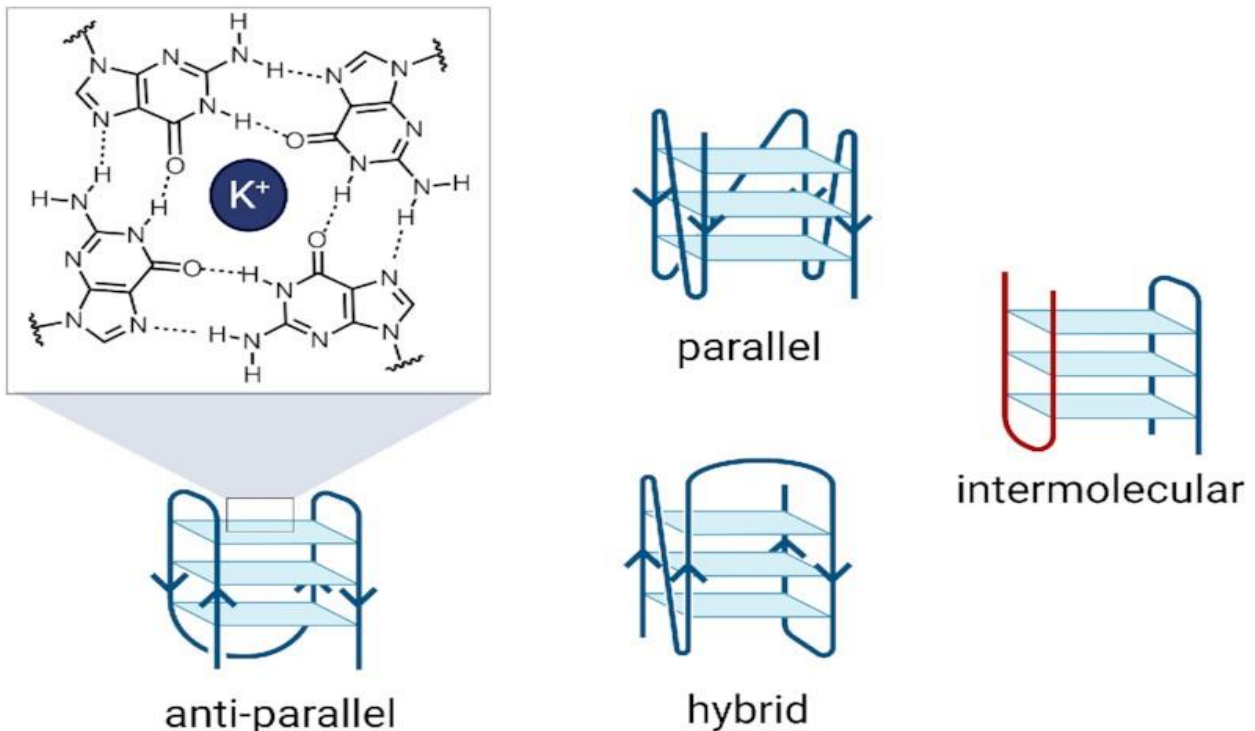


Figure 1.3. G-quadruplex structures and their topology.

G4s constitute of four guanine bases held together by Hoogsteen hydrogen bonding in a square planar arrangement (G-tetrad) and further stabilized by monovalent cations. G4s can have different topologies among them are: anti-parallel, parallel and hybrid structures. If more than one DNA strand is involved in generating the G4, Intermolecular G4s can also be formed (red and blue strands) (adapted from Robinson et al., 2021).

1.2.2 Characterization of G-quadruplexes

G-quadruplex research had been performed extensively in *Tetrahymena* after identifying the role of its telomerase (Yu et al., 1990). and in *S. cerevisiae* because it had been best characterized in terms of structure and function of genetic material (JH et al., 1992). The folding capacity of *Oxytricha* telomeric DNA *in vitro* serves as primer for telomerase led to the observation that antiparallel G4 structures block telomerase (Zahler et al., 1991) This had been proposed to happen in two ways: inhibiting telomerase binding to long telomeric sequences directly, or by modifying the detachment rate of primers from telomerase (Zahler et al., 1991). NMR study of *Oxytricha* telomeric repeats lead to the observation of intermolecular quadruplex conformation (Smith and Feigon, 1992). It had been proposed that G4s could be involved in regulating telomere length, because the telomerase was inhibited by G4s *in vitro* (Smith and Feigon, 1992). Sequencing of yeast (A et al., 1996)

and human genome (International Human Genome Sequencing, 2004) made it possible to start developing computational algorithms for identifying G4 motifs in the genomes (JL, 2008). More than 370000 potentially relevant G4 structures have been identified in the human genome with computational approaches (JL and S, 2005). Based on computational analyses, more than 40% of human genes have G4 motifs on the promoter region, especially on the highly transcribed ones like oncogenes (JL and S, 2007; Lim et al., 2010). G4s can also have the function of a loading platform for the enhancers or repressors of transcription (Y and LH, 2008). The number and nature of human G4s have been shown to be broader with over 700000 G4s with high resolution sequencing based method (Chambers et al., 2015). The formation of G4 was related to oncogenes or tumor suppressors (Chambers et al., 2015). In *S. cerevisiae* genomic distribution of G4s have been associated to more than 500 motifs (Hershman et al., 2008; Paeschke et al., 2011). Formation of G4 structures is not restricted to human. G4 formation is documented to exist in so far, all tested organisms, including viruses, bacteria, yeasts and humans (Mullen et al., 2010; VK et al., 2008). In eukaryotes, the location and regions that have a strong preference to adopt G4 structures are conserved. With the help of a phage display library of different single chain antibody clones, a G-quadruplex structure specific antibody has been identified. The specific antibody termed BG4, was used for the visualization of human DNA G-quadruplex structure with immunofluorescence microscopy (Biffi et al., 2013). G-quadruplexes were shown to be more abundant in the S phase of the cell cycle (Biffi et al., 2013). In the recent years, a method has been developed from ChIP-seq for detection of DNA G4s (Hänsel-Hertsch et al., 2018). To determine G4 formation genome-wide, the BG4 antibody has been used for pull down of secondary structures followed by high-throughput sequencing. G4 ChIP-seq of primary and spontaneously immortalized human keratinocytes, showed that G4s are highly enriched in nucleosome-depleted regions (NDRs) and associated with transcribed genes, suggesting they might have function in chromatin (Hänsel-Hertsch et al., 2018). The G4-ChIP method has the potential to be adapted to other species, like yeast, to identify and confirm conserved roles of G4s at specific regions. Furthermore, a flow cytometry method has been developed for G4 quantification based on the BG4 antibody in human cell lines, blood samples and mouse macrophages (De Magis et al., 2021). It's been suggested that BG-flow can be combined with other cell surface markers to determine G4 levels for diagnostic reasons (De Magis

et al., 2021). Quantifying the G4 abundancy at telomeres with sequencing has not been performed to this date. The fundamental challenge of sequencing telomeres is that the reads of telomeric repeats are repetitive and not accurate enough to distinguish each repeats from one another. Notably, telomere-to-telomere assembly of human X chromosome has been published with ultra-long-read nanopore sequencing which proposes that sequencing of repetitive repeats might be within reach (Miga et al., 2020). Therefore, characterization of G4s at *S. cerevisiae* telomeres could be very helpful for the G4 community.

Due to their special structures, G4s have provided suitable drug targets inside the genome (AK et al., 2005; JL and S, 2005). They can be recognized by synthetic small molecules and there are numerous G4 stabilizing ligands on the market (Daekyu Sun et al., 1997; DJ et al., 2007). The first observation for human G4 formation was that the G-quadruplex stabilizing ligand like BRACO19 blocked the telomerase holoenzyme and led to shortening of telomeres (AM et al., 2005; SM et al., 2002). Furthermore, the Telomeric G-overhang can fold to G4 and is resistance to extension by telomerase. The G-quadruplex ligand, 3H-360A, has been shown to have strong selectivity toward telomeric G-overhang *in vitro* (Granotier et al., 2005). Metaphase spreads of normal and cancer cells treated with 3H-360A, showed that it was preferentially binding to terminal regions (Granotier et al., 2005). In human telomeres the shelterin complex is binding to double stranded DNA and G-overhang and protects the chromosome ends (D et al., 2004; DE LANGE, 2005). A small synthetic molecule which stabilizes folded G4s, known as pyridostatin (PDS), has been first shown to interact with human telomeres and affect the integrity of shelterin and resulting in a DNA damage response (Rodriguez et al., 2008). Pyridostatin has been extensively used for G4 related studies. It has been shown that at lower concentrations PDS interacts with non-telomeric loci before targeting telomeres at higher doses. Genes containing PQS, like SRC protooncogene are more likely to be affected by PDS. PDS has been reported to induce replication and transcription dependent DNA damage, leading to cell cycle arrest. High throughput sequencing of PDS treated cells associated to γ H2AX DNA damage marker indicated that it targets sequences which are able to fold into G4s (Rodriguez et al., 2012). In *S. cerevisiae*, N-methyl mesoporphyrin IX (NMM) and Phen-DC3 are the two commercially available G4 ligands that have been shown to enter the cells. NMM causes up regulation of foci with G4 forming potentials in promoters or ORFs

(Hershman et al., 2008). NMM has been proposed to bind more specifically to parallel G4s (JM et al., 2012). NMM bound G4s have been shown to impair G4 unfolding by the RecQ helicase (Huber et al., 2002). Phen-DC3 binds to G4s with high affinity and specificity and can enter living cells (Anne De Cian et al., 2007; Chung et al., 2014; D et al., 2008). Phen-DC3 treatment of yeast cells inhibits G4 unwinding by Pif1 helicase (Piazza et al., 2010).

1.2.3 Potential functions of G-quadruplexes at telomeres

Formation and existence of G4s *in vivo* was debatable for a long time and the structures were considered to be *in vitro* artifacts. One of the scientific community's concerns was that G4 formation is too slow to regulate processes *in vivo* and too stable which hinders processes like replication (Bochman et al., 2012). *S. cerevisiae* essential protein Rap1 has been shown to promote the formation of parallel G4s *in vitro* (Giraldo and Rhodes, 1994). The β subunit of the *Oxytricha* telomere-binding protein (TEBP β) acts as chaperone and facilitate G4 formation *in vitro* (Fang and Cech, 1993). These *in vitro* findings strengthened the potential *in vivo* functions of G4s. The first direct *in vivo* evidence for G4 structure formation was observed in ciliates telomeres by using antibodies originated by ribosome display against telomeric TG structures (Schaffitzel et al., 2001). This observation was further validated *in vivo* in *Stylonychia*. It was demonstrated that telomeric G4 formation is promoted by two telomere binding proteins, TEBP α and TEBP β (Paeschke et al., 2005). Furthermore, it has been proposed that TEBP β phosphorylation in S phase is required for G4 unfolding (Paeschke et al., 2005). *Tetrahymena* telomerase can use parallel intermolecular G-quadruplexes as substrate and extend them, however intramolecular antiparallel G-quadruplexes blocked the telomerase extension (Oganesian et al., 2006). During DNA replication, G4s are unfolded by helicases and telomerase. The telomerase seems to be actively involved in telomeric G-quadruplex DNA structure unfolding *in vivo*. Significantly, the telomerase is recruited to telomeres by phosphorylated TEBP β , and hence telomerase recruitment is cell-cycle regulated (Paeschke et al., 2008). One of the most descriptive *in vivo* G4 dynamic is the model proposed in *Stylonychia* (Fig. 1.4). TEBP α and TEBP β bind to telomeres and promote G4 formation in G1 and G2. In S phase, TEBP β is phosphorylated and recruits telomerase together with RecQ helicase. The helicase actively unwinds G4s in the replication band and facilitates telomerase action (Postberg et al., 2012).

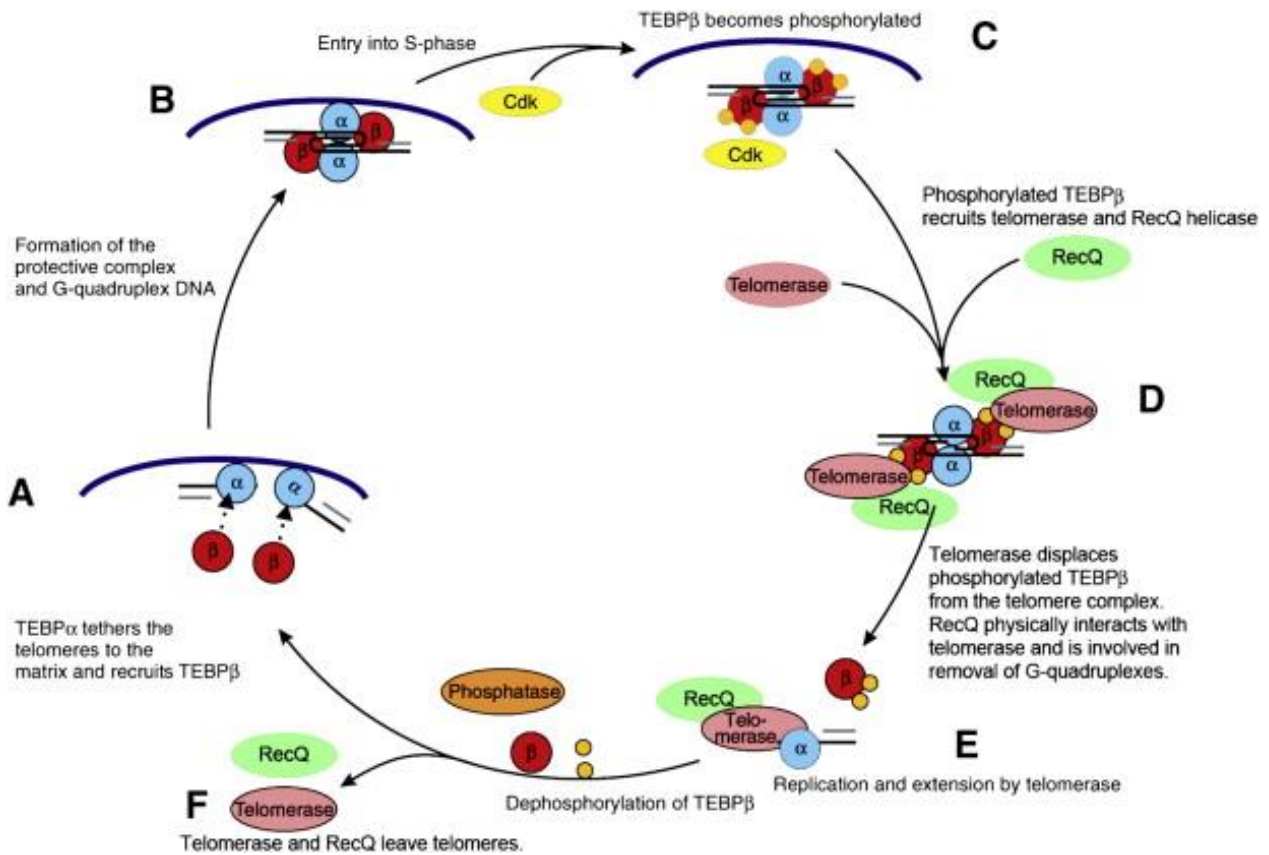


Figure 1.4. A model for the regulation of telomeric G4 structure.

In G1 and G2 phases TEBP α and TEBP β assist telomeric G4 formation. TEBP β gets phosphorylated in s phase. A complex composed of telomerase and RecQ-like helicase associates within the replication band. The complex is recruited to the telomeres by phosphorylated TEBP β . RecQ-like helicase is resolving G4s in the replicating telomere. At the end of S-phase TEBP β is dephosphorylated. Subsequently the original telomere conformation is restored, letting out the telomerase-RecQ complex from the telomere.

G4 structures can be considered as double-edged swords with both genome stabilizing and destabilizing functions that need to be balanced through sensitive regulatory machinery. G4s have been proposed to protect telomeres with compromised capping function and contribute to telomere length maintenance (Paeschke et al., 2010). It has been reported that a purified conformational stable human telomeric G4 is recognized by human telomerase and the telomerase partially unwinds parallel intermolecular conformations *in vitro* (Moye et al., 2015). Unresolved G4s can impair telomere replication and induce genome instability. It has been shown that the catalytic dead mutant of the WRN helicase results in loss of the telomeric lagging strand, meaning that WRN is needed to unfold G4s on the telomeric lagging strand (L et al., 2004). In *S. cerevisiae* the absence

of the Pif1 helicase induces replication fork stalling due to unresolved G4s (Paeschke et al., 2011). The DNA helicase Pif1, which efficiently unwinds G4 structures *in vitro*, has been shown to negatively regulate telomerase activity (Phillips et al., 2015).

Different telomeric proteins have also been indicated to have G4 associated functions. Apart from the Rap1 protein, the *S. cerevisiae* telomerase subunit Est1, has been shown to elevate the formation of parallel G-quadruplexes *in vitro* (Zhang et al., 2010). Est1 mutant cells that are incapable of G4 unfolding *in vitro*, show telomere shortening and senescence (Zhang et al., 2010). Since Est1p and TEBP β both promote G4 formation, it has been proposed that they have equivalent function in telomerase regulation (Zhang et al., 2010). Cdc13 has been shown to partially unwind G4s and facilitate telomere replication (Lin et al., 2001). In human, the POT1 protein, homologue of Cdc13 in yeast, can inhibit or facilitate telomerase action depending on where it is located at the 3'-end (Lei et al., 2005). The *S. cerevisiae*, *cdc13-1* mutant which loses the ability to inhibit exonucleolytic resection of the 5' strand at elevated temperatures, has been proposed to form G4s at G-rich ss DNA and rescue compromised telomere capping *in vitro* (Smith et al., 2011).

One of the G4 binding proteins which has been recently identified with a yeast one-hybrid (Y1H) screen in our group is the Zuo1 protein. Upon UV damage, Zuo1 is recruited to the damage sites by G4 formation, this results in the stability of G4 and stimulate binding of the nucleotide excision repair(NER) machinery. Zuo1 has been shown to maintain genome stability through helping the recruitment of NER and promoting the formation of G4s. Because telomeric sequences have a strong potential to form G4s, we speculate that Zuo1 is involved in regulating telomeric G4s (Magis et al., 2020)(De Magis et al., 2020). If Zuo1 binding changes due to telomere length or if Zuo1 interacts with telomeric proteins needs to be investigated.

Overall, these findings inspires us to postulate the evolutionary conserved functions of ss DNA associated telomeric proteins and the G4 forming potentials of G-overhang, points out potential roles of G4s in telomeres which needs to be further investigated. Although telomeric G4 structures have been studied extensively *in vitro*, little is known about the biological formation and functions of these structures at eukaryotic chromosomal ends.

Because, genome wide analyses always exclude telomeric regions, the functional relevance of telomeric G4 might be more challenging to reveal.

1.3 Aim of the study

The thesis aims to shed light on some basic questions regarding telomere dynamics. Chromosomes termini structure and their intact regulation are of prominent importance in maintaining genome integrity of eukaryotic cells. In this project we tried to address some of open questions regarding telomeres in correlation to G4 structures in *S. cerevisiae*. Addition of telomeric sequences to internal regions in the genome is unfavorable for genome stability and should be avoided. The telomerase enzyme is extending the telomeres when they are critically short. The first aim was to understand where the telomerase subunits are located when they are not attached to telomeres. We provide a map of Est2 binding sites inside the genome. Established by my colleagues in the lab, Est2 binds to multiple internal genomic loci termed as non-telomere binding sites (NTBS). We reveal that Est2 binding to NTBS is regulated during cell cycle and is independent of other telomerase subunits. We could reveal that Est2 binding with NTBS is associated with three dimensional organization of chromosomes. As the second aim, we evaluated the folding kinetics of G-overhang in collaboration with Tomasaka and Trantirek group. Followed by this, we characterize when G4 form at telomeres in *S. cerevisiae* and what contribution this has for telomere function such as protection or telomerase regulation. We modified the ChIP-seq protocol from human to ChIP-qPCR and monitored G4 enrichment at specific telomeric Loci. Third aim was to better understand if G4s form independent of telomere length or in association with telomeric proteins. Lastly, we characterized binding of Zuo1 G4 stabilizing protein in telomeres with respect to telomere length and its correlation with telomeric proteins.

2. Material and methods

2.1 Strains, constructs, and media

All the yeast strains, plasmids and primers are listed in Table 1,2,3 respectively. Deletions eliminated entire ORFs and were created according to (Sikorski and Hieter, 1989). Myc tagging was performed as described (Longtine et al., 1998). Tagged proteins were expressed from endogenous loci and promoters. The *pif1-m2* mutant was created as described (Schulz and Zakian, 1994). The tagging and deletions were confirmed with PCR and sequencing (Table 1., list of yeast strains). RNH1OE plasmid and STM1OE were generous gifts from Brian Luke and Brad Johnson lab respectively (Table 2, list of plasmids).

2.2 Chromatin Immunoprecipitation (ChIP)

2.2.1 Myc- tagged ChIP

Chromatin Immunoprecipitation was performed as described previously (Fisher et al., 2004) with minor changes. 50 ml of yeast strains were grown in standard YPD media to reach the exponential growth phase, OD₆₀₀ = 0.5 (Biochrom). The cells were crosslinked with 1% Formaldehyde (Roth) for 5 min (25°C, 200rpm) and quenched with 125 mM glycine for 5 min (25°C, 200rpm). The cells were centrifuged at 4000 rpm for 5min at 4°C and the pellet was washed with ice-cold HBS buffer (50 mM HEPES pH 7.5, 140mM NaCl) and ChIP lysis buffer (50 mM HEPES pH 7.5, 140mM NaCl, 1mM EDTA pH-8.0, IGEPAL 1%, Sodium deoxycholate 0.1 %) respectively. The pellet was resuspended in 400 µl of ChIP lysis buffer supplemented with protease inhibitor cocktail (Sigma Aldrich) and snap frozen in liquid Nitrogen by immersing the bottom of tubes. At this point the samples can be stored at -80 °C. For lysis, glass beads were added to the screw cap tubes, filled up to meniscus and the cells were beaten in the FastPrep (MP Biomedicals FastPrep-24) two times (6.0 m/s, 1 min). The glass beads were removed and the samples were centrifuged at 14000 rpm for 30min at 4°C. The pellet was resolved in 500µl ChIP lysis buffer supplemented with protease inhibitor cocktail. The chromatin was sheared in Bioruptor (Bioruptor Pico, Diagenode) under high-power mode for 7 cycles (30 sec On, 30 sec OFF), the tubes were kept in ice. Samples were centrifuged at 10000 rpm for 5min at 4°C and the supernatants were transferred to prechilled LoBind tubes (Eppendorf). To remove any traces of cell debris, the samples were centrifuged again at 10000 rpm for

15min at 4°C and the supernatants were transferred to prechilled LoBind tubes (Eppendorf). 1% of the sample was taken separately as Input DNA. 8µl of c-Myc antibody (Clontech) was added to the sheared chromatin and incubated at 4 °C for an hour. In the meanwhile, 80 µl Dynabeads-Protein G was prepared and used for one sample. The beads were pulled down on magnetic rack, washed 3 times with ChIP lysis buffer. After the washes, the beads were pulled down and resuspend in ChIP lysis buffer supplemented with protease inhibitor cocktail. The beads were added to each c-Myc antibody containing samples and incubated at 4°C on a rotator (Phoenix, RS-RD 5) for 1 h. The beads were pulled down on the magnetic racks, the supernatant was discarded and the beads were washed with 2 times with SDS buffer (50 mM HEPES pH 7.5, 140mM NaCl, 1mM EDTA pH-8.0, 0,025% SDS), once with high salt buffer (50 mM HEPES pH 7.5, 1M NaCl, 1mM EDTA pH-8.0), once Tris-lithium buffer (20mM Tris-Cl pH-7.5, 1mM EDTA pH-8.0, IGEPAL 0,05%, Sodium deoxycholate 0.1 %, LiCl 1,06 %) Two more wash steps were performed with TE buffer (10 mM Tris-Cl pH 8.0, 1 mM EDTA). The wash buffer was removed and 140µl TE buffer with 1% SDS were added to the Input samples as well. The samples and the inputs were incubated at 65°C (Eppendorf Thermomixer), first for 2 minutes, then the beads were removed and they were kept at 65°C overnight for reverse crosslinking. The immunoprecipitated and the input DNA were purified using MinElute Kit (Qiagen) following the manufacturer's protocol. DNA was eluted in 25µl ddH₂O. The enrichment of G4s and percentage of input recovery was quantified using qPCR with specific primers (Table 3).

2.2.2 BG4 ChIP

BG4 Chromatin Immunoprecipitation was performed as described previously (Hänsel-Hertsch et al., 2018) with minor changes for *S. cerevisiae*. Briefly, 50 ml of yeast strains were grown in standard YPD media to reach the exponential growth phase, OD₆₀₀ =0.5 (Biochrom). The cells were crosslinked with 1% Formaldehyde (Roth) for 10 min (25°C, 200rpm) and quenched with 125 mM glycine for 10 min (25°C, 200rpm). The cells were centrifuged at 4000 rpm for 5min at 4°C and the pellet was washed with ice-cold HBS buffer (50 mM HEPES pH 7.5, 140mM NaCl) and ChIP lysis buffer (50 mM HEPES pH 7.5, 140mM NaCl, 1mM EDTA pH-8.0, IGEPAL 1%, Sodium deoxycholate 0.1 %) respectively. The pellet was resuspended in 400 µl of ChIP lysis buffer supplemented with protease inhibitor cocktail (Sigma Aldrich) and snap frozen in liquid Nitrogen by immersing

the bottom of tubes. At this point the samples can be stored at -80 °C. For lysis, glass beads were added to the screw cap tubes, filled up to meniscus and the cells were beaten in the FastPrep (MP Biomedicals FastPrep-24) two times (6.0 m/s, 1 min). The glass beads were removed and the samples were centrifuged at 14000 rpm for 30min at 4°C. The pellet was resolved in 500µl ChIP lysis buffer supplemented with protease inhibitor cocktail. The chromatin was sheared in Bioruptor (Bioruptor Pico, Diagenode) under high-power mode for 7 cycles (30 sec On, 30 sec OFF), the tubes were kept in ice. Samples were centrifuged at 10000 rpm for 5min at 4°C and the supernatants were transferred to prechilled LoBind tubes (Eppendorf). To remove any traces of cell debris, the samples were centrifuged again at 10000 rpm for 15min at 4°C and the supernatants were transferred to prechilled LoBind tubes (Eppendorf). The RNA digestion was performed by adding 2µl RNase A (10 mg/ml, Invitrogen) followed by 20 min incubation at 37°C and 1400 rpm (Eppendorf Thermomixer). Quantity of DNA was measured with Qubit-Fluorometer (Invitrogen) according to manufactures instructions. Same quantity of DNA (4µg) was used for BG4 ChIP and 1% was taken separately as Input DNA (0.04 µg). The samples were incubated using 0.5 µg of recombinant BG4 for 1 µg chromatin and 1% BSA at 16°C for 2h on rotator (RS-RD 5, Phoenix). In the meanwhile, the Anti-FLAG magnetic beads (Sigma Aldrich) were prepared. 40 µl of Anti-FLAG magnetic beads was used for one sample. The beads were pulled down on magnetic rack, washed 3 times with ChIP lysis buffer supplemented with 1% BSA. After the washes, the beads were pulled down and resuspend in ChIP lysis buffer supplemented with 1% BSA and protease inhibitor cocktail. The beads were added to each BG4 antibody containing samples and incubated at 16°C on a rotator (Phoenix, RS-RD 5) for 1 h. The beads were pulled down on the magnetic racks, the supernatant was discarded and the beads were washed 3 times with 200µl ice-cold wash buffer (100 mM KCl, 10 mM Tris pH 7.4, 0.1% Tween 20). Two more wash steps were performed at 37°C, 200 µl wash buffer was added and the beads were rotated for 10 head over tails. The wash buffer was removed and 75 µl TE buffer (10 mM Tris-Cl pH 8.0, 1 mM EDTA) supplemented with 1 µl Proteinase K (20mg/ml) were added, the same were added to the Input samples. The samples and t

he inputs were incubated at 37°C for 1h and 1400rpm rotation (Eppendorf Thermomixer), followed by another 2h incubation at 65°C and 1400rpm rotation. At this point, the samples can be kept at 16°C over night. The next day, the beads were pulled down in magnetic

racks and the supernatants were transferred to new microtubes. The immunoprecipitated and the input DNA were purified using MinElute Kit (Qiagen) following the manufacturer's protocol. DNA was eluted in 25µl ddH₂O. The enrichment of G4s and percentage of input recovery was quantified using qPCR with specific primers (Table 3).

2.3 Cell cycle synchrony and confirmation of DNA content with fluorescence-activated cell sorting (FACS)

Cell cycle synchrony was performed as previously described (Paeschke et al., 2011) with some modifications. Briefly, *bar1Δ* strain were grown in standard YPD medium + Glucose (2%) at 30°C, 200rpm until OD₆₀₀ =0.2 was reached. The cells were incubated at 24°C, 200rpm for 3h with 5µg/ml α-factor (Genescript) to arrest the cells in the G1 phase. The cells were checked for "shmoos" formation under the microscope (E200, Nikon). Cells were fixed for 5 minutes (1ml EDTA 0.5 M, NaN₃ 0.3% w/v) for FACS analysis to confirm G1 arrest of cells. 50ml sample was taken for ChIP experiment. The remaining culture was filtered with and resuspended in fresh YPD + Glucose (2%) to arrest the cells in S and G2/M. To fractionate S-phase, the cells were incubated with 250mM (early), 150mM (mid) and 75mM (late) Hydroxyurea (HU) at 30°C, 200rpm for 2h. 5ml of samples were added to fixative solution (1ml EDTA 0.5 M, NaN₃ 0.3% w/v) for FACS analysis to confirm S-phase arrest. 50ml of the sample was taken for the ChIP experiment. To arrest the cells in G2/M, 15 µg/ml Nocodazole was used. 5ml of samples were added to fixative solution (1ml EDTA 0.5 M, NaN₃ 0.3% w/v) for FACS analysis to confirm G2/M arrest. 50ml of the sample was taken for the ChIP experiment. To verify cell cycle synchrony FACS, fixed cells were pelleted and washed twice in 1ml Sodium citrate (50mM) buffer. The cells were resuspended in ethanol (70%) and incubated at -20°C for 30min. The cells were washed with Sodium citrate (50mM) buffer and resuspended in 500 µl of sodium citrate (50mM) + 10 µl RNase A (10mg/ml, Invitrogen), incubated at 37°C for 1h. The cells were incubated for another 2h at 50°C with 2 µl of proteinase K (20mg/ml, Sigma Aldrich). The cells were sonicated for 3 cycles (30 sec on/off) using bioruptor (Bioruptor Pico, Diagenode). 500 µl of sodium citrate (50mM) + 2 µl SYTOX Green (Invitrogen) were added to the cells before sorting. The DNA content and cell cycle was measured by BD FACS Canto II using the parameters FSC Log 200V, SSC Log 300V, GFP Lin 416V, FSC threshold 5000, flowrate high and record 10000 events.

2.4 BG4 purification and validation

BG4 antibody was expressed and purified as described previously (Biffi et al., 2013). Briefly, the pSang10-BG4 plasmid was transformed to *E. Coli* BL21(DE3) competent cells, supplemented with 50µg/ml Kanamycin for selection. four single colonies were inoculated in 5ml standard 2xTY medium (16 g/L Tryptone, 10 g/L Yeast extract, 5 g/L NaCl), supplemented with 1% Glucose and 50µg/ml Kanamycin and incubated overnight at 37°C, 200rpm (Ecotron, Infors HT). The starting cultures were inoculated in 4x 500ml (2L flasks) 2xTY medium, supplemented with 1% Glucose and 50µg/ml Kanamycin, grew for 3-4 h at 37°C, 200rpm until OD600= 0.6 (Biochrom) was reached. IPTG was added to a final concentration of 0.5mM to induce BG4 expression, the cells were grown overnight at 25°C, 200rpm. The cells were centrifuged at 4000 g for 30 min at 4°C. The supernatant was discarded and the pellet was resuspend in 160 ml ice cold TES buffer (Tris 50Mm pH8.0, Sucrose 20%, EDTA 1mM) and stirred for 10 minutes on ice. 240 ml TES 1:5 diluted was added and stirred for another 15 min, on ice. Samples were centrifuged at 16000 g for 30 min at 4°C. The pellet was discarded and the supernatant was filtered through a 0.45µM membrane, on ice. The filtered flow through was incubated with 6 ml of previously washed Ni-NTA magnetic beads (Qiagen) for 1 h at 4°C on rotator. The mixture was transferred to Nickel affinity column and the saturated beads were washed 6 times, with 50 ml cold wash buffer (PBS pH8.0, 100 mM NaCl, 10 mM Imidazole). The BG4 was eluted from the beads with 5ml elution buffer (PBS pH8.0, 250 mM Imidazole). Imidazole was removed by multiple washes at 4000g and 4°C using the Amicon Ultra-15 Centrifugal Filter Unit (Merck) with Intracellular salt buffer (25 mM HEPES pH 7.6, 110 mM KCl, 10.5 mM NaCl, 1 mM MgCl₂) and concentrated to 500µL. The purity of the expressed BG4 was confirmed by SDS-PAGE and immunofluorescence.

2.5 Telomere healing assay

Telomere healing assays were performed essentially as previously described (Bianchi et al., 2004; Strecker et al., 2017; Zhang and Durocher, 2010) with minor modifications. The TG80-HO and N80-HO strains (Phillips et al., 2015) were used as positive and negative controls respectively. Briefly, the strains were grown on XY media (20 g/L bactopectone, 10 g/L yeast extract, 0.1 g/L adenine, 0.2 g/L tryptophan) + Glucose (2%) overnight and subculture to XY + raffinose (2%) to reach the density of 2.5-7.5x10⁶ cells/mL or OD600 =0.75. To synchronize the cells in G2/M Nocodazole (Sigma Aldrich) was added to a final

concentration of 15 µg/mL and incubated for at 30°C, 200rpm for 2h. Galactose (3%) was added to induce HO endonuclease expression, incubated at 30°C, 200rpm for 4 h. The cells were plated on XY + Glucose (2%) before and after addition of galactose and grown for 2-3 days. The number of colonies were counted and replica plated to a media containing α-amino adipic acid (α-AA) or SD-Lys to identify cells that have lost the distal LYS2 gene. Frequency of telomere addition was calculated as the percent of post-galactose surviving colonies that are α-AA resistant (α-AA/XY).

2.6 Southern blot telomeres

S.cerevisiae genomic DNA was extracted from a saturated 5 ml overnight yeast culture using the Epicenter MasterPure™ Yeast DNA Purification Kit (MPY80200). 10 µg gDNA was digested overnight, in a final volume of 50 µL, at 37°C with XhoI. The digested DNA was loaded on 0.8% agarose gel with EtBr and TAE (0.4 M Tris acetate pH-8.3, 0.01 M EDTA) and ran at 100 V for 5 hours. The DNA in the gel was cross linked with 120 mJ in UV-crosslinked (Stratalinker 1800, Stratagene). The gel was incubated in denaturing solution (1.5 M NaCl, 0.5 M NaOH) for 30 min RT on rocking platform and another 30 min in Blotting solution (1.5 M NaCl, 0.25 M NaOH). The gel was transferred to Hybond N+ membrane (GE Healthcare Life Sciences) using overnight capillary flow. The transferred membrane were UV-crosslinked (Stratalinker 1800,Stratagene) and pre-hybridized in 20 ml pre-warmed DIG easy hyb buffer (Roche) for 1h at 39°C. 5ml TG DIG-labelled probe created from DIG Oligonucleotide 3'-End Labelling Kit (Roche) was denatured at 68°C for 10 min and incubated overnight with prehybridized membrane at 39°C. The membrane was washed 2x for 5 min with pre-warmed 2X SSC (17,5 g NaCl, 8,8 g Sodium citrate, pH 7.0) + 0.1% SDS at 39°C. The membrane was washed 2x for 20 min with pre-warmed 0,5X SSC and 0.1% SDS at 39°C. The membrane was blocked for 30 min at RT in 2ml 10x blocking solution (DIG labelling kit, Roche) and 18ml maleic acid buffer (11,67 g Maleic acid, 8,76 g NaCl pH to 7.5). The blocked membrane was incubated with 2 µl AP-coupled anti-DIG Fab in 20 ml 1x blocking solution for 30 min at RT. The membrane was washed 4x for 15 min with 1x DIG washing buffer (11,8 g Maleic acid, 8,76 g NaCl, 3 ml Tween-20, pH 7.5) at RT. The membrane was placed in plastic sheet protector and incubated for 5 min in the dark with 20 µl CSPD in 2 ml detection buffer (15,8 g Tris HCl, 5,8 g NaCl, pH 9.5). The membrane was exposed to ChemiDoc XRS+ System (Bio Rad) to check the telomere length.

2.7 Spot assay

The strains were grown in standard YPD medium + Glucose (2%) at 30°C, 200rpm until OD600 =0,8 was reached. 200 µl was transferred to a sterile 96-well plate. 10 fold serially diluted samples were plated as 5 µl droplets on YPD or selective yeast media and grown for 2-3 days at 23° or 30°C to evaluate the viability of the mutants.

2.8 Co-Immunoprecipitation

1 of yeast strains were grown in standard YPD media to reach the exponential growth phase, OD600 =0.7 (Biochrom). The samples were centrifuged 3000 rpm at 4°C for 5 min and washed 2x with 30 ml cold ddH₂O with the same settings. The cells were washed with lysis buffer (50 mM HEPES pH 7.5, 140mM NaCl, 1mM EDTA pH-8.0, IGEPAL 1%, Sodium deoxycholate 0.1 %) and centrifuged 3000 rpm at 4°C for 5 min. the pellet was resuspended in 400 µl of lysis buffer supplemented with protease inhibitor cocktail (Sigma Aldrich) and snap frozen in liquid Nitrogen by immersing the bottom of tubes. At this point the samples can be stored at -80 °C. For lysis, the glass beads were added to the screw cap tubes, filled up to meniscus and the cells were beaten in the FastPrep (MP Biomedicals FastPrep-24) two times (6.0 m/s, 1 min). The glass beads were removed and the samples were centrifuged at 14000 rpm for 30min at 4°C. The RNA digestion was performed by adding 2µl RNase A (10 mg/ml, Invitrogen) followed by 20 min incubation at 37°C and 1400 rpm (Eppendorf Thermomixer). Then 1 µl Proteinase K (20mg/ml) was added and incubated at 37°C for 20 min and 1400rpm rotation (Eppendorf Thermomixer). 20 µl was taken as the Input control. 8µl anti-myc (Takara) antibody was added and incubated for 2h at 4°C. In the meanwhile, 80 µl of magnetic protein G Dynabeads was washed 3x times with 1 ml lysis buffer. The beads were resuspend again in 80µl lysis buffer supplemented with protease inhibitor cocktail (Sigma Aldrich). 80µl beads were added to each sample and incubated over night at 4°C. The beads were pull down on a magnet and washed 6x with 1 ml TBS (50 mM Tris-Cl, pH 7.5, 150 mM NaCl) supplemented with protease inhibitor cocktail (Sigma Aldrich). To detach the samples from the beads, 50 µl 1x SDS loading dye (62.5 mM Tris-HCl pH 6.8, 2.5 % SDS, 0.002 % Bromophenol Blue, 0.7135 M β-mercaptoethanol, 10 % glycerol) was added and boiled at 95°C for 5min. The samples were checked with on western blot using the specific antibodies.

2.9 Hi-C

The Hi-C 2.0 protocol was adapted and modified from (Belaghzal et al., 2017) for usage in yeast cells. Diploid cells of *S. cerevisiae* were cultured in YPD media to reach the exponential phase. Afterwards, fixation of the cells was achieved by adding 3% formaldehyde to 100 ml of the cell suspension (OD₆₀₀ 0.50-0.8) and incubation for 20 min at 30°C with 250 rpm agitation. The reaction was stopped by adding 0.35 M glycine and 5 min incubation at 30°C and 250 rpm agitation. The cells were centrifuged and washed in water. Subsequently, the cells were again centrifuged and snap frozen in liquid nitrogen for storage at -80°C. Next, the cells were thawed and washed in spheroplasting buffer (SB; 1 M Sorbitol, 50 mM Tris pH 7.5). An amount of 10 µg/ml 100T zymolase with 0.5% β-mercaptoethanol was added to the SB and incubated for 10 min at 35°C for cell digestion. Then, the cells were washed in restriction enzyme buffer NEB3.1 and the chromatin was solved by adding 0.01% SDS and incubation at 65°C for 5 min. Afterwards, Triton X-100 was supplemented to 1%. Overnight incubation with 400 U DpnII at 37°C and 400 rpm was performed for chromatin digestion. On the next day, DpnII was heat-inactivated at 65°C for 20 min and to the ends of the DNA new nucleotides with biotin-14-dCTP were added by using the Klenow fragment DNA polymerase I at 23°C for 4 h with 10 seconds agitation at 900 rpm every 5 min. The sample was diluted 1:2 and the cross-linked DNA ends were ligated at 16°C for 4 h by using the T4 DNA ligase in 1x T4 ligation buffer with supplemented 1% Triton and 0.1mg/ml BSA.

The subsequent crosslinking was achieved by overnight incubation at 65°C with supplemented 400 µg/ml proteinase K. In order to increase the reaction an additional amount of 400 µg/ml proteinase K was added and incubated for 2 h at 65°C. Afterwards, the DNA purification was performed using phenol:chloroform:isoamylalcohol for extraction and ethanol for precipitation. The purified DNA pellet was dissolved in TLE buffer (10 mM Tris pH 8.0, 0.1 mM EDTA) and concentrated in an Amicon filter with 30 kDa cutoff. Next, the sample was incubated with 10 µg/ml RNase A at 37°C for 30 min. In order to remove biotin from unligated ends the sample was treated with 0.3 U/µl T4 DNA polymerase and 25 µM dGTP and 25 µM dATP at 20°C for 4 h. The reaction was terminated at 75°C for 20 min. After washing in an Amicon filter with a 30 kDa cutoff the DNA was fragmented in a Covaris M220 (Duty factor 20%, 200 cycles/burst, 240 sec at 20°C). Afterwards, T4 DNA polymerase, T4 Polynucleotide Kinase and Klenow fragment DNA polymerase I were

added to the sample for reparation of the DNA ends. For the purpose of enrichment of biotinylated fragments, the sample was incubated with streptavidin beads (C1) and afterwards, DNA ends were A tailed with a subsequent on-beads ligation of barcode adapters (NextFlex, Bio Scientific) was accomplished. Finally, the obtained library was minimally PCR amplified and send for next generation sequencing using paired end 75 bp reads on a NextSeq550 device (Illumina, Brighton Genomics).

3. Results

3.1 Identification of Non Telomeric Binding Sites (NTBS)

Experiments and data described in 3.1 were generated by members of the Paeschke group before I started my PhD and were the basis for my own experiments. At the time of writing my thesis this data is still unpublished but submitted with me as a co-first author. I will describe this data below to lay the foundation for my own experimental work.

3.1.1 Telomerase catalytic subunit (Est2) binds to endogenous regions

To monitor telomerase binding affinity for endogenous regions (Gallardo et al., 2008; Obodo et al., 2016; Ouenzar et al., 2017; Schmidt et al., 2016), we tagged the telomerase catalytic subunit Est2 endogenously with 13 Myc at its C-terminus. We performed Chromatin Immunoprecipitation (ChIP) after Est2.Myc13 was crosslinked with formaldehyde, to get a genome wide binding profile. The immunoprecipitated Est2.Myc13 and input DNA were labelled fluorescently and hybridized to whole genome DNA microarray (ChIP-chip). We used the ChIPOTle 2.0 program (Buck et al., 2005) with a significance cut-off of 0.05 for identifying the binding sites. The regions which were detectable in three out of five biological repeats were selected as Est2 binding targets. Est2.Myc13 ChIP-chip analyses led to the detection of 978 non-telomeric binding sites (NTBS) after excluding the telomeric sequences. The average length of NBS is 240 bp across all the chromosomes (Table 5, list of NTBS) (Fig. 3.1A, S1A). These sequences are significantly more G-rich than the average GC content of the yeast genome (NTBS: 52 % GC; yeast genome: 38 % GC) (p-value <0.001). The TG-richness of NTBS looks similar to telomeric repeats analysed by MEME motif (Fig. 3.1B, E-value 1.1e-69). NTBS overlapping to important genomic regions (annotated by *S. cerevisiae* genome database (SGD)) such as ARS, promoter or binding sites of specific proteins, was correlated bioinformatically. The p-value was calculated based on 10.000 random datasets. NTBS significantly overlap with regions known to be bound by telomerase regulatory factors. These include Pif1 sites (Paeschke et al., 2011) (361/978)[p<0.0001], pif1-m2 sites (430/978) [p<0.0001], R-loops (Chan et al., 2014; Wahba et al., 2016) (84/978) [p<0.0001], G-quadruplex (G4) regions (Capra et al., 2010) (35/978) [p<0.0001], DNA damage marker γ -H2A sites (Capra et al., 2010) (294/978) [p<0.0001] and Pol II sites (Paeschke et al., 2011) (354/978) (Fig. S1B-F).

To validate Est2 binding to endogenous regions, we performed ChIP and quantitative PCR (ChIP-qPCR) with specific primers designed to detect 4 different NTBS (NTBS #1- NTBS #4). We used a primer directed against the right arm telomere on Chromosome VI (Telo VI-R) as positive control and ARO1 a region known to be low in telomere binding proteins as negative control (Chan et al., 2008). Est2.Myc binding was significantly enriched (2-3 fold) in four NTBS in comparison to the ARO1 negative control (Fig. 3.1C comparison to the negative control (Fig. 3.1C).

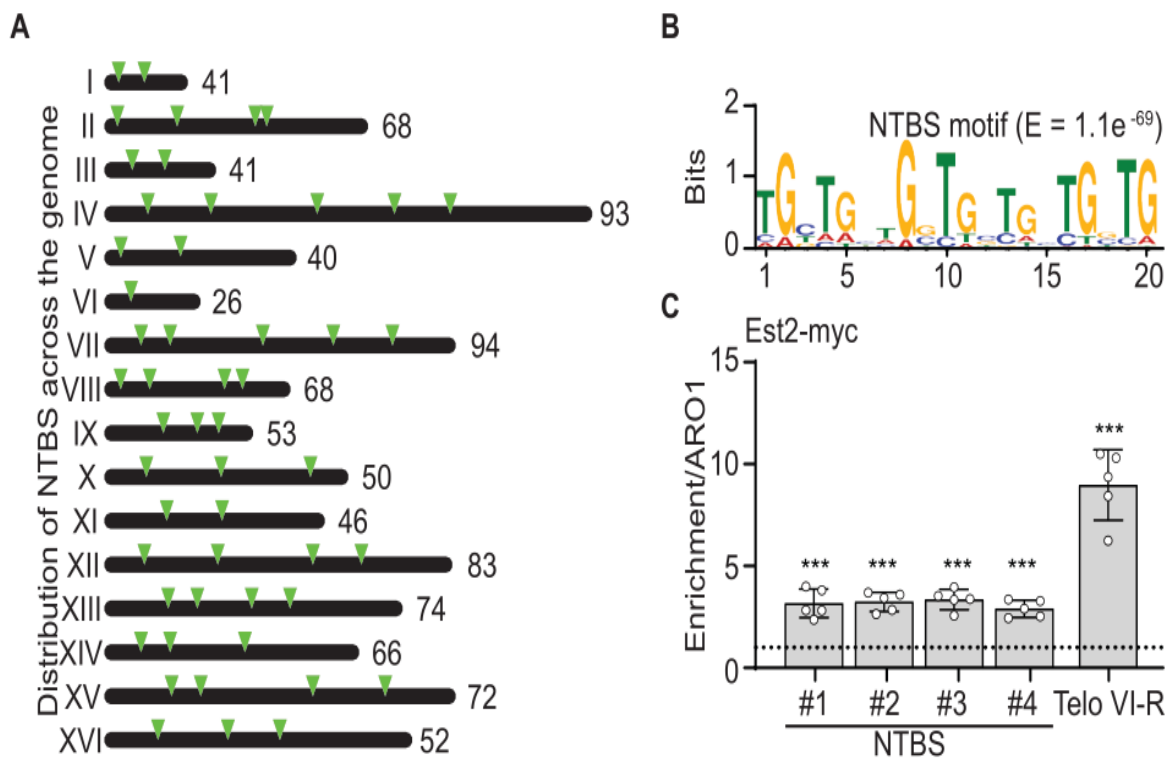


Figure 3.1. Est2 binding across the yeast genome

A. Est2 binding across the *S. cerevisiae* genome. Each triangle represents a non-telomeric binding site (NTBS) of Est2 on chromosome. All the sites were present in at least 3 out of 5 independent experiments. **B.** NTBS regions MEME motif. The binding sites were TG-rich. (E-value 1.1e-069) **C.** ChIP-qPCR of four different NTBS regions (see Table 5 for specification of the region). Est2 binding to telomere VI-R was used as positive control. Reported values are normalized to input and ARO1 (non-telomeric control). Data are represented as mean \pm Standard error mean (SEM) of n = 5 biological replicates. Statistical significance was calculated to ARO1 levels and determined using Student's t-test. ** p-value < 0.01 and *** p-value < 0.001.

3.1.2 Like telomeres, Est2 binding to NTBS is regulated during the cell cycle

Published data indicates that for a functional telomerase holoenzyme, all of its subunits should be present (Evans and Lundblad, 1999; Hughes et al., 2000; Lendvay et al., 1996; Lundblad and Szostak, 1989; Taggart et al., 2002). At telomeres, Est2 functions together

with Est1 and Est3 in a complex (Lendvay et al., 1996; Wellinger and Zakian, 2012). The binding of Est1 and Est3 to different NTBS was monitored with CHIP-qPCR (Fig. 3.2A-B). Neither Est1, nor Est3 shows significant binding to NTBS. Est2 binds to NTBS alone and is most likely in an inactive state. It is already known that Est2 association to telomeres is cell cycle regulated and occurs in late S phase, when telomere extension takes place if needed (Chan et al., 2008; Fisher et al., 2004; Wellinger and Zakian, 2012). To monitor Est2 binding during cell cycle to NTBS, cell cycle synchrony was done in yeast after arresting the cells in G1 with α -factor and releasing them to S-phase as has been done previously (Fisher et al., 2004). The synchrony of the cells was examined by Fluorescence-activated cell sorting (FACS) (Fig. S2A). We monitored Est2 binding to four NTBS, the positive (Telo VI-R) and negative control (ARO1) throughout the cell cycle by CHIP-qPCR. As it was previously published, Est2 binding to telomeres peaks at the end of S-phase (Fisher et al., 2004) (Fig. 3.2C). However, Est2 binding to NTBS peaks in G1 and late S/G2 phase (Fig. 3.2D).

Apart from Est1 and Est3, Est2 binding to telomeres depends on TLC1 as well (Chan et al., 2008; Evans and Lundblad, 1999; Fisher et al., 2004; Hughes et al., 2000; Taggart et al., 2002; Tuzon et al., 2011) We monitored the abundance of Est2 binding to telomeres throughout the cell cycle in the absence of Est1 and TLC1 with CHIP-qPCR. In agreement with previously published data, Est2 binding to telomeres is reduced in *est1 Δ* and *tlc1 Δ* (Fig. 3.2C) (Chan et al., 2008). At NTBS, Est2 binding is increased in *est1 Δ* cells in late S/G2 phase (Fig. 3.2E, Fig. S2B-D, white triangles). A similar trend was observed for Est2 binding to NTBS in *tlc1 Δ* , which was significantly elevated during cell cycle with a strong peak in mid S-phase (Fig. 3.2E, Fig. S2B-D, white squares). We speculate Est2 is not capable of distinguishing between NTBS and telomeres in the absence of TLC1, which is a main component for Est2 binding to telomeres (Chen et al., 2018; Gallardo et al., 2008; Hughes et al., 2000; Lendvay et al., 1996). Our data also indicates that without TLC1, there is an Est2 abundance in the cells and more Est2 is free for binding to NTBS.

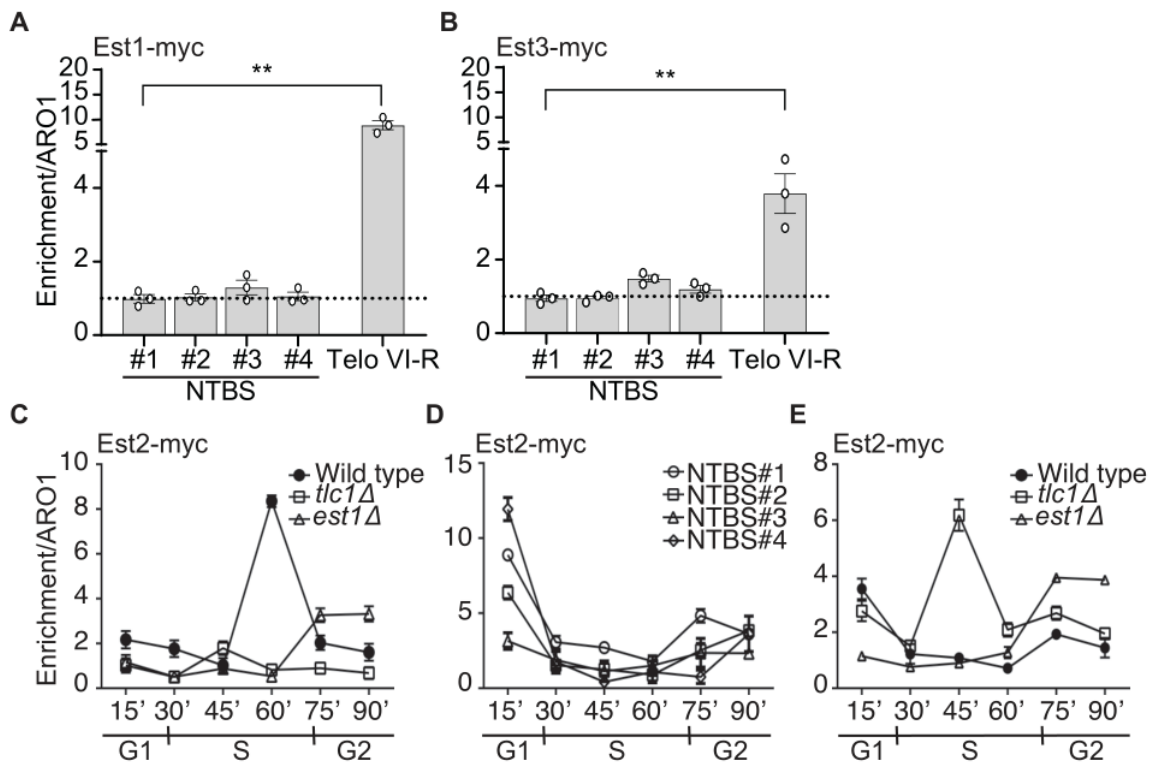


Figure 3.2. Est2 binding to NTBS changes in the absence of Est1 and TLC1

analysis of Est1 and Est3 to four NTBS and one telomere (VI-R) (A-B). **A.** Est1 binding to NTBS **B.** Est3-NTBS binding. Bars represent enrichment over ARO1. Data are represented as mean \pm SEM for $n=3$ biological replicates. Statistical significance was determined using Student's t-test. * p -value < 0.05 and ** p -value < 0.01 . **C.** Est2 binding in synchronized cultures. For this, cells were synchronized using α -factor and released in the cell cycle. Est2 binding to telomere VI-R in wildtype background (closed circles) in absence of TLC1 (open squares) and in the absence of Est1 (open triangles). **D.** Est2 binding to four NTBS in wildtype background. **E.** Est2 binding to NTBS#1 in wildtype, *tlc1Δ*, *est1Δ* (Fig. S2B-D for NTBS #2 -#4). Data are represented as mean \pm SEM for $n=3$ biological replicates.

3.1.3 Est2 is not recruited to NTBS via canonical telomerase recruitment proteins

Telomerase recruitment to telomeres is regulated via Cdc13, Est1 and yKu70/80, which are necessary proteins for telomere maintenance (Chan et al., 2008; Fisher et al., 2004; Lin and Zakian, 1996; Nugent et al., 1996; Qi and Zakian, 2000). yKu70/80 is important for Est2 binding to telomeres in G1, while Cdc13 together with Est1 recruits Est2 during S/G2 phase. In order to understand which proteins are associated with Est2 binding to NTBS, we first analysed the known telomerase recruitment factors. Both Cdc13 and yku70 were tagged endogenously with MYC and their binding to 4 NTBS as well as the positive and negative control, was monitored by CHIP-qPCR (Fig. 3.3A-B). Our data did not indicate significant binding to the four different NTBS for both Cdc13 and yKu70. However,

Cdc13 is enriched nearly 30 fold and yKu70 over 100 fold at telomeres (Fig. 3.3A-B) (Chan et al., 2008). We propose that both proteins do not have a major role in regulating Est2 and NTBS interaction. Since our data reveals no correlation to known telomere recruitment factors, we examined another hypothetical model called the “replication fork model” to investigate Est2 binding to NTBSs. We checked for the co-migration of telomerase with the replication fork (Greider, 2016; Matmati et al., 2020) and observed a significant overlap of NTBS with replication fork pausing sites (Fig. S1). We assumed if the pauses in replication give rise to Est2 binding, the binding of Est2 to NTBSs should correlate to replication fork progression. To investigate this, we generated a tagged catalytic subunit of Polymerase 2 (DNA Pol2) and monitored Pol2 progression. This experiment was performed in synchronized yeast cells using DNA Pol2 tagged to measure the time of binding by ChIP-qPCR. Our results indicate that the binding of Est2 and DNA Pol2 does not overlap spatially and temporally and thus, suggests a replication fork independent mechanism for Est2 binding to NTBS (Fig. 3.3C).

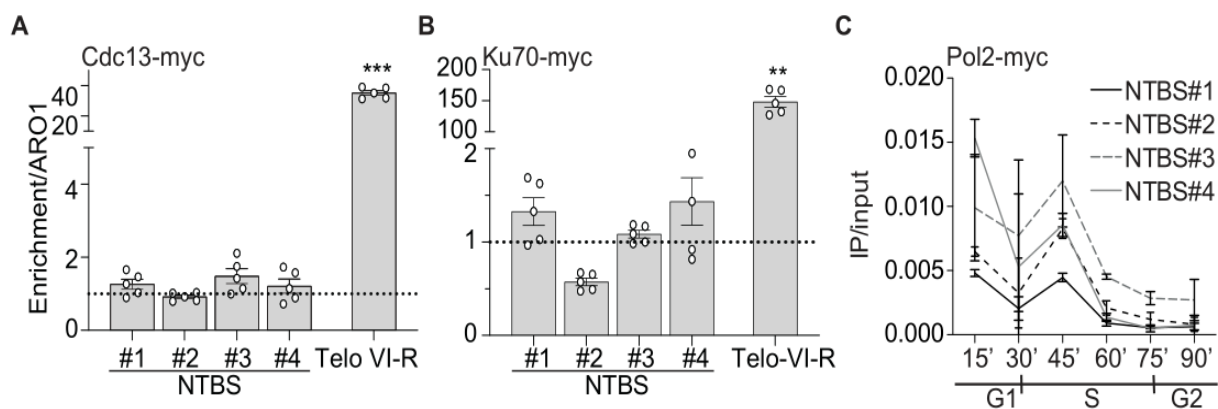


Figure 3.3. Est2 is recruited via an alternative pathway to NTBS

A. Cdc13 was tagged endogenously and binding to four NTBS and telomere VI-R was monitored by ChIP-qPCR in asynchronous cultures. **B.** Ku70 is tagged endogenously and binding to NTBS and telomere VI-R was monitored by ChIP-qPCR in asynchronous cultures. **C.** DNA Pol2 occupancy was monitored throughout the cell cycle to NTBS and telomeres. Representative data of DNA Pol2 binding to NTBS#1-4, normalized to input. The significance was calculated using Student's t-test. * p-value <0.05, ** p-value <0.01 and *** p-value <0.001.

3.1.4 3D organization of chromatin involved in Est2 and NTBS interaction

Because telomere extension is a tightly regulated mechanism, other proteins and mechanisms have been proposed to positively and negatively regulate Est2 recruitment in addition to Cdc13 and yKu70. These include Mlh1 (Jia et al., 2017; Jia and Chai, 2018), Pif1 (negative regulator of telomerase) (Boule et al., 2005; Phillips et al., 2015), R-loop formation (TERRA) (Balk et al., 2013; Cerritelli and Crouch, 2009; Graf et al., 2017), Rad51-Rad52 (Epum et al., 2020), and RNaseP components (Garcia et al., 2020). We checked Est2 binding to NTBS with ChIP-qPCR in the absence of these regulatory factors to identify their potential role in Est2 and NTBS interaction. We observed no significant changes in Est2 binding to NTBS after deletion of Mlh1 (*mlh1Δ*), Pif1 mutation (*pif1-m2*), or reduction in R-loops (overexpression of RNaseH1) (Fig. S3A-C). The Heterochromatic state of telomeres has been reported to affect telomerase access to telomeres. Histone deacetylase complex is responsible for deacetylation of core histones and changing the heterochromatin state (Bernstein et al., 2000). We performed ChIP-qPCR and monitored Est2 binding in the absence of Sin3 (*sin3Δ*) which is a component of histone deacetylase complex. Our data revealed minor to no significant changes on Est2 binding to NTBS (Fig. S3E).

Furthermore, we analysed another hypothesis following a three-dimensional model in which the telomerase first makes several contacts with internal chromosomal regions before binding to telomeric regions (Schmidt et al., 2016). To test association of 3D chromosome configuration in Est2 binding to NTBSs we implemented the chromosome conformation capture technique called Hi-C (Fig. 3.4 A). We compared the interactions of NTBS-NTBS and NTBS-telomeric regions and calculated the average contact possibilities (Fig. 3.4 B). NTBS with an average mean Hi-C contact possibility are closer to one another. This accounted for 841 of 978 (86%) of all NTBS regions. Furthermore, 137 (14%) of the NTBS indicate significantly closer contact to telomeric regions compared to randomized control regions (p-value $2.2e^{-16}$) (Fig. 3.4C). These results implicate that Est2 binding to NTBSs brings telomeric regions to closer proximity via chromatin organizational event.

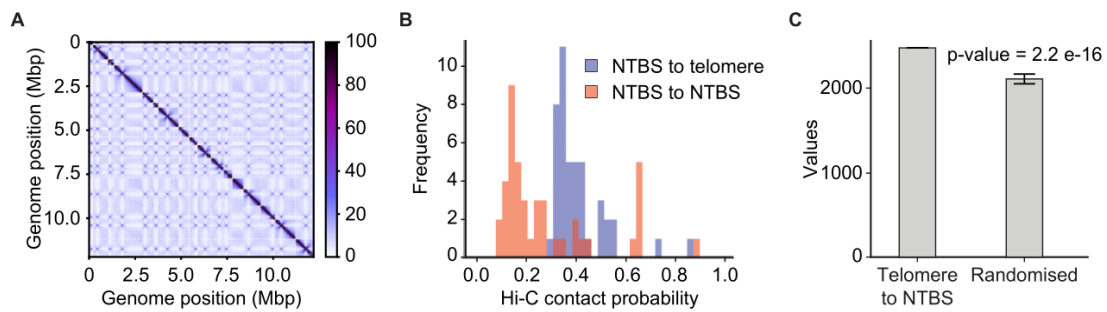


Figure 3.4. Hi-C data

A. Hi-C contact map of interchromosomal events. Contacts are plotted at 5 kb resolution. **B.** Histogram of the Hi-C contact possibility of NTBS-NTBS and NTBS-telomeres. Hi-C data show that NTBS are nearer to each other than to telomeres in roughly 86 out of 100 cases. **C.** Telomere-NTBS are more probable than random chance (p -value = $2.2e-16$).

3.2 Telomeric G-overhang as the means of telomere maintenance

The experiments and data described in 3.2 were done in collaboration with Trantirek and Tomaska group. The *in vitro* experiments were performed by our collaborators. The scientific observations have been published in Journal of Biological Chemistry, 2020 with me as a co-first author. I will describe this data below to lay the foundation for my own experimental work.

3.2.1 Oligonucleotides simulating telomeric G-overhang with different length form G4s with diverse topologies

Telomeric G-overhang is a conserved characteristic among many organisms, however the length of the telomeric G-tail varies between them. The G-overhang in human varies between 50-250 nucleotides during the cell cycle (Makarov et al., 1997; WE et al., 1997). *S. cerevisiae* has a short telomeric G-tail (9-15 nucleotides) during most of the cell cycle, which gets extended to 30-100 nucleotides in only a small window in late S phase (M et al., 2004; Wellinger et al., 1993). The length of G-overhang defines its capability to fold into G4 (P et al., 2015; Tran et al., 2011). In humans the G-overhang has the capacity to form a G4 throughout the cell cycle, however in *S. cerevisiae* the G-overhang should be unable to form G-quadruplexes for most of the cell cycle because the length of ssDNA is too short (P et al., 2015; Tran et al., 2011). It has been reported that the abundant short telomeric motif (5'-GTGTGGGTGTG-3') in *S. cerevisiae* has the potential to form other

alternative structures. These are a combination of parallel/antiparallel fold-back structures referred to as a G-hairpin (Gajarský et al., 2017). To examine the folding topology of telomeric G4 DNA in *S. cerevisiae* and its correlation with nucleotide composition and length of the fragment, we designed 10 DNA oligonucleotides (ONG) corresponding to various length with 21-33 nucleotides derived from native telomeric DNA (Table 4, list of ONG). We used CD spectroscopy and non-denaturing PAGE to analyse the fragments. The constructs were categorized into three different groups according to the CD spectra (Fig. 3.5). Group I: ONG1–6 indicated CD spectra highlighted by two major bands, a negative peak at ~240 nm, and a positive peak at ~260 nm; which characteristic of a parallel G4 (Fig. 3.5). Group II: ONG9 and ONG10 indicated CD spectra with a negative band at ~265 nm and a positive band at ~290 nm; this is the sign of anti-parallel G4 (Fig. 3.5). Group III: ONG7 and ONG8 displayed CD spectra with two major positive bands at ~260 nm and ~290 nm, showing these ONGs as a mixture of parallel and anti-parallel G4 structures (Fig. 3.5). Note, although the CD spectra of ONG1-6 and ONG9-10 were showing parallel and anti-parallel G4 structures respectively, further analysis of spectra indicated that these constructs are similar to ONG7 and ONG8. They can form at least two different G4 conformations that consist a mixture of dominant and minor G4 species. The data supports the idea that the extended telomeric G-overhangs in S phase have the potential to fold into different G4s, whereas short telomeric G-overhangs in the rest of the cell cycle are capable of folding to G-hairpin (Gajarský et al., 2017).

3.2.2 Telomeric DNA secondary structures, impede Cdc13 binding

The link between telomerase and the potential length dependant folding of G-overhang is not understood so far. We speculate the ability of Cdc13 to bind to the secondary G-overhang structures may influence its association to the ssDNA and play a role in telomerase recruitment. We monitored the ability of Cdc13 to bind a variety of oligonucleotides with secondary structures *in vitro*. We expressed the Oligonucleotide/Oligosaccharide-Binding (OB)-fold domain of Cdc13, residues 497–694 (Cdc13-DBD) in *E. coli* BL21(DE3) and purified the protein with affinity chromatography. The binding efficiency of the purified protein was confirmed to be similar to previously published works (Fig. S4) (Anderson et al., 2002; Hughes et al., 2000). The pre-formed complex between Cdc13-DBD and unlabelled competitor ONG1 (telomeric parallel G4), ONG9 (anti-parallel G4) or ONG11 (G-hairpin structures), was incubated with a radioactively [³²P]-labelled

probe (ONG11). The ability of the unlabelled oligonucleotides to outcompete the binding of the [32 P]-labelled ONG11 was evaluated by electrophoretic mobility shift assay (EMSA). Our results revealed that the folded oligonucleotides (K⁺) have less potential to displace the labelled probe from Cdc13-DBD in comparison to their unfolded state (Fig. 3.6A). Based on our analyses, Cdc13 has lower tendency for both potential telomeric G-hairpin (ONG11) and G4 (ONG1) secondary structures than the same oligonucleotides in their ssDNA form (Fig. 3.6).

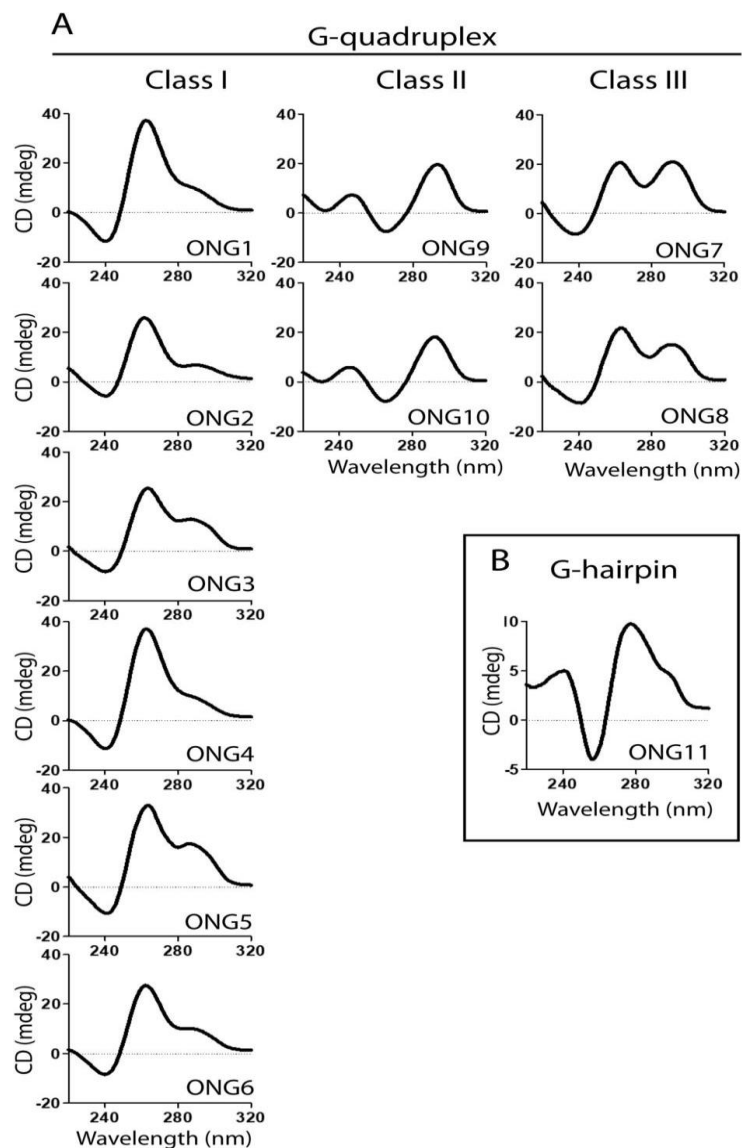


Figure 3.5. Oligonucleotides mimicking telomeric G-tails form distinct non-B DNA structures.

CD spectra of constructs mimicking long (A) and short (B) telomeric G-tails (see Table 4). CD spectra were evaluated at RT in K⁺S buffer with 50 μ M DNA concentration. The spectra was evaluated 24 hours post sample annealing.

Furthermore, it has been shown that parallel and antiparallel G4s have different effects on telomeres (Oganesian et al., 2006; Paeschke et al., 2008; Zahler et al., 1991). We assessed the binding of oligonucleotides with different topologies to Cdc13-DBD (Fig. 3.6B). Our results indicate similar competitor pattern for ONG1 (parallel) and ONG9 (antiparallel). It can be inferred that it is the presence of a secondary structure rather than its topology which dictates Cdc13 binding affinity.

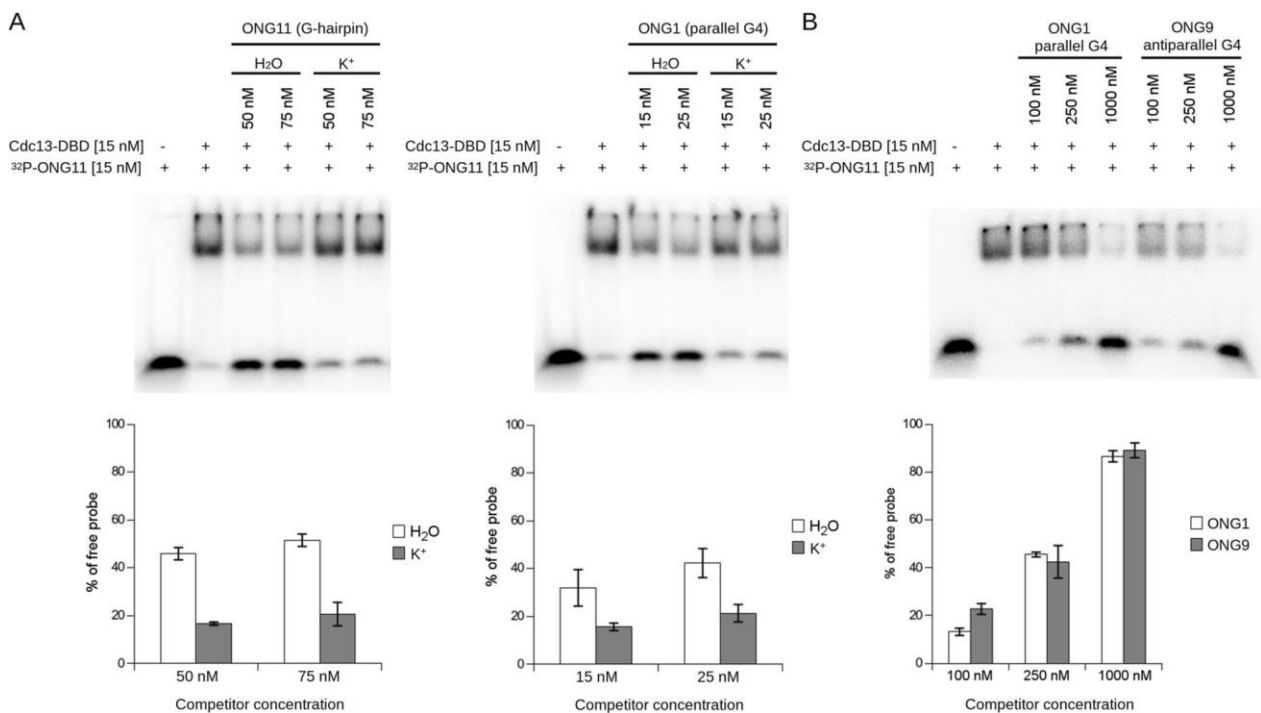


Figure 3.6. Secondary structures forming on telomeric DNA decrease the binding of Cdc13-DBD.

A. EMSA radioactively labelled ONG11 was used as a probe and ONG11 and ONG1 as unlabelled competitors. **B.** EMSA with radioactively labelled ONG11 as a probe and folded ONG1 (parallel G4) and ONG9 (anti-parallel G4) as competitors, indicating that G4 conformation does not impact Cdc13-DBD binding. Quantification of the free probe, mean \pm s.d , n = 2, independent replicas.

3.2.3 Folding kinetics of G-tails impact Cdc13 association to telomeres

Our data indicated that G4 and G-hairpin have different folding kinetics (Fig. S6) and their ability to impede Cdc13 binding may refer to their function on telomeres *in vivo*. To evaluate Cdc13 association to secondary telomeric oligonucleotides folding for different time points and compare their kinetics, we performed EMSA. Unfolded, [³²P]-labelled ONG11 and competitors (ONG1 (quickly folded parallel G4) and ONG11 (slowly folded G-

hairpin)) were evaluated either in water for the unfolded state, or in 1x K⁺ buffer for the folded state. This was done at multiple time points after the beginning of folding. First we observed formation kinetics of ONG1 and ONG11 (Fig. S5). Our results indicate that unlike the G-hairpin (ONG11) folding which takes several hours, G4 (ONG1) folding is completed after 20 min in K⁺ buffer (Fig. S5). The G-hairpin (ONG11) has an occurring folding and loses its engagement ability with increasing time, however ONG1 only requires 20 minutes after annealing to act poorly as a competitor (Fig. 3.7).

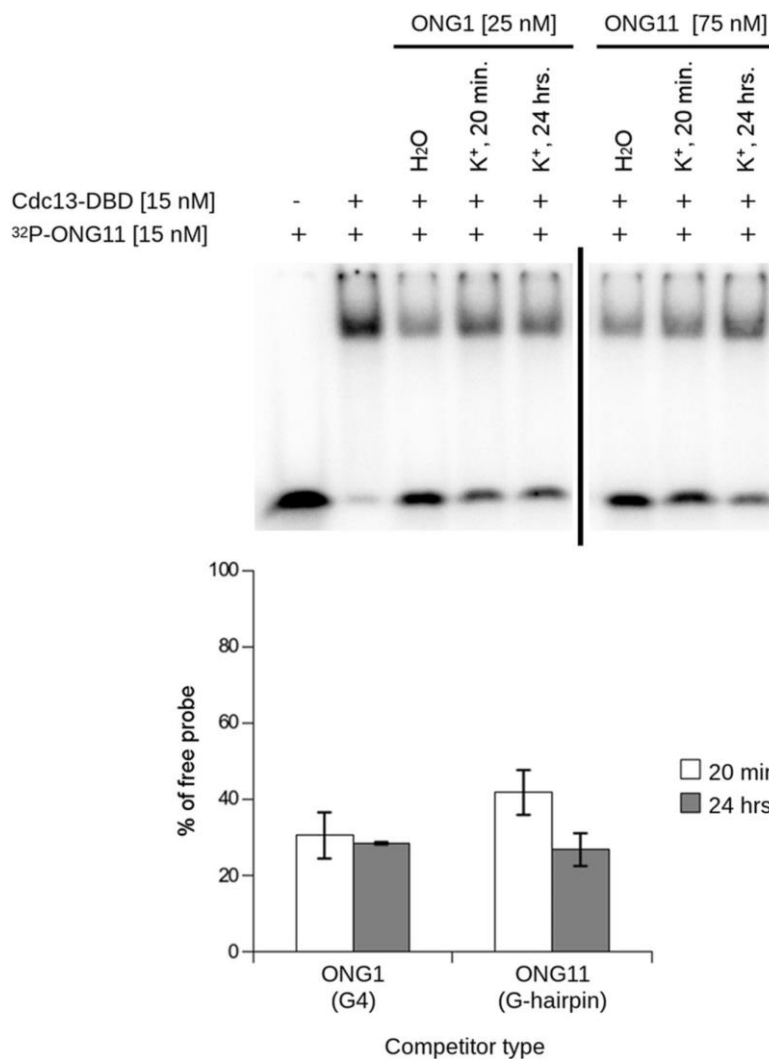


Figure 3.7. Diverse formation kinetics of G-hairpin and G4 affect their Cdc13-DBD binding ability.

Top, EMSA with [³²P]-labelled ONG11. ONG1 and ONG11 were unlabeled competitors allowed to fold in 1x K⁺ buffer for the indicated times. ONG11 (G-hairpin) shows decreased binding of Cdc13-DBD between 20 min and 24 h, ONG1 (parallel G4) does not show time-dependent change. Bottom, quantification of the free probe, mean ± S.D., n = 2, independent replicas.

To exclude the possibility of Cdc13 engagement in with the folding of non-B DNA structures in EMSA, we performed NMR with ONG1 and ONG11 in a time-resolved manner, in the presence of equimolar amounts of Cdc13. 100 μ M of thermally denatured ONG solutions were mixed into a 100 μ M solution of Cdc13-DBD. The NMR spectra of the resulting combinations were collected after 30, 90, and 150 min (Fig. 3.8A). Altogether, the changes observed in the time-dependant NMR of ONG1 and ONG11 in the presence of Cdc13-DBD were similar to those observed in its absence (Fig. 3.6 B). The data suggests that Cdc13-DBD does not influence ONG1/ONG11 non-B DNA structure folding. Importantly, the NMR experiment based on the ability of Cdc13-DBD to bind to G4 or G-hairpin, revealed that there was no difference in quadruplex/G-hairpin correlation time (rotational diffusion coefficient) upon complex formation. This indicates that Cdc13 is not capable of forming a stable complex with G4 or G-hairpin structure (Fig. 3.8C).

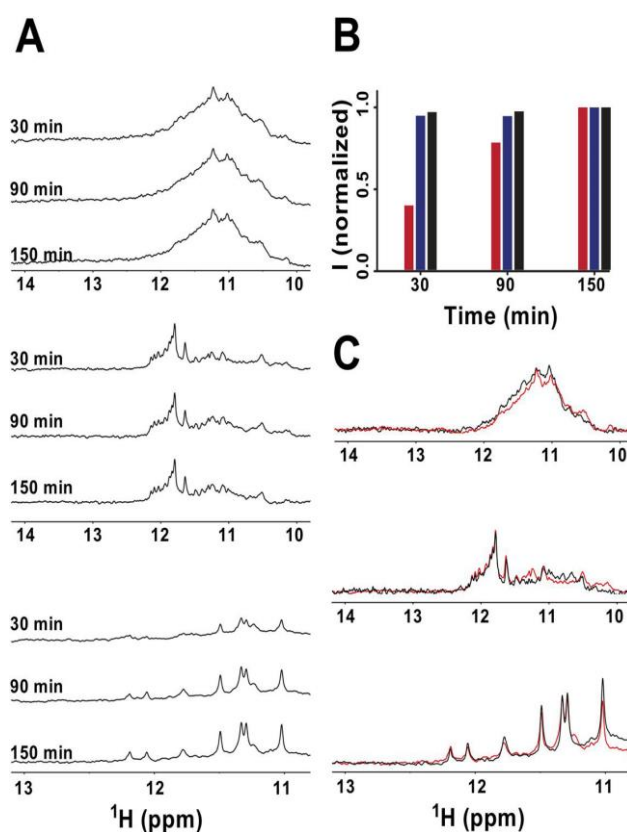


Figure 3.8. Cdc13-DBD does not impede with G-hairpin or G4 folding kinetics and does not form a stable complex with them either.

A. Imino regions of the 1D ^1H NMR spectra of an equimolar mixture of ONG1 (top), ONG9 (middle), ONG11 (bottom) and Cdc13-DBD were done in the indicated times. **B.** Timing of the formation process for ONG1 (black box), ONG9 (blue box) and ONG11 (red box) in the presence of equimolar amounts of Cdc13-DBD as estimated from normalized time-dependent changes in the

intensity of imino signals (I) from NMR spectra presented in **A**. The imino signal intensities at $t = 30$ and $t = 90$ min were normalized to those collected at 150 min. The NMR spectra were done with 1-1 echo pulse sequence with an excitation maximum set to 12 ppm. **C**. Overlay of the imino regions of the 1D ^1H NMR spectra of ONG1 (top), ONG9 (middle), and ONG11 (bottom) measured in K+TD buffer in the absence (black) and in the presence of equimolar amounts of Cdc13-DBD (red).

3.2.4 G4 occupancy differs through the cell cycle at the telomeric region and is in accordance with the length of the G-overhang

So far, direct evidence that telomeres in yeast fold into G4 structures is missing *in vivo*. To monitor G4 enrichment in *S. cerevisiae* telomeres, we adapted the ChIP-seq method using the G4 specific antibody, BG4 to ChIP-qPCR. BG4 has been previously shown to bind with high selectivity to G4 structures *in vitro* and *in vivo* (Biffi et al., 2013; Hänsel-Hertsch et al., 2018). We expressed and purified the recombinant BG4 as previously described and validated its binding specificity with ELISA. G4 abundance at telomeres was quantified with qPCR using primers directed against known telomeric regions on chromosome VI-R and VII-L (Sabourin et al., 2007). Our data show that two telomeric regions VI-R and VII-L were capable of forming G4s *in vivo* (Fig. 3.9A). As an additional control, we treated the cells with 10 μM of G4 binding ligand Phen-DC₃ (Piazza et al., 2010). Our results implicate slight increase in G4 abundance after Phen-DC₃ (~1.5 fold) in comparison to the non-treated wild type cells (Fig. 3.9A) To observe if G4 formation is in accordance with the changes of the G-overhang during the cell cycle, we performed BG4-ChIP in synchronous cells. The cells were arrested in G1 phase with alpha factor and released synchronously into cell cycle (Graf et al., 2017; Paeschke et al., 2011). The synchrony of the cells was measured by FACS (Fig. 3.9B). After synchronization we monitored G4 levels by performing BG4 ChIP-qPCR. The minimum telomeric G4 enrichment was shown in the early S phase, with a slight increase in the mid S phase and the highest level (2–3-fold) of accumulation in the late S phase (Fig. 3.9C). As mentioned before, the temperature sensitive *cdc13-1* mutant loses the capping ability and has longer G-rich ssDNA (Hayashi and Murakami, 2002; Smith et al., 2011). We speculate that long G-overhangs might form G4s at elevated temperatures as means of protection. We performed BG4-ChIP in *cdc13-1* strain at permissive (23°C) and non-permissive temperatures (37°C) and quantified the telomeric G4 levels. We evaluate increased G4 enrichment at non-permissive temperature in comparison to permissive temperature (Fig. 3.9D). Our results correlate with the *in vitro* observations that G4 structures preferentially

form during the time when long telomeric overhangs are present at the chromosome ends (M et al., 2004; Wellinger et al., 1993).

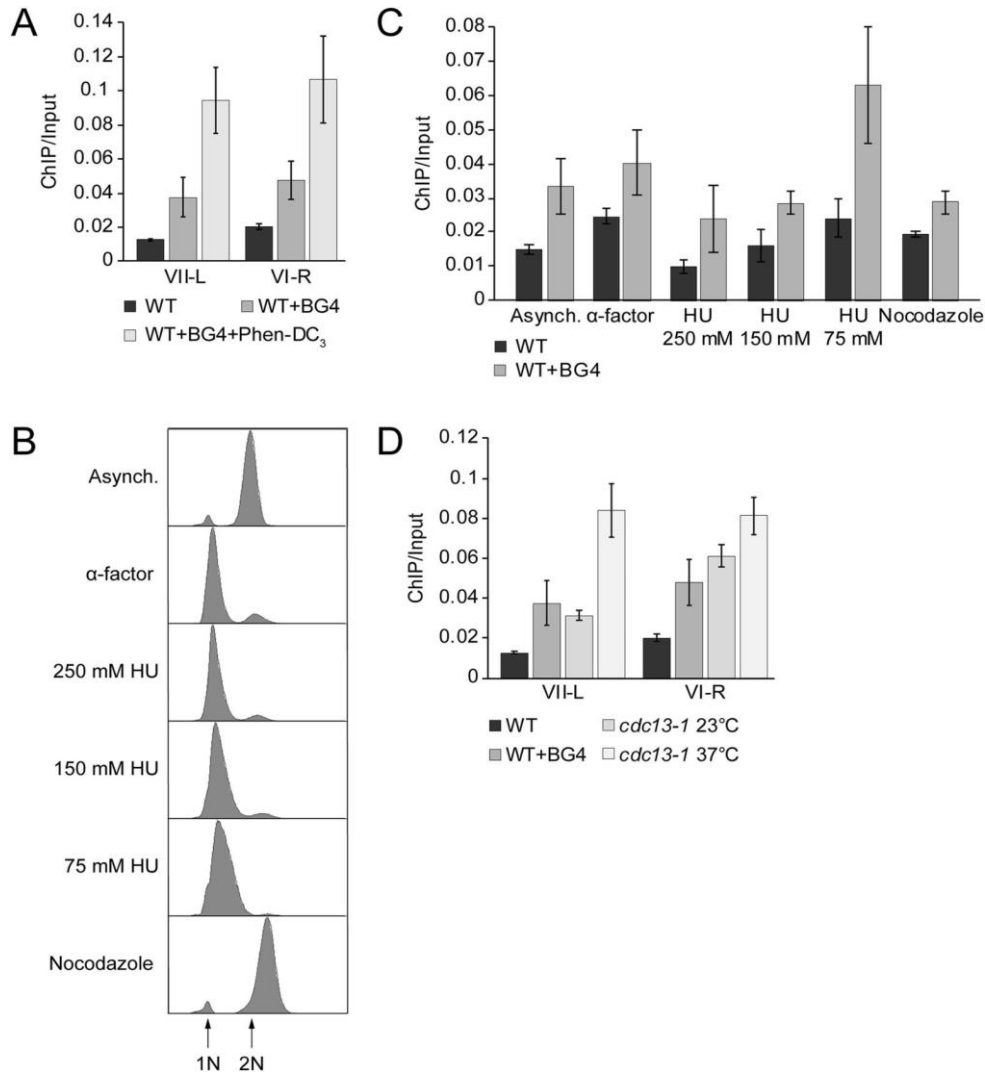


Figure 3.9. G4 enrichment in *S. cerevisiae* telomeres

A. BG4 ChIP-qPCR in wild type strain at two different telomeric (VI-R, VII-L) regions. ChIP-qPCR was performed in the absence of BG4 antibody and 10 μ M Phen-DC3 to determine the specific binding of BG4. Data was normalized to input (ChIP/Input). **B.** FACS analysis of yeast DNA content to confirm cell synchrony. **C.** BG4 ChIP-qPCR of G4s in during cell cycle at telomere VII-L. BG4 ChIP signals were normalized to input. Significance was calculated based on Student's t-test comparing 75 mM HU to the other cell cycle phases. G4 level at 75 mM HU in comparison to other cell cycle phases was significantly higher according to the t-test $p < 0.02$. Only in G1 arrest (α -factor) a significance of $p = 0.1$ was calculated. **D.** BG4 ChIP-qPCR in *cdc13-1* mutant at non-permissive temperature (37°C). As control, the BG4 ChIP was done in *cdc13-1* mutant at permissive temperature (23°C) and WT strain. The means of at least three biological replicates are plotted. Error bars represent \pm SEM.

3.2.5 Characterization of G4s at short and long telomeres in *S. cerevisiae*

To better understand the function of G4s at yeast telomeres and their correlation to telomere length, we monitored G4s at short and long telomeres. If G4s contribute in telomerase recruitment to short telomeres or protecting them from degradation, we speculated to see more G4 abundance. Deletion of certain telomeric proteins like Ku70 or the MRX components like Rad50 and Mre11 is associated with showing a short telomere phenotype (Boulton and Jackson, 1998). We analysed short telomeres with either long or short telomeric overhangs with BG4 ChIP-qPCR. First, we analysed G4 formation at short telomeres which have elongated (*yku70Δ*) or shortened (*rad50Δ*, *mre11Δ*) overhangs, respectively. We observe significantly less G4 formation (p -value < 0.01) at VII-L telomeric short in *rad50Δ* and *mre11Δ* strains (Fig. 3.10 A,B). On the contrary, *ku70Δ* strain the cells have short telomeres and long overhangs the G4 levels did not change (Fig. 3.10C)

To fully understand the question whether G4 structures preferentially form at short or long telomeres or are independent of the telomere length, we performed BG4 ChIP followed by qPCR, in the strains where the overall telomere length is elongated like *pif1-m2* or *rif2Δ* strains (Schulz and Zakian, 1994; Wotton and Shore, 1997). In the *pif1-m2* mutant a point mutation in the second start site prevents the expression of nuclear Pif1 (Schulz and Zakian, 1994). The telomeres are elongated because telomerase binding is no longer negatively regulated by Pif1 helicase (Zhou et al., 2000). Our data reveal a significant increase (~10 fold, p -value 0.014) of telomeric G4 levels in *pif1-m2* strains in comparison to wild type strain (Fig. 3.10D). In *rif2Δ* strain, telomeres are elongated because the check point kinase tel1 loses its preference for short telomeres (McGee et al., 2010). Our G4 ChIP results in *rif2Δ* strain show similar or slightly more (not significant) G4 levels than wild type (Fig. 3.10E). Another helicase, that is known to bind to telomeres and regulates telomerase is the RecQ helicase Sgs1 (Johnson et al., 2001). In the absence of Sgs1, telomeres have no severe telomere length effect. (Johnson et al., 2001). BG4 ChIP-qPCR in *sgs1Δ* strain show minor changes in G4 level (-1.5 fold decrease) in comparison to the wild type strain (Fig. 3.10F). Overall, G4 abundance does not correlate with telomere length but rather seems to be associated with the presence of telomeric proteins.

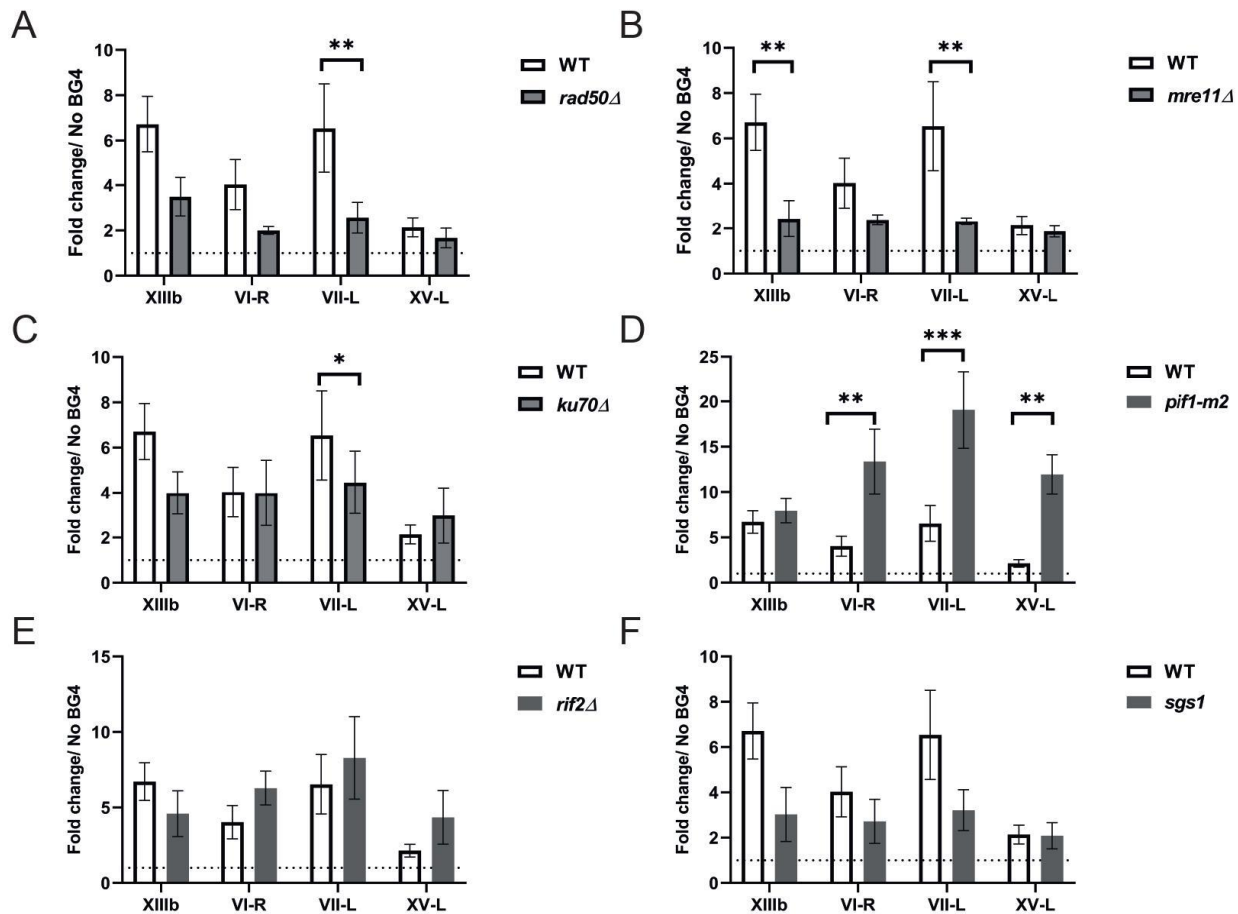


Figure 3.10. G4 abundance at short and long telomere

A-B. Representative of BG4 ChIP-qPCR in the absence of the MRX complex components. *rad50Δ* and *mre11Δ* short telomere strains at different telomeric (VI-R, VII-L, XV-L) and non-telomeric (XIIIb) regions. **C.** BG4 ChIP-qPCR in *ku70Δ* short telomere strain. **D.** G4 ChIP-qPCR in *pif1-m2* strain with long telomere phenotype. **E.** BG4 ChIP-qPCR in *rif2Δ* strain with long telomeres. **F.** BG4 ChIP-qPCR in *sgs1Δ* strain. Data are presented as mean \pm SEM of $n = 3$ biological replicates. Statistical significance was calculated as fold change in comparison to no BG4 control. Significance of the represented data was determined using Student's t-test of comparing similar regions for G4 abundance between WT and mutants. * p-value < 0.05 ** p-value < 0.01 and *** p-value < 0.001

3.2.6 G4 motif adjacent to a DSB does not induce telomere addition

We asked whether telomeric G4 structures support the difference between a DSB and a telomere. For this we adapted an established assay in which we use a galactose-inducible HO endonuclease and a HO recognition site adjacent to either a telomeric region (TG80), a random control (N80) 14, 52 or a G4 region (G480). Upon galactose induction, HO endonuclease cleaves the HO site and creates a DSB (Bianchi et al., 2004; Strecker et al., 2017) (Fig. 3.11 A). The DSB will be repaired by either telomere addition or break

repair. This can be monitored by plating, due to specific selection marker (LYS2) near the cut site,. If a telomeric sequence is next to the break, telomere addition takes places and the cells lose the ability to grow on LYS2 deficient plates (Bianchi et al., 2004; Strecker et al., 2017). No telomere addition has been observed if a control sequence (N80) was inserted next to the DSB, the lesion is repaired by HR and LYS2 marker is retained. Integrated G4 sites adjacent to the HO cut site, have been selected from two strong G4 motifs, in Chromosome IV (location 1525213- 1525292) and Chromosome IX (location 356348-356427), reported to fold into G4 structures *in vitro* (Capra et al., 2010). If the G4 itself would recruit telomerase, we expected to observe telomere addition after the HO cut. Based on our observation, we did not see telomere addition in the two strains with G4 motifs (Fig. 3.11B). The repair was similar to N80 strain(Fig. 3.11B).

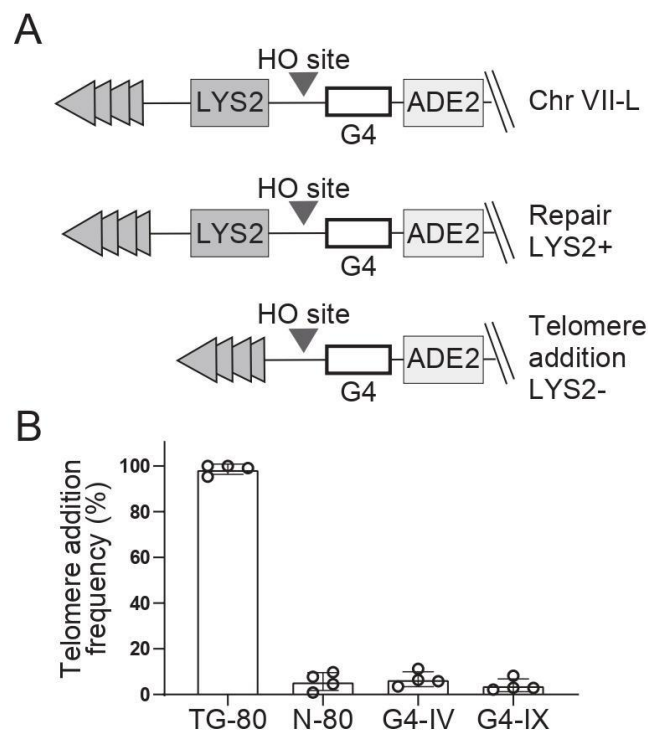


Figure 3.11. Telomere addition adjacent to G4-IV and G4-IX motifs.

A. Schematic representation of telomere addition next to the HO endonuclease recognition site. In these strains, upon galactose induction HO endonuclease induces a DSB which is then decided to be repaired as DSB or telomere, depending on the adjacent sequence (Strecker et al., 2017)

B. Telomere addition frequency was determined in normal growth condition and calculated as previously. The calculation was done using a genetic assay based on loss of distal LYS2 gene. TG80 and N80 were used as positive and negative control. TG80 contains 80 bp TG₁₋₃; N80 contains 80 bp lambda DNA. The bars are plotted as mean \pm SEM of n = 3 biological replicates.

3.3 Characterization of Zuo1 as a telomeric G4 binding protein

3.3.1 Zuo1 binds to *S. cerevisiae* telomeres without affecting telomere length

Our group has recently identified Zuo1 as a novel G4 binding protein, validated by *in vitro* and *in vivo* experiments (Magis et al., 2020). We showed that Zuo1 binding supports G4s, particularly in the context of DNA repair and in response to UV damage. Zuo1 bound G4s supported the recruitment of the NER machinery (Magis et al., 2020). *S. cerevisiae* shows a slower growth phenotype and is more sensitive to UV damage in the absence of Zuo1 and we have found telomeric sequences have a greater potential to fold into G4s and many repair proteins are involved in telomere maintenance as well. Therefore, we asked the question, whether Zuo1 is associated to telomeres. The first step to observe the impact of Zuo1 on telomeres was to check telomere length in the absence of Zuo1 with southern blot. No length effect on *S. cerevisiae* telomeres has been evaluated in the absence of Zuo1 (Fig. 3.12A). Furthermore we monitored telomeric length in the double deletion of Zuo1 and important telomeric proteins including *zuo1Δpif1-m2*, *zuo1Δku70Δ* and *zuo1Δsgs1Δ*. Our results did not show any changes in telomere length in double deletions (Fig.3.12A). The length of telomeric G-tail changes through cell cycle and is longest in S phase, when it is extended by telomerase (Jurikova et al., 2020). During this time is it most kinetically favourable to form G4s We performed ChIP-qPCR with endogenously tagged Zuo1.Myc13 in synchronous cells. The synchrony of the cells was confirmed by FACS. Zuo1 binding was monitored by ChIP-qPCR using primers directed against known regions VI-R, VII-L. Our data indicates Zuo1 binding to telomeres changes during cell cycle and decreases in S phase when telomere extension is happening and telomerase is active (Fig. 3.12B). Furthermore, we performed BG4 ChIP-qPCR in the absence of Zuo1 and checked telomeric VI-R, VII-L, XV-L (McGee et al., 2010) regions and a G4 region located on Chromosome XIII (location 250435-250911 (YML009W-B)) which has been characterized to fold into G4 in the endogenous region (Paeschke et al., 2011). Our results indicate a significant decrease in G4 abundance in telomeric VI-R (p-value < 0.05) and VII-L (p-value < 0.01) in *zuo1Δ* strain in comparison to wild type (Fig. 3.12C). BG4 ChIP-qPCR in the *zuo1Δ* strain in synchronous cells revealed significantly less (p-value < 0.05) G4 abundance in mid and late S phase in the VI-R telomeres of *zuo1Δ* strain in comparison to the wild type (Fig. 3.12D).

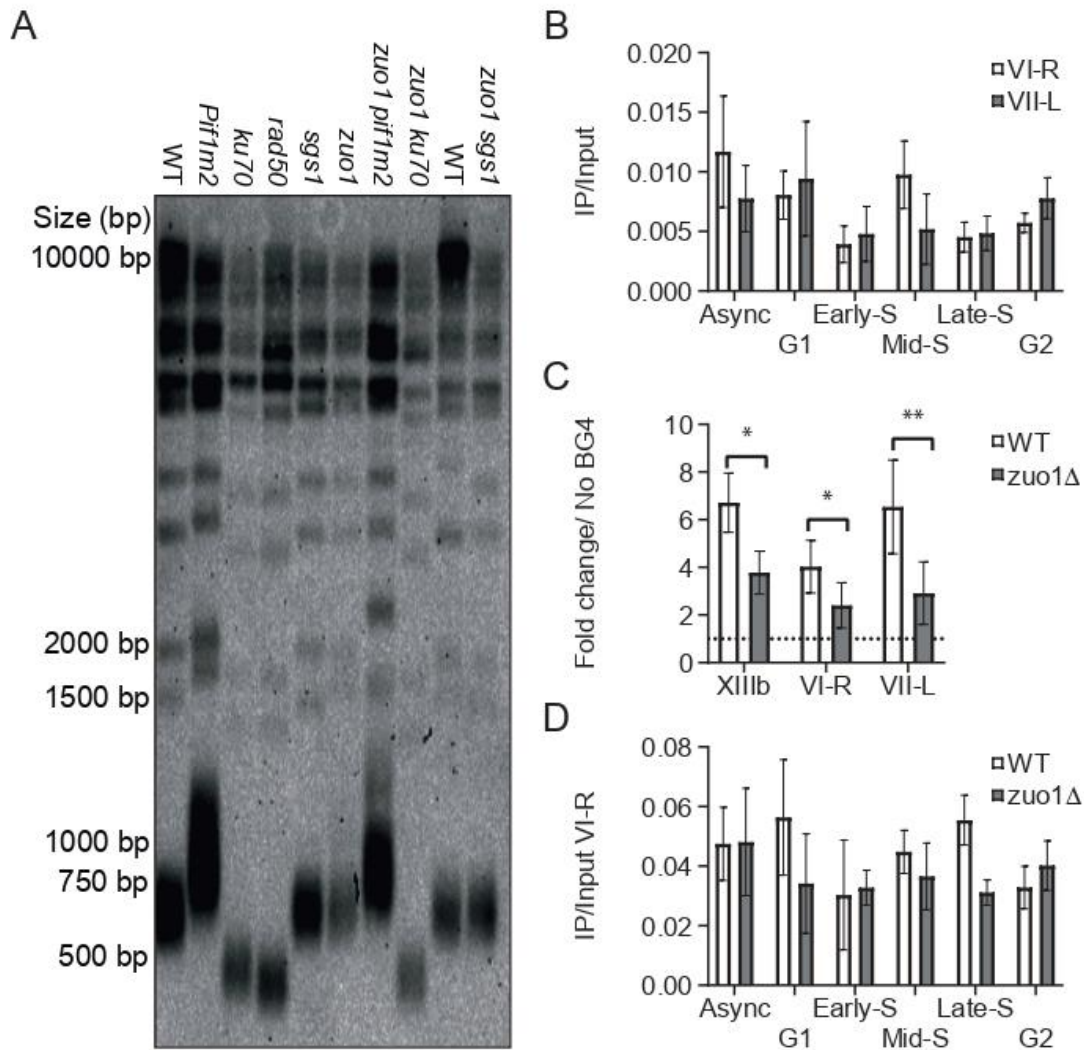


Figure 3.12. Zuo1 binds to telomeres but has no length effect

A. Southern blot for telomere length TG DIG-labelled probe to label telomeric sequences. **B.** ChIP-qPCR of synchronous Zuo1.Myc in VI-R and VII-L telomeric regions. **C.** BG4 ChIP-qPCR in *zuo1Δ* strain in comparison to WT in telomeric regions (VI-R, VII-L) as well as the endogenous G4 motif (XIIIb). **D.** BG4 ChIP-qPCR in cell cycle synchronized *zuo1Δ* strain in comparison to WT in VI-R and VII-L telomeric regions. Data are presented as mean \pm SEM of $n = 3$ biological replicates. Statistical significance was compared to WT levels at different regions or time point of the cell cycle. Significance of the represented data was determined using Student's t-test. * p-value < 0.05 ** p-value < 0.01 and *** p-value < 0.001

3.3.2 Zuo1 binds more to short telomeres

To address if Zuo1 binding to telomeres depends on telomere length, we evaluated Zuo1 binding in the short telomeric background. Our ChIP-qPCR analyses in the endogenously tagged Zuo1.Myc *rad50Δ* strain indicates significantly increased Zuo1 binding to VI-R (p-value < 0.05), VII-L (p-value < 0.001) and XV-L (p-value < 0.05) telomeric regions (Fig.

3.13A) We observed the same pattern for Zuo1.Myc *mre11Δ* (Fig. 3.13B). To further investigate Zuo1 binding in short telomeres with longer G-overhangs, we performed ChIP-qPCR in the Zuo1.Myc *ku70Δ* strain. Our data indicates significantly increased Zuo1 binding to VI-R (p-value < 0.001), VII-L (p-value < 0.001) and XV-L (p-value < 0.05) telomeric regions (Fig. 3.13C) We coupled an inducible short telomere system (Phillips et al., 2015; Strecker et al., 2017) with ChIP-qPCR analyses in order to characterize G4 formation at critically short telomeres. In this system the cells have a modified chromosome VII-L in which a cassette containing telomeric repeats flanked by recognition sites (FRT – for the Flp specific recombinase) were positioned next to the telomere (Sabourin et al., 2007) (Fig. S7). The strain had an integrated copy of galactose inducible FLP1 recombinase which causes recombination between two FRT sites (Fig. S7). The generated telomere on chromosome VII-L will be around 100bp (Sabourin et al., 2007). All other telomeres will have wild type length. The VI-R telomere was used as internal control. To better understand Zuo1 binding to short telomeres we included the VIII inducible short telomere strain. We performed ChIP-qPCR in Zuo1.Myc tagged short inducible telomere strain. Our qPCR analyses revealed increased Zuo1 binding (p-value < 0,001) to short VII-L telomere in comparison to wild type VI-R (Fig. 3.13D).

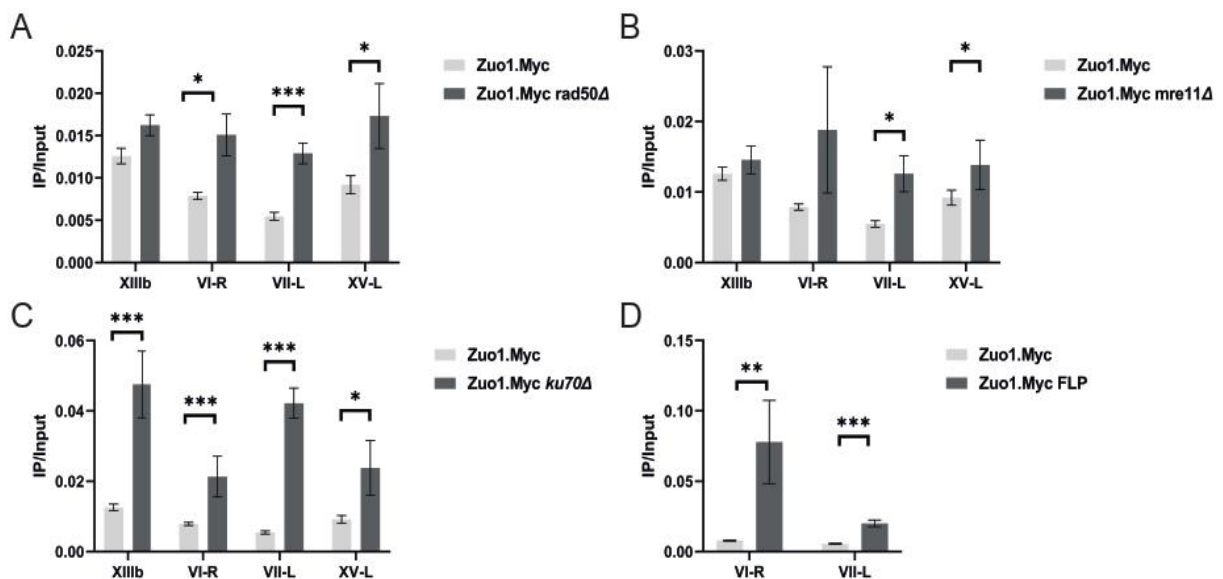


Figure 3.13. Zuo1 binding to short telomere

A-B. ChIP-qPCR in the absence of the MRX complex. Zuo1.Myc *rad50Δ* and Zuo1.Myc *mre11Δ* strain at different telomeric (VI-R, VII-L) and non-telomeric (XIIIb) region. **C.** ChIP-qPCR in Zuo1.Myc *ku70Δ* strain. **D.** ChIP-qPCR in Zuo1.Myc tagged Flp short inducible telomere strain. Data are presented as mean \pm Standard error mean (SEM) of n = 3 biological replicates. Statistical significance was compared to Zuo1.Myc levels. Significance of the represented data was determined using Student's t-test. * p-value < 0.05 ** p-value < 0.01 and *** p-value < 0.001.

3.3.3 Zuo1 binds to a population of long telomeres

To investigate correlation of Zuo1 with telomere length we asked if Zuo1 binding to telomeres changes with their elongation. Our ChIP and qPCR analyses in Zuo1.Myc *pif1-m2* showed increased binding to VI-R (p-value < 0.001), VII-L (p-value < 0.001) and XV-L (p-value < 0.05) telomeric regions.(Fig. 3.14A). In order to further validate Zuo1 interaction with Pif1 helicase, we did ChIP-qPCR in the Pif1.Myc *zuo1Δ* strain. The binding of Pif1 to VI-R and VII-L telomeres was decreased (p-value < 0.001) in the absence of Zuo1 (Fig 3.14B). However, in Zuo1.Myc *rif2Δ* strain which has long telomeres, Zuo1 binding was decreased (Fig. 3.14C). In order to understand if the result is specific to the absence of G4 unwinding helicases, we did Zuo1.Myc ChIP-qPCR in the absence of RecQ helicase Sgs1. Notably, there was more Zuo1 binding to telomeres VII-L and XV-L (p-value < 0.05) in the Zuo1.Myc *sgs1Δ* (Fig. 3.14E). Another interesting aspect of telomere regulation which has been reported in the past years is the negative regulation of telomere length by SUMOylation (LE et al., 2011). SUMO has been reported to help with Cdc13-Stn1 interaction and restrain telomerase activity (LE et al., 2011). To evaluate potential Zuo1 involvement in interacting with the Smt3 SUMO protein and indirect effect on telomerase activity we performed ChIP-qPCR in the Smt3.Myc strain in the absence of Zuo1. Our results indicate that Smt3 binding to telomeric VI-R (p-value < 0.001), VII-L (p-value < 0.05) and XV-L (p-value < 0.001) regions decrease as well as the XIIIb G4 motif (Fig. 3.14D).

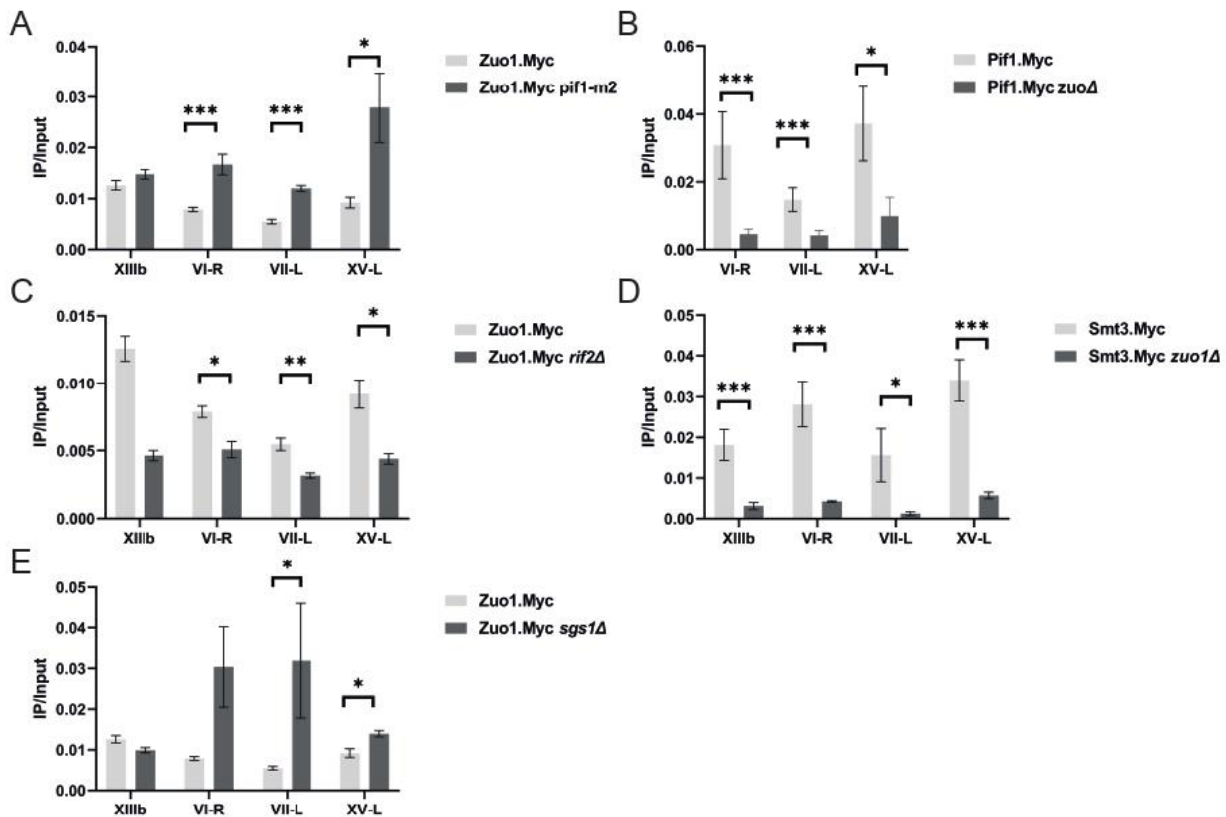


Figure 3.14. Zuo1 binding to long telomeres.

A. ChIP-qPCR in *Zuo1.Myc pif1-m2* (long telomere phenotype) in telomeric (VI-R, VII-L, XV-L) as well as non-telomeric (XIIIb) region. **B.** ChIP-qPCR of *Pif1.Myc zuo1Δ* strain, in comparison to *Pif1.Myc*. **C.** ChIP-qPCR of *Zuo1.Myc rif2Δ* strain binding to telomeric regions VI-R, VII-L and XV-L. **D.** ChIP-qPCR of *Smt3.Myc zuo1Δ* strain. **E.** ChIP-qPCR of *Zuo1.Myc sgs1Δ* strain. Data are presented as mean \pm Standard error mean (SEM) of $n = 3$ biological replicates. Statistical strain significance was compared to WT binding levels. Significance of the represented data was determined using Student's t-test. * p-value < 0.05 ** p-value < 0.01 and *** p-value < 0.001.

3.3.4 Zuo1 binds more to telomeres when the natural capping is compromised

To further investigate the possible function of Zuo1 on yeast telomeres, we considered Zuo1 as a G4 interactor and its potential function to be involved in telomere maintenance. To identify Zuo1 interacting proteins tagged Zuo1 endogenously with Myc13 and pulled down via immunoprecipitation, followed by Mass spectrometry. The Mass spectrometry results showed Stm1 protein as a Zuo1 interacting partner with a high affinity (Table 6). As mentioned in chapter 3.2, telomeric G-overhangs and their potential to form G4s can be considered as means of telomere maintenance, especially when the natural capping is compromised (Jurikova et al., 2020). It has been shown that in the *cdc13-1* temperature sensitive strain, which loses the ability to stop the end resection of the 5' end and has extended G-overhangs, G4s can play a positive role in the maintenance of telomere length

(Jurikova et al., 2020). Furthermore overexpression of the Stm1 G4 binding protein in the *cdc13-1* can rescue growth of these cells at semi-permissive temperature (SPT, 30 °C)(Hayashi and Murakami, 2002). Stm1 is a G4 binding protein which associates with telomeres and subtelomeric regions. Rescue of *cdc13-1* temperature sensitivity with STM1 overexpression have been proposed to be associated to G4 capping for telomere protection. Because we pulled down Stm1 in the Zuo1.Myc mass spectrometry, we asked the question if Zuo1 as a G-quadruplex binding proteins (G4BP) is also involved in telomere capping when the natural capping is compromised. To address this, we first validated our mass spectrometry data by performing Co-Immunoprecipitation in Zuo1.Myc Stm1.6xHA tagged strain and confirmed with western blot. We could confirm Zuo1 and Stm1 interaction in comparison to the Input sample and the no tag controls (Fig. 3.15A). Next, We asked the question whether Zuo1 overexpression or its absence can affect the *cdc13-1* temperature sensitivity like STM1. To address this, we created the pSTM1 *zuo1Δ* as well as Zuo1 overexpression (pZuo1OE) strain in the *cdc13-1* mutant and monitored their growth with spot assay at permissive temperature (PT, 22 °C) or at semi-permissive temperature (SPT, 30 °C) (see table 1 for strains list). We were able to reproduce the rescue of the *cdc13-1* strain with Stm1 overexpression (pSTM1 overexpression) at SPT as it has been shown previously (Fig. 3.15B). Based on our experiment, we did not see any growth differences in the overexpression or absence of Zuo1. However the rescue of the *cdc13-1* mutant growth defect with Stm1 overexpression was also observed in absence of *zuo1Δ* strains (Fig. 3.15B). To check Zuo1 binding in the temperature sensitive strain, we performed CHIP-qPCR in the *cdc13-1* strain in which Zuo1 was endogenously tagged with Myc at PT (23°C) and SPT (30°C). Our analyses indicated increased Zuo1 binding at SPT in comparison to wild type (Fig. 3.15C). We performed CHIP-qPCR to calculate the impact of Zuo1 presence in Stm1 binding to telomeres quantitatively. In the *zuo1Δ* mutants, Stm1 binding to telomeres was significantly decreased in VI-R (p-value < 0.05), VII-L (p-value < 0.001) and XV-L (p-value < 0.001) regions as well as the XIIIb G4 motif (p-value < 0.05) (Fig. 3.15D). This finding further confirmed the interplay with G4s and telomeres.

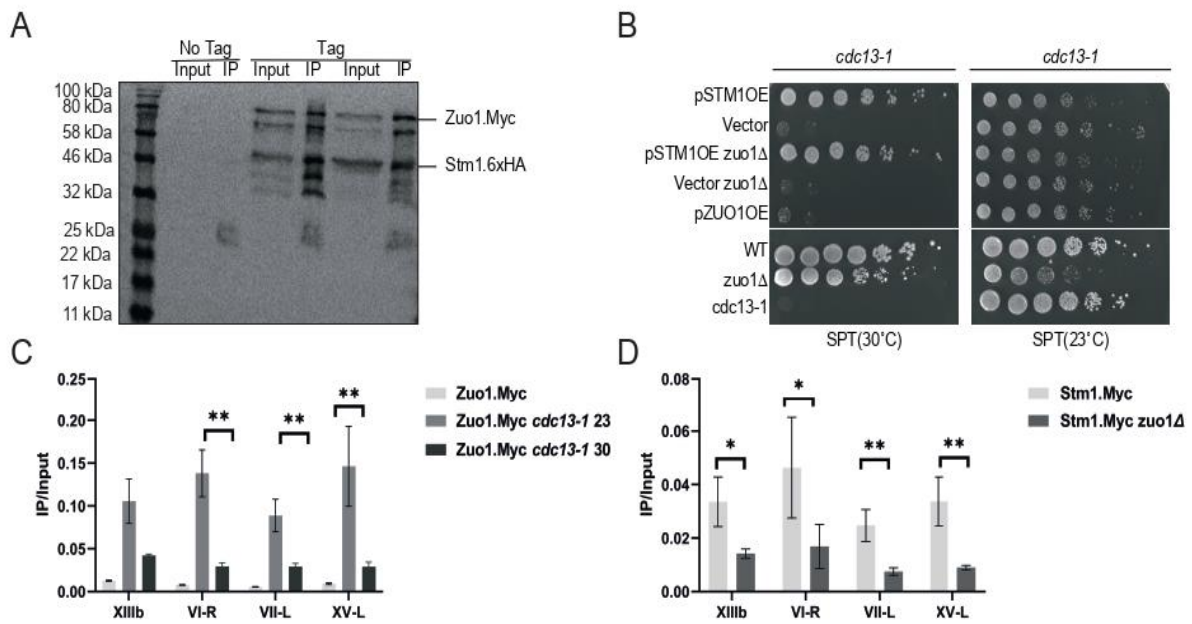


Figure 3.15. Interaction of Zuo1 with STM1

A. CoIP Zuo1 and Sm1. **B.** Spot assay *cdc13-1* mutants carrying pSTM1, pZuo1OE or vector alone at two permissive temperature (PT, 22 °C) or at semi-permissive temperature (SPT, 30 °C) **C.** ChIP-qPCR of Zuo1.Myc *cdc13-1* mutant binding to 3 telomeric regions as well as non-telomeric (XIIIb) at PT and SPT. **D.** ChIP-qPCR of Stm1.Myc *zuo1Δ* strain. Data are presented as mean \pm Standard error mean (SEM) of $n = 3$ biological replicates. Statistical significance was compared to WT binding levels. Significance of the represented data was determined using Student's t-test. * p-value < 0.05 ** p-value < 0.01 and *** p-value < 0.001.

4. Discussion

4.1 Non Telomeric Binding Sites (NTBS) as parking spots for telomerase catalytic subunit Est2

This chapter of the thesis has been accepted for publication, with me as one of the lead-(first) authors (Pandey et al (accepted) at BMC). The obtained data are discussed in detail in the manuscript, which you can find in the appendix.

Multiple studies have reported how telomerase is recruited to telomeres and distinguishes DSB from telomeres (Pennaneach et al., 2006; Phillips et al., 2015; Schulz and Zakian, 1994; Wellinger and Zakian, 2012). One finding is that the catalytic subunit of telomerase, Est2, is expressed through the whole cell cycle but assembling to telomeres during late S phase (Chan et al., 2008). The exact localization of Est2 and where it is binding when it is not attached to telomeres was not clear. We monitored genome wide binding of Est2 protein in *S. cerevisiae*. We identified non telomeric binding sites (NTBS) of Est2, addressed how it is recruited to these regions and the possible outcome of this interaction (Fig. 3.1). Our data shows that Est2 binds to TG rich internal regions and these regions mimic the telomeric repeats.(Fig. 3.1). It is not fully understood why specific regions in the genome are more prone to telomerase action and *de novo* telomere addition (Bianchi et al., 2004; Obodo et al., 2016; Putnam et al., 2004). This is important particularly for cancers which have up-regulated telomerase activity or DNA repair or impaired genome stability because of telomere addition to endogenous regions (A and A, 2017; Davoli and Lange, 2012; J et al., 2015; Pennaneach et al., 2006; SE and RA, 2010). In unchallenged conditions, Est2 binding to NTBS is independent of the Est1 and Est3 subunits of telomerase (Fig. 3.2). Our data correlate with two recent studies which identified sites of repair-associated telomere addition (SiRTA) (Obodo et al., 2016) after DNA damage or deep sequencing of yeast cells with an overload of DNA damage (Ouenzar et al., 2017). We did not see an overlap of NTBS to these published telomere addition sites. This could be due to monitoring Est2 binding in normal conditions, whereas these studies were in response to DNA damage. The second reason could be our strong cut off which might lead to underrepresentation of peaks (a peak needs to be present in 3 of 5 experiments). Telomerase recruitment to telomeres involves different protein complexes including Ku complex, CST complex, Pif1 and assembly of the telomerase subunits (Chan et al., 2008;

Conrad et al., 1990; Fisher et al., 2004; Gallardo et al., 2008; Lin and Zakian, 1996; J Lingner et al., 1997; Qi and Zakian, 2000; Taggart et al., 2002; Tuzon et al., 2011; Wotton and Shore, 1997; Zhou et al., 2000). We asked if Est2 binding to NTBS entails the same mechanism as telomerase binding to telomeres. The classical telomerase recruitment factors did not indicate a direct effect in Est2 binding to NTBS(Fig. 3.3). Our data did not indicate replication pausing (Greider, 2016) or heterochromatin formation(Fig. 3.3, Fig. S3) to be involved in the Est2 binding to NTBS.

We further analysed another hypothesis for Est2 binding to NTBS. A three-dimensional model has been proposed, at which telomerase first makes several contacts with internal chromosomal regions before binding to telomeric regions (Schmidt et al., 2016). 3D organization of telomeres and their tethering to the nuclear periphery changes during cell cycle and is deformed in cancer cells (Chuang et al., 2004; Rutledge et al., 2015; Schalbetter et al., 2017). We asked if 3D organization of chromosomes is involved in Est2 binding to NTBS. We compared our chromosome conformation capture results using the Hi-C method with previously published Hi-C analyses from *S. cerevisiae* (Belton and Dekker, 2015). Our Hi-C contact probability showed that NTBS regions are in closer proximity to each other and to telomeres than expected by randomized control regions (Fig. 3.4). This suggests that chromatin organization and telomeres conformation bring Est2 near NTBS. We speculate because of the TG rich nature of these regions, Est2 interacts with them. The possible function of Est2 binding to endogenous regions is not studied yet. Our data provides insights that endogenous regions of the genome could potentially be the contact regions for Est2 during the three-dimensional diffusion model. Whether this binding and the genome organization is altered in the presence and absence of other telomerase regulators and during survivor formation, still needs to be studied in detail.

Our data leads to a model that under normal conditions, Est2 binds to telomeres in S-phase, whereas it binds to NTBS regions during G1 and G2 phases (Fig. 4.1). NTBS regions are closer to each other in a 3D organization and Est2 is “parked” and sequestered at these NTBS in an inactive manner (Fig. 4.1). We speculate that intermolecular G-quadruplexes support this interactions. Since telomeres and NTBS both overlap G4 regions (Capra et al., 2010) (35/978) [$p < 0.0001$] (Fig. S1B), we suggest that they could

be involved in telomere regulation and help to maintain nuclear architecture (L and J, 2009; Paeschke et al., 2005; Traczyk et al., 2020). Intriguingly, Rap1 promotes G4 formation (Traczyk et al., 2020) and overlapping its binding sites with NTBS would be the next step to better understand the biological relevance of these sequences. Our data indicates a novel mechanism about where and how telomerase is interacting within the genome through 3D organization and can recognize between endogenous regions and telomeric ends.

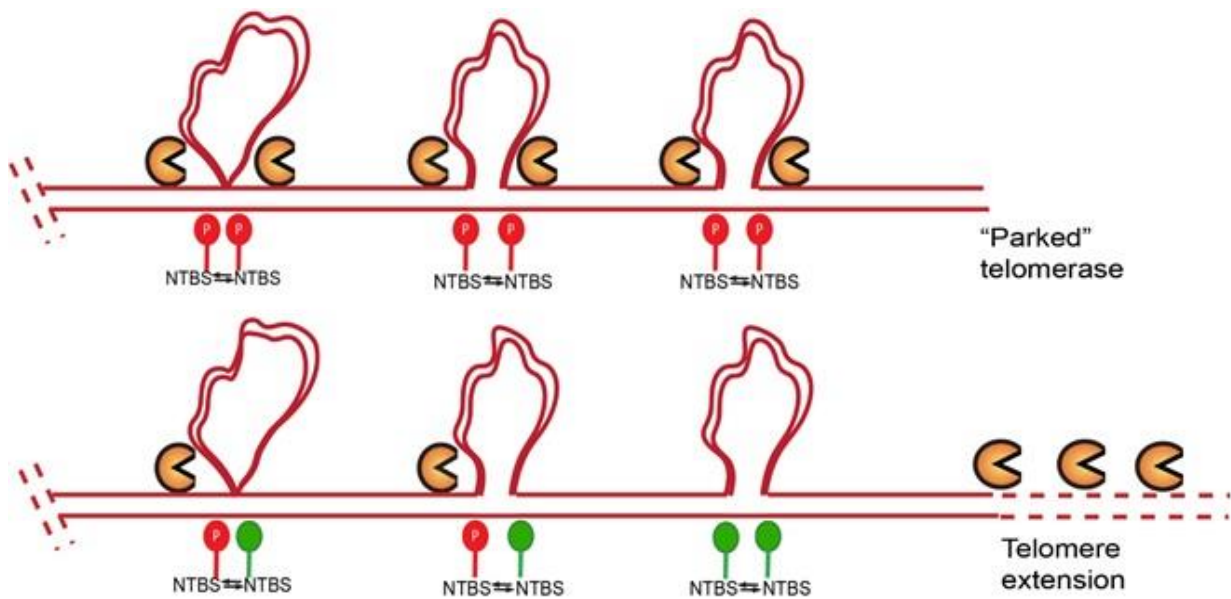


Figure 4.1. Parking model for telomerase.

Est2 enzyme is parked at NTBS regions (denoted by red, occupied parking spots) awaiting its action at telomeres during S-phase for telomere elongation where there is a loss of Est2-NTBS interaction (denoted by green, vacant parking spots).

4.2 Telomeric G-overhang as the means of telomere maintenance

This chapter of the thesis has been published (Jurikova et al 2020, JBC Journal). I am listed as one of the lead (first) authors. The obtained data are discussed in detail in the manuscript which you can find in the appendix.

The CST (Cdc13, Stn1, Ten1) is responsible for capping the ss DNA and protecting the telomeric ends (Gopalakrishnan et al., 2017; LE et al., 2011; Li et al., 2009; Shen et al., 2014; Sun et al., 2009). The Cdc13 protein goes through post translational modifications and associates with the telomerase subunit Est1 for telomerase recruitment (Boule et al., 2005; Rigo et al., 2017). Besides the protein modifications, non-B DNA structures formed

on the G-overhang might also have an effect on telomere which is not clear yet. We show that oligonucleotides mimicking telomeric DNA of the G-overhang which is generated in S phase of cell cycle in *S. cerevisiae* can fold into anti-parallel and parallel intramolecular G4s (Fig. 3.5). Our data shows that the formation of the antiparallel structure is more kinetically favourable (Fig. S6). Our observations reveal that both structures have the capacity to displace Cdc13 from the ss DNA. Despite the possibility of forming both parallel and anti-parallel G4 in a specific sequence (Fig. 3.6). Comparing the ability of parallel and anti-parallel G4s to displace Cdc13 from ssDNA points that their role is neither correlating with their folding topology nor is related to the kinetically preferred conformation.

In contrast to previously published data that Cdc13 and Cdc13-DBD show similar binding affinity for tetra-molecular parallel G4 as well as the unfolded ssDNA (Lin et al., 2001), our data implicates that binding of Cdc13 to different topologies of telomeric G4s is weaker than its binding to ssDNA (Fig. 3.6, Fig 3.7). Unlike the previously published data (Lin et al., 2001) our results show that Cdc13-DBD does not involve in denaturation of the intramolecular G4 structure (Fig. 3.8). We speculate the differences are due to the distinct nature of the two studies including different topologies and cation concentrations, as different unfolding rate has been reported for human POT1-TPP1 telomeric complex (MR et al., 2016). Notably our sequences are generated from most represented repeats in *S. cerevisiae* telomeres (Gajarský et al., 2017) and might reflect the situation more closely *in vivo*. Our results indicate that Cdc13 has stronger binding affinity for ssDNA in comparison to G4 which impairs its binding (Fig 3.6).

To evaluate the physiological relevance of non-B DNA structures we monitored the binding capacity of Cdc13-DBD to short (G-hairpin) and long (G4) telomeric overhangs. Both structures showed decreased ability to form a stable complex with Cdc13-DBD in comparison to unfolded ssDNA (Fig. 3.7, Fig 3.8). The doubling time of *S. cerevisiae* is almost 90min and the S phase is 10 minutes. The secondary DNA structures should be folded in this time window. There is less than 10 min for a G4 to fold in a long telomeric G-tail and less than 80 min for G-hairpin in the short G-tails. The short G-tail present in most of the cell cycle is bound by CST complex to inhibit telomerase recruitment and is not favourable to form secondary structures. Cdc13 goes through post-translational modifications which mediates telomerase recruitment (Chandra et al., 2001; LE et al.,

2011; Li et al., 2009; Shen et al., 2014; Zhang et al., 2010). The telomerase elongated G-tails are likely to quickly form G4 which could lead to Cdc13 dissociation from the G tail because of its low affinity. It has been reported that G4s might act as telomeres cap when the natural capping by Cdc13 is compromised (Smith et al., 2011). After unwinding G4 by telomerase (Paeschke et al., 2008) and helicases (Boule et al., 2005; Sun et al., 1999) the G-tail might be bound again by Cdc13. With the help of the G4 specific antibody BG4, we have pulled down and characterized G4 formation in *S. cerevisiae* telomeres *in vivo*. In accordance with these findings, we evaluated increased G4 levels in late S phase and in the *cdc13-1* mutant (Fig. 3.9) We speculate that more G4s at longer G-tails compromise the impaired natural capping of telomeres in *cdc13-1* strain, particularly at higher temperatures due to their stable nature. In the time frame of each cell cycle, the short G-overhang with the G-hairpin forming potential is mostly in its unfolded state, which has a high affinity to bind to Cdc13 (Fig. 4.2)(Jurikova et al., 2020). We propose a model that non-B DNA structures form as a kinetically regulating mechanism for binding of Cdc13 to telomeric G-overhangs (Fig. 4.2). To our knowledge, these data shows for the first time secondary structures at G-overhang might have a role in regulating yeast telomeres.

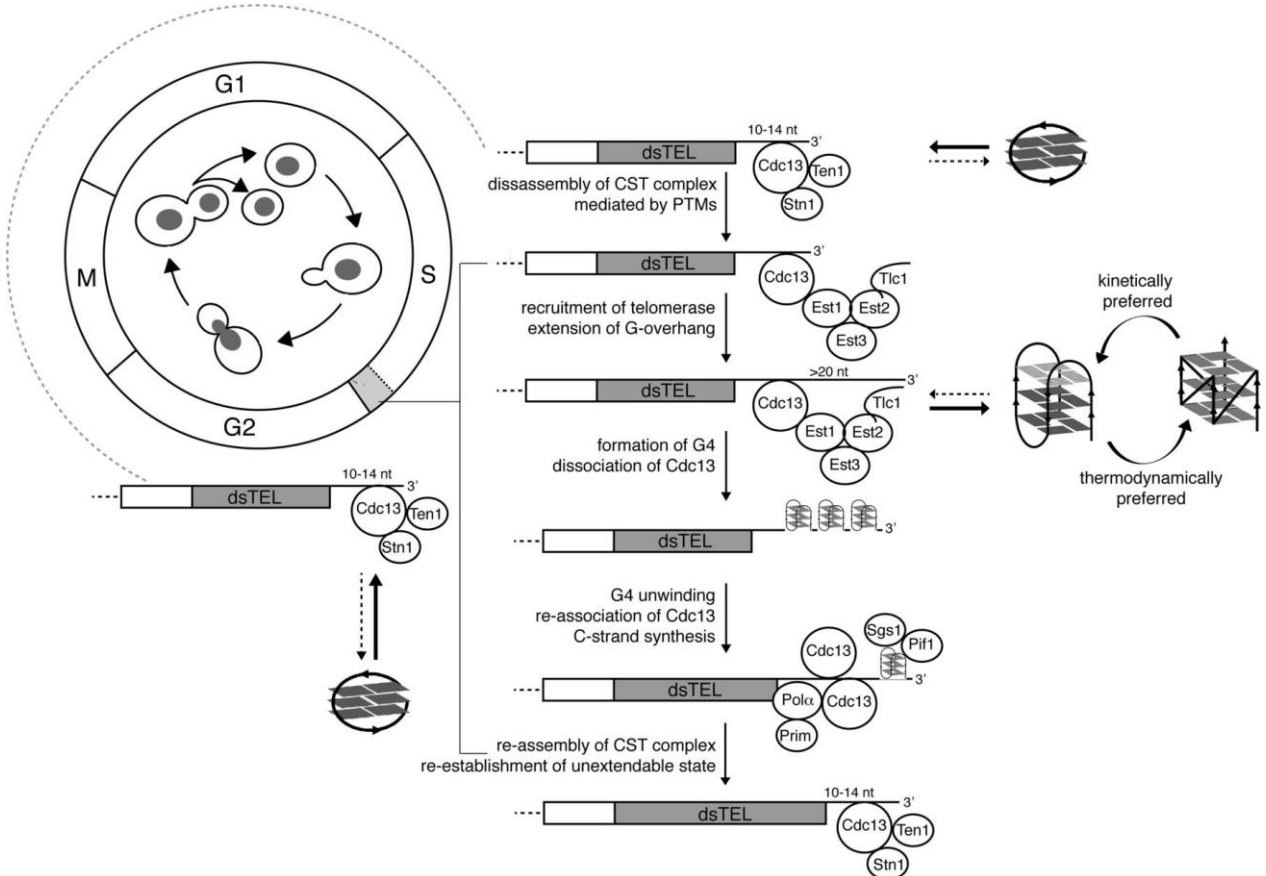


Figure 4.2. potential function of non-B DNA structures formed in the G-tail of telomeres in *S. cerevisiae*.

In S phase, the Cdc13 goes through post-translational modifications (PTM), which contributes to telomerase recruitment. In late S phase when the overhang is elongated, there is a small window for G4 formation. We propose the potentially formed G4s protect the ss DNA before they are unwinded by helicases. The light grey box in the cell cycle corresponds to a late S phase.; Pol α , DNA polymerase α (Jurikova et al., 2020).

To further understand the link between G4s, telomere length and their association with telomere binding proteins, we performed BG4 ChIP-qPCR in different telomeric backgrounds. Short telomere strains, specifically in the absence of MRX components, indicate less G4 in telomeric region (Fig.3.10). However, the *ku70 Δ* strain with short telomeres but long G-overhangs does not show difference on G4 enrichment except for the VII-L telomeric region (Fig.3.10). We suggest less G4 enrichment could be because only a subset of G4s (e.g. Antiparallel intermolecular) forming, which are favourable for telomerase activity (Moye et al., 2015) and the rest are resolved by helicases (Sauer and Paeschke, 2017). Whether helicases are more active at short telomere or only a specific family of G4s are formed, is not clear and should be further studied. The *pif1-m2* strain with long telomere strain indicate elevated G4 binding to telomeres in comparison to WT (Fig.3.10). This agrees with previous findings, that Pif1 unwinds G4 structures in the absence G4 structures form at endogenous sites (Paeschke et al., 2013; Phillips et al., 2015; Strecker et al., 2017). One possible explanation is that telomerase is more active when it is not negatively regulated by Pif1, leading to longer telomeres and more unresolved G4s. On the contrary, *rif2 Δ* strain with long telomere shows similar G4 like WT.(Fig. 3.10) Absence of RecQ helicase, Sgs1, indicate similar G4 abundancy at telomeres like WT(Fig. 3.10). It can be implied that long telomeres do not enhance the formation of G4 structures but rather the abundancy is regulated by Pif1 helicase. Furthermore, telomere healing assay after induction of DSB next to G4 motif, demonstrates that a single G4 motif is not sufficient for telomere addition at endogenous sites after a DSB. (Fig. 3.11). Here, we identify when G4 form at telomeres in *S. cerevisiae*. Overall,G4 contribution for telomere function depends not only on the telomere length but also on the presence of specific telomere binding proteins. The next striking questions to address would be to observe similar effects in human cells, the to clarify the *in vivo* functions of G4s at telomeres and identify the proteins involved in G4 regulation.

4.3 Zuo1 as a G-quadruplex binding protein

Telomere associated proteins are the key modulators for preserving telomere homeostasis (Wellinger and Zakian, 2012). Apart from proteins, the unique structural features of telomeric sequences (e.g. G4 forming potential) have been shown to play positive and negative roles in maintaining genome integrity (Rhodes and Lipps, 2015). Controversial data exist that challenge the function and relevance of G4s to telomeres. *In vivo* circumstances of telomeric G4 formation and the interacting protein partners are the topic of heated debate. It is of critical importance to identify their function and associated proteins. Previous work from the Paeschke lab has identified Zuo1 has a novel G4 binding and stabilizing protein.(Magis et al., 2020). Besides its biological role as a ribosome associated chaperone (W et al., 1998), Zuo1 supports G4 formation at internal sites, where its function is essential after UV irradiation (Magis et al., 2020). G4 stabilized by Zuo1, supports the recruitment of nucleotide excision repair (NER) proteins after UV damage (Magis et al., 2020). Because in initial studies, I could reveal that Zuo1 binds robustly to telomeres, we hypothesized that Zuo1 may also support G4 formation at telomeres and by this contribute to distinguishing telomeres from DSB. This in line with published finding that Zuo1 binding to internal G4s prevents the action of HR and NHEJ (Magis et al., 2020). Therefore, we raised the hypothesis that Zuo1 supports G4 formation at telomeres where it actively participates in preventing telomeres recognition as DSB.

If Zuo1 was essential for regulating telomere length, we would expect major telomere length alterations in the cells lacking Zuo1. However, I did not observe visible changes in telomere length in the absence of Zuo1.(Fig. 3.12). To further elucidate Zuo1 impact on telomere length, I have generated Zuo1 double deletions in the absence of telomere associated proteins. Ku70 together with Ku80 is involved in telomerase recruitment to telomeres (Fisher et al., 2004) and NHEJ (Gravel et al., 1998; Lieber et al., 1997; Martin et al., 1999). Double deletion of Zuo1 and the Ku70 protein, which has short telomere phenotype (Boulton and Jackson, 1998) did not reveal direct telomere length changes.(Fig. 3.12). Deletion of Zuo1 in the absence of Pif1 helicase, a negative regulator of telomerase (Phillips et al., 2015), did not show direct effect on telomere length in the southern blot. Double deletion of Zuo1 and recQ helicase Sgs1 also did not change telomere length (Fig. 3.12). In unchallenged conditions, Zuo1 double deletion with G4 unwinding helicases or NHEJ component (Ku70), does not affect telomere length.

Telomere binding proteins are cell cycle regulated and that their relevance for telomere length was detectable in particular cell cycle phase or by showing a specific telomeric phenotype (Bianchi et al., 2004; Fisher et al., 2004; Levy and Blackburn, 2004). To evaluate Zuo1 impact as a mediator for HR or NHEJ at telomeres and its binding dependency on telomere length, I performed ChIP in strains, deficient of specific telomeric proteins, harboring short telomeres. Zuo1 binding in the short telomere strains in the absence of the MRX components (Zuo1.Myc *rad50Δ* and Zuo1.Myc *mre11Δ* strains) indicates higher enrichment at VI-R and VII-L telomeres (Fig.3.13). Absence of the MRX complex did not lead to changes in Zuo1 binding to internal region (XIIIb) (Fig.3.13). In accordance with our previous observation that absence of MRX components did not change Zuo1 binding to internal regions (Magis et al., 2020), we suggest increased Zuo1 binding is not HR driven but rather specific for telomeric role of the MRX complex. Increased Zuo1 binding to short telomere *ku70Δ* strain points out to its binding preferences for short telomeres. Elevated Zuo1 binding in the short inducible telomere strain, also supports Zuo1 preferential binding for short telomeres (Fig. 3.13). Telomeres shorten in each cell cycle and only the short telomeres are extended by telomerase (J Lingner et al., 1997; Joachim Lingner et al., 1997). A potential function of Zuo1 at telomeres, could be to support them from being recognized as DSB when they get shorter. It can be inferred that telomeric role of Zuo1 is different from its generic role as J-protein cochaperone of Hsp70 (JK et al., 2013; Prunuske et al., 2012) and is most likely G4 related.

One of the key factors for the cells to distinguish short telomeres from DSB is due to their sensitivity to the Pif1 helicase, which negatively regulates telomerase (Phillips et al., 2015; Strecker et al., 2017) Telomeric DNA sequences of 34bp to 125 bp are considered as critically short telomeres and preferentially elongated (Chang et al., 2007; Sabourin et al., 2007; Strecker et al., 2017) Pif1 is binding and acting at wild type length or longer telomeres and is insensitive to short telomeres (Phillips et al., 2015). The mechanism by which Pif1 inhibits telomerase from telomere-DSB transition is not clear. I observed more G4s in the *pif1-m2* long telomere strain compared to WT, which is in line with previous publications showing that Pif1 is the major helicase, unwinding G4 DNA in yeast (Paeschke et al., 2013, 2011; Ribeyre et al., 2009) (Fig. 3.10). We speculate that high levels of G4s (Fig. 3.10), and not the long telomere phenotype, leads to increased Zuo1

binding to telomeres in *pif1-m2*. Because lengthened telomeres, for example in *rif2Δ* are not sufficient to recruit Zuo1. It can be inferred that having longer telomere does not correlate with more Zuo1 binding and is specific for presence or absence of specific telomere associated proteins.

Because there is an interplay between telomere conformation and its associated proteins during cell cycle (Schmidt et al., 2016; Wellinger and Zakian, 2012), we monitored Zuo1 in synchronous cells at telomere VI-R and VII-L. Telomerase binding, in particular Est2 attachment to telomeres, which leads to their extension, happens in late S phase (Chan et al., 2008; Fisher et al., 2004; Wellinger and Zakian, 2012). I observed decreased Zuo1 binding to telomeres in late S phase (Fig. 3.12). In contrast, G4s change throughout cell cycle and show higher abundance in S phase (Jurikova et al., 2020). These two findings indicate that Zuo1 function at telomeres may not be easily explained by changes in G4 levels. Furthermore, the telomerase subunit Est1 can form G4s *in vitro* and the cells carrying Est1 mutant, which were incapable of forming G4, show telomere shortening and senescence (Zhang et al., 2010). One possibility is that Zuo1 is not coupled to telomeric G4s in late S phase because there should be enough space for telomerase activity or potential G4 resolution

We show that G4 levels change during cell cycle and they are more abundant during S phase in *S. cerevisiae* (Jurikova et al., 2020). To address the link between Zuo1 and telomeric G4s, we monitored G4 levels in Zuo1 deficient cells. In the Absence of Zuo1, we determined, both in synchronous and asynchronous cells, a decrease in G4 levels compared to WT.(Fig.3.12). On one hand parallel, intermolecular G4s have been shown to be a target for telomerase *in vitro* (Moye et al., 2015; Paeschke et al., 2008). On the other hand antiparallel G4s have been reported to block telomerase and sequester at the 3' end *in vitro* (Zahler et al., 1991; Zaug et al., 2005). G4 resolution has been reported to happen in ciliates during S phase (Paeschke et al., 2005). It is likely that Zuo1 support the formation of a specific G4 population, and could be the missing link to address the controversial observations. If Zuo1 would support formation of G4s as substrates or obstacles for telomerase recruitment and telomere elongation, we would expect to observe telomere length alterations in the *pif1-m2* strain. However, Zuo1 absence did not lead to any length effect in the *pif1-m2* strain (Fig. 3.12). One possible explanation is that

the Rif1 protein, which has been shown to generate G4s *in vitro* (Masai et al., 2019), is occupying the long telomeres, hence the G4s and modulates Zuo1 binding sites. We observed decreased G4 level in short telomeres (Fig. 3.10) and suggest that Zuo1 binding to short telomeres might be increased as means of supporting G4 formation at telomeres. If Zuo1 supports the formation of a particular G4 conformation needs to be further studied.

Based on *in vitro* observations, G4s have been proposed to be involved in capping mechanism to protect the ends when the natural capping is disrupted (Smith et al., 2011). To puzzle Zuo1 role as a G4 interacting protein and characterize its protein counterparts, we pulled down Zuo1.Myc followed by mass spectrometry. Stm1 was one of the top proteins interacting with Zuo1 (Table 6). Stm1 binds to ribosome and is more abundant in nutrient and replication stress (T et al., 1995). Stm1 is involved in telomere maintenance and is also G4 binding protein (G4BP) (Hayashi and Murakami, 2002; MW et al., 2004). Previous study, reported Stm1 overexpression to rescue the temperature sensitivity of *cdc13-1* mutants via G4 (Smith et al., 2011). Furthermore, at elevated temperature, more G4s were evaluated in the *cdc13-1* mutant with long G-overhang at (Jurikova et al., 2020). We speculated Zuo1 and Stm1 interaction to be the missing link for the proposed G4 dependent telomere capping. However, neither Zuo1 overexpression, nor its deletion rescue or affect the growth of *cdc13-1* strain at tested temperatures (Fig. 3.15). Zuo1 presence does not affect the *cdc13-1* strain temperature sensitivity. Interestingly, Zuo1 binding to *cdc13-1* temperature sensitive strain was more at permissive temperature (23°C) (Fig. 3.15). Stm1 binding is dramatically decreased in the absence of Zuo1 (Fig. 3.15). Overall, we propose Zuo1-Stm1 interaction to be involved in G4 related telomere capping. However the interaction should be further investigated in the future to find out the missing binding parameter.

Future experiments, require monitoring Zuo1 and G4 landscape at telomeres in the *tlc1-tm* mutant strain. The *tlc1-tm* strain carries a mutant TLC1 and subsequently the telomerase is incapable of adding sequences that can form consensus G4s (Chang et al., 2007; Strecker et al., 2017). This would bring more insight whether Zuo1 binding to telomeres depending on G4s. It is possible that Zuo1 does not play an essential role at telomeres in unchallenged conditions and it is needed upon stress, like DNA damage. A telomere screen in unchallenged and under stress conditions (e.g. in response to

damaging agents) with the double deletion of Zuo1 and telomeric proteins could be helpful to characterize its binding partners. Multiple studies have shown G4 ligands to affect cellular senescence and telomere shortening (Beauvarlet et al., 2019; Gaikwad et al., 2020; Riou et al., 2002) Another future direction is to evaluate Zuo1 and telomeric G4s when the cells go through senescence. Whether Zuo1 effect at telomeres is limited to DNA G4s or it affects other structures like the telomeric RNA, TERRA is another open question which needs to be investigated. TERRA levels are cell cycle regulated, peak in early S-phase and accumulate at short telomeres(Graf et al., 2017). It is likely that G4 stabilization at telomeres, due to overexpression of Zuo1 will lead, not only to more G4s, but also to elevated TERRA levels. These speculations will give rise future studies related to biological roles of Zuo1 and secondary structures at telomeres.

4.4 Future perspectives

It is important to address possible parallels between our observations in yeast and human telomeres. Considering that the length of human G-overhang is sufficient for G4 formation throughout the cell cycle, it would be interesting to study the folding kinetics of human ssDNA-binding protein and its ability to compete with G-overhang secondary structures. Moreover, our analyses reveal that the G4 levels are generally less in short telomeric strains. Whether helicases are more active at short telomeres or only a specific family of G4s are formed, is not clear and should be further studied. Further investigation of Zuo1 function at telomeres will also provide new insights to better understand its function and benefit as a G4 binding protein.

5. Abstract

Telomeres are specialized nucleoprotein structures at the end of linear eukaryotic chromosomes, vital for safeguarding of genetic material. They inhibit nucleolytic degradation, end to end fusion and unwanted recombination. The telomerase enzyme impedes telomere shortening, but is not expressed in most somatic cells. On one hand telomerase absence results in telomere shortening, leading to aging. On the other hand telomerase reactivation is a hallmark of many cancer cells. Furthermore, *de novo* telomere addition to internal regions should be avoided to maintain genome integrity. Eukaryotic cells have developed different regulatory mechanisms to outcompete these challenges. To our knowledge, the destiny of telomerase components and where they are located throughout the cell cycle is not fully understood. Here, we entailed *S. cerevisiae* as model organism and identified the genome-wide binding sites of the telomerase catalytic subunit Est2. Specific internal sequences (termed NTBS) showed preference for inactive Est2 binding, when it is not attached to telomeres. 3D conformation of chromosome has been proposed to establish a boundary between Est2 association to telomeres and NTBS.

The terminal part of eukaryotic telomeres contains a single stranded G-overhang, which is capped by telomeric proteins such as Cdc13 in yeast. The G-overhang gets extended in late S phase of the cell cycle. Several lines of evidence have revealed the G-overhang potential for forming non-B DNA structures. We studied the folding kinetics of different oligonucleotides resembling the G-overhang. Here, we revealed that depending on the length, they can form G-quadruplexes (G4) or G-hairpins *in vitro*. Regardless of their topology, these structures impede Cdc13 binding *in vitro*. The formation of G4s has been shown to be more likely in late S phase when the overhang is longer. We proposed a model explaining the potential function of non-B DNA structures formed in the G-overhang in a time and length dependant manner.

Despite the rising evidence for G4 functions at telomeres, little is known about their *in vivo* abundancy, the correlation to telomere length and telomeric proteins. We entailed a previously established method with the help of a G4 specific antibody (BG4) to pull down G4s at yeast telomeres. Here, we show that telomeric G4 landscape at changes throughout the cell cycle. G4 abundancy is generally less at short telomeres, however it

does not necessarily depend on telomere length and is more related to the presence of telomeric proteins.

Finally, we characterized the telomeric abundancy of the recently identified G4 stabilizing protein, Zuo1. Despite the G-rich nature of telomeres, the *in vivo* relevance of G4 formation and the underlying mechanisms at telomeres is poorly understood. Absence of Zuo1 did not show a length effect on telomeres. Zuo1 binding to the studied telomeres changes during the cell cycle and is less abundant in late S phase. Zuo1 binding to telomeres have been increased in the *pif1-m2* strain, pointing out it is related to more abundant G4. Furthermore, we reveal Zuo1 interaction with G4 associated telomeric protein Stm1. However the exact underlying mechanism should be further clarified.

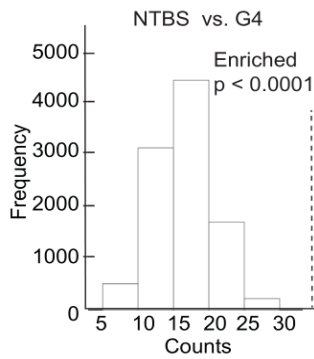
6. Supplementary figures

6.1 NTBS supplementary figures

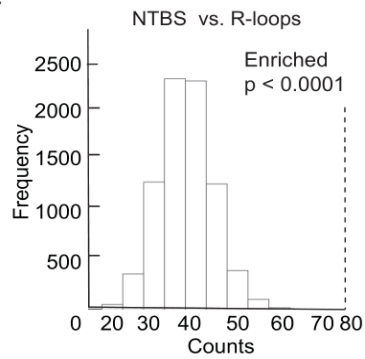
A



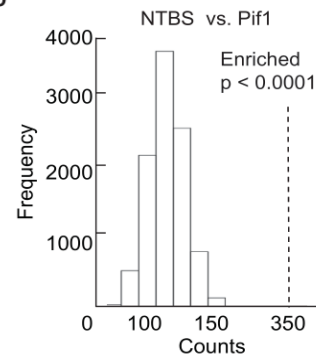
B



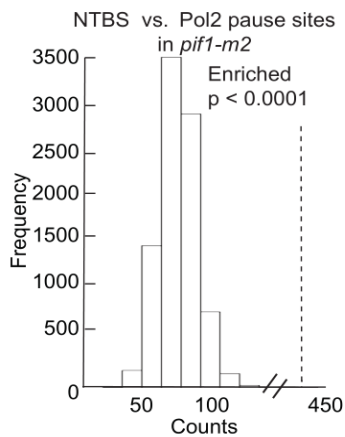
C



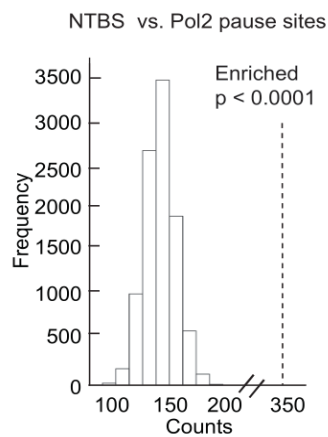
D



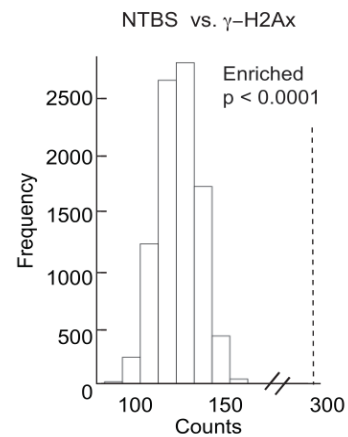
E



F

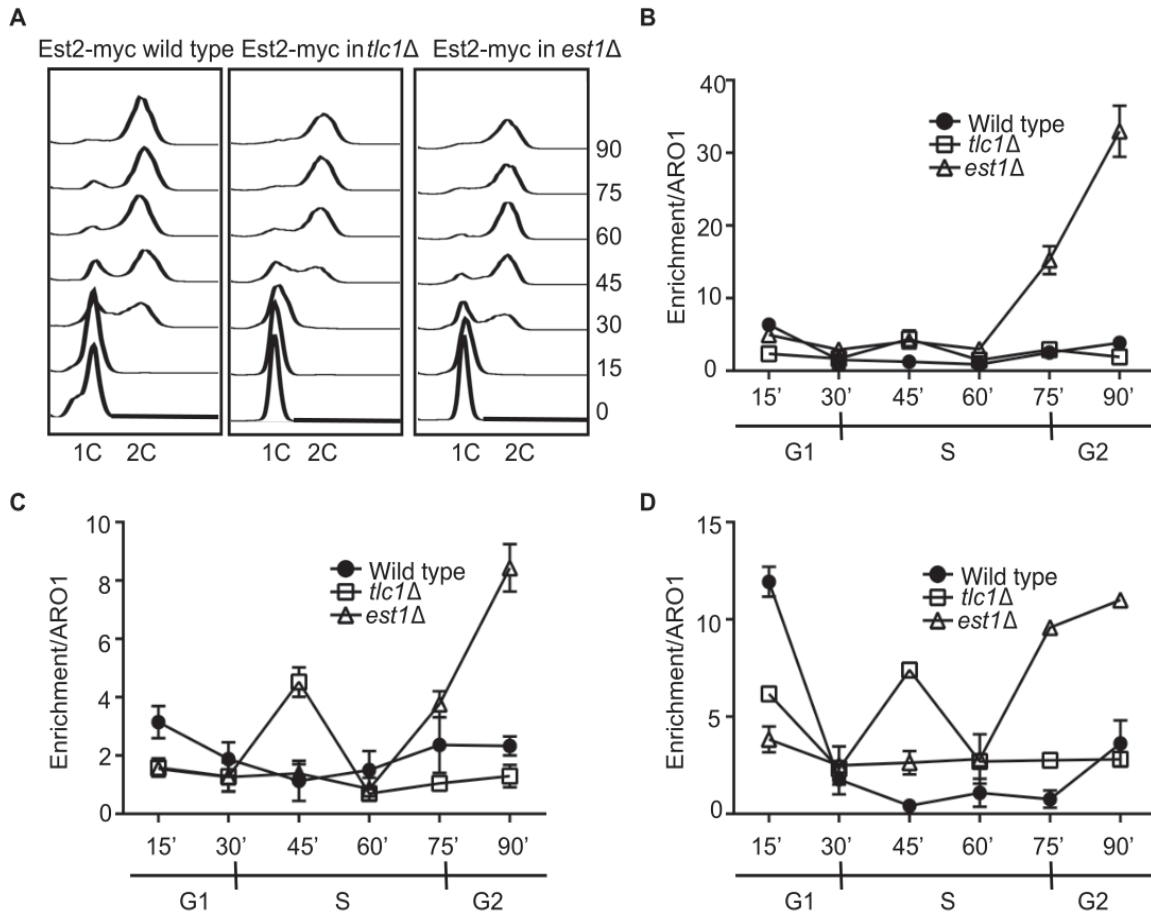


G



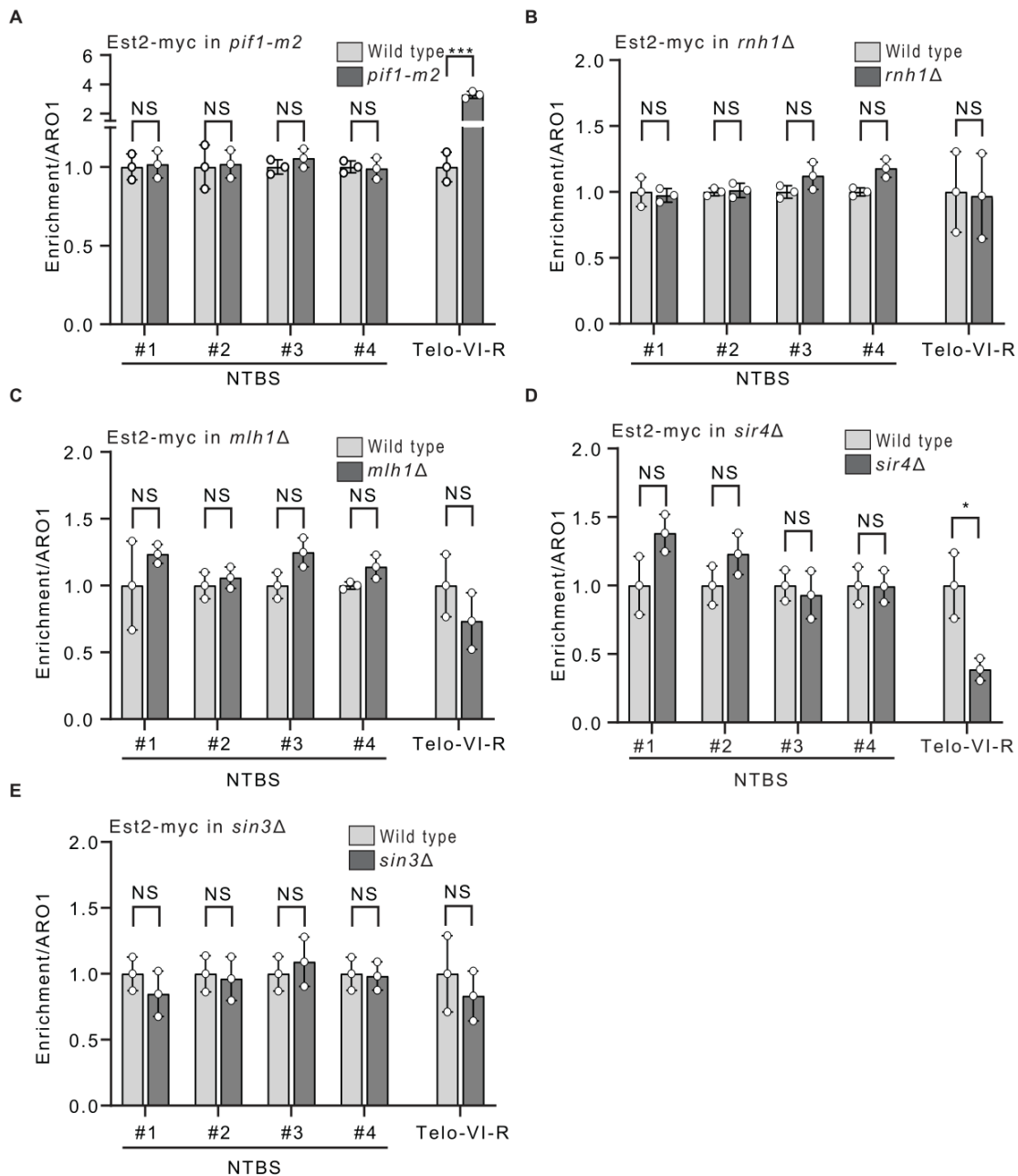
Supplementary figure S1.

A. IGV snapshot of NTBS #1-4 in yeast genome. **B-F.** computational calculations indicating the overlap of genomic traits with NTBS P-value shows statistical significance of their enrichment between specific trait and NTBS. NTBS vs, **B.** G4s, **C.** R-loops, **D.** Pif1 binding sites, **E.** pif1-m2 binding sites, **F.** DNA Pol2 sites, **G.** gamma-H2A(X) binding sites.



Supplementary figure S2.

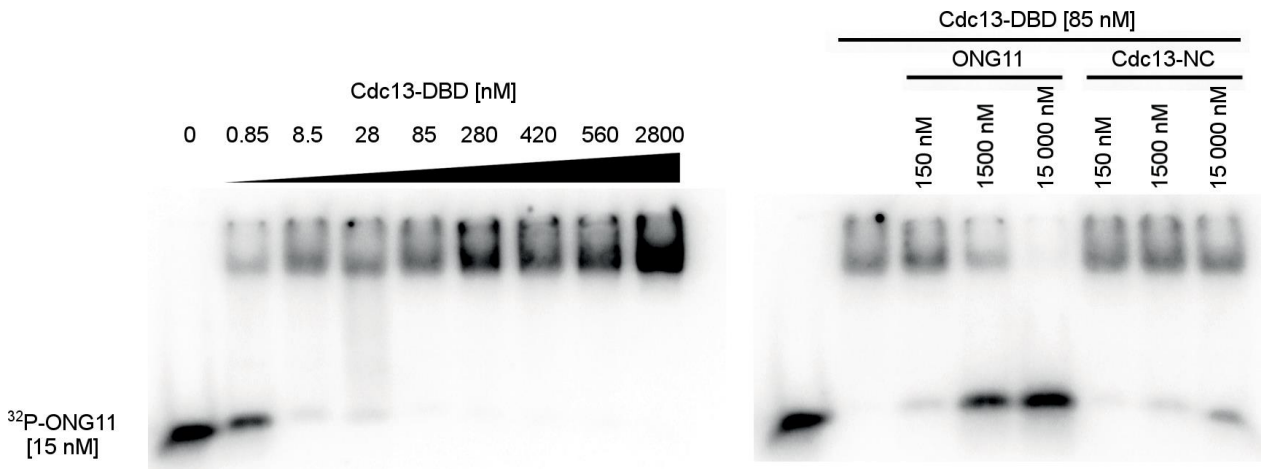
A. Confirming cell cycle stages with FACS analysis in wildtype, *tlc1Δ* and *est1Δ*. **B-D.** Est2 attachment to NTBS #2-#4 in wildtype (closed circles), *tlc1Δ* (open squares) and *est1Δ* (open triangles). Plotted data are standard mean \pm SEM for $n=3$ replicates.



Supplementary figure S3.

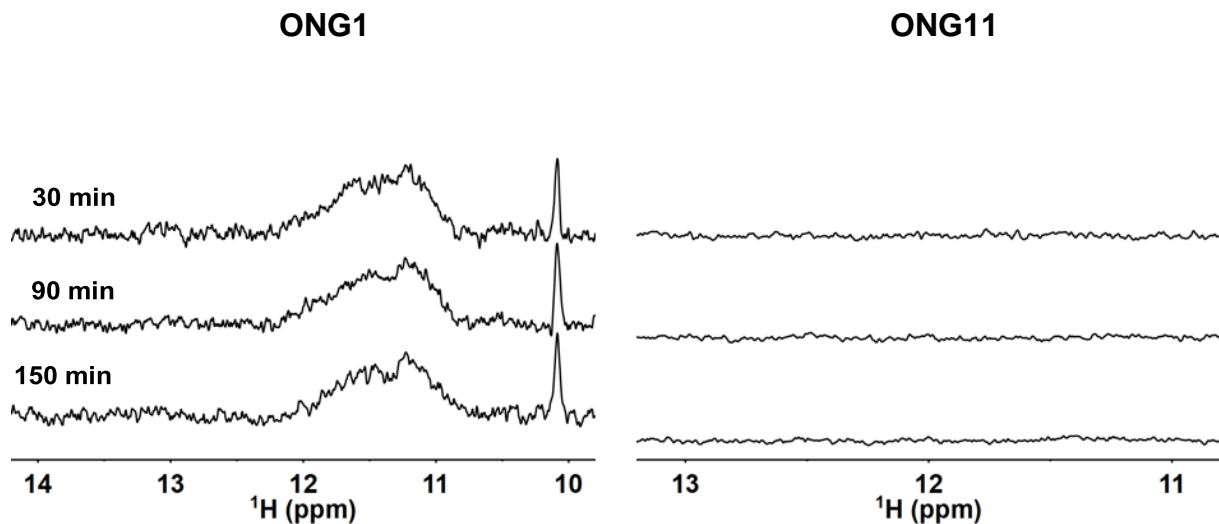
A. ChIP-qPCR of Est2-NTBS binding in *pif1-m2* (dark grey bars) cells compared to wildtype condition (light grey bars) **B.** Overexpression of RNaseH1 and resolving R-loops (dark grey bars) compared to wildtype (light grey bars). **C.** Binding in *mlh1Δ* cells compared to wildtype. **D.** Est2-NTBS interaction in *sin3Δ*. **E.** Est2-NTBS interaction in *sir4Δ* cells. No statistically significant enrichment to NTBS sites were observed for all the tested conditions. Data represented are mean \pm SEM. Statistical significance was calculated in comparison to ARO1 levels at respective cell cycle stages for $n=3$ biological replicates and determined using Student's t-test. No statistically significant enrichment to NTBS sites were observed for all the tested conditions.

6.2 Telomeric G-overhang supplementary figures



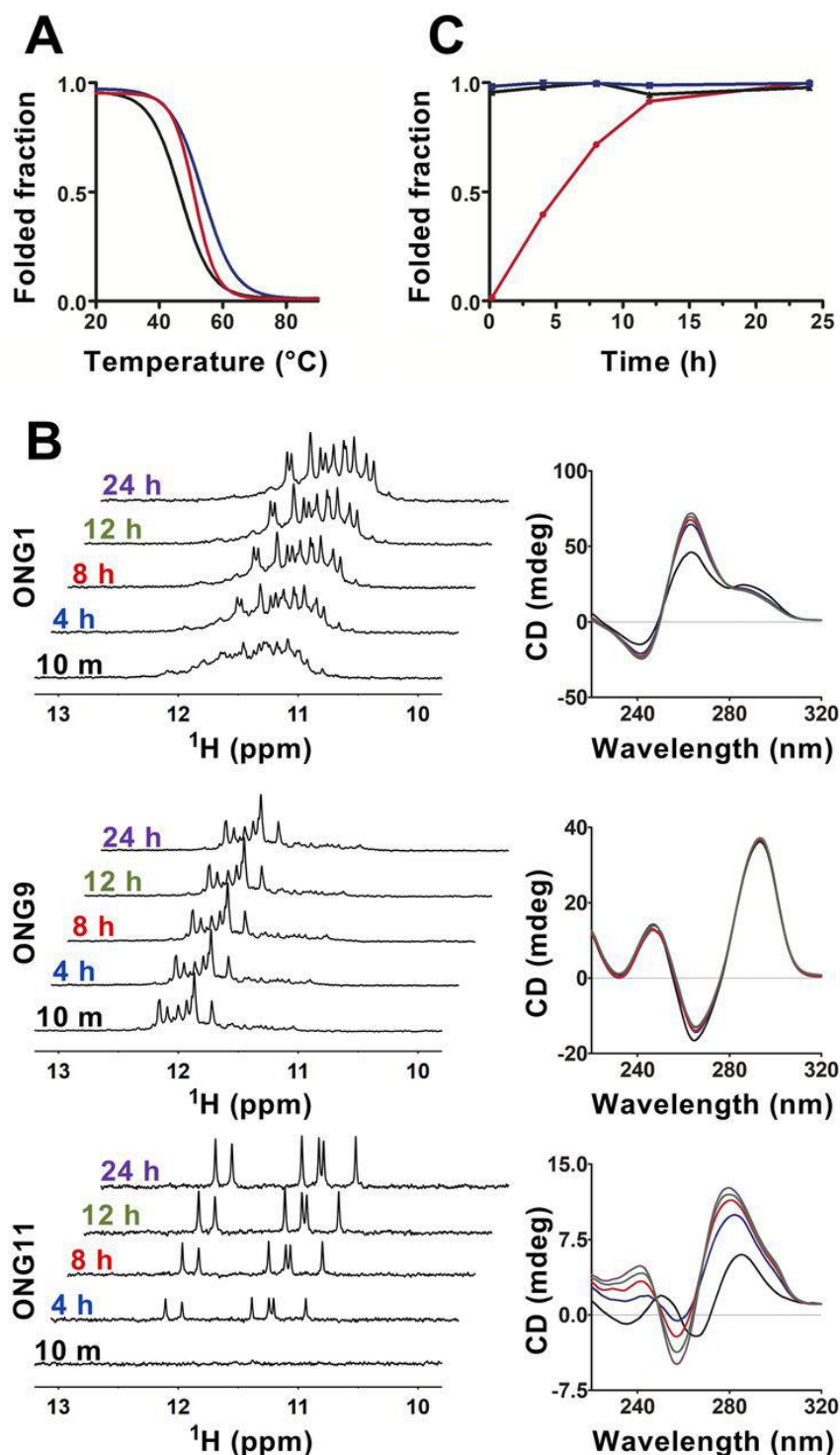
Supplementary figure S4.

Confirmation of Cdc13 binding properties with EMSA. Left: [^{32}P]-labelled ONG11 binding by Cdc13-DBD was assayed in direct EMSA with increasing protein concentration. Right: unlabelled competitors in an EMSA with [^{32}P]-labelled ONG11 to confirm the binding preference of Cdc13-DBD. ONG11 is a previously described binding motif of Cdc13, whereas Cdc13-NC (5'-TGTGGGTGTG-3') has been used as a negative control for Cdc13 binding previously (Anderson et al., 2002; Hughes et al., 2000).



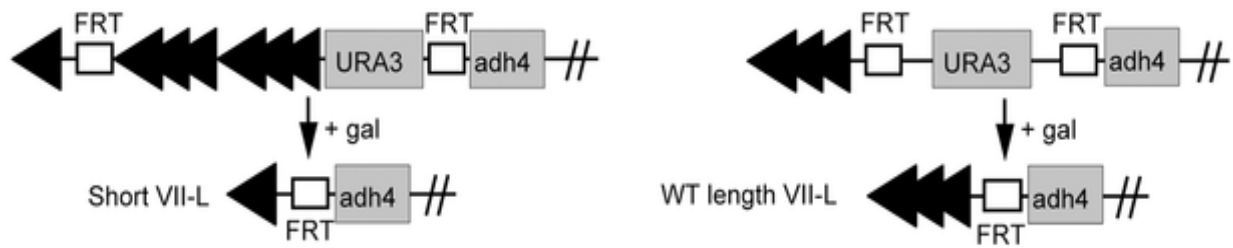
Supplementary figure S5.

Time dependant development of imino region of 1D ^1H NMR spectra from 50 mM ONG1 and ONG11 in cellular lysate. The spectra were evaluated using 1-1 echo pulse sequence at 25 $^{\circ}\text{C}$.



Supplementary figure S6.

A. CD melting curves of ONG1 (black; apparent T_m = 46.3 °C), ONG9 (blue; apparent T_m = 53.5 °C), and ONG11 (red; apparent T_m = 50.7 °C). **B.** Imino region of 1D ¹H NMR and CD (right) of ONG1, ONG9, and ONG11 evaluated at indicated time points. NMR spectra were acquired using a zgpgw5 pulse sequence. **C.** Time course of the folding process for ONG1 (black, triangle), ONG9 (blue, square) and ONG11 (red, circle) evaluated from normalized time-dependent changes of imino signals in NMR of A.

**Supplementary figure S7.**

Schematic representation of chromosome VII-L inducible short telomere constructs. In these strains, upon galactose induction Flp1 recombinase recognizes the two FRT sites and causes recombination (adapted from Phillips et al., 2015)

7. List of figures and tables

Figure 1.1. <i>Saccharomyces cerevisiae</i> telomere.	10
Figure 1.2. Telomere replication.....	17
Figure 1.3. G-quadruplex structures and their topology.	21
Figure 1.4. A model for the regulation of telomeric G4 structure.....	25
Figure 3.1. Est2 binding across the yeast genome	38
Figure 3.2. Est2 binding to NTBS changes in the absence of Est1 and TLC1	40
Figure 3.3. Est2 is recruited via an alternative pathway to NTBS	41
Figure 3.4. Hi-C data.....	43
Figure 3.5. Oligonucleotides mimicking telomeric G-tails form distinct non-B DNA structures.	45
Figure 3.6. Secondary structures forming on telomeric DNA decrease the binding of Cdc13-DBD.....	46
Figure 3.7. Diverse formation kinetics of G-hairpin and G4 affect their Cdc13-DBD binding ability.....	47
Figure 3.8. Cdc13-DBD does not impede with G-hairpin or G4 folding kinetics and does not form a stable complex with them either.....	48
Figure 3.9. G4 enrichment in <i>S. cerevisiae</i> telomeres.....	50
Figure 3.10. G4 abundancy at short and long telomere	52
Figure 3.11. Telomere addition adjacent to G4-IV and G4-IX motifs.....	53
Figure 3.12. Zuo1 binds to telomeres but has no length effect	55
Figure 3.13. Zuo1 binding to short telomere	57
Figure 3.14. Zuo1 binding to long telomeres.....	58
Figure 3.15. Interaction of Zuo1 with STM1	60
Figure 4.1. Parking model for telomerase.	63
Figure 4.2. potential function of non-B DNA structures formed in the G-tail of telomeres in <i>S. cerevisiae</i>	66
Supplementary figure S1.....	75
Supplementary figure S2.....	75
Supplementary figure S3.....	76
Supplementary figure S4.....	77
Supplementary figure S5.	77

Supplementary figure S6.....	78
Supplementary figure S7.....	79
Table 1: Yeast Strains.....	82
Table 2: Bacteria and plasmids.....	84
Table 3: Primers.....	86
Table 4: Oligonucleotides created for screening the conformational space of extended telomeric ssDNA from <i>S. cerevisiae</i>	87
Table 5: List of NTBS.....	87
Table 6: Zuo1.Myc Mass spectrometry associated proteins	118

8. Tables

Table 1: Yeast Strains

Strain	Genotype	Source
YPH499	<i>MATa ura3-52 lys2-801_amber ade2-101_ochre trp1-Δ63 his3-Δ200 leu2-Δ1</i>	V. Zakian lab
W303	<i>MATa ura3-1 trp1Δ 2 leu2-3, 112 his3-11,15 ade2-1 can1-100</i>	R. Rothstein
EST2-MYC	YPH499 Est2-G8-Myc18::TRP1 bar1::KAN	KP
EST2-MYC <i>pif1-m2</i>	YPH499 Est2-G8-Myc18::TRP1 <i>pif1-m2</i>	KP
CDC13-MYC	W303 Cdc13-Myc13::HIS3	V. Geli lab
EST1-MYC	YPH499 Est1-Myc13::TRP1	SP (this study)
EST3-MYC	YPH499 Est3-Myc13::TRP1	SP (this study)
KU80-MYC	W303 Cdc13-Myc13::HIS3	SP (this study)
CDC13-MYC	W303 Cdc13-Myc13::HIS3 bar1::KAN	SP (this study)
H2aS129a	W303 S129A mutation in Histone H2A protein	KP
POL2-MYC	YPH499 Pol2::Myc13::TRP1	SP (this study)
Gal-HO	W303 <i>mnt2::LYS2 lys2Δ ade2Δ leu2::GAL-HO</i>	A. Bianchi lab
Est2-G8-Myc <i>tlc1Δ yku80-135i</i>	YPH501 Est2-G8-Myc18::TRP1/EST2 <i>tlc1Δ::LEU2/TLC1 yKU80-135i/Ku80 Tel VII-L::URA3/ Tel VII-L::URA3</i>	V. Zakian lab
Est2-G8-Myc <i>est1Δ</i>	YPH501 Est2-G8-Myc18::TRP1/EST2 <i>est1Δ::HIS3/EST1 Tel VII-L::URA3/ Tel VII-L::URA3</i>	V. Zakian lab
Est2-G8-Myc <i>cdc13-2</i>	YPH501 Est2-G8-Myc18::TRP1/EST2 <i>cdc13-2/CDC13 Tel VII-L::URA3/ Tel VII-L::URA3</i>	V. Zakian lab
Est2-G8-Myc <i>est1Δ</i>	YPH501 Est2-G8-Myc18::TRP1/EST2 <i>est1Δ::HIS3/EST1 Tel VII-L::URA3/ Tel VII-L::URA3</i>	V. Zakian lab
Est2-G8-Myc <i>rad52Δ</i>	yph499 Est2-G8-Myc18::TRP1 <i>rad52::LEU2</i>	SP (this study)
NTBS#1-HO tagged strain	Gal-HO NTBS#1-HO::LYS2 bar1::KAN Rad5+	SP (this study)
NTBS#2-HO tagged strain	Gal-HO NTBS#2-HO::LYS2 bar1::KAN Rad5+	SP (this study)

NTBS#3-HO tagged strain	Gal-HO NTBS#3-HO::LYS2 bar1::KAN Rad5+	SP (this study)
NTBS#4-HO tagged strain	Gal-HO NTBS#4-HO::LYS2 bar1::KAN Rad5+	SP (this study)
NTBS#5-HO tagged strain	Gal-HO NTBS#5-HO::LYS2 bar1::KAN Rad5+	SP (this study)
NTBS#6-HO tagged strain	Gal-HO NTBS#6-HO::LYS2 bar1::KAN Rad5+	SP (this study)
NTBS#7-HO tagged strain	Gal-HO NTBS#7-HO::LYS2 bar1::KAN Rad5+	SP (this study)
NTBS#8-HO tagged strain	Gal-HO NTBS#8-HO::LYS2 bar1::KAN Rad5+	SP (this study)
NTBS#9-HO tagged strain	Gal-HO NTBS#9-HO::LYS2 bar1::KAN Rad5+	SP (this study)
N80-HO tagged strain	Gal-HO N80-HO::LYS2 bar1::NAT Rad5+	A. Bianchi lab
TG80-HO tagged strain	Gal-HO TG80-HO::LYS2 bar1::NAT Rad5+	A. Bianchi lab
MH74	yph499 Est2-G8-Myc18::TRP1 mlh1::LEU	TS (this study)
TS17	yph499 Est2-G8-Myc18::TRP1 pRS425-Gal (pBL211)::LEU	TS (this study)
TS18	yph499 Est2-G8-Myc18::TRP1 RNH1 proteinA HA 6HIS (pBL291)::URA	TS (this study)
EST2-MYC <i>sin3Δ</i>	Est2-G8-Myc18::TRP1 sin3::LEU	MH (this study)
EST2-MYC <i>sir4Δ</i>	Est2-G8-Myc18::TRP1 sir4::LEU	MH (this study)
G4.IV-HO tagged strain	Gal-HO G4.IV-HO::LYS2 bar1::KAN Rad5+	MH (this study)
G4.IX-HO tagged strain	Gal-HO G4.IX-HO::LYS2 bar1::KAN Rad5+	MH (this study)
<i>rif2Δ</i>	W303 <i>rif2</i> ::NATMX	M. Chang lab
Zuo1.Myc <i>rif2Δ</i>	W303 Zuo1.Myc::TRP1 <i>rif2</i> ::NATMX	MH (this study)
<i>pif1-m2</i>	W303 <i>pif1-m2</i>	KP
Zuo1.Myc <i>pif1-m2</i>	W303 Zuo1.Myc::TRP1 <i>pif1-m2</i>	MH (this study)
Zuo1.Myc <i>cdc13-1</i>	W303 Zuo1.Myc::TRP1 <i>cdc13-1</i>	MH (this study)
<i>cdc13-1</i>	W303 <i>cdc13-1</i>	M. Chang lab
<i>ku70Δ</i>	W303 <i>ku70</i> ::KAN	M. Chang lab

<i>rad50Δ</i>	W303 <i>rad50::LEU</i>	MH (this study)
Zuo1.Myc <i>ku70Δ</i>	W303 Zuo1.Myc::TRP1 <i>ku70::KAN</i>	MH (this study)
Zuo1.Myc <i>rad50Δ</i>	W303 Zuo1.Myc::TRP1 <i>rad50::LEU</i>	MH (this study)
<i>mre11Δ</i>	W303 <i>mre11::TRP</i>	KW (Paeschke lab)
Zuo1.Myc <i>mre11Δ</i>	W303 Zuo1.Myc::HIS3 <i>mre11::TRP</i>	MH (this study)
Zuo1.Myc Gal-Flp1	<i>lev220 Gal-Flp1::LEU2</i>	KP
Smt3.Myc <i>zuo1Δ</i>	W303 Smt3.Myc::TRP <i>zuo1Δ::HIS3</i>	MH (this study)
Pif1.Myc <i>zuo1Δ</i>	W303 Pif1.Myc::TRP <i>zuo1Δ::HIS3</i>	MH (this study)
Stm1.Myc <i>zuo1Δ</i>	W303 Stm1.Myc::TRP <i>zuo1Δ::HIS3</i>	MH (this study)
<i>sgs1Δ</i>	W303 <i>sgs1Δ::KAN</i>	MH (this study)
Zuo1.Myc <i>sgs1Δ</i>	W303 Zuo1.Myc::TRP1 <i>sgs1Δ::KAN</i>	MH (this study)
<i>zuo1Δ</i>	W303 <i>zuo1Δ::KAN</i>	SG (Paeshcke lab)
<i>zuo1Δ ku70Δ</i>	W303 <i>zuo1Δ::HIS3 ku70::KAN</i>	MH (this study)
<i>zuo1Δ pif1-m2</i>	W303 <i>zuo1Δ::KAN pif1-m2</i>	MH (this study)
<i>zuo1Δ sgs1Δ</i>	W303 <i>zuo1Δ::HIS3 sgs1::KAN</i>	MH (this study)
Zuo1.Myc Stm1.HA	W303 Zuo1.Myc::TRP Stm1.HA::HYG	MH (this study)
<i>cdc13-1</i> pSTM1OE	W303 <i>cdc13-1 YEplac195 STM1::URA3</i>	Johnson lab
<i>cdc13-1</i> Vector	W303 <i>cdc13-1 YEplac195::URA3</i>	Johnson lab
<i>cdc13-1</i> pSTM1OE	W303 <i>cdc13-1 YEplac195 STM1::URA3</i>	MH (this study)
<i>zuo1Δ</i>	<i>zuo1Δ::KAN</i>	
<i>cdc13-1</i> Vector <i>zuo1Δ</i>	W303 <i>cdc13-1 YEplac195::URA3 zuo1Δ::KAN</i>	MH (this study)
<i>cdc13-1</i> pZUO1OE	W303 <i>cdc13-1 YEplac195 Zuo1::URA3</i>	MH (this study)

Table 2: Bacteria and plasmids

Bacterial	Plasmid	strain	Antibiotic	Purpose
PML10	PML10	DH5α	Ampicillin	Myc13-KAN
PML11	PML11	DH5α	Ampicillin	MYC-13-TRP
PML12	PML12	DH5α	Ampicillin	Myc-13-HIS
pFA6-KanMX	pFA6-KanMX6	DH5α	Ampicillin	for amplification of KanMX to delete genes
pRS305	pRS305	DH5α	Ampicillin	LEU2
pRS306	pRS306	DH5α	Ampicillin	URA3
pFA6a- NATMX	pFA6a	DH5α	Ampicillin	

NTBS#5-HO plasmid	pRS415	DH5 α	Ampicillin	for integration into Gal-HO strain
NTBS#4-HO plasmid	pRS415	DH5 α	Ampicillin	for integration into Gal-HO strain
NTBS#1-HO plasmid	pRS415	DH5 α	Ampicillin	for integration into Gal-HO strain
NTBS#2-HO plasmid	pRS415	DH5 α	Ampicillin	for integration into Gal-HO strain
NTBS#3-HO plasmid	pRS415	DH5 α	Ampicillin	for integration into Gal-HO strain
NTBS#6-HO plasmid	pRS415	DH5 α	Ampicillin	for integration into Gal-HO strain
NTBS#7-HO plasmid	pRS415	DH5 α	Ampicillin	for integration into Gal-HO strain
NTBS#8-HO plasmid	pRS415	DH5 α	Ampicillin	for integration into Gal-HO strain
NTBS#9-HO plasmid	pRS415	DH5 α	Ampicillin	for integration into Gal-HO strain
RNAseH1 control plasmid	pRS425-Gal (pBL211)::LEU	DH5 α	Ampicillin	Control plasmid for RNAse H1 overexpression experiments
RNAseH1 overexpression plasmid	RNH1 proteinA HA 6HIS (pBL291)::URA	DH5 α	Ampicillin	RNAse H1 overexpression plasmid with URA marker for selection
G4IX-HO plasmid	pAB348	DH5 α	Ampicillin	for integration into Gal-HO strain
G4IV-HO plasmid	pAB349	DH5 α	Ampicillin	for integration into Gal-HO strain
YEplac195-STM1	YEplac195	DH5 α	Ampicillin	STM1 OE from Johnson lab
YEplac195	YEplac195	DH5 α	Ampicillin	Control vector from Johnson lab
YEplac195-ZUO1	YEplac195	DH5 α	Ampicillin	Zuo1 OE plasmid

Table 3: Primers

Name	Sequence	Purpose
NTBS#1-FP	CTCACTTCGTTTCCGCTGTC	qPCR for Est2-NTBS binding
NTBS#1-RP	CAGCAGCGTACTTTTCTGGG	qPCR for NTBS
NTBS#2-FP	TCACATCTTCCTCCGCTGTT	qPCR for NTBS
NTBS#2-RP	TCTGGGCAGTGGAAGAAGAG	qPCR for NTBS
NTBS#3-FP	GGTCCCTAGTTGTGGCTGAA	qPCR for NTBS
NTBS#3-RP	ACAACAGCAACCAGACATCG	qPCR for NTBS
NTBS#4-FP	GATGTTGGACAGCTTGGACG	qPCR for NTBS
NTBS#4-RP	CAAGGACAACCTCAGCGATGG	qPCR for NTBS
NTBS#5-FP	CCGTGGACCAGGTACCTAAA	qPCR for NTBS
NTBS#5-RP	GGAGAAATTATCTGCTCCTATTTT	qPCR for NTBS
NTBS#6-FP	CCCTCTGACATGGCAAATTC	qPCR for NTBS
NTBS#6-RP	CATGCTTGAATGGTCAATGG	qPCR for NTBS
NTBS#7-FP	CAATCCGGGTAATGGTAAACGT	qPCR for NTBS
NTBS#7-RP	TGTCTTCAGTCATTTGCCTGG	qPCR for NTBS
NTBS#8-FP	AAAAGCCAATTGTCTGCGGT	qPCR for NTBS
NTBS#8-RP	GGGGTACTTCTGTTAGCGTTG	qPCR for NTBS
NTBS#9-FP	AGGCTTCGCATTTCGAGTTTA	qPCR for NTBS
NTBS#9-RP	GTTCAACTTCCGCTTCTTGG	qPCR for NTBS
ARO1-FP	TGCTGCAGTCACAATTCCTC	qPCR control primers
ARO1-RP	GGCTCTAGAAGTGCCACCTG	qPCR control primers
TELO-6L-FP	CAACTTGCGTGAATCGAAGA	qPCR control primers
TELO-6L-RP	CTGTTCGATGATGCCTGCTAA	qPCR control primers
ChIP-HO-SBR27-FP	TACGCTGGTTTGCATAAAGG	qPCR for enrichment of protein at HO region
ChIP-HO-SBR27-RP	GGTTTCTTGTCTGGTTTCTC	qPCR for enrichment of protein at HO region
non γ -H2AX-FP	CGAAGTATACCGTGCGTC	qPCR for non γ -H2AX region
non γ -H2AX-RP	AGCTTCTTGCTGCTCTATG	qPCR for non γ -H2AX region
non γ -H2AX-FP	GAGGACGAAACGATTGATG	qPCR for non γ -H2AX region
non γ -H2AX-RP	AGATAATGAGCCACGGTAC	qPCR for non γ -H2AX region
Nco1-G4-Chr9-F	CCATGGCCATGGGGAGGGTACGGTGGGTAAT A	Inducible telomere with Gal-HO
Ecor1-G4-Chr9-R	GAATTCGAATTCTTCCAACAATGGCAATGGAAT T	Inducible telomere with Gal-HO
Nco1-G4-Chr4-F	CCATGGCCATGGGGTTCGGTTGGTGGTAGTAC A	Inducible telomere with Gal-HO
Ecor1-G4-Chr4-R	GAATTCGAATTCTCCCCACTCGTTACCCTGACT C	Inducible telomere with Gal-HO
VII-L FP	TGATATGTGTTACGCAGAATAC	qPCR for telomeric region

VII-L RP	TGAGAAGCACCGCAATG	qPCR telomeric region
XV-L FP	TAACCCTGTCCAACCTGTCT	qPCR telomeric region
XV-L RP	ATACTATAGCATCCGTGGGC	qPCR telomeric region
G4 ChrXIII	GCTTCAGCCTGGGGTAAC	qPCR internal G4 motif
G4 ChrXIII	GGCACCATTAGATTACCAC	qPCR internal G4 motif

Table 4: Oligonucleotides created for screening the conformational space of extended telomeric ssDNA from *S. cerevisiae*.

	Length (nt)	Sequence (5' → 3')	Structural type	Dominant topology
ONG1	33	GTGTGGGTGTGGTGTGGGTGTGGTG TGGGTGTG	G-quadruplex	parallel
ONG2	22	GTGTGGGTGTGGTGTGGGTGTG	G-quadruplex	parallel
ONG3	32	GTGTGGGTGTGGTGTGGGTGTGGTG TGGGTGT	G-quadruplex	parallel
ONG4	32	TGTGGGTGTGGTGTGGGTGTGGTGT GGGTGTG	G-quadruplex	parallel
ONG5	30	GTGTGGGTGTGGTGTGGGTGTGGTG TGGGT	G-quadruplex	parallel
ONG6	30	TGGGTGTGGTGTGGGTGTGGTGTGG GTGTG	G-quadruplex	parallel
ONG7	27	TGGGTGTGGTGTGGGTGTGGTGTGG GT	G-quadruplex	mixture
ONG8	26	TGTGGTGTGGGTGTGGTGTGGGTGT G	G-quadruplex	mixture
ONG9	21	TGGGTGTGGTGTGGGTGTGGT	G-quadruplex	antiparallel
ONG10	21	TGGTGTGGGTGTGGTGTGGGT	G-quadruplex	antiparallel
ONG11	11	GTGTGGGTGTG	G-hairpin	-

Table 5: List of NTBS

Chromosome	Start	End	Length	WT coverage
chr1	12050	12549	500	4
chr1	31850	32749	900	3
chr1	38250	38649	400	3
chr1	44050	44249	200	3
chr1	46350	46849	500	3
chr1	56950	57249	300	3
chr1	59350	59649	300	4
chr1	60850	61049	200	3

chr1	61450	61649	200	4
chr1	62050	62549	500	5
chr1	68850	69049	200	3
chr1	69350	69649	300	3
chr1	75150	75449	300	3
chr1	75850	76249	400	3
chr1	83650	83749	100	4
chr1	83950	84249	300	4
chr1	100750	100849	100	3
chr1	106650	107349	700	3
chr1	108050	108449	400	3
chr1	109150	109949	800	3
chr1	112050	112149	100	3
chr1	112250	112449	200	3
chr1	112550	112649	100	4
chr1	113350	113449	100	3
chr1	113550	113649	100	3
chr1	113750	113849	100	3
chr1	114850	114949	100	3
chr1	115250	115749	500	3
chr1	116350	116449	100	3
chr1	119350	119649	300	4
chr1	128850	129049	200	3
chr1	129350	129449	100	3
chr1	130050	130349	300	3
chr1	139950	140449	500	4
chr1	140950	141249	300	3
chr1	142850	142949	100	3
chr1	149650	149749	100	3
chr1	192950	193049	100	5
chr1	194150	194349	200	4

chr1	195050	195349	300	3
chr1	72850	73049	200	5
chr10	62000	62299	300	3
chr10	62900	63099	200	3
chr10	80900	81099	200	3
chr10	93900	94099	200	3
chr10	94200	94599	400	4
chr10	147100	147399	300	4
chr10	166500	166799	300	3
chr10	168200	168399	200	4
chr10	171600	171699	100	3
chr10	178200	178299	100	3
chr10	289500	290099	600	3
chr10	314900	315099	200	3
chr10	315700	316099	400	3
chr10	332600	332799	200	4
chr10	338300	338699	400	4
chr10	361200	361599	400	3
chr10	366200	366299	100	3
chr10	399900	399999	100	3
chr10	411700	411999	300	3
chr10	420100	420299	200	3
chr10	426100	426299	200	3
chr10	443700	443999	300	3
chr10	464300	464599	300	4
chr10	464900	465699	800	5
chr10	466900	466999	100	4
chr10	467200	467699	500	3
chr10	469900	470499	600	3
chr10	519400	519599	200	3
chr10	524000	524199	200	3

chr10	532300	532399	100	3
chr10	547000	547299	300	3
chr10	548700	548799	100	3
chr10	548900	549099	200	3
chr10	555200	555299	100	3
chr10	571000	571099	100	3
chr10	571300	571899	600	3
chr10	573100	573199	100	3
chr10	577900	577999	100	3
chr10	578600	578799	200	3
chr10	595100	595299	200	3
chr10	621200	621499	300	3
chr10	622100	622499	400	4
chr10	623600	624199	600	3
chr10	635600	635799	200	3
chr10	638300	638499	200	4
chr10	663900	664299	400	3
chr10	703900	704099	200	4
chr10	704700	704899	200	4
chr10	714300	714999	700	4
chr10	572100	572299	200	5
chr11	17450	17949	500	4
chr11	23050	23549	500	3
chr11	33950	34149	200	3
chr11	39550	39749	200	3
chr11	101550	101749	200	3
chr11	102750	103249	500	5
chr11	106050	106149	100	4
chr11	108350	108749	400	3
chr11	118050	118149	100	3
chr11	145750	146049	300	3

chr11	164950	165249	300	3
chr11	169650	170849	1200	3
chr11	226750	226949	200	3
chr11	246150	246649	500	3
chr11	275250	275749	500	3
chr11	279150	279449	300	4
chr11	280250	280449	200	3
chr11	283150	283449	300	3
chr11	283550	284049	500	4
chr11	311050	311249	200	3
chr11	327050	327149	100	5
chr11	334350	334649	300	3
chr11	336550	336849	300	3
chr11	339950	340149	200	3
chr11	369750	369849	100	3
chr11	380050	380249	200	4
chr11	380550	380749	200	4
chr11	381350	381449	100	3
chr11	383750	384049	300	3
chr11	387550	387749	200	4
chr11	391750	391949	200	3
chr11	463650	463849	200	4
chr11	464450	464549	100	5
chr11	511750	511849	100	3
chr11	522850	523049	200	3
chr11	524050	524649	600	4
chr11	525950	526149	200	3
chr11	527150	527249	100	3
chr11	527350	528549	1200	3
chr11	528850	529049	200	3
chr11	529150	529349	200	3

chr11	615350	615649	300	3
chr11	635750	636049	300	3
chr11	646750	646849	100	4
chr11	648050	648249	200	3
chr11	259350	259449	100	3
chr12	15000	15099	100	3
chr12	21100	21599	500	3
chr12	95500	95899	400	4
chr12	103700	103899	200	3
chr12	104000	104199	200	3
chr12	105700	105899	200	3
chr12	107100	107399	300	3
chr12	107600	107699	100	3
chr12	113600	113799	200	3
chr12	132400	132499	100	3
chr12	132800	132899	100	4
chr12	178000	178299	300	3
chr12	195900	196099	200	3
chr12	201900	202199	300	3
chr12	233800	234099	300	3
chr12	242700	242799	100	4
chr12	252100	252699	600	3
chr12	259900	260299	400	3
chr12	261800	262099	300	3
chr12	263700	264199	500	3
chr12	324100	324399	300	3
chr12	328400	328499	100	3
chr12	328700	328999	300	4
chr12	340600	340899	300	3
chr12	342200	342399	200	3
chr12	343400	343599	200	4

chr12	351000	351299	300	3
chr12	375000	375399	400	3
chr12	389700	390399	700	3
chr12	411100	411499	400	4
chr12	417900	418199	300	3
chr12	419900	420299	400	3
chr12	440600	441399	800	3
chr12	445900	446499	600	3
chr12	506400	506699	300	3
chr12	511400	511599	200	3
chr12	515600	515799	200	3
chr12	516200	516299	100	4
chr12	535800	535999	200	3
chr12	546700	546799	100	3
chr12	555400	555899	500	4
chr12	567000	567399	400	3
chr12	611800	611999	200	3
chr12	613300	613399	100	3
chr12	647100	648099	1000	3
chr12	659300	659499	200	3
chr12	703500	703799	300	3
chr12	729900	729999	100	3
chr12	736300	737099	800	3
chr12	763900	764099	200	3
chr12	771600	771799	200	3
chr12	778400	778499	100	3
chr12	790900	790999	100	4
chr12	810200	810399	200	3
chr12	814600	814899	300	3
chr12	815100	815299	200	3
chr12	827200	827599	400	4

chr12	829800	829999	200	3
chr12	875700	875999	300	3
chr12	878800	879199	400	4
chr12	879800	880199	400	3
chr12	883400	883499	100	3
chr12	919500	919699	200	3
chr12	923100	923399	300	3
chr12	937700	937999	300	4
chr12	951200	951499	300	4
chr12	954500	954699	200	3
chr12	992100	992199	100	3
chr12	999800	999899	100	3
chr12	1002800	1003099	300	3
chr12	1010700	1010899	200	3
chr12	1011800	1011999	200	3
chr12	1013000	1013199	200	5
chr12	1013300	1013499	200	5
chr12	1013700	1013899	200	3
chr12	1014800	1015299	500	3
chr12	1031900	1032099	200	4
chr12	1038200	1038599	400	4
chr12	806500	806799	300	5
chr12	369200	369399	200	3
chr12	837700	837999	300	3
chr13	16000	16199	200	3
chr13	20100	20299	200	3
chr13	23000	23099	100	3
chr13	45200	45499	300	3
chr13	53400	53499	100	3
chr13	68800	68899	100	3
chr13	86500	86799	300	3

chr13	92200	92499	300	3
chr13	95700	95899	200	3
chr13	100700	100799	100	3
chr13	119800	119999	200	3
chr13	120200	120799	600	4
chr13	123400	123599	200	3
chr13	146800	147099	300	3
chr13	157200	157899	700	3
chr13	162400	162799	400	3
chr13	170800	170999	200	4
chr13	210300	210399	100	3
chr13	222900	223199	300	3
chr13	241900	242299	400	3
chr13	248300	248399	100	4
chr13	250600	250699	100	4
chr13	272200	272699	500	3
chr13	279000	279499	500	4
chr13	282200	282399	200	3
chr13	304900	305199	300	3
chr13	352800	352999	200	4
chr13	354200	354299	100	4
chr13	389400	389599	200	3
chr13	464300	464499	200	3
chr13	470200	470499	300	4
chr13	476800	476899	100	3
chr13	484300	484499	200	3
chr13	484600	484799	200	5
chr13	485000	485199	200	3
chr13	491500	491599	100	3
chr13	493000	493099	100	3
chr13	534300	534499	200	3

chr13	539700	539899	200	4
chr13	546500	546799	300	3
chr13	588500	588799	300	3
chr13	593600	593699	100	3
chr13	624400	624599	200	3
chr13	627100	627699	600	3
chr13	644500	644599	100	3
chr13	667500	667899	400	3
chr13	668000	668199	200	3
chr13	673700	674099	400	5
chr13	676100	676499	400	3
chr13	695800	695899	100	3
chr13	700600	700999	400	3
chr13	702200	702499	300	3
chr13	723000	723099	100	3
chr13	726800	727099	300	3
chr13	735300	735699	400	3
chr13	757700	757799	100	3
chr13	771300	771399	100	3
chr13	818500	818599	100	3
chr13	820400	820699	300	3
chr13	820900	821099	200	3
chr13	859700	859999	300	3
chr13	860200	860299	100	3
chr13	862200	862499	300	3
chr13	873600	873999	400	4
chr13	874100	874199	100	3
chr13	879000	879499	500	3
chr13	888200	888499	300	5
chr13	891100	891399	300	3
chr13	908600	908999	400	4

chr13	911200	911799	600	3
chr13	250400	250599	200	4
chr13	703100	703499	400	3
chr14	26000	26599	600	3
chr14	33700	34399	700	4
chr14	34900	35099	200	3
chr14	36700	36899	200	3
chr14	53500	53599	100	3
chr14	59300	59499	200	3
chr14	65900	66199	300	4
chr14	88400	88899	500	4
chr14	106000	106099	100	3
chr14	109700	109799	100	3
chr14	115400	115999	600	3
chr14	118000	118299	300	3
chr14	172900	173199	300	3
chr14	173300	173499	200	3
chr14	187900	187999	100	3
chr14	188400	188599	200	3
chr14	189900	190399	500	3
chr14	190600	190699	100	3
chr14	195500	195799	300	3
chr14	199000	199499	500	5
chr14	242200	242399	200	3
chr14	268000	268399	400	3
chr14	275000	275099	100	4
chr14	318200	318499	300	3
chr14	344100	344299	200	3
chr14	346000	346099	100	3
chr14	347500	347799	300	3
chr14	350500	350599	100	3

chr14	358000	358699	700	3
chr14	367800	367899	100	3
chr14	391300	391599	300	3
chr14	394100	394199	100	4
chr14	408900	409099	200	3
chr14	414000	414299	300	4
chr14	414400	414599	200	3
chr14	428000	428199	200	3
chr14	477100	477299	200	3
chr14	477500	477599	100	3
chr14	477700	477999	300	3
chr14	480000	480299	300	3
chr14	489500	489699	200	3
chr14	490600	490699	100	3
chr14	491900	492499	600	3
chr14	504200	504599	400	3
chr14	506400	506599	200	3
chr14	518600	518799	200	3
chr14	530100	530399	300	3
chr14	531100	531299	200	4
chr14	558300	558399	100	3
chr14	579900	579999	100	4
chr14	603800	604099	300	3
chr14	642000	642199	200	3
chr14	651200	651299	100	3
chr14	653700	653899	200	3
chr14	654800	654999	200	3
chr14	655600	656299	700	4
chr14	664600	664899	300	3
chr14	693800	694099	300	3
chr14	694700	694899	200	3

chr14	704400	704599	200	4
chr14	707600	707899	300	3
chr14	709000	709199	200	3
chr14	715200	715399	200	3
chr14	733600	733799	200	3
chr14	570700	571299	600	4
chr15	20050	20149	100	3
chr15	20750	21049	300	3
chr15	30250	30449	200	5
chr15	34750	35149	400	3
chr15	54050	54349	300	3
chr15	74550	74949	400	3
chr15	75250	75349	100	3
chr15	80650	80749	100	3
chr15	162450	162649	200	3
chr15	197650	197949	300	3
chr15	198250	198549	300	3
chr15	202250	202349	100	3
chr15	203450	204049	600	3
chr15	207550	207849	300	3
chr15	212650	212849	200	3
chr15	213050	213249	200	3
chr15	219650	219849	200	3
chr15	254450	254749	300	4
chr15	268950	269749	800	3
chr15	286850	286949	100	3
chr15	290050	290149	100	4
chr15	318650	319149	500	3
chr15	341450	341949	500	3
chr15	344650	344949	300	3
chr15	346650	346749	100	4

chr15	377350	377549	200	3
chr15	381850	382149	300	3
chr15	409250	409449	200	3
chr15	428050	428449	400	3
chr15	455950	456249	300	3
chr15	457350	457449	100	3
chr15	460450	460649	200	3
chr15	479850	480149	300	4
chr15	482750	482849	100	3
chr15	493750	494049	300	3
chr15	509450	509649	200	3
chr15	536650	536849	200	4
chr15	542850	543449	600	3
chr15	559350	559749	400	3
chr15	588750	589049	300	3
chr15	622950	623349	400	3
chr15	628550	628849	300	3
chr15	677050	677849	800	4
chr15	688850	688949	100	3
chr15	761950	762149	200	3
chr15	771450	771549	100	3
chr15	798150	798449	300	4
chr15	805950	806049	100	3
chr15	829450	829549	100	3
chr15	831550	831749	200	3
chr15	833850	834049	200	4
chr15	861450	861649	200	3
chr15	863050	863249	200	3
chr15	880050	880149	100	3
chr15	919750	919849	100	3
chr15	921750	921949	200	3

chr15	925950	926049	100	3
chr15	942850	942949	100	4
chr15	956250	956649	400	3
chr15	1008350	1008549	200	3
chr15	1011350	1011749	400	4
chr15	1018050	1018349	300	3
chr15	1018650	1018849	200	3
chr15	1060550	1060749	200	4
chr15	1069750	1069949	200	3
chr15	480950	481049	100	5
chr15	344950	345349	400	5
chr15	29750	29949	200	4
chr15	236250	236449	200	4
chr15	271150	271249	100	4
chr16	47600	48599	1000	3
chr16	75600	76199	600	3
chr16	83700	84499	800	3
chr16	107700	107899	200	3
chr16	111700	113099	1400	3
chr16	115800	115999	200	3
chr16	124500	124999	500	3
chr16	133300	133899	600	3
chr16	203700	203999	300	3
chr16	226900	227199	300	3
chr16	228900	229199	300	4
chr16	266400	266699	300	3
chr16	278200	278999	800	3
chr16	296200	296399	200	3
chr16	303400	303599	200	4
chr16	311000	311399	400	3
chr16	350800	350899	100	3

chr16	371600	371999	400	4
chr16	372400	372799	400	3
chr16	380300	380399	100	3
chr16	387200	387399	200	4
chr16	389200	389699	500	3
chr16	393400	393899	500	3
chr16	464600	464999	400	3
chr16	498400	498499	100	3
chr16	505000	505499	500	3
chr16	539400	539499	100	3
chr16	553600	553699	100	3
chr16	574600	574699	100	3
chr16	610900	611099	200	3
chr16	628200	628299	100	3
chr16	642800	642899	100	4
chr16	644500	644999	500	5
chr16	646700	646899	200	3
chr16	647500	647699	200	3
chr16	649400	649799	400	3
chr16	665600	665799	200	3
chr16	752900	752999	100	3
chr16	753500	753699	200	3
chr16	811000	811299	300	4
chr16	830000	830199	200	5
chr16	832200	832499	300	4
chr16	869300	869799	500	3
chr16	875700	875899	200	3
chr16	886500	886599	100	3
chr16	893300	893399	100	4
chr16	898500	898799	300	3
chr16	899000	899599	600	3

chr16	900300	900499	200	3
chr16	900700	901299	600	3
chr16	433800	433899	100	4
chr2	67600	67699	100	3
chr2	68400	68699	300	3
chr2	70100	70299	200	3
chr2	70900	71199	300	4
chr2	72200	72299	100	3
chr2	72600	72999	400	4
chr2	81300	81499	200	3
chr2	106000	106199	200	3
chr2	122800	123299	500	3
chr2	130600	130799	200	3
chr2	145400	145499	100	3
chr2	163700	164099	400	3
chr2	169100	169299	200	4
chr2	178100	178399	300	3
chr2	180300	180499	200	3
chr2	181700	181999	300	3
chr2	182700	183099	400	3
chr2	202500	202799	300	3
chr2	215700	215799	100	3
chr2	235600	235899	300	5
chr2	257800	257899	100	3
chr2	268300	268499	200	3
chr2	269800	270399	600	3
chr2	299900	300399	500	3
chr2	309700	309899	200	3
chr2	334800	335099	300	3
chr2	377500	378199	700	4
chr2	380500	380799	300	3

chr2	382500	382599	100	3
chr2	389000	389199	200	3
chr2	393400	394199	800	3
chr2	395500	395699	200	4
chr2	412500	412599	100	3
chr2	414300	414499	200	5
chr2	428600	428699	100	4
chr2	429800	430599	800	3
chr2	455300	455499	200	3
chr2	463000	463799	800	4
chr2	475400	475499	100	3
chr2	482400	482599	200	3
chr2	482800	482999	200	3
chr2	492200	492599	400	3
chr2	503600	504199	600	3
chr2	563600	563799	200	4
chr2	564000	564099	100	4
chr2	577700	577799	100	3
chr2	612500	612899	400	3
chr2	613500	613699	200	3
chr2	616400	616699	300	3
chr2	639800	639899	100	3
chr2	660400	660999	600	3
chr2	661700	661999	300	3
chr2	699200	699799	600	3
chr2	701600	701899	300	3
chr2	703200	703299	100	4
chr2	703600	703999	400	3
chr2	734900	735999	1100	3
chr2	736500	737099	600	3
chr2	739000	739299	300	3

chr2	740100	740799	700	3
chr2	775800	776199	400	3
chr2	777300	777399	100	3
chr2	780400	780599	200	3
chr2	782100	782299	200	3
chr2	464000	464199	200	5
chr2	128400	128599	200	3
chr3	28700	28899	200	3
chr3	32600	32899	300	3
chr3	49000	49999	1000	3
chr3	50700	51199	500	5
chr3	53900	54099	200	3
chr3	60400	60599	200	3
chr3	63000	63299	300	4
chr3	66400	66799	400	3
chr3	69600	69799	200	3
chr3	70800	71199	400	4
chr3	77400	77699	300	3
chr3	93100	93699	600	3
chr3	102100	102499	400	4
chr3	104800	105199	400	4
chr3	106000	106299	300	3
chr3	156200	156499	300	3
chr3	164500	164599	100	3
chr3	189800	190199	400	3
chr3	209300	209499	200	3
chr3	210700	211399	700	3
chr3	212000	212299	300	3
chr3	213100	213299	200	3
chr3	214000	214299	300	4
chr3	216400	216699	300	3

chr3	216800	216999	200	3
chr3	222000	222599	600	3
chr3	226300	226399	100	3
chr3	226600	226899	300	4
chr3	242600	243499	900	3
chr3	249500	249799	300	4
chr3	251500	251899	400	4
chr3	253600	253899	300	3
chr3	266200	266499	300	3
chr3	268800	269099	300	3
chr3	269900	269999	100	3
chr3	271800	271899	100	3
chr3	279500	279699	200	3
chr3	283400	283599	200	3
chr3	304400	304599	200	4
chr3	226400	226599	200	4
chr3	11300	11799	500	3
chr4	18000	18199	200	3
chr4	43200	43299	100	3
chr4	54800	55199	400	3
chr4	59800	60099	300	3
chr4	62700	62999	300	4
chr4	67000	67199	200	4
chr4	122900	123199	300	3
chr4	125900	126299	400	3
chr4	133800	133999	200	3
chr4	145900	146199	300	3
chr4	148400	148699	300	3
chr4	149300	149899	600	3
chr4	151200	151399	200	3
chr4	151500	151599	100	3

chr4	176100	176199	100	3
chr4	195600	195799	200	3
chr4	197400	197599	200	3
chr4	206000	206599	600	5
chr4	231200	231599	400	3
chr4	265600	265699	100	3
chr4	285900	286499	600	3
chr4	288000	288299	300	4
chr4	301900	301999	100	3
chr4	342900	343299	400	3
chr4	351900	352099	200	3
chr4	384600	384999	400	3
chr4	390400	390499	100	3
chr4	393300	393499	200	3
chr4	458500	458799	300	3
chr4	461200	461499	300	3
chr4	484500	484799	300	4
chr4	526100	526299	200	3
chr4	546900	547099	200	3
chr4	550000	550199	200	3
chr4	564100	564499	400	3
chr4	601700	601799	100	3
chr4	633600	634199	600	3
chr4	635900	636199	300	3
chr4	677800	677999	200	3
chr4	692500	692699	200	3
chr4	695000	695299	300	3
chr4	697700	697999	300	4
chr4	709000	709099	100	3
chr4	724600	724699	100	3
chr4	742300	742599	300	3

chr4	743100	743199	100	3
chr4	759500	759699	200	3
chr4	768400	768899	500	3
chr4	806600	807099	500	3
chr4	808600	808799	200	3
chr4	809600	809899	300	3
chr4	834200	834399	200	3
chr4	836900	837799	900	5
chr4	842800	842899	100	3
chr4	864500	864699	200	5
chr4	867400	867599	200	3
chr4	868500	868699	200	3
chr4	927900	928099	200	4
chr4	928700	928899	200	3
chr4	931500	932099	600	3
chr4	932200	932699	500	3
chr4	939300	939399	100	3
chr4	955400	955699	300	3
chr4	968500	968699	200	3
chr4	1002800	1003199	400	3
chr4	1024200	1024399	200	3
chr4	1089300	1089699	400	3
chr4	1183600	1183799	200	4
chr4	1237500	1238099	600	4
chr4	1239400	1239999	600	3
chr4	1253400	1253799	400	4
chr4	1280400	1280499	100	4
chr4	1291600	1291699	100	4
chr4	1293300	1293499	200	3
chr4	1307200	1307299	100	3
chr4	1335600	1335799	200	3

chr4	1344300	1344599	300	5
chr4	1345900	1346099	200	3
chr4	1410400	1410699	300	3
chr4	1413000	1413099	100	3
chr4	1419600	1419899	300	3
chr4	1429500	1430199	700	3
chr4	1442800	1442999	200	3
chr4	1444800	1445299	500	3
chr4	1460100	1460299	200	3
chr4	1467300	1467599	300	3
chr4	1467800	1467899	100	3
chr4	1475300	1475399	100	3
chr4	1478100	1478299	200	5
chr4	1308400	1308599	200	5
chr4	1307700	1307999	300	5
chr5	43500	43699	200	4
chr5	44000	44199	200	4
chr5	49300	49399	100	3
chr5	52800	53099	300	3
chr5	72900	73099	200	3
chr5	79000	79499	500	5
chr5	81500	82299	800	3
chr5	86900	87299	400	3
chr5	119000	119199	200	3
chr5	159900	160099	200	3
chr5	190100	190199	100	3
chr5	236000	236299	300	3
chr5	236800	236999	200	4
chr5	257400	257499	100	3
chr5	265300	265399	100	4
chr5	268000	268199	200	3

chr5	280500	280599	100	4
chr5	285600	286199	600	3
chr5	323500	323699	200	3
chr5	333600	333699	100	3
chr5	333800	334199	400	4
chr5	334400	335699	1300	3
chr5	340200	340699	500	4
chr5	341400	341599	200	3
chr5	350800	351099	300	3
chr5	379600	379899	300	3
chr5	381600	381899	300	3
chr5	413800	413899	100	3
chr5	425000	425399	400	3
chr5	427800	428099	300	3
chr5	460900	461199	300	3
chr5	464000	464399	400	3
chr5	468700	468799	100	3
chr5	475200	475499	300	5
chr5	475600	475799	200	3
chr5	511500	511899	400	3
chr5	544900	544999	100	4
chr5	545200	545499	300	3
chr5	546100	546199	100	3
chr6	34800	34999	200	3
chr6	35200	35599	400	3
chr6	44900	45399	500	3
chr6	52600	52899	300	3
chr6	56400	57199	800	3
chr6	72300	72799	500	3
chr6	75300	75799	500	4
chr6	76600	76999	400	3

chr6	91400	91799	400	3
chr6	93800	94399	600	5
chr6	105300	105499	200	5
chr6	112500	112699	200	3
chr6	163600	163799	200	3
chr6	189200	189399	200	3
chr6	195700	195899	200	3
chr6	208500	208799	300	3
chr6	210700	211399	700	3
chr6	211500	211699	200	3
chr6	223400	223699	300	3
chr6	224300	224899	600	4
chr6	227700	228199	500	3
chr6	228600	228799	200	3
chr6	240600	240899	300	4
chr6	248900	248999	100	3
chr6	250200	250499	300	3
chr6	115400	115499	100	3
chr7	10250	10849	600	3
chr7	22950	23149	200	3
chr7	24150	24849	700	3
chr7	40250	40649	400	3
chr7	41950	42349	400	3
chr7	54950	55149	200	4
chr7	55550	55649	100	3
chr7	57250	57349	100	3
chr7	57950	58149	200	3
chr7	75150	75349	200	3
chr7	83450	83749	300	3
chr7	85550	85849	300	3
chr7	92050	92149	100	3

chr7	93350	93549	200	3
chr7	108750	109049	300	3
chr7	143650	143749	100	3
chr7	189450	189549	100	3
chr7	191550	191749	200	3
chr7	198450	198749	300	3
chr7	225050	225249	200	3
chr7	227150	227349	200	3
chr7	270450	270649	200	4
chr7	271150	271849	700	4
chr7	272850	273249	400	4
chr7	273950	274049	100	3
chr7	279550	279749	200	3
chr7	308250	308649	400	3
chr7	364150	364649	500	3
chr7	372250	372549	300	3
chr7	378950	379149	200	4
chr7	379250	379449	200	3
chr7	383850	384049	200	4
chr7	384350	384549	200	4
chr7	387250	387549	300	3
chr7	398950	399549	600	3
chr7	417850	418249	400	3
chr7	431450	431949	500	3
chr7	442650	442849	200	3
chr7	447550	448049	500	3
chr7	450450	450849	400	4
chr7	451150	451349	200	3
chr7	453250	454149	900	3
chr7	458350	458649	300	3
chr7	473850	473949	100	3

chr7	492950	493149	200	3
chr7	495650	495849	200	3
chr7	516050	516149	100	3
chr7	517250	518049	800	4
chr7	519050	519349	300	4
chr7	519450	519849	400	4
chr7	519950	520349	400	4
chr7	529250	529849	600	4
chr7	547150	547449	300	3
chr7	575950	576149	200	3
chr7	583550	583649	100	3
chr7	598050	598249	200	3
chr7	612250	612349	100	3
chr7	613150	613749	600	4
chr7	616350	616649	300	3
chr7	640850	641049	200	3
chr7	641150	641349	200	4
chr7	646450	646649	200	3
chr7	651650	651849	200	3
chr7	673250	673349	100	3
chr7	740250	740549	300	3
chr7	741050	741649	600	3
chr7	755950	756449	500	3
chr7	798850	799149	300	3
chr7	835350	835549	200	3
chr7	847550	848449	900	3
chr7	890550	890849	300	3
chr7	900950	901149	200	3
chr7	906150	906449	300	4
chr7	906750	907049	300	4
chr7	908150	908749	600	3

chr7	914250	914749	500	3
chr7	916250	916449	200	3
chr7	921450	921649	200	4
chr7	940750	941249	500	4
chr7	960350	960549	200	3
chr7	960650	960749	100	3
chr7	971050	971149	100	4
chr7	980050	980349	300	3
chr7	1004950	1005049	100	3
chr7	1009450	1009549	100	3
chr7	1009650	1009949	300	3
chr7	1048950	1049749	800	4
chr7	1051250	1051549	300	3
chr7	1058150	1058449	300	3
chr7	1064150	1064549	400	3
chr7	1068050	1068649	600	3
chr7	279950	280249	300	5
chr8	24700	25299	600	3
chr8	33700	33999	300	3
chr8	36900	37399	500	4
chr8	37600	37899	300	3
chr8	39100	39399	300	3
chr8	47800	47899	100	3
chr8	49600	49899	300	3
chr8	51400	51599	200	3
chr8	52300	52599	300	4
chr8	75700	75999	300	3
chr8	95700	95899	200	3
chr8	96100	96299	200	3
chr8	99400	99999	600	3
chr8	120400	120599	200	3

chr8	121000	121299	300	4
chr8	123200	123399	200	4
chr8	124900	125099	200	3
chr8	125200	125499	300	3
chr8	140800	141099	300	4
chr8	142500	143099	600	4
chr8	144700	145099	400	5
chr8	158900	158999	100	3
chr8	160000	160299	300	3
chr8	161800	162199	400	4
chr8	169300	169599	300	3
chr8	173700	173899	200	3
chr8	175500	175899	400	3
chr8	176100	176299	200	3
chr8	177600	177799	200	3
chr8	187200	187399	200	3
chr8	189000	189199	200	3
chr8	191000	191699	700	3
chr8	219600	219699	100	3
chr8	225900	225999	100	4
chr8	235400	235499	100	4
chr8	235800	235999	200	4
chr8	236100	236199	100	4
chr8	247200	247299	100	3
chr8	247400	247599	200	3
chr8	272900	273399	500	3
chr8	282700	282899	200	3
chr8	295000	295099	100	3
chr8	311000	311299	300	4
chr8	313100	313499	400	4
chr8	318700	319399	700	3

chr8	329500	329599	100	3
chr8	337000	337199	200	3
chr8	341100	341499	400	3
chr8	363600	363799	200	3
chr8	371000	371099	100	3
chr8	385700	385999	300	3
chr8	418000	418099	100	3
chr8	420700	420999	300	3
chr8	421700	422099	400	3
chr8	457700	457799	100	3
chr8	472400	472499	100	3
chr8	476600	476799	200	3
chr8	483500	483999	500	3
chr8	484200	484599	400	3
chr8	484800	484999	200	3
chr8	485600	485799	200	3
chr8	498200	498599	400	4
chr8	499400	499999	600	3
chr8	500300	500499	200	3
chr8	511600	511899	300	3
chr8	517800	517999	200	3
chr8	189400	189599	200	5
chr9	25800	26199	400	3
chr9	48600	48699	100	4
chr9	76700	77099	400	3
chr9	83000	83099	100	3
chr9	84100	84299	200	3
chr9	84500	84599	100	3
chr9	95100	95599	500	3
chr9	100800	100999	200	3
chr9	128800	129599	800	5

chr9	131400	131499	100	3
chr9	157900	158099	200	3
chr9	159600	159899	300	3
chr9	161400	161899	500	3
chr9	169100	169299	200	3
chr9	176900	176999	100	3
chr9	178300	178799	500	3
chr9	179100	179299	200	3
chr9	179900	180099	200	3
chr9	192700	192999	300	3
chr9	218700	218999	300	4
chr9	255300	255699	400	5
chr9	267500	267699	200	5
chr9	269500	270499	1000	4
chr9	274400	274599	200	3
chr9	275600	275899	300	3
chr9	276000	276099	100	3
chr9	286000	286099	100	3
chr9	286900	286999	100	3
chr9	292800	293099	300	3
chr9	317200	317299	100	3
chr9	365800	365899	100	3
chr9	366200	366399	200	3
chr9	371700	371999	300	3
chr9	378600	378799	200	3
chr9	378900	379099	200	3
chr9	383400	383599	200	3
chr9	383800	383899	100	4
chr9	389400	390199	800	3
chr9	390300	390899	600	3
chr9	392800	393399	600	3

chr9	398100	398299	200	3
chr9	409300	409399	100	3
chr9	413500	413699	200	3
chr9	414500	414599	100	3
chr9	421300	421599	300	4
chr9	422400	422699	300	3
chr9	392500	392799	300	5
chr9	54500	54899	400	4
chr9	23500	24099	600	4
chr9	25600	25699	100	4
chr9	128300	128399	100	4
chr9	159900	159999	100	4

Table 6: Zuo1.Myc Mass spectrometry associated proteins

Accession	Description	Abundance ratio: Zuo1MYC/ WT	Coverage [%]	Score Mascot	Ensemble Gene ID
P40961	Prohibitin-1 OS= <i>Saccharomyces cerevisiae</i> (strain ATCC 204508 / S288c)	100	6	31	YGR132C
P53551	Histone H1 OS= <i>Saccharomyces cerevisiae</i> (strain ATCC 204508 / S288c)	100	12	69	YPL127C
P49723	Ribonucleoside-diphosphate reductase small chain 2	100	8	80	YGR180C
P25491	Mitochondrial protein import protein MAS5 OS= <i>Saccharomyces cerevisiae</i> (strain ATCC 204508 / S288c)	100	12	36	YNL064C
P22202	Heat shock protein SSA4 OS= <i>Saccharomyces cerevisiae</i> (strain ATCC 204508 / S288c)	100	16	942	YER103W

P32466	Low-affinity glucose transporter HXT3 OS= <i>Saccharomyces cerevisiae</i> (strain ATCC 204508 / S288c)	100	5	91	YDR345C
P20967	2-oxoglutarate dehydrogenase, mitochondrial OS= <i>Saccharomyces cerevisiae</i> (strain ATCC 204508 / S288c)	100	4	32	YIL125W
P32527	Zuotin OS= <i>Saccharomyces cerevisiae</i> (strain ATCC 204508 / S288c)	100	64	2325	YGR285C
P07257	Cytochrome b-c1 complex subunit 2, mitochondrial OS= <i>Saccharomyces cerevisiae</i> (strain ATCC 204508 / S288c)	100	10	182	YPR191W
P36008	Elongation factor 1-gamma 2 OS= <i>Saccharomyces cerevisiae</i> (strain ATCC 204508 / S288c)	100	10	245	YKL081W
Q12230	Sphingolipid long chain base-responsive protein LSP1 OS= <i>Saccharomyces cerevisiae</i> (strain ATCC 204508 / S288c)	100	10	86	YPL004C
P41940	Mannose-1-phosphate guanyltransferase OS= <i>Saccharomyces cerevisiae</i> (strain ATCC 204508 / S288c)	100	9	148	YDL055C
P00815	Histidine biosynthesis trifunctional protein OS= <i>Saccharomyces cerevisiae</i> (strain ATCC 204508 / S288c)	100	4	0	YCL030C
P25605	Acetolactate synthase small subunit, mitochondrial OS= <i>Saccharomyces cerevisiae</i> (strain ATCC 204508 / S288c)	100	22	222	YCL009C

P40531	Protein GVP36 OS= <i>Saccharomyces cerevisiae</i> (strain ATCC 204508 / S288c)	100	7	66	YIL041W
P39015	Suppressor protein STM1 OS= <i>Saccharomyces cerevisiae</i> (strain ATCC 204508 / S288c)	100	16	138	YLR150W
P36421	Tyrosine—tRNA ligase, cytoplasmic OS= <i>Saccharomyces cerevisiae</i> (strain ATCC 204508 / S288c)	100	9	105	YGR185C
P25087	Sterol 24-C-methyltransferase OS= <i>Saccharomyces cerevisiae</i> (strain ATCC 204508 / S288c)	100	8	13	YML008C
P00359	Glyceraldehyde-3-phosphate dehydrogenase 3 OS= <i>Saccharomyces cerevisiae</i> (strain ATCC 204508 / S288c)	100	37	4584	YGR192C

9. References

- A, G., BG, B., H, B., RW, D., B, D., H, F., F, G., JD, H., C, J., M, J., EJ, L., HW, M., Y, M., P, P., H, T., SG, O., 1996. Life with 6000 genes. *Science* 274, 546–567. <https://doi.org/10.1126/SCIENCE.274.5287.546>
- A, T., A, N., 2017. Endogenous DNA Damage as a Source of Genomic Instability in Cancer. *Cell* 168, 644–656. <https://doi.org/10.1016/J.CELL.2017.01.002>
- Abdallah, P., Luciano, P., Runge, K.W., Lisby, M., Géli, V., Gilson, E., Teixeira, M.T., 2009. A two-step model for senescence triggered by a single critically short telomere. *Nat. Cell Biol.* 2009 118 11, 988–993. <https://doi.org/10.1038/ncb1911>
- AK, T., M, J., S, N., 2005. Highly prevalent putative quadruplex sequence motifs in human DNA. *Nucleic Acids Res.* 33, 2901–2907. <https://doi.org/10.1093/NAR/GKI553>
- AM, B., F, D., CM, S., AP, R., MJ, M., JA, D., S, N., 2005. The G-quadruplex-interactive molecule BRACO-19 inhibits tumor growth, consistent with telomere targeting and interference with telomerase function. *Cancer Res.* 65, 1489–1496. <https://doi.org/10.1158/0008-5472.CAN-04-2910>
- Anbalagan, S., Bonetti, D., Lucchini, G., Longhese, M.P., 2011. Rif1 supports the function of the CST complex in yeast telomere capping. *PLoS Genet.* 7, 1002024. <https://doi.org/10.1371/journal.pgen.1002024>
- and, A.T.P., Patel, D.J., 2003. Two-Repeat Human Telomeric d(TAGGGTTAGGGT) Sequence Forms Interconverting Parallel and Antiparallel G-Quadruplexes in Solution: Distinct Topologies, Thermodynamic Properties, and Folding/Unfolding Kinetics. *J. Am. Chem. Soc.* 125, 15021–15027. <https://doi.org/10.1021/JA037616J>
- Anderson, E.M., Halsey, W.A., Wuttke, D.S., 2002. Delineation of the high-affinity single-stranded telomeric DNA-binding domain of *Saccharomyces cerevisiae* Cdc13. *Nucleic Acids Res.* 30, 4305–4313. <https://doi.org/10.1093/NAR/GKF554>
- Anne De Cian, ‡, Elsa DeLemos, †, Jean-Louis Mergny, ‡, Marie-Paule Teulade-Fichou, *,† and, Monchaud†, D., 2007. Highly Efficient G-Quadruplex Recognition by Bisquinolinium Compounds. *J. Am. Chem. Soc.* 129, 1856–1857. <https://doi.org/10.1021/JA067352B>

- Aparicio, O.M., Billington, B.L., Gottschling, D.E., 1991. Modifiers of Position Effect Are Shared between Telomeric and Silent Mating-Type Loci in *S. cerevisiae*, *Cell*.
- Arora, R., Lee, Y., Wischnewski, H., Brun, C.M., Schwarz, T., Azzalin, C.M., 2014. RNaseH1 regulates TERRA-telomeric DNA hybrids and telomere maintenance in ALT tumour cells. *Nat. Commun.* 5, 5220. <https://doi.org/10.1038/ncomms6220>
- B, K., MT, T., P, L., N, E.-B., SM, G., MN, S., I, G., P, A., E, G., V, G., M, L., 2009. The DNA damage response at eroded telomeres and tethering to the nuclear pore complex. *Nat. Cell Biol.* 11, 980–987. <https://doi.org/10.1038/NCB1910>
- Balk, B., Maicher, A., Dees, M., Klermund, J., Luke-Glaser, S., Bender, K., Luke, B., 2013. Telomeric RNA-DNA hybrids affect telomere-length dynamics and senescence. *Nat. Struct. Mol. Biol.* 20, 1199–1205. <https://doi.org/10.1038/nsmb.2662>
- Beauvarlet, J., Bensadoun, P., Darbo, E., Labrunie, G., Rousseau, B., Richard, E., Draskovic, I., Londono-Vallejo, A., Dupuy, J.-W., Nath Das, R., Guédin, A., Robert, G., Orange, F., Croce, S., Valesco, V., Soubeyran, P., Ryan, K.M., Mergny, J.-L., Djavaheri-Mergny, M., 2019. Modulation of the ATM/autophagy pathway by a G-quadruplex ligand tips the balance between senescence and apoptosis in cancer cells. *Nucleic Acids Res.* 47, 2739. <https://doi.org/10.1093/NAR/GKZ095>
- Belaghzal, H., Dekker, J., Gibcus, J.H., 2017. Hi-C 2.0: An optimized Hi-C procedure for high-resolution genome-wide mapping of chromosome conformation. *Methods* 123, 56–65. <https://doi.org/10.1016/j.ymeth.2017.04.004>
- Belton, J.M., Dekker, J., 2015. Hi-C in Budding Yeast. *Cold Spring Harb Protoc* 2015, 649–661. <https://doi.org/10.1101/pdb.prot085209>
- Bernstein, B.E., Tong, J.K., Schreiber, S.L., 2000. Genomewide studies of histone deacetylase function in yeast. *Proc Natl Acad Sci U S A* 97, 13708–13713. <https://doi.org/10.1073/pnas.250477697>
- Bianchi, A., Negrini, S., Shore, D., 2004. Delivery of Yeast Telomerase to a DNA Break Depends on the Recruitment Functions of Cdc13 and Est1. *Mol. Cell* 16. <https://doi.org/10.1016/J.MOLCEL.2004.09.009>
- Bianchi, A., Shore, D., 2007. Increased association of telomerase with short telomeres in

- yeast. *Genes Dev.* 21, 1726–1730. <https://doi.org/10.1101/GAD.438907>
- Biffi, G., Tannahill, D., McCafferty, J., Balasubramanian, S., 2013. Quantitative visualization of DNA G-quadruplex structures in human cells. *Nat. Chem.* 5, 182. <https://doi.org/10.1038/nchem.1548>
- Bochman, M.L., Paeschke, K., Zakian, V.A., 2012. DNA secondary structures: stability and function of G-quadruplex structures. *Nat. Rev. Genet.* 2012 1311 13, 770–780. <https://doi.org/10.1038/nrg3296>
- Bonaglia, M.C., Giorda, R., Beri, S., Agostini, C. De, Novara, F., Fichera, M., Grillo, L., Galesi, O., Vetro, A., Ciccone, R., Bonati, M.T., Giglio, S., Guerrini, R., Osimani, S., Marelli, S., Zucca, C., Grasso, R., Borgatti, R., Mani, E., Motta, C., Molteni, M., Romano, C., Greco, D., Reitano, S., Baroncini, A., Lapi, E., Cecconi, A., Arrigo, G., Patricelli, M.G., Pantaleoni, C., D'Arrigo, S., Riva, D., Sciacca, F., Bernardina, B.D., Zoccante, L., Darra, F., Termine, C., Maserati, E., Bigoni, S., Priolo, E., Bottani, A., Gimelli, S., Bena, F., Brusco, A., Gregorio, E. di, Bagnasco, I., Giussani, U., Nitsch, L., Politi, P., Martínez-Frias, M.L., Martínez-Fernández, M.L., Guardia, N.M., Bremer, A., Anderlid, B.-M., Zuffardi, O., 2011. Molecular Mechanisms Generating and Stabilizing Terminal 22q13 Deletions in 44 Subjects with Phelan/McDermid Syndrome. *PLOS Genet.* 7, e1002173. <https://doi.org/10.1371/JOURNAL.PGEN.1002173>
- Bonetti, D., Clerici, M., Anbalagan, S., Martina, M., Lucchini, G., Longhese, M.P., 2010. Shelterin-Like Proteins and Yku Inhibit Nucleolytic Processing of *Saccharomyces cerevisiae* Telomeres. *PLOS Genet.* 6, e1000966. <https://doi.org/10.1371/JOURNAL.PGEN.1000966>
- Bonetti, D., Martina, M., Clerici, M., Lucchini, G., Longhese, M.P., 2009. Multiple Pathways Regulate 3' Overhang Generation at *S. cerevisiae* Telomeres. *Mol. Cell* 35, 70–81. <https://doi.org/10.1016/J.MOLCEL.2009.05.015>
- Bonetti, D., Rinaldi, C., Vertemara, J., Notaro, M., Pizzul, P., Tisi, R., Zampella, G., Longhese, M.P., 2020. DNA binding modes influence Rap1 activity in the regulation of telomere length and MRX functions at DNA ends. *Nucleic Acids Res.* 48, 2424–2441.

- Boulé, J.-B., Zakian, V.A., 2006. Roles of Pif1-like helicases in the maintenance of genomic stability. *Nucleic Acids Res.* 34, 4147–4153. <https://doi.org/10.1093/NAR/GKL561>
- Boule, J.B., Vega, L.R., Zakian, V.A., 2005. The yeast Pif1p helicase removes telomerase from telomeric DNA. *Nature* 438, 57–61. <https://doi.org/10.1038/nature04091>
- Boulton, S.J., Jackson, S.P., 1998. Components of the Ku-dependent non-homologous end-joining pathway are involved in telomeric length maintenance and telomeric silencing. *EMBO J.* 17, 1819. <https://doi.org/10.1093/EMBOJ/17.6.1819>
- Buck, M.J., Nobel, A.B., Lieb, J.D., 2005. ChIPOTle: a user-friendly tool for the analysis of ChIP-chip data, *Genome Biology*. BioMed Central. <https://doi.org/10.1186/GB-2005-6-11-R97>
- Capra, J.A., Paeschke, K., Singh, M., Zakian, V.A., 2010. G-Quadruplex DNA Sequences Are Evolutionarily Conserved and Associated with Distinct Genomic Features in *Saccharomyces cerevisiae*. *PLoS Comput. Biol.* 6, e1000861. <https://doi.org/10.1371/journal.pcbi.1000861>
- Cerritelli, S.M., Crouch, R.J., 2009. Ribonuclease H: the enzymes in eukaryotes. *FEBS J* 276, 1494–1505. <https://doi.org/10.1111/j.1742-4658.2009.06908.x>
- Chambers, V.S., Marsico, G., Boutell, J.M., Di Antonio, M., Smith, G.P., Balasubramanian, S., 2015. High-throughput sequencing of DNA G-quadruplex structures in the human genome 33, 877–881. <https://doi.org/10.1038/nbt.3295>
- Chan, A., Boule, J.B., Zakian, V.A., Boulé, J.-B., Zakian, V.A., 2008. Two pathways recruit telomerase to *Saccharomyces cerevisiae* telomeres. *PLoS Genet* 4, e1000236. <https://doi.org/10.1371/journal.pgen.1000236>
- Chan, C.S.M., Tye, B.K., Herskowitz, I., 1983. A family of *Saccharomyces cerevisiae* repetitive autonomously replicating sequences that have very similar genomic environments. *J. Mol. Biol.* 168, 505–523. [https://doi.org/10.1016/S0022-2836\(83\)80299-X](https://doi.org/10.1016/S0022-2836(83)80299-X)
- Chan, Y.A., Aristizabal, M.J., Lu, P.Y.T., Luo, Z., Hamza, A., Kobor, M.S., Stirling, P.C., Hieter, P., 2014. Genome-Wide Profiling of Yeast DNA:RNA Hybrid Prone Sites with

- DRIP-Chip. PLoS Genet. 10, e1004288.
<https://doi.org/10.1371/journal.pgen.1004288>
- Chandra, A., Hughes, T.R., Nugent, C.I., Lundblad, V., 2001. Cdc13 both positively and negatively regulates telomere replication. *Genes Dev.* 15, 404.
<https://doi.org/10.1101/GAD.861001>
- Chang, M., Arneric, M., Lingner, J., 2007. Telomerase repeat addition processivity is increased at critically short telomeres in a Tel1-dependent manner in *Saccharomyces cerevisiae*. *Genes Dev.* 21, 2485–94. <https://doi.org/10.1101/gad.1588807>
- Chen, H., Xue, J., Churikov, D., Hass, E.P., Shi, S., Lemon, L.D., Luciano, P., Bertuch, A.A., Zappulla, D.C., Geli, V., Wu, J., Lei, M., 2018. Structural Insights into Yeast Telomerase Recruitment to Telomeres. *Cell* 172, 331-343 e13.
<https://doi.org/10.1016/j.cell.2017.12.008>
- Chen, Q., Ijima, A., Greider, C.W., 2001. Two Survivor Pathways That Allow Growth in the Absence of Telomerase Are Generated by Distinct Telomere Recombination Events. *Mol. Cell. Biol.* 21, 1819–1827. <https://doi.org/10.1128/mcb.21.5.1819-1827.2001>
- Chuang, T.C., Moshir, S., Garini, Y., Chuang, A.Y., Young, I.T., Vermolen, B., van den Doel, R., Mougey, V., Perrin, M., Braun, M., Kerr, P.D., Fest, T., Boukamp, P., Mai, S., 2004. The three-dimensional organization of telomeres in the nucleus of mammalian cells. *BMC Biol* 2, 12. <https://doi.org/10.1186/1741-7007-2-12>
- Chung, W.J., Heddi, B., Hamon, F., Teulade-Fichou, M.-P., Phan, A.T., 2014. Solution Structure of a G-quadruplex Bound to the Bisquinolinium Compound Phen-DC3. *Angew. Chemie Int. Ed.* 53, 999–1002. <https://doi.org/10.1002/ANIE.201308063>
- Cl, N., V, L., 1998. The telomerase reverse transcriptase: components and regulation. *Genes Dev.* 12, 1073–1085. <https://doi.org/10.1101/GAD.12.8.1073>
- Conrad, M.N., Wright, J.H., Wolf, A.J., Zakian, V.A., 1990. RAP1 protein interacts with yeast telomeres in vivo: overproduction alters telomere structure and decreases chromosome stability. *Cell* 63, 739–750.
- Cusanelli, E., Romero, C.A.P., Chartrand, P., 2013. Telomeric Noncoding RNA TERRA Is

Induced by Telomere Shortening to Nucleate Telomerase Molecules at Short Telomeres. *Mol. Cell* 51, 780–791. <https://doi.org/10.1016/J.MOLCEL.2013.08.029>

D'Amours, D., Jackson, S.P., 2001. The yeast Xrs2 complex functions in S phase checkpoint regulation. *Genes Dev.* 15, 2238. <https://doi.org/10.1101/GAD.208701>

D, L., MS, O., J, Q., Z, S., 2004. Telosome, a mammalian telomere-associated complex formed by multiple telomeric proteins. *J. Biol. Chem.* 279, 51338–51342. <https://doi.org/10.1074/JBC.M409293200>

D, M., C, A., H, B., N, S., F, R., V, G., A, D.C., JL, M., MP, T.-F., 2008. Ligands playing musical chairs with G-quadruplex DNA: a rapid and simple displacement assay for identifying selective G-quadruplex binders. *Biochimie* 90, 1207–1223. <https://doi.org/10.1016/J.BIOCHI.2008.02.019>

D, S., A, B., 2009. Telomere length regulation: coupling DNA end processing to feedback regulation of telomerase. *EMBO J.* 28, 2309–2322. <https://doi.org/10.1038/EMBOJ.2009.195>

Daekyu Sun, †, Brian Thompson, ‡, Brian E. Cathers, ‡, Miguel Salazar, ‡, Sean M. Kerwin, ‡, John O. Trent, §, Terence C. Jenkins, §, Stephen Neidle, *, A., Laurence H. Hurley*, ‡, 1997. Inhibition of Human Telomerase by a G-Quadruplex-Interactive Compound. *J. Med. Chem.* 40, 2113–2116. <https://doi.org/10.1021/JM970199Z>

Davé, A., Pai, C.C., Durley, S.C., Hulme, L., Sarkar, S., Wee, B.Y., Prudden, J., Tinline-Purvis, H., Cullen, J.K., Walker, C., Watson, A., Carr, A.M., Murray, J.M., Humphrey, T.C., 2020. Homologous recombination repair intermediates promote efficient de novo telomere addition at DNA double-strand breaks. *Nucleic Acids Res.* 48, 1271–1284. <https://doi.org/10.1093/nar/gkz1109>

Davoli, T., Lange, T. de, 2012. Telomere-driven tetraploidization occurs in human cells undergoing crisis and promotes transformation of mouse cells. *Cancer Cell* 21, 765. <https://doi.org/10.1016/J.CCR.2012.03.044>

DE LANGE, T., 2005. Telomere-related Genome Instability in Cancer. *Cold Spring Harb. Symp. Quant. Biol.* 70, 197–204. <https://doi.org/10.1101/sqb.2005.70.032>

De Magis, A., Kastl, M., Brossart, P., Heine, A., Paeschke, K., 2021. BG-flow, a new flow

- cytometry tool for G-quadruplex quantification in fixed cells. *BMC Biol.* 2021 19:1 19, 1–12. <https://doi.org/10.1186/S12915-021-00986-6>
- Diede, S.J., Gottschling, D.E., 1999. Telomerase-Mediated Telomere Addition In Vivo Requires DNA Primase and DNA Polymerases α and δ . *Cell* 99, 723–733. [https://doi.org/10.1016/S0092-8674\(00\)81670-0](https://doi.org/10.1016/S0092-8674(00)81670-0)
- DJ, P., AT, P., V, K., 2007. Human telomere, oncogenic promoter and 5'-UTR G-quadruplexes: diverse higher order DNA and RNA targets for cancer therapeutics. *Nucleic Acids Res.* 35, 7429–7455. <https://doi.org/10.1093/NAR/GKM711>
- E, P., K, B., V, L., 2001. Cdc13 delivers separate complexes to the telomere for end protection and replication. *Cell* 104, 387–396. [https://doi.org/10.1016/S0092-8674\(01\)00226-4](https://doi.org/10.1016/S0092-8674(01)00226-4)
- EH, B., JG, G., 1978. A tandemly repeated sequence at the termini of the extrachromosomal ribosomal RNA genes in *Tetrahymena*. *J. Mol. Biol.* 120, 33–53. [https://doi.org/10.1016/0022-2836\(78\)90294-2](https://doi.org/10.1016/0022-2836(78)90294-2)
- EJ, E., L, J.-T., 2008. On helicases and other motor proteins. *Curr. Opin. Struct. Biol.* 18, 243–257. <https://doi.org/10.1016/J.SBI.2008.01.007>
- Epum, E.A., Mohan, M.J., Ruppe, N.P., Friedman, K.L., 2020. Interaction of yeast Rad51 and Rad52 relieves Rad52-mediated inhibition of de novo telomere addition. *PLoS Genet* 16, e1008608. <https://doi.org/10.1371/journal.pgen.1008608>
- Evans, S.K., Lundblad, V., 1999. Est1 and Cdc13 as comediators of telomerase access. *Science* (80-.). 286, 117–120. <https://doi.org/10.1126/science.286.5437.117>
- F, H., FR, N., G, V.H., K, D., SM, G., 2002. Live imaging of telomeres: yKu and Sir proteins define redundant telomere-anchoring pathways in yeast. *Curr. Biol.* 12, 2076–2089. [https://doi.org/10.1016/S0960-9822\(02\)01338-6](https://doi.org/10.1016/S0960-9822(02)01338-6)
- Fang, G., Cech, T.R., 1993. The β subunit of *Oxytricha* telomere-binding protein promotes G-quartet formation by telomeric DNA. *Cell* 74, 875–885. [https://doi.org/10.1016/0092-8674\(93\)90467-5](https://doi.org/10.1016/0092-8674(93)90467-5)
- Feuerhahn, S., Iglesias, N., Panza, A., Porro, A., Lingner, J., 2010. TERRA biogenesis,

- turnover and implications for function. *FEBS Lett.* 584, 3812–3818. <https://doi.org/10.1016/j.febslet.2010.07.032>
- Fisher, T.S., Taggart, A.K., Zakian, V.A., 2004. Cell cycle-dependent regulation of yeast telomerase by Ku. *Nat Struct Mol Biol* 11, 1198–1205. <https://doi.org/10.1038/nsmb854>
- Flynn, R.L., Cox, K.E., Jeitany, M., Wakimoto, H., Bryll, A.R., Ganem, N.J., Bersani, F., Pineda, J.R., Suva, M.L., Benes, C.H., Haber, D.A., Boussin, F.D., Zou, L., 2015. Alternative lengthening of telomeres renders cancer cells hypersensitive to ATR inhibitors. *Science (80-.)*. 347, 273–277. <https://doi.org/10.1126/science.1257216>
- Förstemann, K., Lingner, J., 2001. Molecular Basis for Telomere Repeat Divergence in Budding Yeast. *Mol. Cell. Biol.* 21, 7277–7286. <https://doi.org/10.1128/mcb.21.21.7277-7286.2001>
- Fourel, G., Revardel, E., Koering, C.E., Gilson, É., 1999. Cohabitation of insulators and silencing elements in yeast subtelomeric regions. *EMBO J.* 18, 2522–2537. <https://doi.org/10.1093/EMBOJ/18.9.2522>
- Gaikwad, S.M., Phyo, Z., Arteaga, A.Q., Gorjifard, S., Calabrese, D.R., Connors, D., Huang, J., Michalowski, A.M., Zhang, S., Liu, Z.-G., Schneekloth, J.S., Mock, B.A., 2020. A Small Molecule Stabilizer of the MYC G4-Quadruplex Induces Endoplasmic Reticulum Stress, Senescence and Pyroptosis in Multiple Myeloma. *Cancers* 2020, Vol. 12, Page 2952 12, 2952. <https://doi.org/10.3390/CANCERS12102952>
- Gajarský, M., Živković, M.L., Stadlbauer, P., Pagano, B., Fiala, R., Amato, J., Tomáška, L., Šponer, J., Plavec, J., Trantírek, L., 2017. Structure of a Stable G-Hairpin. *J. Am. Chem. Soc.* 139, 3591–3594. <https://doi.org/10.1021/JACS.6B10786>
- Gallardo, F., Olivier, C., Dandjinou, A.T., Wellinger, R.J., Chartrand, P., 2008. TLC1 RNA nucleo-cytoplasmic trafficking links telomerase biogenesis to its recruitment to telomeres. *EMBO J* 27, 748–757. <https://doi.org/10.1038/emboj.2008.21>
- Garcia, P.D., Leach, R.W., Wadsworth, G.M., Choudhary, K., Li, H., Aviran, S., Kim, H.D., Zakian, V.A., 2020. Stability and nuclear localization of yeast telomerase depend on protein components of RNase P/MRP. *Nat. Commun.* 11, 2173.

<https://doi.org/10.1038/s41467-020-15875-9>

- Garvik, B., Carson, M., Hartwell, L., 1995. Single-stranded DNA arising at telomeres in *cdc13* mutants may constitute a specific signal for the RAD9 checkpoint. *Mol. Cell. Biol.* 15, 6128–6138. <https://doi.org/10.1128/MCB.15.11.6128>
- Gilson, E., Roberge, M., Giraldo, R., Rhodes, D., Gasser, S.M., 1993. Distortion of the DNA Double Helix by RAP1 at Silencers and Multiple Telomeric Binding Sites. *J. Mol. Biol.* 231, 293–310.
- Giraldo, R., Rhodes, D., 1994. The yeast telomere-binding protein RAP1 binds to and promotes the formation of DNA quadruplexes in telomeric DNA. *EMBO J.* 13, 2411–20.
- Gopalakrishnan, V., Tan, C.R., Li, S., 2017. Sequential phosphorylation of CST subunits by different cyclin-Cdk1 complexes orchestrate telomere replication. *Cell Cycle* 16, 1271. <https://doi.org/10.1080/15384101.2017.1312235>
- Graf, M., Bonetti, D., Lockhart, A., Serhal, K., Kellner, V., Maicher, A., Jolivet, P., Teixeira, M.T., Luke, B., 2017. Telomere Length Determines TERRA and R-Loop Regulation through the Cell Cycle. *Cell* 170, 72-85.e14. <https://doi.org/10.1016/j.cell.2017.06.006>
- Grandin, N., Damon, C., Charbonneau, M., N, G., C, D., M, C., 2001. Ten1 functions in telomere end protection and length regulation in association with Stn1 and Cdc13 20. <https://doi.org/10.1093/EMBOJ/20.5.1173>
- Grandin, N., Reed, S.I., Charbonneau, M., 1997. Stn1, a new *Saccharomyces cerevisiae* protein, is implicated in telomere size regulation in association with Cdc13. *Genes Dev.* 11, 512–527. <https://doi.org/10.1101/GAD.11.4.512>
- Granotier, C., Pennarun, G., Riou, L., Hoffschir, F., Gauthier, L.R., De Cian, A., Gomez, D., Mandine, E., Riou, J.-F., Mergny, J.-L., Mailliet, P., Dutrillaux, B., Boussin, F.D., 2005. Preferential binding of a G-quadruplex ligand to human chromosome ends. *Nucleic Acids Res.* 33, 4182–4190.
- Gravel, S., Larrivée, M., Labrecque, P., Wellinger, R.J., 1998. Yeast Ku as a Regulator of Chromosomal DNA End Structure. *Science* (80-.). 280, 741–744.

<https://doi.org/10.1126/SCIENCE.280.5364.741>

- Greider, C.W., 2016. Regulating telomere length from the inside out: the replication fork model. *Genes Dev.* 30, 1483–91. <https://doi.org/10.1101/gad.280578.116>
- Greider, C.W., Blackburn, E.H., 1985. Identification of a Specific Telomere Terminal Transferase Activity in Tetrahymena Extracts. *Cell* 43, 405–413.
- Grossi, S., Puglisi, A., Dmitriev, P. V., Lopes, M., Shore, D., 2004. Pol12, the B subunit of DNA polymerase α , functions in both telomere capping and length regulation. *Genes Dev.* 18, 992–1006. <https://doi.org/10.1101/GAD.300004>
- Hänsel-Hertsch, R., Spiegel, J., Marsico, G., Tannahill, D., Balasubramanian, S., 2018. Genome-wide mapping of endogenous G-quadruplex DNA structures by chromatin immunoprecipitation and high-throughput sequencing. *Nat. Protoc.* 13, 551–564. <https://doi.org/10.1038/nprot.2017.150>
- Hardy, C.F., Sussel, L., Shore, D., 1992. A RAP1-interacting protein involved in transcriptional silencing and telomere length regulation. *Genes Dev.* 6, 801–814. <https://doi.org/10.1101/GAD.6.5.801>
- Hayashi, N., Murakami, S., 2002. STM1, a gene which encodes a guanine quadruplex binding protein, interacts with CDC13 in *Saccharomyces cerevisiae*. *Mol. Genet. Genomics* 267, 806–813. <https://doi.org/10.1007/s00438-002-0712-3>
- Hershman, S.G., Chen, Q., Lee, J.Y., Kozak, M.L., Yue, P., Wang, L.-S., Johnson, F.B., 2008. Genomic distribution and functional analyses of potential G-quadruplex-forming sequences in *Saccharomyces cerevisiae*. *Nucleic Acids Res.* 36, 144–156. <https://doi.org/10.1093/nar/gkm986>
- Hirano, Y., Sugimoto, K., 2007. Cdc13 telomere capping decreases Mec1 association but does not affect Tel1 association with DNA ends. *Mol. Biol. Cell* 18, 2026–2036. <https://doi.org/10.1091/MBC.E06-12-1074>
- Horowitz, H., Thorburn, P., Haber, J.E., 1984. Rearrangements of highly polymorphic regions near telomeres of *Saccharomyces cerevisiae*. *Mol. Cell. Biol.* 4, 2509–2517. <https://doi.org/10.1128/mcb.4.11.2509-2517.1984>

- Huber, M.D., Lee, D.C., Maizels, N., 2002. G4 DNA unwinding by BLM and Sgs1p: substrate specificity and substrate-specific inhibition. *Nucleic Acids Res.* 30, 3954. <https://doi.org/10.1093/NAR/GKF530>
- Hughes, T.R., Weilbaecher, R.G., Walterscheid, M., Lundblad, V., 2000. Identification of the single-strand telomeric DNA binding domain of the *Saccharomyces cerevisiae* Cdc13 protein. *Proc. Natl. Acad. Sci.* 97, 6457–6462. <https://doi.org/10.1073/PNAS.97.12.6457>
- I, D., RJ, W., 1998. Processing of telomeric DNA ends requires the passage of a replication fork. *Nucleic Acids Res.* 26, 5365–5371. <https://doi.org/10.1093/NAR/26.23.5365>
- IR, G., RA, H., KG, S., KA, H., A, C., 1999. In vivo analysis of functional regions within yeast Rap1p. *Mol. Cell. Biol.* 19, 7481–7490. <https://doi.org/10.1128/MCB.19.11.7481>
- Ivessa, A.S., Zhou, J.-Q., Schulz, V.P., Monson, E.K., Zakian, V.A., AS, I., JQ, Z., VP, S., EK, M., VA, Z., 2002. *Saccharomyces Rrm3p*, a 5' to 3' DNA helicase that promotes replication fork progression through telomeric and subtelomeric DNA. *Genes Dev.* 16, 1383–1396. <https://doi.org/10.1101/GAD.982902>
- J, M., Y, L., N, B., PJ, C., T, de L., 2015. Chromothripsis and Kataegis Induced by Telomere Crisis. *Cell* 163, 1641–1654. <https://doi.org/10.1016/J.CELL.2015.11.054>
- J, S., Y, Y., K, W., N, M., TY, Y., YC, L., DC, D., BC, F., JJ, L., NF, L., M, L., 2011. Structural bases of dimerization of yeast telomere protein Cdc13 and its interaction with the catalytic subunit of DNA polymerase α . *Cell Res.* 21, 258–274. <https://doi.org/10.1038/CR.2010.138>
- JD, W., 1972. Origin of concatemeric T7 DNA. *Nat. New Biol.* 239, 197–201. <https://doi.org/10.1038/NEWBIO239197A0>
- JH, W., DE, G., VA, Z., 1992. *Saccharomyces* telomeres assume a non-nucleosomal chromatin structure. *Genes Dev.* 6, 197–210. <https://doi.org/10.1101/GAD.6.2.197>
- Jia, P., Chai, W., 2018. The MLH1 ATPase domain is needed for suppressing aberrant formation of interstitial telomeric sequences. *DNA Repair* 65, 20–25.

<https://doi.org/10.1016/j.dnarep.2018.03.002>

- Jia, P., Chastain, M., Zou, Y., Her, C., Chai, W., 2017. Human MLH1 suppresses the insertion of telomeric sequences at intra-chromosomal sites in telomerase-expressing cells. *Nucleic Acids Res* 45, 1219–1232. <https://doi.org/10.1093/nar/gkw1170>
- JK, D., FC, P., LA, H., AJ, P., BF, V., EA, C., 2013. Unfolding of the C-terminal domain of the J-protein Zuo1 releases autoinhibition and activates Pdr1-dependent transcription. *J. Mol. Biol.* 425, 19–31. <https://doi.org/10.1016/J.JMB.2012.09.020>
- JL, H., 2008. Hunting G-quadruplexes. *Biochimie* 90, 1140–1148. <https://doi.org/10.1016/J.BIOCHI.2008.01.014>
- JL, H., S, B., 2007. G-quadruplexes in promoters throughout the human genome. *Nucleic Acids Res.* 35, 406–413. <https://doi.org/10.1093/NAR/GKL1057>
- JL, H., S, B., 2005. Prevalence of quadruplexes in the human genome. *Nucleic Acids Res.* 33, 2908–2916. <https://doi.org/10.1093/NAR/GKI609>
- JM, N., SP, B., JL, M., LA, Y., 2012. Interaction of human telomeric DNA with N-methyl mesoporphyrin IX. *Nucleic Acids Res.* 40, 5432–5447. <https://doi.org/10.1093/NAR/GKS152>
- Johnson, F.B., Marciniak, R.A., McVey, M., Stewart, S.A., Hahn, W.C., Guarente, L., 2001. The *Saccharomyces cerevisiae* WRN homolog Sgs1p participates in telomere maintenance in cells lacking telomerase. *EMBO J.* 20, 905. <https://doi.org/10.1093/EMBOJ/20.4.905>
- JR, W., MK, R., TR, C., 1989. Monovalent cation-induced structure of telomeric DNA: the G-quartet model. *Cell* 59, 871–880. [https://doi.org/10.1016/0092-8674\(89\)90610-7](https://doi.org/10.1016/0092-8674(89)90610-7)
- Jurikova, K., Gajarsky, M., Hajikazemi, M., Nosek, J., Prochazkova, K., Paeschke, K., Trantirek, L., Tomaska, L., 2020. Role of folding kinetics of secondary structures in telomeric G-overhangs in the regulation of telomere maintenance in *Saccharomyces cerevisiae*. *J. Biol. Chem.* jbc.RA120.012914. <https://doi.org/10.1074/jbc.ra120.012914>

- Kang, C., Zhang, X., Ratliff, R., Moyzis, R., Rich, A., 1992. Crystal structure of four-stranded *Oxytricha* telomeric DNA. *Nat.* 1992 3566365 356, 126–131. <https://doi.org/10.1038/356126a0>
- Keener, R., Connelly, C.J., Greider, C.W., 2019. Tel1 Activation by the MRX Complex Is Sufficient for Telomere Length Regulation but Not for the DNA Damage Response in *Saccharomyces cerevisiae*. *Genetics* 213, 1271–1288. <https://doi.org/10.1534/GENETICS.119.302713>
- L, C., RE, V., CI, H., J, K., 2004. Defective telomere lagging strand synthesis in cells lacking WRN helicase activity. *Science* 306, 1951–1953. <https://doi.org/10.1126/SCIENCE.1103619>
- L, H., PS, M., 1961. The serial cultivation of human diploid cell strains. *Exp. Cell Res.* 25, 585–621. [https://doi.org/10.1016/0014-4827\(61\)90192-6](https://doi.org/10.1016/0014-4827(61)90192-6)
- L, O., J, K., 2009. Telomeric armor: the layers of end protection. *J. Cell Sci.* 122, 4013–4025. <https://doi.org/10.1242/JCS.050567>
- Larrivée, M., Wellinger, R.J., 2006. Telomerase- and capping-independent yeast survivors with alternate telomere states. *Nat. Cell Biol.* 2006 87 8, 741–747. <https://doi.org/10.1038/ncb1429>
- LE, H., X, L., I, C., Y, Y., X, Z., 2011. SUMOylation regulates telomere length homeostasis by targeting Cdc13. *Nat. Struct. Mol. Biol.* 18, 920–926. <https://doi.org/10.1038/NSMB.2100>
- Lei, M., Zaug, A.J., Podell, E.R., Cech, T.R., 2005. Switching Human Telomerase On and Off with hPOT1 Protein in Vitro*. *J. Biol. Chem.* 280, 20449–20456. <https://doi.org/10.1074/JBC.M502212200>
- Lendvay, T.S., Morris, D.K., Sah, J., Balasubramanian, B., Lundblad, V., 1996. Senescence mutants of *Saccharomyces cerevisiae* with a defect in telomere replication identify three additional EST genes. *Genetics* 144, 1399–1412.
- Levy, D.L., Blackburn, E.H., 2004. Counting of Rif1p and Rif2p on *Saccharomyces cerevisiae* Telomeres Regulates Telomere Length. *Mol. Cell. Biol.* 24, 10857–10867. <https://doi.org/10.1128/MCB.24.24.10857-10867.2004>

- Li, B., Lustig, A.J., 1996. A novel mechanism for telomere size control in *Saccharomyces cerevisiae*. *Genes Dev.* 10, 1310–1326. <https://doi.org/10.1101/GAD.10.11.1310>
- Li, S., Makovets, S., Matsuguchi, T., Blethrow, J.D., Shokat, K.M., Blackburn, E.H., 2009. Cdk1-dependent phosphorylation of Cdc13 coordinates telomere elongation during cell cycle progression. *Cell* 136, 50. <https://doi.org/10.1016/J.CELL.2008.11.027>
- Lieber, M.R., Grawunder, U., Wu, X., Yaneva, M., 1997. Tying loose ends: roles of Ku and DNA-dependent protein kinase in the repair of double-strand breaks. *Curr. Opin. Genet. Dev.* 7, 99–104. [https://doi.org/10.1016/S0959-437X\(97\)80116-5](https://doi.org/10.1016/S0959-437X(97)80116-5)
- Lim, K.W., Lacroix, L., Yue, D.J.E., Lim, J.K.C., Lim, J.M.W., Phan, A.T., 2010. Coexistence of Two Distinct G-Quadruplex Conformations in the hTERT Promoter. *J. Am. Chem. Soc.* 132, 12331–12342. <https://doi.org/10.1021/JA101252N>
- Lin, J.J., Zakian, V.A., 1996. The *Saccharomyces* CDC13 protein is a single-strand TG1-3 telomeric DNA-binding protein in vitro that affects telomere behavior in vivo. *Proc Natl Acad Sci U S A* 93, 13760–13765.
- Lin, Y.-C., Shih, J.-W., Hsu, C.-L., Lin, J.-J., 2001. Binding and Partial Denaturing of G-quartet DNA by Cdc13p of *Saccharomyces cerevisiae* *. *J. Biol. Chem.* 276, 47671–47674. <https://doi.org/10.1074/JBC.M104989200>
- Lingner, Joachim, Cech, T.R., Hughes, T.R., Lundblad, V., 1997. Three ever shorter telomere (EST) genes are dispensable for in vitro yeast telomerase activity. *Proc. Natl. Acad. Sci. U. S. A.* 94, 11190–11195. <https://doi.org/10.1073/pnas.94.21.11190>
- Lingner, J, Hughes, T.R., Shevchenko, A., Mann, M., Lundblad, V., Cech, T.R., 1997. Reverse transcriptase motifs in the catalytic subunit of telomerase. *Science* (80-.). 276, 561–567. <https://doi.org/10.1126/SCIENCE.276.5312.561>
- Liu, C., Mao, X., Lustig, A.J., 1994. Mutational analysis defines a C-terminal tail domain of RAP1 essential for telomeric silencing in *Saccharomyces cerevisiae*. *Genetics* 138, 1025–1040. <https://doi.org/10.1093/genetics/138.4.1025>
- Longtine, M.S., McKenzie, A., Demarini, D.J., Shah, N.G., Wach, A., Brachat, A., Philippsen, P., Pringle, J.R., McKenzie 3rd, A., Demarini, D.J., Shah, N.G., Wach, A., Brachat, A., Philippsen, P., Pringle, J.R., 1998. Additional modules for versatile and

- economical PCR-based gene deletion and modification in *Saccharomyces cerevisiae*. *Yeast* 14, 953–961. [https://doi.org/10.1002/\(SICI\)1097-0061\(199807\)14:10<953::AID-YEA293>3.0.CO;2-U](https://doi.org/10.1002/(SICI)1097-0061(199807)14:10<953::AID-YEA293>3.0.CO;2-U)
- Luciano, P., Coulon, S., Faure, V., Corda, Y., Bos, J., Brill, S.J., Gilson, E., Simon, M.-N., Géli, V., 2012. RPA facilitates telomerase activity at chromosome ends in budding and fission yeasts. *EMBO J.* 31, 2034. <https://doi.org/10.1038/EMBOJ.2012.40>
- Luke, B., Panza, A., Redon, S., Iglesias, N., Li, Z., Lingner, J., 2008. The Rat1p 5' to 3' Exonuclease Degrades Telomeric Repeat-Containing RNA and Promotes Telomere Elongation in *Saccharomyces cerevisiae*. *Mol. Cell* 32. <https://doi.org/10.1016/J.MOLCEL.2008.10.019>
- Lundblad, V., Blackburn, E.H., 1993. An alternative pathway for yeast telomere maintenance rescues est1- senescence. *Cell* 73, 347–360. [https://doi.org/10.1016/0092-8674\(93\)90234-H](https://doi.org/10.1016/0092-8674(93)90234-H)
- Lundblad, V., Szostak, J.W., 1989. A mutant with a defect in telomere elongation leads to senescence in yeast. *Cell* 57, 633–643. [https://doi.org/10.1016/0092-8674\(89\)90132-3](https://doi.org/10.1016/0092-8674(89)90132-3)
- M, B., Y, P., AJ, L., 2001. Intrachromatid excision of telomeric DNA as a mechanism for telomere size control in *Saccharomyces cerevisiae*. *Mol. Cell. Biol.* 21, 6559–6573. <https://doi.org/10.1128/MCB.21.19.6559-6573.2001>
- M, C., NV, H., J, P., 2002. The solution structure of d(G(4)T(4)G(3))(2): a bimolecular G-quadruplex with a novel fold. *J. Mol. Biol.* 320, 911–924. [https://doi.org/10.1016/S0022-2836\(02\)00569-7](https://doi.org/10.1016/S0022-2836(02)00569-7)
- M, G., C, G., NF, L., 2001. Checkpoint activation in response to double-strand breaks requires the Mre11/Rad50/Xrs2 complex. *Nat. Cell Biol.* 3, 844–847. <https://doi.org/10.1038/NCB0901-844>
- M, G., MN, L., DR, D., 1962. Helix formation by guanylic acid. *Proc. Natl. Acad. Sci. U. S. A.* 48, 2013–2018. <https://doi.org/10.1073/PNAS.48.12.2013>
- M, G., SM, G., 1996. Nuclear organization and transcriptional silencing in yeast. *Experientia* 52, 1136–1147. <https://doi.org/10.1007/BF01952113>

- M, L., C, L., RJ, W., 2004. The generation of proper constitutive G-tails on yeast telomeres is dependent on the MRX complex. *Genes Dev.* 18, 1391–1396. <https://doi.org/10.1101/GAD.1199404>
- M, R.-L., G, R., A, W., N, F., R, K., OJ, R., 2011. Dynamics of Sir3 spreading in budding yeast: secondary recruitment sites and euchromatic localization. *EMBO J.* 30, 1012–1026. <https://doi.org/10.1038/EMBOJ.2011.30>
- M, Y., N, H., A, M., F, I., 1998. Y'-Help1, a DNA helicase encoded by the yeast subtelomeric Y' element, is induced in survivors defective for telomerase. *J. Biol. Chem.* 273, 33360–33366. <https://doi.org/10.1074/JBC.273.50.33360>
- Magis, A. De, Götz, S., Hajikazemi, M., Fekete-Szücs, E., Caterino, M., Juranek, S., Paeschke, K., 2020. Zuo1 supports G4 structure formation and directs repair toward nucleotide excision repair. *Nat. Commun.* 2020 111 11, 1–12. <https://doi.org/10.1038/s41467-020-17701-8>
- Makarov, V.L., Hirose, Y., Langmore, J.P., 1997. Long G Tails at Both Ends of Human Chromosomes Suggest a C Strand Degradation Mechanism for Telomere Shortening. *Cell* 88, 657–666. [https://doi.org/10.1016/S0092-8674\(00\)81908-X](https://doi.org/10.1016/S0092-8674(00)81908-X)
- Makovets, S., Blackburn, E.H., 2009. DNA damage signalling prevents deleterious telomere addition at DNA breaks. *Nat Cell Biol* 11, 1383–1386. <https://doi.org/10.1038/ncb1985>
- Mandell, E.K., Gelinias, A.D., Wuttke, D.S., Lundblad, V., 2011. Sequence-specific binding to telomeric DNA is not a conserved property of the Cdc13 DNA binding domain. *Biochemistry* 50, 6289–6291. https://doi.org/10.1021/BI2005448/SUPPL_FILE/BI2005448_SI_001.PDF
- Marcand, S., Brevet, V., Gilson, E., 1999. Progressive cis-inhibition of telomerase upon telomere elongation. *EMBO J.* 18. <https://doi.org/10.1093/emboj/18.12.3509>
- Marcand, S., Pardo, B., Gratias, A., Cahun, S., Callebaut, I., 2008. Multiple pathways inhibit NHEJ at telomeres. *Genes Dev.* 22, 1153–1158. <https://doi.org/10.1101/GAD.455108>
- Martin, S.G., Laroche, T., Suka, N., Grunstein, M., Gasser, S.M., 1999. Relocalization of

- Telomeric Ku and SIR Proteins in Response to DNA Strand Breaks in Yeast. *Cell* 97, 621–633. [https://doi.org/10.1016/S0092-8674\(00\)80773-4](https://doi.org/10.1016/S0092-8674(00)80773-4)
- Marvin, M.E., Griffin, C.D., Eyre, D.E., Barton, D.B.H., Louis, E.J., 2009. In *Saccharomyces cerevisiae*, yKu and Subtelomeric Core X Sequences Repress Homologous Recombination Near Telomeres as Part of the Same Pathway. *Genetics* 183, 441–451. <https://doi.org/10.1534/GENETICS.109.106674>
- Masai, H., Fukatsu, R., Kakusho, N., Kanoh, Y., Moriyama, K., Ma, Y., Iida, K., Nagasawa, K., 2019. Rif1 promotes association of G-quadruplex (G4) by its specific G4 binding and oligomerization activities. *Sci. Rep.* 9. <https://doi.org/10.1038/s41598-019-44736-9>
- Matmati, S., Lambert, S., Géli, V., Coulon, S., Geli, V., Coulon, S., 2020. Telomerase Repairs Collapsed Replication Forks at Telomeres. *Cell Rep* 30, 3312-3322 e3. <https://doi.org/10.1016/j.celrep.2020.02.065>
- McClintock, B., 1939. The Behavior in Successive Nuclear Divisions of a Chromosome Broken at Meiosis. *Proc. Natl. Acad. Sci. U. S. A.* 25, 405. <https://doi.org/10.1073/PNAS.25.8.405>
- McGee, J.S., Phillips, J.A., Chan, A., Sabourin, M., Paeschke, K., Zakian, V.A., 2010. Reduced Rif2 and lack of Mec1 target short telomeres for elongation rather than double-strand break repair. *Nat. Struct. Mol. Biol.* 17, 1438–1445. <https://doi.org/10.1038/nsmb.1947>
- MD, V., RJ, W., 2007. The cell division cycle puts up with unprotected telomeres: cell cycle regulated telomere uncapping as a means to achieve telomere homeostasis. *Cell Cycle* 6, 1161–1167. <https://doi.org/10.4161/CC.6.10.4224>
- MD, V., RJ, W., 2006. DNA degradation at unprotected telomeres in yeast is regulated by the CDK1 (Cdc28/Clb) cell-cycle kinase. *Mol. Cell* 24, 127–137. <https://doi.org/10.1016/J.MOLCEL.2006.07.035>
- Meier, B., Driller, L., Jaklin, S., Feldmann, H.M., 2001. New Function of CDC13 in Positive Telomere Length Regulation. *Mol. Cell. Biol.* 21, 4233. <https://doi.org/10.1128/MCB.21.13.4233-4245.2001>

- Mersaoui, S.Y., Bonnell, E., Wellinger, R.J., 2018. Nuclear import of Cdc13 limits chromosomal capping. *Nucleic Acids Res.* 46, 2975. <https://doi.org/10.1093/NAR/GKY085>
- Meselson, M., Stahl, F.W., 1958. THE REPLICATION OF DNA IN ESCHERICHIA COLI. *Proc. Natl. Acad. Sci. U. S. A.* 44, 671. <https://doi.org/10.1073/PNAS.44.7.671>
- Miga, K.H., Koren, S., Rhie, A., Vollger, M.R., Gershman, A., Bzikadze, A., Brooks, S., Howe, E., Porubsky, D., Logsdon, G.A., Schneider, V.A., Potapova, T., Wood, J., Chow, W., Armstrong, J., Fredrickson, J., Pak, E., Tigyi, K., Kremitzki, M., Markovic, C., Maduro, V., Dutra, A., Bouffard, G.G., Chang, A.M., Hansen, N.F., Wilfert, A.B., Thibaud-Nissen, F., Schmitt, A.D., Belton, J.-M., Selvaraj, S., Dennis, M.Y., Soto, D.C., Sahasrabudhe, R., Kaya, G., Quick, J., Loman, N.J., Holmes, N., Loose, M., Surti, U., Risques, R. ana, Graves Lindsay, T.A., Fulton, R., Hall, I., Paten, B., Howe, K., Timp, W., Young, A., Mullikin, J.C., Pevzner, P.A., Gerton, J.L., Sullivan, B.A., Eichler, E.E., Phillippy, A.M., 2020. Telomere-to-telomere assembly of a complete human X chromosome. *Nat.* 2020 5857823 585, 79–84. <https://doi.org/10.1038/s41586-020-2547-7>
- Misino, S., Bonetti, D., Luke-Glaser, S., Luke, B., 2018. Increased TERRA levels and RNase H sensitivity are conserved hallmarks of post-senescent survivors in budding yeast. *Differentiation* 100, 37–45. <https://doi.org/10.1016/j.diff.2018.02.002>
- ML, B., CP, J., VA, Z., 2011. The Pif1 family in prokaryotes: what are our helicases doing in your bacteria? *Mol. Biol. Cell* 22, 1955–1959. <https://doi.org/10.1091/MBC.E11-01-0045>
- Moravec, M., Wischnewski, H., Bah, A., Hu, Y., Liu, N., Lafranchi, L., King, M.C., Azzalin, C.M., 2016. TERRA promotes telomerase-mediated telomere elongation in *Schizosaccharomyces pombe*. *EMBO Rep.* 17, 999–1012. <https://doi.org/10.15252/embr.201541708>
- Moye, A.L., Porter, K.C., Cohen, S.B., Phan, T., Zyner, K.G., Sasaki, N., Lovrecz, G.O., Beck, J.L., Bryan, T.M., 2015. Telomeric G-quadruplexes are a substrate and site of localization for human telomerase. *Nat. Commun.* 6, 1–12. <https://doi.org/10.1038/ncomms8643>

- MR, M., M, R., W, H.-S., M, de la F., SM, B., ME, H., DJ, T., 2016. POT1-TPP1 Binding and Unfolding of Telomere DNA Discriminates against Structural Polymorphism. *J. Mol. Biol.* 428, 2695–2708. <https://doi.org/10.1016/J.JMB.2016.04.031>
- Mullen, M.A., Olson, K.J., Dallaire, P., Major, F., Assmann, S.M., Bevilacqua, P.C., 2010. RNA G-Quadruplexes in the model plant species *Arabidopsis thaliana*: prevalence and possible functional roles. *Nucleic Acids Res.* 38, 8149. <https://doi.org/10.1093/NAR/GKQ804>
- MW, V.D., LD, N., RG, W., DV, M., 2004. Stm1p, a G4 quadruplex and purine motif triplex nucleic acid-binding protein, interacts with ribosomes and subtelomeric Y' DNA in *Saccharomyces cerevisiae*. *J. Biol. Chem.* 279, 24323–24333. <https://doi.org/10.1074/JBC.M401981200>
- Myung, K., Chen, C., Kolodner, R.D., 2001. Multiple pathways cooperate in the suppression of genome instability in *Saccharomyces cerevisiae*. *Nature* 411, 1073–1076. <https://doi.org/10.1038/35082608>
- N, G., M, C., 2007. Mrc1, a non-essential DNA replication protein, is required for telomere end protection following loss of capping by Cdc13, Yku or telomerase. *Mol. Genet. Genomics* 277, 685–699. <https://doi.org/10.1007/S00438-007-0218-0>
- Negrini, S., Ribaud, V., Bianchi, A., Shore, D., 2007. DNA breaks are masked by multiple Rap1 binding in yeast: implications for telomere capping and telomerase regulation. *Genes Dev.* 21, 292–302. <https://doi.org/10.1101/GAD.400907>
- Nugent, C.I., Hughes, T.R., Lue, N.F., Lundblad, V., 1996. Cdc13p: a single-strand telomeric DNA-binding protein with a dual role in yeast telomere maintenance. *Science (80-.)*. 274, 249–252. <https://doi.org/10.1126/SCIENCE.274.5285.249>
- Obodo, U.C., Epum, E.A., Platts, M.H., Seloff, J., Dahlson, N.A., Velkovsky, S.M., Paul, S.R., Friedman, K.L., 2016. Endogenous Hot Spots of De Novo Telomere Addition in the Yeast Genome Contain Proximal Enhancers That Bind Cdc13. *Mol Cell Biol* 36, 1750–1763. <https://doi.org/10.1128/MCB.00095-16>
- Oganesian, L., Moon, I.K., Bryan, T.M., Jarstfer, M.B., 2006. Extension of G-quadruplex DNA by ciliate telomerase 25, 1148–1159.

- Olovnikov, A.M., 1973. A theory of marginotomy: The incomplete copying of template margin in enzymic synthesis of polynucleotides and biological significance of the phenomenon. *J. Theor. Biol.* 41, 181–190. [https://doi.org/10.1016/0022-5193\(73\)90198-7](https://doi.org/10.1016/0022-5193(73)90198-7)
- Ouenzar, F., Lalonde, M., Laprade, H., Morin, G., Gallardo, F., Tremblay-Belzile, S., Chartrand, P., 2017. Cell cycle-dependent spatial segregation of telomerase from sites of DNA damage. *J Cell Biol* 216, 2355–2371. <https://doi.org/10.1083/jcb.201610071>
- P, M., D, S., 2001. Multiple interactions in Sir protein recruitment by Rap1p at silencers and telomeres in yeast. *Mol. Cell. Biol.* 21, 8082–8094. <https://doi.org/10.1128/MCB.21.23.8082-8094.2001>
- P, Š., S, F.-T., K, B., R, F., M, V., L, T., 2015. Unique *C. elegans* telomeric overhang structures reveal the evolutionarily conserved properties of telomeric DNA. *Nucleic Acids Res.* 43, 4733–4745. <https://doi.org/10.1093/NAR/GKV296>
- Paeschke, K., Bochman, M.L., Garcia, P.D., Cejka, P., Friedman, K.L., Kowalczykowski, S.C., Zakian, V.A., 2013. Pif1 family helicases suppress genome instability at G-quadruplex motifs. *Nature* 497, 458–462. <https://doi.org/10.1038/nature12149>
- Paeschke, K., Capra, J.A., Zakian, V.A., 2011. DNA replication through G-quadruplex motifs is promoted by the *Saccharomyces cerevisiae* Pif1 DNA helicase. *Cell* 145, 678–691. <https://doi.org/10.1016/j.cell.2011.04.015>
- Paeschke, K., Juranek, S., Simonsson, T., Hempel, A., Rhodes, D., Lipps, H.J., 2008. Telomerase recruitment by the telomere end binding protein- β facilitates G-quadruplex DNA unfolding in ciliates. *Nat. Struct. Mol. Biol.* 15, 598–604. <https://doi.org/10.1038/nsmb.1422>
- Paeschke, K., McDonald, K.R., Zakian, V.A., 2010. Telomeres: structures in need of unwinding. *FEBS Lett.* 584, 3760–3772. <https://doi.org/10.1016/j.febslet.2010.07.007>
- Paeschke, K., Simonsson, T., Postberg, J., Rhodes, D., Lipps, H.J., 2005. Telomere end-binding proteins control the formation of G-quadruplex DNA structures in vivo. *Nat. Struct. Mol. Biol.* 12, 847–854. <https://doi.org/10.1038/nsmb982>

- Palladino, F., Laroche, T., Gilson, E., Axelrod, A., Pillus, L., Gasser, S.M., 1993. SIR3 and SIR4 proteins are required for the positioning and integrity of yeast telomeres. *Cell* 75, 543–555. [https://doi.org/10.1016/0092-8674\(93\)90388-7](https://doi.org/10.1016/0092-8674(93)90388-7)
- Pardo, B., Marcand, S., 2005. Rap1 prevents telomere fusions by nonhomologous end joining. *EMBO J.* 24, 3117–3127. <https://doi.org/10.1038/SJ.EMBOJ.7600778>
- Pennaneach, V., Putnam, C.D., Kolodner, R.D., 2006. Chromosome healing by de novo telomere addition in *Saccharomyces cerevisiae*. *Mol. Microbiol.* 59, 1357–1368. <https://doi.org/10.1111/J.1365-2958.2006.05026.X>
- Phan, A.T., Luu, K.N., Patel, D.J., 2006. Different loop arrangements of intramolecular human telomeric (3+1) G-quadruplexes in K⁺ solution. *Nucleic Acids Res.* 34, 5715. <https://doi.org/10.1093/NAR/GKL726>
- Phillips, J.A., Chan, A., Paeschke, K., Zakian, V.A., 2015. The Pif1 Helicase, a Negative Regulator of Telomerase, Acts Preferentially at Long Telomeres. *PLOS Genet.* 11, e1005186. <https://doi.org/10.1371/journal.pgen.1005186>
- Piazza, A., Boulé, J.-B., Lopes, J., Mingo, K., Largy, E., Teulade-Fichou, M.-P., Nicolas, A., 2010. Genetic instability triggered by G-quadruplex interacting Phen-DC compounds in *Saccharomyces cerevisiae*. *Nucleic Acids Res.* 38. <https://doi.org/10.1093/nar/gkq136>
- Prunuske, A.J., Waltner, J.K., Kuhn, P., Gu, B., Craig, E.A., 2012. Role for the molecular chaperones Zuo1 and Ssz1 in quorum sensing via activation of the transcription factor Pdr1. *Proc. Natl. Acad. Sci.* 109, 472–477. <https://doi.org/10.1073/PNAS.1119184109>
- Puglisi, A., Bianchi, A., Lemmens, L., Damay, P., Shore, D., 2008. Distinct roles for yeast Stn1 in telomere capping and telomerase inhibition. *EMBO J.* 27, 2328. <https://doi.org/10.1038/EMBOJ.2008.158>
- Putnam, C.D., Pennaneach, V., Kolodner, R.D., 2004. Chromosome healing through terminal deletions generated by de novo telomere additions in *Saccharomyces cerevisiae*. *Proc Natl Acad Sci U S A* 101, 13262–13267. <https://doi.org/10.1073/pnas.0405443101>

- Qi, H., Zakian, V.A., 2000. The *Saccharomyces* telomere-binding protein Cdc13p interacts with both the catalytic subunit of DNA polymerase alpha and the telomerase-associated est1 protein. *Genes Dev* 14, 1777–1788.
- Qian, W., Wang, J., Jin, N.-N., Fu, X.-H., Lin, Y.-C., Lin, J.-J., Zhou, J.-Q., 2009. Ten1p promotes the telomeric DNA-binding activity of Cdc13p: implication for its function in telomere length regulation. *Cell Res.* 2009 197 19, 849–863. <https://doi.org/10.1038/cr.2009.67>
- Qin, M., Chen, Z., Luo, Q., Wen, Y., Zhang, N., Jiang, H., Yang, H., 2015. Two-Quartet G-Quadruplexes Formed by DNA Sequences Containing Four Contiguous GG Runs. *J. Phys. Chem. B* 119, 3706–3713. <https://doi.org/10.1021/JP512914T>
- R, A., D, J., B, F., U, R., 2020. Limiting homologous recombination at stalled replication forks is essential for cell viability: DNA2 to the rescue. *Curr. Genet.* 66, 1085–1092. <https://doi.org/10.1007/S00294-020-01106-7>
- RC, P., HC, C., CI, N., 2007. The role of Stn1p in *Saccharomyces cerevisiae* telomere capping can be separated from its interaction with Cdc13p. *Genetics* 177, 1459–1474. <https://doi.org/10.1534/GENETICS.107.078840>
- RE, H., RL, S., A, R., BR, C., T, N., KL, B., KW, R., 2007. Tel1p preferentially associates with short telomeres to stimulate their elongation. *Mol. Cell* 27, 851–858. <https://doi.org/10.1016/J.MOLCEL.2007.08.007>
- Redon, S., Reichenbach, P., Lingner, J., 2010. The non-coding RNA TERRA is a natural ligand and direct inhibitor of human telomerase. *Nucleic Acids Res.* 38, 5797–5806. <https://doi.org/10.1093/nar/gkq296>
- Rhodes, D., Lipps, H.J., 2015. G-quadruplexes and their regulatory roles in biology. *Nucleic Acids Res.* 43, 8627–8637. <https://doi.org/10.1093/nar/gkv862>
- Ribeyre, C., Lopes, J., Boulé, J.-B., Piazza, A., Guédin, A., Zakian, V.A., Mergny, J.-L., Nicolas, A., 2009. The Yeast Pif1 Helicase Prevents Genomic Instability Caused by G-Quadruplex-Forming CEB1 Sequences In Vivo. *PLOS Genet.* 5, e1000475. <https://doi.org/10.1371/JOURNAL.PGEN.1000475>
- Rigo, R., Dean, W.L., Gray, R.D., Chaires, J.B., Sissi, C., 2017. Conformational profiling

- of a G-rich sequence within the c-KIT promoter. *Nucleic Acids Res.* 45, 13056. <https://doi.org/10.1093/NAR/GKX983>
- Riou, J.F., Guittat, L., Mailliet, P., Laoui, A., Renou, E., Petitgenet, O., Mégnin-Chanet, F., Hélène, C., Mergny, J.L., 2002. Cell senescence and telomere shortening induced by a new series of specific G-quadruplex DNA ligands. *Proc. Natl. Acad. Sci. U. S. A.* 99, 2672. <https://doi.org/10.1073/PNAS.052698099>
- Ritchie, K.B., Petes, T.D., 2000. The Mre11p/Rad50p/Xrs2p Complex and the Tel1p Function in a Single Pathway for Telomere Maintenance in Yeast. *Genetics* 155, 475–479. <https://doi.org/10.1093/GENETICS/155.1.475>
- RJ, W., K, E., P, L., VA, Z., 1996. Evidence for a new step in telomere maintenance. *Cell* 85, 423–433. [https://doi.org/10.1016/S0092-8674\(00\)81120-4](https://doi.org/10.1016/S0092-8674(00)81120-4)
- RL, K., AD, M., 1993. A gene with specific and global effects on recombination of sequences from tandemly repeated genes in *Saccharomyces cerevisiae*. *Genetics* 135, 711–718. <https://doi.org/10.1093/GENETICS/135.3.711>
- Rodriguez, R., Miller, K.M., Forment, J. V., Bradshaw, C.R., Nikan, M., Britton, S., Oelschlaegel, T., Xhemalce, B., Balasubramanian, S., Jackson, S.P., 2012. Small molecule-induced DNA damage identifies alternative DNA structures in human genes. *Nat. Chem. Biol.* 8, 301. <https://doi.org/10.1038/NCHEMBIO.780>
- Rodriguez, R., Müller, S., Yeoman, J.A., Trentesaux, C., Riou, J.-F., Balasubramanian, S., 2008. A Novel Small Molecule That Alters Shelterin Integrity and Triggers a DNA-Damage Response at Telomeres. *J. Am. Chem. Soc.* 130, 15758–15759. <https://doi.org/10.1021/JA805615W>
- Roisné-Hamelin, F., Pobiega, S., Jézéquel, K., Miron, S., Dépagne, J., Veaute, X., Busso, D., Du, M.-H. Le, Callebaut, I., Charbonnier, J.-B., Cuniasse, P., Zinn-Justin, S., Marcand, S., 2021. Mechanism of MRX inhibition by Rif2 at telomeres. *Nat. Commun.* 2021 121 12, 1–16. <https://doi.org/10.1038/s41467-021-23035-w>
- Rutledge, M.T., Russo, M., Belton, J.M., Dekker, J., Broach, J.R., 2015. The yeast genome undergoes significant topological reorganization in quiescence. *Nucleic Acids Res* 43, 8299–8313. <https://doi.org/10.1093/nar/gkv723>

- S, F., KC, S., Y, D., K, M., G, F., E, G., N, M., 2004. Chromatin domain boundaries delimited by a histone-binding protein in yeast. *J. Biol. Chem.* 279, 55520–55530. <https://doi.org/10.1074/JBC.M410346200>
- S, M., E, G., D, S., 1997. A protein-counting mechanism for telomere length regulation in yeast. *Science* 275, 986–990. <https://doi.org/10.1126/SCIENCE.275.5302.986>
- Sabourin, M., Tuzon, C.T., Zakian, V.A., 2007. Telomerase and Tel1p Preferentially Associate with Short Telomeres in *S. cerevisiae* 27.
- Sauer, M., Paeschke, K., 2017. G-quadruplex unwinding helicases and their function *in vivo*. *Biochem. Soc. Trans.* BST20170097. <https://doi.org/10.1042/BST20170097>
- SC, T., J, C., B, M., VA, Z., 2000. Telomerase-independent lengthening of yeast telomeres occurs by an abrupt Rad50p-dependent, Rif-inhibited recombinational process. *Mol. Cell* 6, 947–952. [https://doi.org/10.1016/S1097-2765\(05\)00094-8](https://doi.org/10.1016/S1097-2765(05)00094-8)
- Schaffitzel, C., Berger, I., Postberg, J., Hanes, J., Lipps, H.J., Plückthun, A., 2001. In vitro generated antibodies specific for telomeric guanine-quadruplex DNA react with *Stylonychia lemnae* macronuclei. *Proc. Natl. Acad. Sci. U. S. A.* 98, 8572. <https://doi.org/10.1073/PNAS.141229498>
- Schalbetter, S.A., Goloborodko, A., Fudenberg, G., Belton, J.M., Miles, C., Yu, M., Dekker, J., Mirny, L., Baxter, J., 2017. SMC complexes differentially compact mitotic chromosomes according to genomic context. *Nat Cell Biol* 19, 1071–1080. <https://doi.org/10.1038/ncb3594>
- Schmidt, J.C., Zaug, A.J., Cech, T.R., 2016. Live Cell Imaging Reveals the Dynamics of Telomerase Recruitment to Telomeres. *Cell* 166, 1188-1197 e9. <https://doi.org/10.1016/j.cell.2016.07.033>
- Schulz, V.P., Zakian, V.A., 1994. The *Saccharomyces* PIF1 DNA helicase inhibits telomere elongation and de novo telomere formation. *Cell* 76, 145–155. [https://doi.org/10.1016/0092-8674\(94\)90179-1](https://doi.org/10.1016/0092-8674(94)90179-1)
- SE, A., RA, D., 2010. Telomeres and telomerase in cancer. *Carcinogenesis* 31, 9–18. <https://doi.org/10.1093/CARCIN/BGP268>

- Sen, D., Gilbert, W., 1988. Formation of parallel four-stranded complexes by guanine-rich motifs in DNA and its implications for meiosis. *Nat.* 1988 3346180 334, 364–366. <https://doi.org/10.1038/334364a0>
- Shen, Z.-J., Hsu, P.-H., Su, Y.-T., Yang, C.-W., Kao, L., Tseng, S.-F., Tsai, M.-D., Teng, S.-C., 2014. PP2A and Aurora differentially modify Cdc13 to promote telomerase release from telomeres at G2/M phase. *Nat. Commun.* 2014 51 5, 1–12. <https://doi.org/10.1038/ncomms6312>
- Sikorski, R.S., Hieter, P., 1989. A system of shuttle vectors and yeast host strains designed for efficient manipulation of DNA in *Saccharomyces cerevisiae*. *Genetics* 122, 19–27. <https://doi.org/10.1093/GENETICS/122.1.19>
- Singer, M.S., Gottschling, D.E., 1994. TLC1: Template RNA component of *Saccharomyces cerevisiae* telomerase. *Science* (80-.). 266, 404–409. <https://doi.org/10.1126/science.7545955>
- SM, G., JR, H., L, P., M, V., MA, R., S, N., LR, K., 2002. A G-quadruplex-interactive potent small-molecule inhibitor of telomerase exhibiting in vitro and in vivo antitumor activity. *Mol. Pharmacol.* 61, 1154–1162. <https://doi.org/10.1124/MOL.61.5.1154>
- Smith, F.W., Feigon, J., 1992. Quadruplex structure of *Oxytricha* telomeric DNA oligonucleotides. *Nat.* 1992 3566365 356, 164–168. <https://doi.org/10.1038/356164a0>
- Smith, F.W., Lau, F.W., Feigon, J., 1994. d(G3T4G3) forms an asymmetric diagonally looped dimeric quadruplex with guanosine 5'-syn-syn-anti and 5'-syn-anti-anti N-glycosidic conformations. *Proc. Natl. Acad. Sci.* 91, 10546–10550. <https://doi.org/10.1073/PNAS.91.22.10546>
- Smith, J.S., Chen, Q., Yatsunyk, L.A., Nicoludis, J.M., Garcia, M.S., Kranaster, R., Balasubramanian, S., Monchaud, D., Teulade-Fichou, M.P., Abramowitz, L., Schultz, D.C., Johnson, F.B., 2011. Rudimentary G-quadruplex-based telomere capping in *Saccharomyces cerevisiae*. *Nat. Struct. Mol. Biol.* 18, 478–486. <https://doi.org/10.1038/nsmb.2033>
- Strecker, J., Stinus, S., Caballero, M.P., Szilard, R.K., Chang, M., Durocher, D., 2017. A

- sharp Pif1-dependent threshold separates DNA double-strand breaks from critically short telomeres. *Elife* 6, e23783. <https://doi.org/10.7554/eLife.23783>
- Sun, H., Bennett, R.J., Maizels, N., 1999. The *Saccharomyces cerevisiae* Sgs1 helicase efficiently unwinds G-G paired DNAs. *Nucleic Acids Res.* 27, 1978. <https://doi.org/10.1093/NAR/27.9.1978>
- Sun, J., Yu, E.Y., Yang, Y., Confer, L.A., Sun, S.H., Wan, K., Lue, N.F., Lei, M., 2009. Stn1–Ten1 is an Rpa2–Rpa3-like complex at telomeres. *Genes Dev.* 23, 2900. <https://doi.org/10.1101/GAD.1851909>
- Sundquist, W.I., Klug, A., 1989. Telomeric DNA dimerizes by formation of guanine tetrads between hairpin loops. *Nat.* 1989 3426251 342. <https://doi.org/10.1038/342825a0>
- T, U., A, T., Y, K., 1995. A high dose of the STM1 gene suppresses the temperature sensitivity of the tom1 and htr1 mutants in *Saccharomyces cerevisiae*. *Biochim. Biophys. Acta* 1263, 285–288. [https://doi.org/10.1016/0167-4781\(95\)00123-X](https://doi.org/10.1016/0167-4781(95)00123-X)
- Taggart, A.K., Teng, S.C., Zakian, V.A., 2002. Est1p as a cell cycle-regulated activator of telomere-bound telomerase. *Science* (80-.). 297, 1023–1026. <https://doi.org/10.1126/science.1074968>
- Teixeira, M.T., Arneric, M., Sperisen, P., Lingner, J., 2004. Telomere Length Homeostasis Is Achieved via a Switch between Telomerase- Extendible and -Nonextendible States. *Cell* 117, 323–335. [https://doi.org/10.1016/S0092-8674\(04\)00334-4](https://doi.org/10.1016/S0092-8674(04)00334-4)
- Teng, S.-C., Zakian, V.A., 1999. Telomere-Telomere Recombination Is an Efficient Bypass Pathway for Telomere Maintenance in *Saccharomyces cerevisiae*. *Mol. Cell. Biol.* 19, 8083–8093. <https://doi.org/10.1128/mcb.19.12.8083>
- Traczyk, A., Liew, C.W., Gill, D.J., Rhodes, D., 2020. Structural basis of G-quadruplex DNA recognition by the yeast telomeric protein Rap1. *Nucleic Acids Res.* 48, 4562–4571. <https://doi.org/10.1093/nar/gkaa171>
- Tran, P.L.T., Mergny, J.-L., Alberti, P., 2011. Stability of telomeric G-quadruplexes. *Nucleic Acids Res.* 39, 3282. <https://doi.org/10.1093/NAR/GKQ1292>
- Tuzon, C.T., Wu, Y., Chan, A., Zakian, V.A., 2011. The *Saccharomyces cerevisiae*

- telomerase subunit Est3 binds telomeres in a cell cycle- and Est1-dependent manner and interacts directly with Est1 in vitro. *PLoS Genet* 7, e1002060. <https://doi.org/10.1371/journal.pgen.1002060>
- V, S., P, L., V, B., S, G., Y, C., MP, L., E, G., V, G., 2004. RPA regulates telomerase action by providing Est1p access to chromosome ends. *Nat. Genet.* 36, 46–54. <https://doi.org/10.1038/NG1284>
- Vega, L.R., Mateyak, M.K., Zakian, V.A., 2003. Getting to the end: telomerase access in yeast and humans. *Nat. Rev. Mol. Cell Biol.* 2003 412 4, 948–959. <https://doi.org/10.1038/nrm1256>
- Viscardi, V., Bonetti, D., Cartagena-Lirola, H., Lucchini, G., Longhese, M.P., 2007. MRX-dependent DNA Damage Response to Short Telomeres. *Mol. Cell Biol.* 27, 3047–3058. <https://doi.org/10.1091/mbc.e07-03-0285>
- VK, Y., JK, A., P, M., R, K., S, C., 2008. QuadBase: genome-wide database of G4 DNA--occurrence and conservation in human, chimpanzee, mouse and rat promoters and 146 microbes. *Nucleic Acids Res.* 36. <https://doi.org/10.1093/NAR/GKM781>
- Vodenicharov, M.D., Laterreur, N., Wellinger, R.J., 2010. Telomere capping in non-dividing yeast cells requires Yku and Rap1. *EMBO J.* 29, 3007. <https://doi.org/10.1038/EMBOJ.2010.155>
- W, Y., B, S., C, P., W, W., S, K., EA, C., 1998. Zuo1, a ribosome-associated DnaJ molecular chaperone. *EMBO J.* 17, 4809–4817. <https://doi.org/10.1093/EMBOJ/17.16.4809>
- Wahba, L., Costantino, L., Tan, F.J., Zimmer, A., Koshland, D., 2016. S1-DRIP-seq identifies high expression and polyA tracts as major contributors to R-loop formation. *Genes Dev.* 30, 1327–1338. <https://doi.org/10.1101/gad.280834.116>
- WATSON, J.D., CRICK, F.H.C., 1953. Molecular Structure of Nucleic Acids: A Structure for Deoxyribose Nucleic Acid. *Nat.* 1953 1714356 171, 737–738. <https://doi.org/10.1038/171737a0>
- WE, W., VM, T., KE, H., SD, L., JW, S., 1997. Normal human chromosomes have long G-

- rich telomeric overhangs at one end. *Genes Dev.* 11, 2801–2809. <https://doi.org/10.1101/GAD.11.21.2801>
- Wellinger, R.J., Wolf, A.J., Zakian, V.A., 1993. *Saccharomyces telomeres acquire single-strand TG1–3 tails late in S phase.* *Cell* 72, 51–60. [https://doi.org/10.1016/0092-8674\(93\)90049-V](https://doi.org/10.1016/0092-8674(93)90049-V)
- Wellinger, R.J., Zakian, V.A., 2012. Everything you ever wanted to know about *Saccharomyces cerevisiae* telomeres: beginning to end. *Genetics* 191, 1073–1105. <https://doi.org/10.1534/genetics.111.137851>
- Wilkie, A.O.M., Lamb, J., Harris, P.C., Finney, R.D., Higgs, D.R., 1990. A truncated human chromosome 16 associated with α thalassaemia is stabilized by addition of telomeric repeat (TTAGGG)_n. *Nat.* 1990 3466287 346, 868–871. <https://doi.org/10.1038/346868a0>
- Williamson, J.R., Raghuraman, M.K., Cech, T.R., 1989. Monovalent cation-induced structure of telomeric DNA: The G-quartet model. *Cell* 59, 871–880. [https://doi.org/10.1016/0092-8674\(89\)90610-7](https://doi.org/10.1016/0092-8674(89)90610-7)
- Wotton, D., Shore, D., 1997. A novel Rap1p-interacting factor, Rif2p, cooperates with Rif1p to regulate telomere length in *Saccharomyces cerevisiae*. *Genes Dev* 11, 748–760. <https://doi.org/10.1101/GAD.11.6.748>
- Wright, J.H., Zakian, V.A., 1995. Protein-DNA interactions in soluble telosomes from *Saccharomyces cerevisiae*. *Nucleic Acids Res.* 23, 1454–1460. <https://doi.org/10.1093/nar/23.9.1454>
- Wu, Z.J., Liu, J.C., Man, X., Gu, X., Li, T.Y., Cai, C., He, M.H., Shao, Y., Lu, N., Xue, X., Qin, Z., Zhou, J.Q., 2020. CDC13 is predominant over STN1 and TEN1 in preventing chromosome end fusions. *Elife* 9, 1–25. <https://doi.org/10.7554/ELIFE.53144>
- Y, Q., LH, H., 2008. Structures, folding patterns, and functions of intramolecular DNA G-quadruplexes found in eukaryotic promoter regions. *Biochimie* 90, 1149–1171. <https://doi.org/10.1016/J.BIOCHI.2008.02.020>
- Y, T., AK, T., VA, Z., 2001. The role of the Mre11-Rad50-Xrs2 complex in telomerase-mediated lengthening of *Saccharomyces cerevisiae* telomeres. *Curr. Biol.* 11, 1328–

1335. [https://doi.org/10.1016/S0960-9822\(01\)00372-4](https://doi.org/10.1016/S0960-9822(01)00372-4)

- Yu, G.-L., Bradley, J.D., Attardi, L.D., Blackburn, E.H., 1990. In vivo alteration of telomere sequences and senescence caused by mutated Tetrahymena telomerase RNAs. *Nat.* 1990 3446262 344, 126–132. <https://doi.org/10.1038/344126a0>
- Zahler, A.M., Williamson, J.R., Cech, T.R., Prescott, D.M., 1991. Inhibition of telomerase by G-quartet DNA structures. *Nature* 350, 718–720. <https://doi.org/10.1038/350718a0>
- Zakian, V.A., Blanton, H.M., Wetzel, L., 1986. Distribution of telomere-associated sequences in yeast. *Basic Life Sci.* 40, 493–498. https://doi.org/10.1007/978-1-4684-5251-8_37
- Zaug, A.J., Podell, E.R., Cech, T.R., 2005. Human POT1 disrupts telomeric G-quadruplexes allowing telomerase extension in vitro. *Proc. Natl. Acad. Sci.* 102, 10864–10869. <https://doi.org/10.1073/PNAS.0504744102>
- Zhang, M.-L., Tong, X.-J., Fu, X.-H., Zhou, B.O., Wang, J., Liao, X.-H., Li, Q.-J., Shen, N., Ding, J., Zhou, J.-Q., 2010. Yeast telomerase subunit Est1p has guanine quadruplex-promoting activity that is required for telomere elongation. *Nat. Struct. Mol. Biol.* 2010 172 17, 202–209. <https://doi.org/10.1038/nsmb.1760>
- Zhang, W., Durocher, D., 2010. De novo telomere formation is suppressed by the Mec1-dependent inhibition of Cdc13 accumulation at DNA breaks. *Genes Dev* 24, 502–515. <https://doi.org/10.1101/gad.1869110>
- Zhou, J., Monson, E.K., Teng, S.C., Schulz, V.P., Zakian, V.A., 2000. Pif1p helicase, a catalytic inhibitor of telomerase in yeast. *Science* (80-.). 289, 771–774. <https://doi.org/10.1126/SCIENCE.289.5480.771>
- Zou, L., Elledge, S.J., Jeitany, M., Wakimoto, H., Bryll, A.R., Ganem, N.J., Bersani, F., Pineda, J.R., Suvà, M.L., Benes, C.H., Haber, D.A., Boussin, F.D., Zou, L., 2003. Sensing DNA damage through ATRIP recognition of RPA-ssDNA complexes. *Science* 300, 1542–8. <https://doi.org/10.1126/science.1083430>

10. Acknowledgements

- ❖ I would like to express my deepest gratitude to my supervisor, Prof. Dr. Katrin Paeschke for seeing me in ways no one else did before and giving me this opportunity, for always believing in me and being supportive and positive, for having an open door with an intimate smile, not only for science but also as a friend.
- ❖ I would like to thank Dr. Stefan Juranek for his additional supervision and his great help and patience for preparing the figures and lots of scientific troubleshooting.
- ❖ I am thankful to my thesis committee, my second supervisor Prof. Brian Luke for reading my thesis, and Prof. Matthias Geyer and Prof. Oliver Gruss, for the critical and insightful discussions and feedback on my work.
- ❖ I am very grateful to Dr. Satya Pandey for his kind and helpful supervision in the lab as well as our scientific collaboration during my PhD.
- ❖ I am super grateful to Theresa Zacheja for sharing her outstanding technical as well as emotional support.
- ❖ I would like to thank Alessio De Magis for his scientific help and playing the inspiring songs in the lab.
- ❖ At this point, I want to thank all the current and former members of the Paeschke group for the good times and for including me in the conversations by switching from German to English. I want to thank Michaela Limmer for sharing the Mass spectrometry data and Philipp Simon for proofreading my thesis. I am very happy and grateful to my fellow PhD students in the group, Daniel Hilbig, Eike Schwindt, Markus Sauer, Melanie Kastl, Michaela Limmer and Lea Sauer for their friendship, help, the coffee breaks, wild laughter and beers in the balcony, and every scientific or non-scientific discussion.
- ❖ Additionally, I would like to say thanks to the people of the Medical Clinic III at the University Hospital Bonn, especially my friends Andre Gauchel and Pia Sauerborn.
- ❖ I would like to thank my amazing friends Azin and Fabian Lewalder for their unconditional support all along the way.
- ❖ I would like to express my deepest gratitude to my parents for their love and providing me wings to move to Germany and pursuing my scientific career.

11. Supplementary papers

11.1 Publications with PhD candidate as co-author, containing data presented in the thesis



Role of folding kinetics of secondary structures in telomeric G-overhangs in the regulation of telomere maintenance in *Saccharomyces cerevisiae*

Received for publication, February 4, 2020, and in revised form, May 7, 2020. Published, Papers in Press, May 8, 2020, DOI 10.1074/jbc.RA120.012914

Katarina Jurikova^{1,‡}, Martin Gajarsky^{2,‡}, Mona Hajikazemi^{3,‡} , Jozef Nosek⁴ , Katarina Prochazkova¹, Katrin Paeschke³, Lukas Trantirek^{2,5,*} , and Lubomir Tomaska^{1,*}

From the Departments of ¹Genetics and ⁴Biochemistry, Faculty of Natural Sciences, Comenius University in Bratislava, Bratislava, Slovakia, the ²Central European Institute of Technology, Masaryk University, Brno, Czech Republic, the ³Department of Oncology, Hematology, and Rheumatology, University Hospital Bonn, Bonn, Germany, and the ⁵Institute of Biophysics, Czech Academy of Sciences, Brno, Czech Republic

Edited by Craig E. Cameron

The ends of eukaryotic chromosomes typically contain a 3' ssDNA G-rich protrusion (G-overhang). This overhang must be protected against detrimental activities of nucleases and of the DNA damage response machinery and participates in the regulation of telomerase, a ribonucleoprotein complex that maintains telomere integrity. These functions are mediated by DNA-binding proteins, such as Cdc13 in *Saccharomyces cerevisiae*, and the propensity of G-rich sequences to form various non-B DNA structures. Using CD and NMR spectroscopies, we show here that G-overhangs of *S. cerevisiae* form distinct Hoogsteen pairing-based secondary structures, depending on their length. Whereas short telomeric oligonucleotides form a G-hairpin, their longer counterparts form parallel and/or antiparallel G-quadruplexes (G4s). Regardless of their topologies, non-B DNA structures exhibited impaired binding to Cdc13 *in vitro* as demonstrated by electrophoretic mobility shift assays. Importantly, whereas G4 structures formed relatively quickly, G-hairpins folded extremely slowly, indicating that short G-overhangs, which are typical for most of the cell cycle, are present predominantly as single-stranded oligonucleotides and are suitable substrates for Cdc13. Using ChIP, we show that the occurrence of G4 structures peaks at the late S phase, thus correlating with the accumulation of long G-overhangs. We present a model of how time- and length-dependent formation of non-B DNA structures at chromosomal termini participates in telomere maintenance.

More than 80 years ago, Herman Muller and Barbara McClintock predicted that terminal regions of linear chromosomes harbor special functions, and they termed these regions telomeres (1, 2). Their visionary studies showed that telomeres are vital protective caps that prevent nucleolytic degradation of chromosomal ends and their erroneous recognition as double-strand breaks by DNA repair machinery

(3). In addition to this end-protection problem, telomeres must address the end-replication problem caused by the inability of conventional DNA polymerases to complete DNA replication at chromosomal termini. The incomplete synthesis of terminal DNA regions of the chromosomes, referred to as telomeric DNA, results in the shortening of DNA followed by cell senescence and chromosomal instability (4–6).

Telomeric DNA of eukaryotic nuclear chromosomes provides a platform for the assembly of molecular partners involved in mediating telomere functions. In the case of eukaryotic nuclear chromosomes, this platform usually consists of a dsDNA region composed of short GC-rich tandem repeats, terminating with a G-rich 3' ssDNA overhang (G-overhang). Many organisms possess a subtle variation of a vertebrate telomeric repeat of 5'-TTAGGG-3' (7); however, these repeats may be of variable lengths (8) or heterogeneous in sequence, and this is the case in the yeast *Saccharomyces cerevisiae* (9). The length of the G-overhang exhibits interspecific, intercellular, and interchromosomal variations (10, 11). Telomeric DNA is bound by a set of dedicated proteins forming a protective nucleoprotein structure comprising a number of telomere-binding proteins that often exhibit binding specificity (3, 12). Examples include the dsDNA-binding protein Rap1 and the G-overhang-binding protein Cdc13 in *S. cerevisiae*. Telomere shortening is most often prevented via extension by telomerase, a ribonucleoprotein enzymatic complex that includes an RNA template and a reverse transcriptase subunit, followed by the fill-in synthesis of the C-rich strand mediated by primase, Pol α , which maintains the number of tandem repeats within a relatively stable interval (13–16).

The other means of protecting the very tip of the chromosome is based on inherent evolutionarily conserved characteristics of the G-overhang (*i.e.* its ability to fold into non-B DNA structures, which are considered as its universal epigenetic hallmark) (17). The G-rich telomeric DNA from the vast majority of eukaryotes displays a propensity to form a four-stranded structure called a G-quadruplex (G4) (10, 18–20) that relies on the formation of planar guanine tetrads (G-quartets) marked by a Hoogsteen base-pairing-type guanine-guanine pattern.

This article contains supporting information.

✂ Author's Choice—Final version open access under the terms of the Creative Commons CC-BY license.

‡ These authors contributed equally to this work.

* For correspondence: Lukas Trantirek, lukas.trantirek@ceitec.muni.cz; Lubomir Tomaska, lubomir.tomaska@uniba.sk.

Present address for Katarina Jurikova: Dept. of Cellular, Computational, and Integrative Biology - CIBIO, University of Trento, Trento, Italy.

G4 formation at telomeres has been demonstrated to alter telomerase activity (21–25). Currently, controversial data exist that link G4 formation and function to telomeres. In detail, antiparallel G4 structures block telomerase (24), whereas intramolecular parallel G4 structures support telomerase binding to telomeres (21, 22). Telomeric G4 structures interact with a number of telomere-associated proteins. Helicases involved in telomere maintenance, Sgs1 in *S. cerevisiae*, human WRN and BLM, and widely conserved Pif1, all bind and unwind G4 structures (26–31). Est1, a subunit of budding yeast telomerase involved in the recruitment of the complex to a G-overhang, was shown to bind G4 structures and promote their formation (32, 33). Human telomerase, which also displays G4 binding, was found to partially unwind and extend the G4 structure (34). Additionally, observations that the processivity of telomerase and association with telomeres can be impaired by ligands stabilizing telomeric G4 structures both *in vitro* and *in vivo* not only marked telomeric G4 structures as potential molecular targets suitable for anticancer therapy but also further demonstrated that G4 formation is an essential component for telomere function and maintenance (34–38). Additionally, G4 also interacts with telomere-binding proteins; in *S. cerevisiae*, Rap1 stimulates G4 formation *in vitro* (39, 40), and a functional interplay between the formation of G4 structures and Cdc13 binding has been suggested by both *in vitro* and *in vivo* experiments (41, 42). These data suggest a link between G4 and telomere function in budding yeast; however, the mechanistic details of their participation remain elusive.

In vertebrates, including humans, the length of telomeric G-overhangs fluctuates between 50 and 250 nt during the cell cycle (43, 44). As only four human telomeric DNA tandem repeats are required for the formation of a G4 structure (45), the capacity to form a G4 is maintained throughout the whole cell cycle. In contrast, in *S. cerevisiae*, the G-overhang is rather short (9–14 nt) throughout most of the cell cycle and is extended to 30–100 nt only in the late S phase (46, 47). As the capacity to form a G4 structure depends on the length of the ssDNA (17, 19), the overhangs are presumably unable to form a G4 during most of the cell cycle. However, shorter telomeric ssDNA may adopt an alternative structure. Recently, our group demonstrated that the abundant short (11-nt) sequence motif (5'-GTGTGGGTGTG-3'), covering more than 90% of irregular telomeric DNA in *S. cerevisiae*, folds into a novel DNA structure that is a mixture of parallel/antiparallel fold-back structures stabilized by guanine-guanine base pairs, herein referred to as a G-hairpin (48).

In this study, we investigated the stereochemical properties of model oligonucleotides emulating telomeric G-overhangs of different lengths with regard to the kinetics of non-B DNA structure formation, their folding topologies, and their capacity to interact with Cdc13. We found that the formation of a stable secondary structure in both long and short telomeric G-overhangs impairs the binding to Cdc13. Additionally, whereas the formation of non-B DNA structures in a long telomeric G-overhang proceeds on the time scale of relevant biological processes (e.g. the S phase), the time required for the formation of a G-hairpin structure notably exceeds the duration of the cell cycle. Our results suggest that the

physiological roles of non-B DNA structures in telomeric G-overhangs are to tune the interaction between Cdc13 and telomeric DNA. We propose a kinetically based model for the initial phase of the telomerase catalytic cycle involving the recruitment of Cdc13 to a telomeric G-overhang. In this model, the folding kinetics of non-B DNA structures of G-overhangs play the role of a switch in the control of Cdc13 binding to a G-overhang, indicating that it may be involved in telomerase recruitment.

Results

Oligonucleotides of different lengths emulating telomeric ssDNA overhangs from *S. cerevisiae* fold into intramolecular G4 structures with different topologies

The oligonucleotide-emulating short telomeric ssDNA overhang (11 nt) of *S. cerevisiae* (ONG11) was recently shown to fold into an intramolecular G-hairpin (48). In contrast, previous CD and NMR studies on oligonucleotides emulating extended (>19-nt) telomeric DNA indicated the formation of G4 structures (17, 19). As the folding topology of a G4 is known to strongly depend on the nucleotide composition and length of the investigated fragment, we conducted an analysis of 10 different DNA constructs corresponding to various lengths with 21–33-nt-long truncations derived from the native (irregular) telomeric DNA of *S. cerevisiae* (Table 1) using CD spectroscopy and nondenaturing PAGE.

As seen in Fig. S1, the migration rates of all the constructs in nondenaturing PAGE were consistent with the formation of monomolecular species. The shapes of the CD spectra, acquired 24 h after annealing, were indicative of the formation of G4 structures for all the constructs. Based on the shapes of the CD spectra, the individual constructs were clustered into three distinct classes (Fig. 1). Class I (ONG1–6) displayed CD spectra marked by two dominant bands, one negative at ~240 nm and one positive at ~260 nm; this is the characteristic spectrum of a parallel G4. Class II (ONG9 and ONG10) displayed CD spectra with a dominant negative band at ~265 nm and a positive band at ~290 nm; this is a characteristic spectrum of an antiparallel G4. Class III (ONG7 and ONG8) displayed CD spectra with two dominant positive bands at ~260 and ~290 nm, indicating that the constructs exist as a mixture of parallel and antiparallel G4 structures. Note, however, that although the shapes of the CD spectra of ONG1–6 and ONG9–10 were indicative of having parallel and antiparallel G4 structures, respectively, the detailed analysis of spectral data revealed that these constructs are similar to ONG7 and ONG8 and capable of adopting at least two distinct G4 topologies that co-exist as a mixture of dominant and minor G4 species (for the detailed analysis of ONG1 and ONG9, which are representative of Class I and Class II constructs, see the next paragraph). Altogether, the presented data indicate that whereas short telomeric overhangs that are present at telomeres for the majority of the cell cycle have the propensity to form G-hairpin (48), the extended telomeric overhangs in the late S phase have the capacity to fold into topologically diverse G4 structures.

Length-dependent folding kinetics of telomeric overhangs

Table 1

List of oligonucleotide constructs employed for screening the conformational space of extended telomeric ssDNA from *S. cerevisiae*. Structural types and topologies of non-B DNA structures were assigned on the basis of CD spectra (Fig. 1)

	Length	Sequence (5' → 3')	Structural type	Dominant topology
	<i>nt</i>			
ONG1	33	GTGTGGGTGTGGTGTGGGTGTGGTGTGGGTGTG	G-quadruplex	Parallel
ONG2	22	GTGTGGGTGTGGTGTGGGTGTG	G-quadruplex	Parallel
ONG3	32	GTGTGGGTGTGGTGTGGGTGTGGTGTGGGTGT	G-quadruplex	Parallel
ONG4	32	TGTGGGTGTGGTGTGGGTGTGGTGTGGGTGTG	G-quadruplex	Parallel
ONG5	30	GTGTGGGTGTGGTGTGGGTGTGGTGTGGGT	G-quadruplex	Parallel
ONG6	30	TGGGTGTGGTGTGGGTGTGGTGTGGGTGTG	G-quadruplex	Parallel
ONG7	27	TGGGTGTGGTGTGGGTGTGGTGTGGGT	G-quadruplex	Mixture
ONG8	26	TGTGGTGTGGTGTGGTGTGGGTGTG	G-quadruplex	Mixture
ONG9	21	TGGGTGTGGTGTGGGTGTGGT	G-quadruplex	Antiparallel
ONG10	21	TGGTGTGGGTGTGGTGTGGGT	G-quadruplex	Antiparallel
ONG11	11	GTGTGGGTGTG	G-hairpin	

Distinct secondary structures in short and extended telomeric overhangs have similar thermodynamic stabilities, but they notably differ in their folding kinetics

As any biological action of DNA secondary structures is jointly governed not only by conformational features but also by thermodynamic and kinetics factors, we set out to characterize the thermodynamic stability and estimate the folding kinetics for (i) the DNA G-hairpin being representative of a secondary structural element in a short telomeric overhang (ONG11) and (ii) parallel and antiparallel G4 structures forming in the model of an extended telomeric overhang (ONG1). However, as the antiparallel form cannot be kinetically isolated within the ONG1 context, we used ONG9, which almost exclusively adopts an antiparallel G-quadruplex structure (see below), as a model emulating antiparallel G-quadruplex that is forming in the context of a long telomeric overhang. To obtain thermodynamic stability information, the CD melting profiles for ONG1, ONG9, and ONG11 were acquired at pH 7.2 in K⁺S buffer. As shown in Fig. 2A, the melting temperatures for these structures were markedly similar, ranging from 46.3 to 53.5 °C. The acquired melting profiles indicate that formation of G-hairpin in a short telomeric overhang as well as antiparallel and parallel G-quadruplex structures in an extended telomeric overhang is plausible under physiologically relevant temperatures.

Despite the different appearances in the CD spectra of ONG1 and ONG9 (Fig. 1), the time-resolved CD and NMR measurements revealed similarities in their folding. The NMR spectrum of ONG1 acquired at *t* = 10 min was unresolved and characteristic of a polymorphic mixture of at least two G4 species, whereas the NMR spectrum of ONG1 acquired at *t* = 4 h displayed ~12 resolved signals (the number expected for a single three-G-tetrad-based G4 structure) (see Fig. 2B). These time-dependent changes in the NMR spectral pattern are a characteristic indication of the kinetic control of G4 formation, where the kinetically preferred G4 topology is distinct from that corresponding to the thermodynamically preferred state (49). Hyperchromic and hypochromic shifts in the CD spectra of ONG1 observed at ~260 and ~285 nm, respectively, between *t* = 10 min and *t* = 4 h (Fig. 2), suggested both the antiparallel and parallel G4 structures as being the kinetically and thermodynamically preferred conformations, respectively. The behavior of ONG9 seemingly differed from that of ONG1; the NMR spectra displayed two independent sets of imino signals

regardless of the data acquisition time: eight strong well-resolved signals in the region of 11.6–12.3 ppm (from dominant species) and ~12 very weak signals (from minor species) in the region of 10.8–11.6 ppm (Fig. 2B). Whereas the number of signals in the region of 11.6–12.3 ppm was consistent with that expected for a G4 consisting of two G-tetrads, the number of signals from the minor species was consistent with a G4 structure consisting of three G-tetrads. The overall appearance of the NMR and CD spectra (Fig. 2) indicated that the ONG9 folds into a mixture of dominant two-tetrad antiparallel and (minor) three-tetrad-based G4 structure. Based on the NMR spectra, the population of the minor species was estimated to be ~5% (Fig. 2B). Importantly, the spectral signatures of both NMR and CD spectra for ONG9 were found to be time-independent (Fig. 2B). This suggests that both dominant and minor species have virtually identical thermodynamic stabilities and that the formation of two-tetrad and three-tetrad G4 structures is, similar to the situation with ONG1, under kinetic control (with a folding rate for the two-tetrad G4 being faster than that for the three-tetrad G4).

Most importantly, the folding of G4 structures (ONG1 and ONG9) proceeded on a time scale dramatically faster than that of the G-hairpin (ONG11). In contrast to the NMR spectrum for ONG9, which was fully developed at *t* = 10 min, the corresponding spectrum of ONG11 was devoid of any signals, indicating the absence of a folded species (G-hairpin) (Fig. 2B). Although imino signals characteristic of G-hairpin formation were detected at *t* = 4 h, their intensities further increased over time, suggesting an ongoing folding process (Fig. 2B). Notably, the time-dependent characteristics of the changes in the NMR spectra of ONG11 were fundamentally distinct from those observed for ONG1. Although the pattern of the NMR spectrum of ONG1 also changed with time, the integral intensities of the imino signals remained constant (Fig. 2C), indicating that the changes in the NMR spectral pattern were not due to changes in the populations of unfolded and folded species but rather due to the refolding of a kinetically preferred G4 structure into a thermodynamically preferred G4 structure (*i.e.* a process that presumes a steady population of the unfolded state) (49). Altogether, the time-resolved CD and NMR data corroborated that G4 structures folded on a time scale that is comparable with or faster than 10 min (resolution limit of our experiment), whereas the G-hairpin folding proceeded on a time scale of several hours (Fig. 2C).

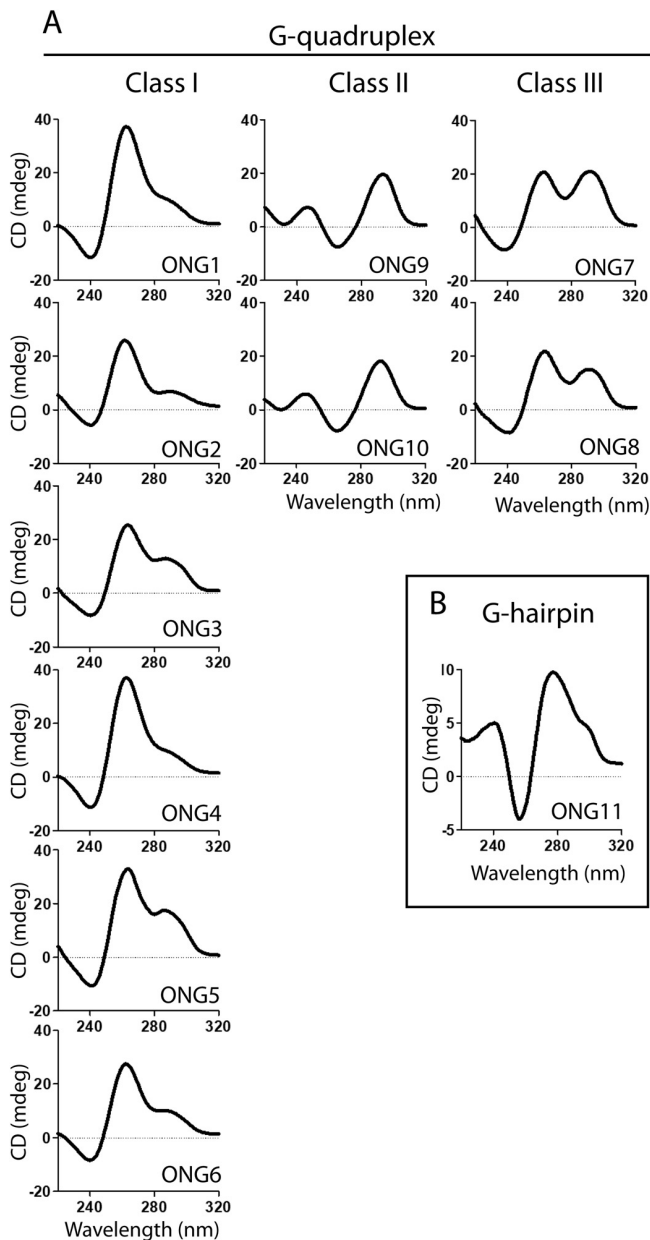


Figure 1. Oligonucleotides emulating long and short telomeric G-overhangs adopt distinct non-B DNA structures. CD spectra of oligonucleotide constructs emulating long (A) and short (B) telomeric G-overhangs (cf. Table 1). CD spectra were measured at RT in K^+S buffer at a DNA concentration of $50 \mu M$. The spectra were measured 24 h after sample annealing.

To assess the relevance of these *in vitro* data to *in vivo* physiological situations, where the folding of these structures might be actively modulated by cellular factors, we compared the folding of ONG1 (a model of a G-quadruplex-forming telomeric overhang), and ONG11 (a model of a G-hairpin-forming short telomeric overhang) in crude yeast cell lysate. Individual constructs were annealed in buffer and then mixed with the cell lysate immediately upon cooling down to room temperature. Whereas the 1D 1H NMR spectrum of ONG1 acquired in the presence of the cell lysate showed, similarly to the situation in the buffer, a characteristic pattern for G4 formation at 10 min, the respective spectrum of ONG11 (G-hairpin) was devoid of

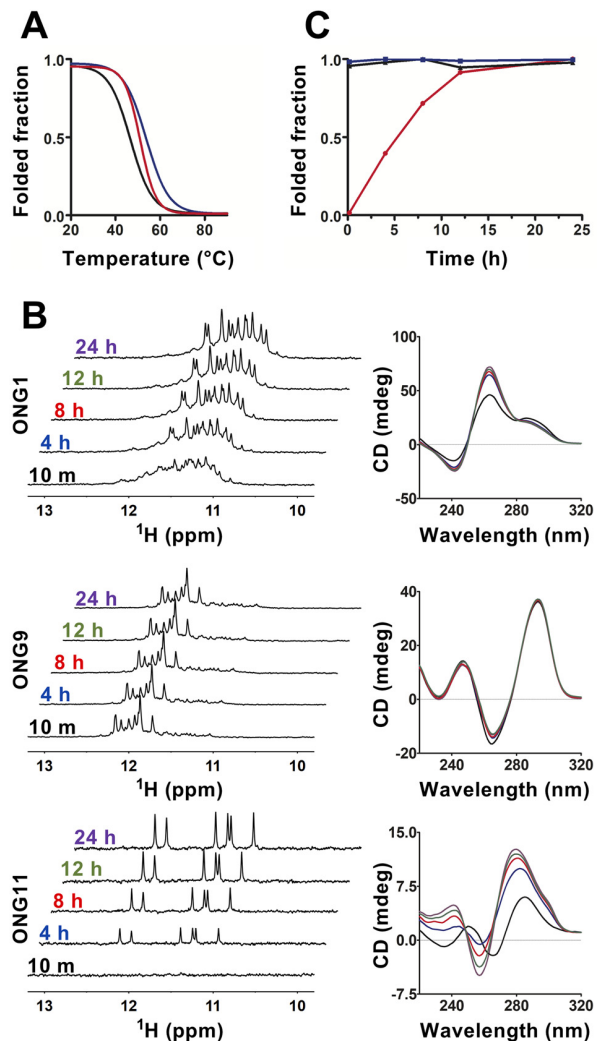


Figure 2. Non-B DNA structures in long and short telomeric G-overhangs have notably distinct formation kinetics. A, normalized CD melting curves for ONG1 (black; apparent $T_m = 46.3^\circ C$), ONG9 (blue; apparent $T_m = 53.5^\circ C$), and ONG11 (red; apparent $T_m = 50.7^\circ C$). B, imino region of 1D 1H NMR (left) and CD (right) spectra of ONG1, ONG9, and ONG11 acquired as a function of time (time points indicated). The NMR and CD spectra were measured in K^+S buffer at a DNA concentration of $50 \mu M$. NMR spectra were acquired using a zgpgpw5 pulse sequence (see “Experimental procedures”). C, time course of the folding process for ONG1 (black, triangle), ONG9 (blue, square), and ONG11 (red, circle) as estimated from the normalized time-dependent changes of imino signals in NMR spectra presented in A.

any imino signals (Fig. S2). The absence of the imino signals in the lysate NMR spectra of ONG11 suggests either that ONG11 remains unfolded at the timescale of the NMR experiment or that ONG11 is bound by high-molecular weight cellular factors (causing relaxation broadening of NMR signals). In either case, these data argue against the existence of the intracellular factors promoting G-hairpin folding, although such activities may be present in intact cells. Together, these results suggest that the formation of secondary structures in short and extended telomeric overhangs is kinetically rather than thermodynamically resolved; in addition, both the structural and formation kinetics should be considered when attempting to assess their relevance *in vivo*.

Length-dependent folding kinetics of telomeric overhangs

Secondary structures in telomeric DNA, regardless of their topology, interfere with Cdc13 binding

Cdc13 binds to G-overhang to mediate the recruitment of telomerase to telomeric DNA (50–52). Analogously to the length of the G-overhang, the activity of telomerase is regulated by the cell cycle. Telomerase is recruited to telomeres in the late S phase, a stage also marked by the presence of long (>30-nt) G-overhangs, resulting from both telomerase action and nuclease resection of the 5' strand (46, 53). The relationship between the telomerase recruitment and length-dependent folding of a G-overhang into DNA secondary structures is currently unknown. As our previous experiments have shown that different secondary structures form on G-overhangs of different lengths with different folding kinetics, the ability of Cdc13 to bind to the secondary structures formed by G-overhangs may influence the presence of Cdc13 on the overhang and thus also may impact telomerase recruitment to telomeres.

To address this issue, we assessed the ability of Cdc13 to bind telomeric oligonucleotides exhibiting various secondary structures *in vitro*. For the experiments, we employed the principal oligonucleotide/oligosaccharide-binding (OB) fold domain of Cdc13 spanning residues 497–694 (Cdc13-DBD), whose DNA-binding properties in terms of dissociation constants are very similar to those of the full-length Cdc13 (K_D of Cdc13-DBD for ONG11 is 0.25–0.5 of the K_D of Cdc13 (54)). We expressed Cdc13-DBD in the *Escherichia coli* BL21(DE3) strain and purified the recombinant protein using affinity chromatography (Fig. S3). The binding properties of the purified protein were assessed and found to correspond to previously published studies (Fig. S4) (55, 56). The binding between Cdc13-DBD and ONG1, ONG9, or ONG11, which are representative of telomeric parallel G4, antiparallel G4, and G-hairpin structures, respectively (Table 1), was assessed with respect to the ssDNA (unfolded) G-hairpin-forming sequence of 5'-GTGTGGG-TGTG-3' (ONG11), which binds to the Cdc13-DBD with high affinity (54). For the purpose of the assay, the preformed complex between Cdc13-DBD and an unlabeled competitor (ONG1, ONG9, or ONG11) was incubated with a radioactively ^{32}P -labeled probe (ONG11), and the capacity of the unlabeled oligonucleotides to outcompete the binding of the ^{32}P -labeled ONG11 was assessed by observing the amount of freely migrating labeled probe on a gel. In each experiment, the competitor DNA was annealed and incubated for the corresponding time in either water (favoring the unfolded state) or $1\times \text{K}^+$ buffer, which favors folding into secondary structures (Fig. S5). The results of electrophoretic mobility shift assays (EMSAs) showed that the competitor oligonucleotides in the folded form (K^+) exhibit a decreased ability to displace the labeled probe from binding to Cdc13-DBD when compared with their unfolded counterparts (Fig. 3A). To further confirm that the displaced free probe is due to the presence of the competitor DNA and not due to other reaction components, we also tested a wider range of competitor concentrations (Fig. S6). These results indicate that for both G-hairpin (ONG11) and G4 (ONG1), Cdc13-DBD has lower affinity toward the secondary structures formed on the telomeric DNA than toward the same oligonucleotides in their ssDNA form.

Previously, parallel and antiparallel G4 structures have been proposed to have different effects on telomerase activity on telomeres (21, 22, 24). For this reason, we assessed the difference in the ability of an oligonucleotide to bind to Cdc13-DBD depending on the topology of the G4 structure it forms (Fig. 3B). Notably, our results show that the folded ONG1 (parallel G4) and ONG9 (antiparallel G4) perform similarly as competitors (Fig. 3B), suggesting that the topology of a G4 does not have an impact on the binding of Cdc13-DBD. This might indicate that it is primarily the presence of a secondary structure on a G-overhang, not its topology, that may determine the Cdc13-binding affinity once a secondary structure is formed.

Kinetics of G-overhang folding influence Cdc13 binding

The formation of secondary structures on telomeric ssDNA and their ability to interfere with Cdc13 binding may implicate their role on telomeres *in vivo*. In particular, our data show that G4 and G-hairpin structures have different folding kinetics, with fast-folding G4 and G-hairpin folding in a span of hours, possibly ruling out its involvement in physiological processes (Fig. 2). To elucidate this possibility, we studied whether the binding of Cdc13-DBD to the telomere-derived oligonucleotides that were allowed to fold for different time periods matched their folding kinetics. We performed EMSA experiments with unfolded, ^{32}P -labeled ONG11 and competitors (ONG1 (quickly folded parallel G4) and ONG11 (slowly folded G-hairpin)) either in water (favoring the unfolded state) or in $1\times \text{K}^+$ buffer (favoring the folded state) at different time points after the initiation of their folding (Fig. 4). Our experiments suggest that the G4 (ONG1) is folded after 20 min in K^+ buffer, whereas the G-hairpin (ONG11) folding takes several hours to be completed (Fig. 2). For this reason, the ability of ONG1 and ONG11 to act as a competitor was evaluated after 20 min and 24 h after folding, as compared with the competitor in water (Fig. 4, top). The quantification of the free-migrating probe shows that the amount of free probe decreases with folding time for the G-hairpin-forming competitor, but it does not change for the competitor DNA folding into G4 (Fig. 4, bottom). These results indicate that, in agreement with our NMR folding kinetics measurements, ONG11 loses its competing ability with increasing time, suggesting an ongoing folding process, and ONG1 performs poorly as a competitor 20 min after annealing, indicating completed folding after the shorter time period. In other words, the loss of the competing ability assayed by EMSA experiments mirrors the folding kinetics of the G-hairpin and G4 structures.

To complement EMSA experiments using oligonucleotide competitors, we performed direct titrations of the Cdc13-DBD using constant concentrations of ONG1, ONG9, and ONG11 that were renatured in $1\times \text{K}^+$ buffer either for 20 min (short folding) or >24 h (long folding). We hypothesized that in the case of ONG1 and ONG9, which form G4 structures quickly (Fig. 2), Cdc13-DBD would exhibit similar affinity to the probes regardless of the time of their folding. In contrast, in the case of ONG11, which is present mostly after 20 min as ssDNA, the binding was compromised when the oligonucleotide was allowed to fold during an extended time period when it reached

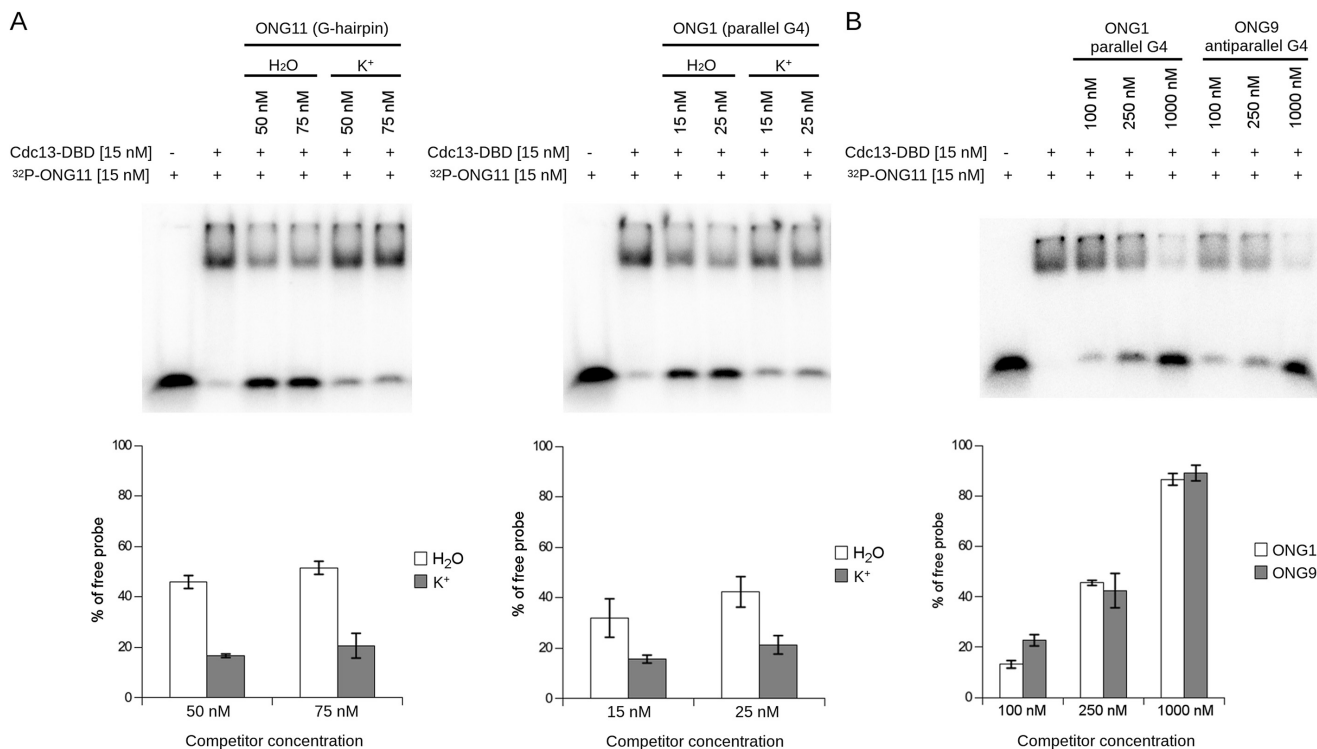


Figure 3. Secondary structures forming on telomeric DNA decrease the binding of Cdc13-DBD. *A, top*, EMSA with radioactively labeled ONG11 as a probe and ONG11 and ONG1 as unlabeled competitors. For the reactions with folded competitors (*labeled K⁺*), the unlabeled DNA oligonucleotides were diluted in $1 \times K^+$ buffer, boiled, allowed to cool, incubated at 22 °C for 72 h, mixed with other components of the EMSA reaction to a final concentration of 50 or 75 nM, incubated for 10 min at 22 °C, and loaded onto the gel. For the reactions with unfolded competitors (*labeled H₂O*), the unlabeled DNA oligonucleotides were diluted in water, boiled, allowed to cool, immediately mixed with other components of the EMSA reaction to a final concentration of 50 or 75 nM, incubated for 10 min at 22 °C, and loaded onto the gel. The labeled probe was boiled and cooled immediately prior to adding to EMSA reactions. For both oligonucleotides, the folded competitors exhibit decreased competing ability (measured as the amount of freely migrating probe) compared with the controls in water. *Bottom*, quantification of the free probe, mean \pm S.D.; $n = 4$ and $n = 3$, independent replicas for ONG1 and ONG11, respectively. *B*, the G4 topology does not impact Cdc13-DBD binding. *Top*, EMSA with radioactively labeled ONG11 as a probe and folded ONG1 (parallel G4) and ONG9 (antiparallel G4) as competitors. The unlabeled DNA oligonucleotides were diluted in $1 \times K^+$ buffer, boiled, incubated at 22 °C for 24 h, and then mixed with other components of the EMSA reaction to a final concentration of 100, 250, or 1000 nM. The labeled probe was boiled and cooled immediately prior to adding to the EMSA reactions. *Bottom*, quantification of the free probe, mean \pm S.D., $n = 2$, independent replicas. *Error bars*, S.D.

the structure of a G-hairpin. These results are shown in Fig. S7 and support this hypothesis. The extent of the inability of Cdc13-DBD to bind to the G-hairpin is not as pronounced as in the case of the experiment presented in Fig. 4; this is probably due to interference of the phosphate group with folding of ONG11 (Fig. S8; *cf.* Note S1). However, the decreased binding of Cdc13-DBD to ONG11 in the case of the long folding is evident and reproducible, and this result supports the scenario that the length-dependent kinetics of folding of telomeric overhangs affect their ability to interact with Cdc13.

EMSA-based experiments also suggested that Cdc13-DBD has a notably lower affinity toward the secondary structures formed on the telomeric DNA than to the same oligonucleotides in their single-stranded form; this implicates that the binding of Cdc13 to telomeric DNA is regulated by DNA folding kinetics. To directly rule out the possibility of interference of Cdc13 with the folding of non-B DNA structures in the course of EMSA, we acquired time-resolved NMR spectra of ONG1, ONG9, and ONG11 in the presence of equimolar amounts of Cdc13. (Note: The spectra were acquired in K^+ TD buffer). After a 100 μ M solution of the ONGs was thermally denatured and cooled for ~ 2 min to room temperature, it was mixed into a 100 μ M solution of Cdc13-DBD. The NMR spectra

of the resulting mixtures were acquired at 30, 90, and 150 min after mixing (Fig. 5). For ONG1 and ONG9, at all of the indicated time points, the overall intensities of imino signals remained essentially constant, whereas the intensity of signals in the respective spectra of ONG11 gradually increased over time (Fig. 5, *A* and *B*). Importantly, the time-dependent changes observed in the spectra of ONG1, ONG9, and ONG11 in the presence of equimolar amounts of Cdc13-DBD paralleled those observed in the absence of Cdc13-DBD (*cf.* Fig. 2C). Note: Compared with the NMR spectra of ONG1 acquired in K^+ S buffer (*cf.* Fig. 2), the spectra measured in K^+ TD buffer, both in the presence and absence of Cdc13-DBD, are unresolved. The unresolved character of the NMR spectrum of ONG1 in the presence/absence of Cdc13-DBD results from the increased G-quadruplex polymorphism of ONG1 in the elution (K^+ TD) buffer required for the measurements in the presence of Cdc13-DBD (see Fig. S9).

Overall the data demonstrate that Cdc13-DBD neither promotes nor hinders ONG1/ONG9/ONG11 folding. Most notably, these data directly provided information on the capacity of Cdc13-DBD to bind to G4/G-hairpin structures. In the NMR experiment, which is based on monitoring the imino signals originating exclusively from folded species, the formation of a

Length-dependent folding kinetics of telomeric overhangs

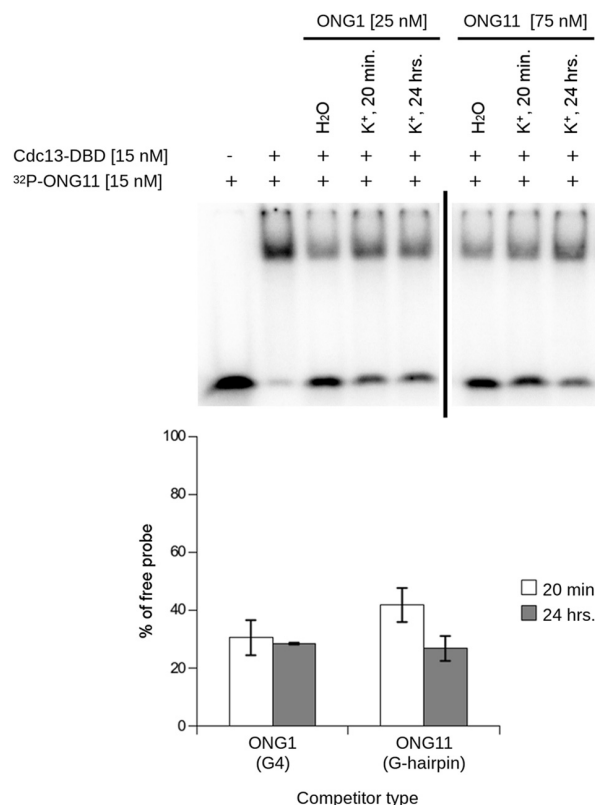


Figure 4. Different folding kinetics of G-hairpin and G-quadruplex affect their ability to bind Cdc13-DBD in a time-dependent manner. *Top*, EMSA with radioactively labeled ONG11. ONG1 and ONG11 were used as unlabeled competitors that were allowed to fold in $1 \times K^+$ buffer for the indicated time periods. Whereas ONG11 (G-hairpin) shows decreased binding of Cdc13-DBD between 20 min and 24 h, ONG1 (parallel G4) does not exhibit this time-dependent change. *Bottom*, quantification of the free probe, mean \pm S.D., $n = 2$, independent replicas. ONG1 and ONG11 were analyzed on separate gels, as indicated by the vertical bar. Error bars, S.D.

complex between Cdc13 and G-quadruplex/G-hairpin would result in a notable increase in the line widths of the signals due to a dramatic change in the quadruplex/G-hairpin correlation time (rotational diffusion coefficient) upon complex formation. The observation of comparable linewidths between the imino signals of G-quadruplex/G-hairpin in the absence and presence of Cdc13 is evidence that neither the G-quadruplex nor the G-hairpin is capable of forming a stable complex with Cdc13 (Fig. 5C). The inability of Cdc13-DBD to bind G-quadruplex DNA is further corroborated by essentially identical CD spectra of both ONG1 and ONG9 acquired in the absence and presence of equimolar amount of the protein (Fig. S10).

G4 occupancy differs through the cell cycle at the telomeric region and is in accordance with the length of the G-overhang

Immunofluorescence visualization of G4 with the BG4 antibody in human cells showed that G4 formation in the endogenous genomic region is modulated during cell cycle progression; the number of BG4 foci reached a maximum as the cells were proceeding through the S phase (57). However, due to the heterogeneous telomeric repeat motif in *S. cerevisiae*, it is unknown whether yeast telomeres produce G4 structures *in*

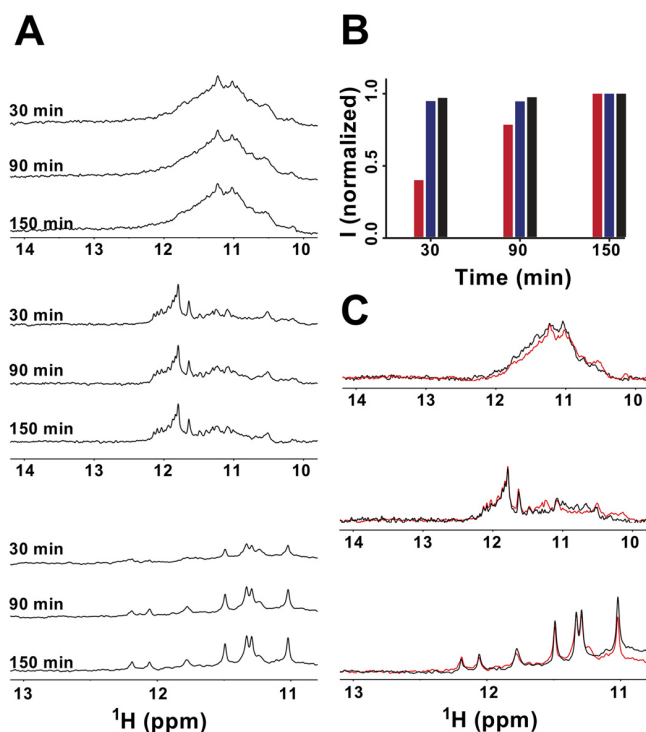


Figure 5. Cdc13-DBD does not form a stable complex with either a G-hairpin or a G-quadruplex and does not interfere with their folding kinetics. *A*, imino regions of the 1D ¹H NMR spectra of an equimolar mixture of ONG1 (top), ONG9 (middle), and ONG11 (bottom) and Cdc13-DBD were acquired as a function of time (indicated). *B*, time course of the folding process for ONG1 (black box), ONG9 (blue box), and ONG11 (red box) in the presence of equimolar amounts of Cdc13-DBD as estimated from normalized time-dependent changes in the intensity of imino signals (*I*) from NMR spectra presented in *A*. The imino signal intensities at $t = 30$ and $t = 90$ min were normalized with respect to those acquired at $t = 150$ min. The NMR spectra were acquired using a 1-1 echo pulse sequence with an excitation maximum set to 12 ppm. *C*, overlay of the imino regions of the 1D ¹H NMR spectra of ONG1 (top), ONG9 (middle), and ONG11 (bottom) measured in K⁺TD buffer in the absence (black) and in the presence of equimolar amounts of Cdc13-DBD (red).

in vivo. To test whether yeast telomeres form G4 structures *in vivo*, we performed ChIP followed by qPCR. Using a specific antibody (BG4) that targets folded G4 structures, in these ChIP experiments, we pulled down G4 regions from the yeast genome. qPCR analysis allowed us to quantitatively measure G4 structure formation at telomeres (Fig. 6A). These data showed that at two telomeres, VI-R and VII-L G4 structures are formed. In untreated control ChIP experiments, in which no BG4 antibody was added, no binding was observed. As an additional control, we treated the cells with the highly specific G-quadruplex ligand, Phen-DC₃ (58). After treatment, an increase in telomeric G4 was detectable after ChIP and qPCR. Next, we tested whether G4 formation is cell cycle-regulated and whether this regulation is in agreement with length changes of the telomere overhang. To address this, *S. cerevisiae* cells were arrested in the G₁ phase with the mating pheromone α factor and released into the cell cycle with varying concentrations of hydroxyurea (HU) to segment the S phase and the anti-microtubule assembly agent, nocodazole, to arrest the cells in G₂ phase (Fig. 6B). Next, we quantitatively measured G4 occupancy at the VII-L telomeric region by ChIP and qPCR. Cell

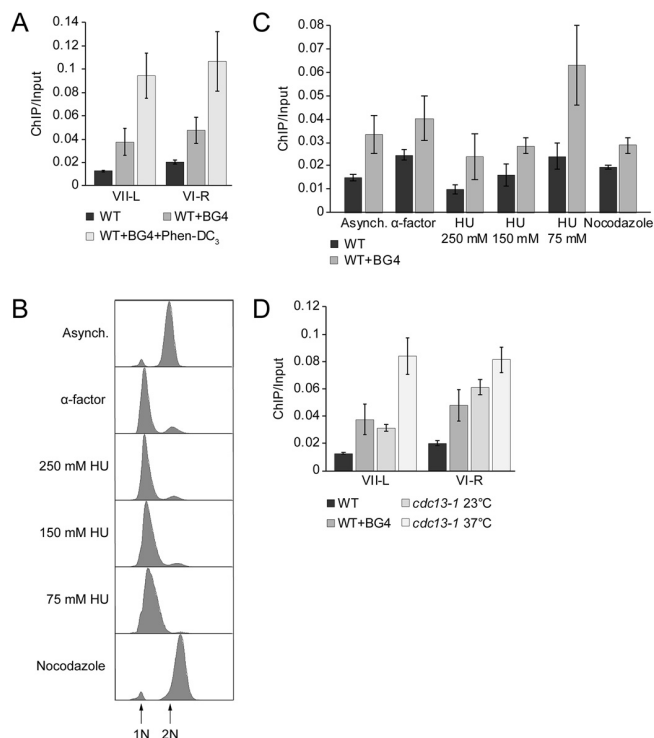


Figure 6. Formation of telomeric G-quadruplexes changes during the cell cycle in *S. cerevisiae*. A–D, formation of G4 at telomeres was monitored by BG4 ChIP and analyzed by qPCR. G4 levels were detected in WT yeast cells. A, BG4 ChIP and qPCR analysis at two different telomeres (telomere VII-L and VI-R). As control, ChIP and qPCR were performed in the absence of BG4 antibody and 10 μM Phen-DC₃ to determine the specific binding of BG4. Data were normalized to input material (*ChIP/Input*). B, FACS analysis of yeast strains to monitor the arrest in specific cell cycle phases. Cells were arrested in G₁ phase with α factor for 3 h. For different S-phase time points, cells were released from G₁ in the presence of the indicated concentrations of HU (early S, 250 mM HU; mid-S phase, 150 mM HU; and late S phase, 75 mM HU). For G₂ phase, cells were treated with 15 $\mu\text{g/ml}$ nocodazole for 2 h. C, BG4 ChIP and qPCR analysis to monitor G4 levels in different cell cycle phases at telomere VII-L. BG4 ChIP signals were normalized to input. Plotted are the means of at least three biological replicates. Error bars represent SEM. Significance was calculated based on Student's *t* test comparing 75 mM HU with the other cell cycle phases. G4 level at 75 mM HU compared with other cell cycle phases was significantly higher according to the *t* test ($p < 0.02$). Only in G₁ arrest (α factor), a significance of $p = 0.1$ was calculated. D, BG4 ChIP and qPCR analysis at two different telomeres (telomere VII-L and VI-R) in *cdc13-1* mutant at nonpermissive temperature (37 °C). As control, the BG4 ChIP was done in *cdc13-1* mutant at permissive temperature (23 °C) and WT strain. We observed 5–6-fold higher enrichment of telomeric G4s in *cdc13-1* strain at nonpermissive temperature compared with WT. Data were normalized to input material (*ChIP/Input*).

cycle progression was controlled by FACS. The lowest level of telomeric G4 enrichment was observed in the early S phase (250 mM HU), with a slight increase in the mid-S phase (150 mM HU) and the highest level (2–3-fold) of accumulation in the late S phase (75 mM HU) (Fig. 6C). As pointed out before, Cdc13 is essential for capping the ssDNA at telomeric ends, and it was demonstrated that G4 DNA might have a capping role when the natural capping is compromised (42). We speculated that more G4 structures should be present at the telomeric region if the Cdc13-dependent capping mechanism is impaired. For this, we used the temperature sensitive *cdc13-1* mutant. In this mutant, telomeres are uncapped if cells are grown under nonpermissive temperature. This uncapping leads to long tracts of guanine-rich single-stranded telomeric DNA

(51). We reasoned that the long G-overhang in *cdc13-1* mutant telomeres might form G4 DNA at elevated temperatures. To test this, we did BG4 ChIP at permissive (23 °C, normal telomeres) and nonpermissive temperatures (37 °C, uncapped telomeres) and checked the telomeric G4 levels. As expected, we observed higher telomeric G4 enrichment in *cdc13-1* strain at nonpermissive temperature (37 °C) compared with permissive temperature (23 °C), as well as WT (Fig. 6D). Notably, these data support *in vitro* observations that G4 structures preferentially form during the time when long telomeric overhangs are present at the chromosome ends (46, 47).

Discussion

It is generally recognized that the major functions of telomeres are mediated by telomere-associated proteins. During most of the cell cycle, Cdc13 associates with proteins Stn1 and Ten1, thus forming the CST complex (59–61) that protects the overhang from exonucleases and prevents access to telomerase (62, 63). Orchestrated by a number of post-translational modifications, the association of Cdc13 with Stn1 and Ten1 is exchanged for the association with the telomerase subunit Est1 during the S phase, thus ensuring the enzyme recruitment to telomeres (33, 50, 64–66). In the late S/G₂ phase, telomere extension is followed by the restoration of CST at the G-overhangs, making them inaccessible to telomerase until the next late S phase (67, 68).

In addition to the regulation of Cdc13 by post-translational modifications and protein-protein interactions, the events taking place at telomeres are affected by the non-B DNA structures adopted by the G-overhang; however, their contribution to telomere function is not yet understood. Here, we showed that the oligonucleotides emulating an extended telomeric DNA overhang that is characteristic of the late S phase of the *S. cerevisiae* cell cycle can form two topologically distinct, antiparallel and parallel, intramolecular G4 structures. Although our data demonstrate that a concurrent formation of both parallel and antiparallel G4 structures is possible in a specific sequence context, the formation of an intramolecular antiparallel G4 appears kinetically favored over the formation of an intramolecular parallel G4. Our observation of comparable capacities of parallel and antiparallel G4 structures to displace Cdc13 from the complex with ssDNA suggests that the biological function of G4 is either not connected with a specific G4 folding topology or is associated with the kinetically preferred antiparallel G4.

Previously, it was shown that Cdc13 and Cdc13-DBD can bind the tetramolecular parallel G4 with a similar affinity as the ssDNA (unfolded) form and that the binding is accompanied by a partial denaturation of the tetramolecular G4 structure, stabilized by Na⁺ cations (41). In contrast to these observations, our data indicate that binding of both intramolecular parallel and antiparallel telomeric G4s bind to Cdc13-DBD is considerably weaker compared with its binding to telomeric DNA in a single-stranded form (Figs. 4 and 5). Moreover, in contrast to the published results (41), our data indicate that Cdc13-DBD does not induce denaturation of the intramolecular G4 structure (Fig. 5 and Fig. S10). We assume that these differences may

Length-dependent folding kinetics of telomeric overhangs

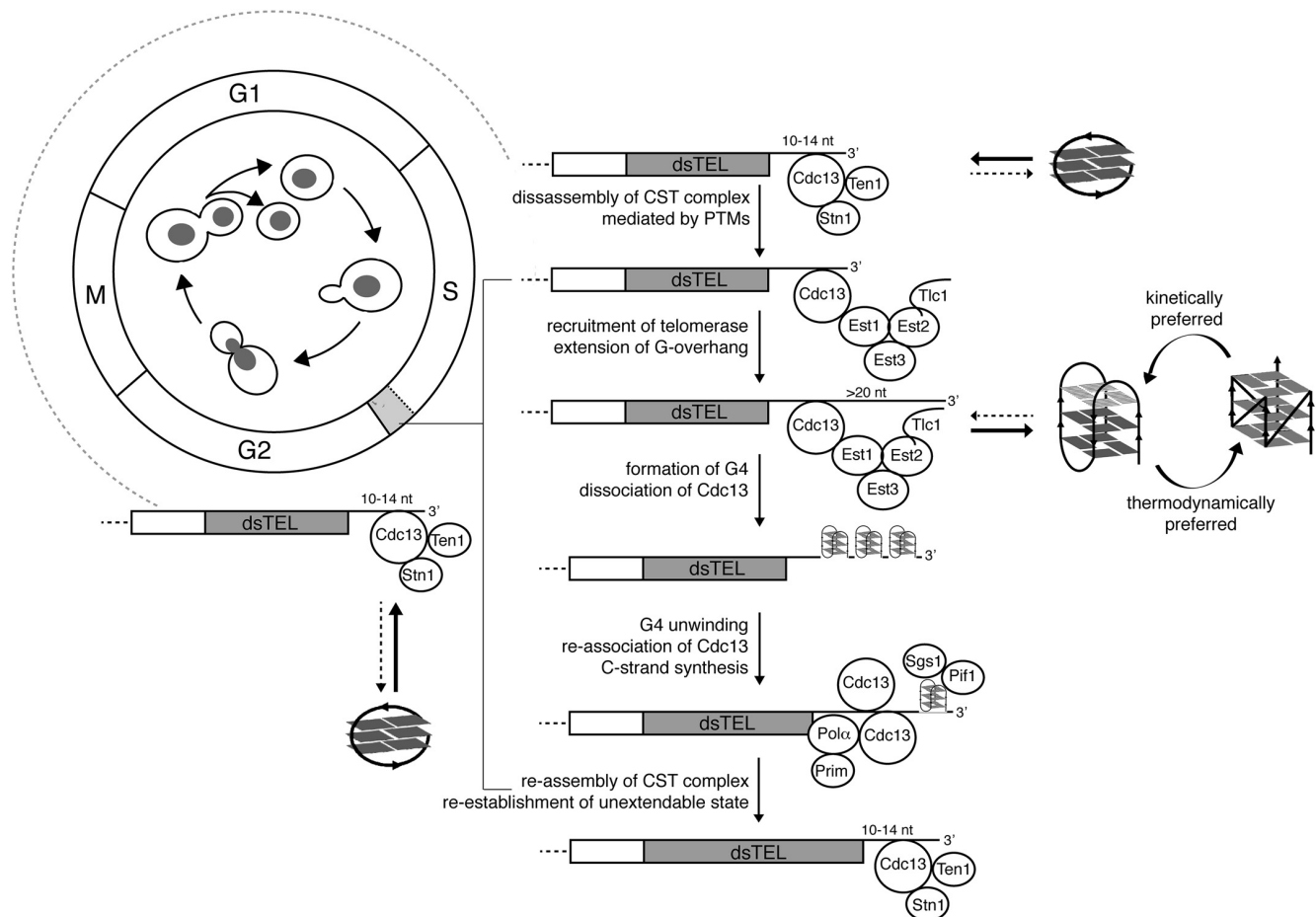


Figure 7. A model summarizing the roles of non-B DNA structures formed by the G-overhang in a time-dependent manner in the maintenance of telomeres in *S. cerevisiae*. See description under "Discussion"; for clarity, the model lacks other important players involved in G-overhang dynamics. The G4s can have distinct numbers of G-tetrads, as indicated by *different shading* of the tetrads. The *light gray box* in the cell cycle corresponds to a late S phase. *PTMs*, post-translational modifications; *Pol α* , DNA polymerase α ; *Prim*, DNA primase.

reflect the different nature of the studied G4 structures (intermolecular *versus* intramolecular, Na^+ - *versus* K^+ -stabilized). In fact, different affinity and rate of unfolding were reported for Na^+ *versus* K^+ G4 interacting with human POT1-TPP1 telomeric protein complex (69). However, our experiments describe the behavior of sequences derived from the most represented repeat in yeast telomeres (48) and may thus more closely reflect the situation *in vivo*.

The limitation of our study is the use of Cdc13-DBD instead of a Cdc13 full-length protein. Although we resorted to this approach due to technical problems with the full-length protein purification, we acknowledge that other domains of Cdc13 can also contribute to its interaction with G4 or G-hairpin structures. However, the affinity toward the telomeric ssDNA motif is similar for the two proteins (54), as is also the previously observed affinity toward the interaction with tetramolecular G4 structure (41), suggesting that their behavior may be similar also for the substrates we studied. The binding of several different substrates can be mediated by the ability of DBD to interact with different secondary structures in a different manner, as is the case for the DBD of the yeast telomeric protein Rap1 and its binding to ssDNA *versus* G4 structure (70).

Our data suggest that Cdc13 preferably binds to G-rich telomeric ssDNA, whereas the formation of intramolecular G4 impairs its binding, regardless of the G4 folding topology. This observation is consistent with the evolution-based argument suggesting that the topology of non-B DNA motifs formed in a G-overhang should be neutral with respect to their function (17). To assess the physiological relevance of non-B DNA structures at long and short telomeric overhangs, we compared the capacity of Cdc13 to bind to unfolded, G-hairpin, and G4 telomeric DNA. Similar to G4, the G-hairpin displayed a diminished capacity to form a stable complex with Cdc13 compared with that of unfolded DNA (Figs. 4 and 5). The binding of Cdc13-DBD observed by EMSA reflects the folding kinetics of different secondary structures, potentially hinting at their physiological roles. The typical time required to complete the cell cycle for *S. cerevisiae* is ~ 90 min, with the S phase spanning < 10 min. Any non-B DNA structure to take part in related biological processes must be formed with a relevant time window (*i.e.* $\ll 10$ min for a G4 within a long telomeric overhang and $\ll 80$ min for a G-hairpin within a short telomeric overhang. For G4 structures, which are known to fold on the time scale of seconds/minutes (71) (Fig. 2C), this condition is fulfilled; for G-hairpins, it is not, as the time required to completely fold this structure exceeds several hours (Fig. 2C).

Within the timeframe of a cell cycle, the short G-overhang sequence displaying a G-hairpin-forming potential predominantly exists in its unfolded form, which, in contrast to both G4 and G-hairpin forms (Figs. 4 and 5), has a high affinity to Cdc13 (Fig. 4). We suggest that non-B DNA structure formation serves as a kinetically controlled switch to regulate the binding of Cdc13 to telomeric G-overhangs (Fig. 7). Whereas the situation *in vivo* may be more complicated because of other proteins interfering with non-B DNA structure formation, our NMR measurements in cell lysates support the possibility that the folding kinetics may be similar to the *in vitro* situation (Fig. S2). To the best of our knowledge, these data show for the first time how the secondary structures forming at a G-rich overhang may play a physiological role in yeast telomeres. Based on our data, we propose a model summarizing how rapid G4 formation on the elongating 3' overhang participates in the telomerase-driven extension of telomeres to fine-tune the regulation of telomerase dissociation. During most of the cell cycle, a short G-overhang is refractory to forming secondary structures and bound by the CST complex that prevents telomerase recruitment. During the S phase, because of post-translational modifications of Cdc13 (33, 50, 64–66), Cdc13 mediates the recruitment of telomerase to telomeres. After elongation by telomerase, the elongated overhangs are prone to form fast-folding G4 structures. The formation of G4s at a G-overhang may be followed by the dissociation of Cdc13 due to its low affinity toward G4 structures. As has been shown previously for stabilized G4 structures at telomeres in the absence of Cdc13, a G4 may transiently act as telomere cap in the absence of Cdc13 (42). After the following unfolding of G4 structures by a concerted action of telomerase (22) and helicases (30, 72), the G-overhang may be bound again by multiple Cdc13 molecules. As a result of these events, there is an increase in the accumulation of telomerase, G4, and Cdc13 at telomeres during the late S phase (Fig. 6). Subsequently, Cdc13-containing ends serve as substrates for C-strand fill-in synthesis machinery (73), thus restoring short, CST-bound G-overhangs that are refractory to telomerase binding and refractory to quickly form a secondary structure (Fig. 7). It is probable that all of these steps are subject to additional levels of regulation, such as the action of various nucleases/helicases and post-translational modifications that may affect the affinity of Cdc13 not only for its protein partners but also for various structures formed by a G-overhang. In addition, currently, it is not clear how the length and structure of individual G-overhangs affect the telomerase activity. Furthermore, our data show the sum of different telomere lengths, and we do not know whether G4s observed by BG4 are only forming at the overhang or if they also form at telomeric dsDNA regions. These and other questions will need to be investigated in detail in future studies.

It is interesting, however, to address possible parallels between yeast and human telomeres based on our observations. Although the length of the human telomeric overhang remains sufficient to form G4 structure throughout the cell cycle, it has been shown that POT1, the main human ssDNA-binding telomeric protein, alone or in complex with TPP1, is capable of unwinding G4 structures *in vitro*, thus enabling telomere extension by telomerase (25, 69). Moreover, the human CST complex (homolog of its yeast counterpart) has also been

described to bind and unfold G4 structures, contributing to removing barriers for replication fork progression (74, 75). These findings suggest an evolutionarily conserved role for G4 structures in telomerase regulation and for CST complex as an interacting partner for G-quadruplexes from yeast to humans.

Conclusions

Formation of non-B DNA structures in the G-overhang is considered to be an epigenetic hallmark of telomeric DNA. In *S. cerevisiae*, these structures involve G-hairpins and topologically distinct classes of intramolecular G4 structures. Here, we propose that the time-dependent formation of non-B DNA structures plays an active regulatory role in telomere maintenance. This study shows for the first time how different lengths of G-overhangs may influence the formation of non-B DNA structures and suggests a possible physiological role for G4s in G-overhangs. Our model connects the time-controlled formation of non-B DNA structures with cell cycle-regulated lengths of G-overhangs and binding by Cdc13. Altogether, our data support a notion of non-B DNA structures in G-overhangs as active players in telomere maintenance and highlight the important role of the time-dependent process of non-B DNA structure formation.

Experimental procedures

Samples for spectroscopic experiments

DNA oligonucleotides (Table 1) were purchased from Sigma–Aldrich and were dissolved in H₂O to yield 1 mM aqueous stock solutions. The oligonucleotide folding was performed by heating the stock solutions to 95 °C for 10 min, followed by cooling them to room temperature. The precise oligonucleotide concentrations were determined from the UV absorbance measured on a NanoDrop 2000c (Thermo Fisher Scientific). The stock solutions were used for the sample preparation for both NMR and CD analyses. The CD and NMR spectra were measured in K⁺S buffer (20 mM potassium phosphate, pH 7.0, 135 mM KCl) unless stated otherwise.

End-labeled oligonucleotide used as an EMSA probe

The oligonucleotide ONG11 (Microsynth, Table 1) was labeled on its 5' end by T4 polynucleotide kinase (Thermo Fisher Scientific) according to the manufacturer's instructions. The unincorporated [γ -³²P]ATP was removed by a Probe Quant G-25 Micro Column (GE Healthcare) equilibrated with water; the probe was stored at 4 °C and boiled immediately prior to each experiment.

Unlabeled oligonucleotides used as EMSA competitors

DNA oligonucleotides were purchased from Sigma–Aldrich (ONG9) or Microsynth (all remaining oligonucleotides) (Table 1). The oligonucleotide working solutions (50 μ M oligonucleotide) in either water or 1 \times K⁺ buffer (20 mM potassium phosphate, pH 7.0, 135 mM KCl, 9% (v/v) glycerol) were prepared by diluting the oligonucleotide stock solutions (100 or 200 μ M oligonucleotides prepared in water) with the appropriate amount of water and/or 4 \times K⁺ buffer. The folding was performed as described above. All oligonucleotides were diluted to the

Length-dependent folding kinetics of telomeric overhangs

working concentrations in water and/or $4\times K^+$ buffer immediately prior to the experiments.

Purification of Cdc13-DBD

The coding sequence for the Cdc13-DBD (residues 497–694) was amplified from genomic DNA of the *S. cerevisiae* strain SCY325 (*MAT α* , *ade2-1*, *his3-11,15*, *leu2-3,112*, *trp1-1*, *ura3-1*, and *can1*) by PCR using the primers Cdc13-DBD-F (5'-phospho-AGGATGAGCAAAATGGCAAGGAA-3') and Cdc13-DBD-R (5'-phospho-CGCGAGATGAGAACCGTTTCTAT-3'). The PCR fragment was ligated into the pGEX-6T-2 vector (GE Healthcare) linearized by *Sma*I and dephosphorylated using alkaline phosphatase. The construct sequence was verified by restriction digestion and sequencing. The expression of the Cdc13-DBD-encoding gene was induced in BL21(DE3) *E. coli* by adding 1 mM isopropyl 1-thio- β -D-galactopyranoside to a mid-log phase culture and subsequently incubating for 4 h at 22 °C and 225 rpm. The cells were washed once with ice-cold PBS, collected, and stored at -80°C . The thawed cells were resuspended in $1\times K^+$ buffer containing 1 mg/ml lysozyme (Sigma-Aldrich), $1\times$ cComplete Protease Inhibitor mixture (Roche Applied Science), 10 $\mu\text{g/ml}$ leupeptin (Applichem), 1 mM DTT (Thermo Fisher Scientific), 10 mM MgCl_2 (Sigma-Aldrich), 30 $\mu\text{g/ml}$ RNase A (Invitrogen), and 10 units/ μl DNase I (Sigma-Aldrich). The suspension was incubated on ice for 15 min followed by sonication (6 \times 20 s, 30% amplitude, model 120 Sonic Dismembrator (Fisher)). Triton X-100 (Sigma-Aldrich) was added to a final concentration of 0.25% (v/v) followed by three additional sonication pulses. After incubating for 5 min on ice, the suspension was centrifuged for 20 min at $10,000\times g$ and 4°C in an SS-34 rotor (Sorvall). The resulting supernatant was mixed with 0.5-ml GSH-agarose beads (Sigma-Aldrich) equilibrated with $1\times K^+$ buffer containing 0.25% Triton X-100 and 1 mM DTT (K^+ TD buffer) with $1\times$ cComplete Protease Inhibitor mixture (Roche Applied Science) and incubated end-over-end for 3 h at 4°C . The beads were then washed three times with K^+ TD buffer containing $1\times$ cComplete Protease Inhibitor mixture (Roche Applied Science) and four times with K^+ TD without the protease inhibitors. The beads were resuspended in 0.7 ml of K^+ TD buffer without protease inhibitors containing the HRV 3°C protease and incubated end-over-end for 3 h at 4°C . The flow-through was collected as the elution fraction. The protein concentration was determined by a Bradford assay (76), and the samples were stored at -80°C .

Yeast lysate preparation

A 500-ml culture of *S. cerevisiae* BY4741 (*MAT α* , *his3 Δ* , *leu2 Δ* , *met15 Δ* , *ura3 Δ*) was grown overnight at 30°C and 180 rpm to a density of 3×10^7 cells/ml. Cells were harvested, resuspended in $1\times K^+$ buffer, and disrupted by FastPrep-24 (MP Biomedicals). Then $1\times K^+$ buffer was added to a final volume of 2 ml, and the extract was sonicated for 60 s at 30% amplitude with the model 120 Sonic Dismembrator (Fisher).

EMSA

All DNA-binding reactions were performed in $1\times K^+$ buffer. After the addition of the labeled probe, the reactions were incu-

bated for 10 min at room temperature and then loaded on a 6% polyacrylamide gel in $0.5\times$ TBE buffer (45 mM Tris borate, 1 mM EDTA, pH 8.0). The electrophoresis was performed in a mini-PROTEAN Tetra Cell R (Bio-Rad) for 18 min at 10 mA/gel. The gels were then fixed with 10% (v/v) methanol and 10% (v/v) acetic acid, vacuum-dried, exposed to a phosphor screen, and visualized using Personal Molecular Imager FX (Bio-Rad).

CD spectroscopy

CD spectra were measured using a JASCO J-815 spectrometer in 1-mm path-length quartz cells placed in a Peltier holder. CD signals are expressed as the difference in the molar absorption of the left- and right-handed circularly polarized light. The molarity was related to the DNA strands. Spectra were acquired at a rate of 100 nm/min and averaged from three measurements.

Nondenaturing PAGE

Nondenaturing PAGE was performed in a temperature-controlled electrophoresis cell (PROTEAN II xi, Bio-Rad) submerged in a cooling system. The gels (16%, 29:1 acrylamide/bisacrylamide) in 16 20-cm glass cassettes were electrophoresed for 22 h at 40 V and 7°C in potassium phosphate buffer. The gels were stained with Stains-All (Sigma-Aldrich).

NMR spectroscopy

The 1D ^1H spectra of the DNA samples were acquired at 700 MHz using a Bruker Avance III NMR spectrometer equipped with a triple resonance room temperature probe using the zgpgw5, p3919 (standard Bruker library) or 1-1 echo pulse sequences (77). All of the spectra were measured in a water solution (90% H_2O , 10% D_2O) at 25°C unless stated otherwise and referenced to the signal of residual H_2O . To assess the folding kinetics from the NMR spectra, the intensity of signals in the imino region (exchangeable protons) normalized to the intensity of signals in the aromatic region (nonexchangeable protons) of the same NMR spectrum was plotted as a function of time.

G4 ChIP

G4 ChIP was performed using the G4 structure-specific antibody (BG4), as described previously (78, 79). Briefly, the BG4 recombinant antibody was prepared using the expression vector pSANG10-3F-BG4 (a gift from Shankar Balasubramanian (Addgene plasmid 55756; RRID:Addgene_55756 (57)) in BL21(DE3) *E. coli*. The purified BG4 solution was concentrated using an Amicon Ultra-15 centrifugal filter unit (Millipore, catalog no. UFC9010). For the ChIP experiment, *S. cerevisiae* strains were grown and cross-linked with 1% (v/v) formaldehyde. Cross-linked samples were immunoprecipitated with anti-FLAG M2 magnetic beads (Sigma-Aldrich) in the presence or absence of the BG4 antibody and 10 μM Phen-DC $_3$ to determine the enrichment. The enrichment of telomeric DNA was confirmed by qPCR with primers Tel_VIII_for (TGATATGTGTTACGCAGAATAC-3'), Tel_VIII_rev (TGAGAAGCACCGCAATG-3'), Tel_VI-R (ATCATTGAGGATCTATAATC-3'), and Tel_VI-R rev (CTTCACTCCATTGCG-3') that are specific for the VII-L

and VI-R telomeric regions. To obtain the fraction of recovery (percentage of input), the results (Cq values) were normalized to the relative input. All data are depicted as the mean \pm S.E., $n = 3$. Error bars indicate the SEM.

Cell cycle analysis

Cell cycle synchrony experiments were performed as described previously (80). Briefly, *S. cerevisiae* cells (W303; *MATa*, *leu2-3,112*, *trp1-1*, *can1-100*, *ura3-1*, *ade2-1*, *his3-11,15*, *bar1Δ::KanMX*) (81) were arrested in the G_1 phase with the α factor at a concentration of 5 $\mu\text{g/ml}$ for 3 h. The cells were checked under the microscope for shmoo formation. G_1 -arrested cells were released into the cell cycle in the presence of different concentrations of HU for early (250 mM), mid (150 mM), and late (75 mM) S-phase arrest and 15 $\mu\text{g/ml}$ nocodazole for G_2 arrest. Samples were taken for DNA content analysis by a BD FACS Canto II. G4 ChIP was performed with cell cycle-arrested cells as described above.

Data availability

All data are contained within the article.

Acknowledgments—We thank members of our laboratories for fruitful discussions. The Ministry of Education, Youth, and Sports of the Czech Republic is acknowledged for its support of access to research infrastructure (CEITEC 2020 LQ1601; CIISB-LM2015043; SYMBIT: CZ.02.1.01/0.0/0.0/15_003/0000477—co-financed by the European Regional Development Funds).

Author contributions—K. J. and M. G. formal analysis; K. J., M. G., M. H., K. Prochazkova, and L. Tomaska investigation; K. J., M. G., and L. Tomaska visualization; K. J., M. G., K. Paeschke, and L. Trantirek methodology; K. J., M. G., L. Trantirek, and L. Tomaska writing—original draft; K. J., M. G., J. N., K. Paeschke, L. Trantirek, and L. Tomaska writing—review and editing; M. G. and L. Trantirek data curation; J. N., K. Paeschke, L. Trantirek, and L. Tomaska supervision; J. N., K. Paeschke, L. Trantirek, and L. Tomaska funding acquisition; L. Trantirek and L. Tomaska conceptualization; L. Trantirek and L. Tomaska project administration.

Funding and additional information—Funding was provided by Slovak Research and Development Agency (APVV) Grants APVV-15-0022 (to L. Tomaska) and APVV-18-0239 (to J. N.), Scientific Grant Agency of the Ministry of Education, Science, Research, and Sport of the Slovak Republic (VEGA) Grants 1/0061/20 (to L. Tomaska) and 1/0027/19 (to J. N.), and Czech Science Foundation GACR Grant 17-12075S and Ministry of Health of the Czech Republic Grants NV19-08-00450 and CEITEC 2020 LQ1601, CIISB-LM2015043, SYMBIT: CZ.02.1.01/0.0/0.0/15_003/0000477 (to L. Trantirek). The Paeschke laboratory is funded by European Research Council Starting Grant 638988-G4DSB.

Conflict of interest—The authors declare that they have no conflicts of interest with the contents of this article.

Abbreviations—The abbreviations used are: G4, G-quadruplex; CST complex, Cdc13-Stn1-Ten1 complex; DBD, DNA-binding do-

main; EMSA, electrophoretic mobility shift assay; qPCR, quantitative PCR; HU, hydroxyurea; nt, nucleotide(s); 1D, one-dimensional.

References

- Muller, H. J. (1938) The remaking of chromosomes. *Collect. Net.* **8**, 182–198
- McClintock, B. (1941) The stability of broken ends of chromosomes in *Zea mays*. *Genetics* **26**, 234–282 [Medline](#)
- de Lange, T. (2018) Shelterin-mediated telomere protection. *Annu. Rev. Genet.* **52**, 223–247 [CrossRef Medline](#)
- Olovnikov, A. M. (1971) [Principle of marginotomy in template synthesis of polynucleotides]. *Dokl. Akad. Nauk SSSR* **201**, 1496–1499 [Medline](#)
- Olovnikov, A. M. (1973) A theory of marginotomy. The incomplete copying of template margin in enzymic synthesis of polynucleotides and biological significance of the phenomenon. *J. Theor. Biol.* **41**, 181–190 [CrossRef Medline](#)
- Watson, J. D. (1972) Origin of concatemeric T7 DNA. *Nat. New Biol.* **239**, 197–201 [CrossRef Medline](#)
- Meyne, J., Ratliff, R. L., and Moyzis, R. K. (1989) Conservation of the human telomere sequence (TTAGGG)_n among vertebrates. *Proc. Natl. Acad. Sci. U.S.A.* **86**, 7049–7053 [CrossRef Medline](#)
- Gunišová, S., Elboher, E., Nosek, J., Gorkovoy, V., Brown, Y., Lucier, J.-F., Laterreur, N., Wellinger, R. J., Tzfati, Y., and Tomáška, L. (2009) Identification and comparative analysis of telomerase RNAs from *Candida* species reveal conservation of functional elements. *RNA* **15**, 546–559 [CrossRef Medline](#)
- Cohn, M., McEachern, M. J., and Blackburn, E. H. (1998) Telomeric sequence diversity within the genus *Saccharomyces*. *Curr. Genet.* **33**, 83–91 [CrossRef Medline](#)
- Henderson, E. R., and Blackburn, E. H. (1989) An overhanging 3' terminus is a conserved feature of telomeres. *Mol. Cell Biol.* **9**, 345–348 [CrossRef Medline](#)
- McElligott, R., and Wellinger, R. J. (1997) The terminal DNA structure of mammalian chromosomes. *EMBO J.* **16**, 3705–3714 [CrossRef Medline](#)
- Lustig, A. J. (2019) Towards the mechanism of yeast telomere dynamics. *Trends Cell Biol.* **29**, 361–370 [CrossRef Medline](#)
- Blackburn, E. H., and Collins, K. (2011) Telomerase: an RNP enzyme synthesizes DNA. *Cold Spring Harb. Perspect. Biol.* **3**, a003558 [CrossRef Medline](#)
- Greider, C. W., and Blackburn, E. H. (1985) Identification of a specific telomere terminal transferase activity in tetrahymena extracts. *Cell* **43**, 405–413 [CrossRef Medline](#)
- Greider, C. W., and Blackburn, E. H. (1987) The telomere terminal transferase of *Tetrahymena* is a ribonucleoprotein enzyme with two kinds of primer specificity. *Cell* **51**, 887–898 [CrossRef Medline](#)
- Lue, N. F. (2018) Evolving linear chromosomes and telomeres: a C-strand-centric view. *Trends Biochem. Sci.* **43**, 314–326 [CrossRef Medline](#)
- Školáková, P., Foldynová-Trantírková, S., Bednářová, K., Fiala, R., Vorlíčková, M., and Trantírek, L. (2015) Unique *C. elegans* telomeric overhang structures reveal the evolutionarily conserved properties of telomeric DNA. *Nucleic Acids Res.* **43**, 4733–4745 [CrossRef Medline](#)
- Sundquist, W. I., and Klug, A. (1989) Telomeric DNA dimerizes by formation of guanine tetrads between hairpin loops. *Nature* **342**, 825–829 [CrossRef Medline](#)
- Tran, P. L. T., Mergny, J.-L., and Alberti, P. (2011) Stability of telomeric G-quadruplexes. *Nucleic Acids Res.* **39**, 3282–3294 [CrossRef Medline](#)
- Williamson, J. R., Raghuraman, M. K., and Cech, T. R. (1989) Monovalent cation-induced structure of telomeric DNA: the G-quartet model. *Cell* **59**, 871–880 [CrossRef Medline](#)
- Oganesian, L., Moon, I. K., Bryan, T. M., and Jarstfer, M. B. (2006) Extension of G-quadruplex DNA by ciliate telomerase. *EMBO J.* **25**, 1148–1159 [CrossRef Medline](#)
- Paeschke, K., Juranek, S., Simonsson, T., Hempel, A., Rhodes, D., and Lipps, H. J. (2008) Telomerase recruitment by the telomere end binding protein- β facilitates G-quadruplex DNA unfolding in ciliates. *Nat. Struct. Mol. Biol.* **15**, 598–604 [CrossRef Medline](#)

Length-dependent folding kinetics of telomeric overhangs

23. Tang, J., Kan, Z. Y., Yao, Y., Wang, Q., Hao, Y. H., and Tan, Z. (2008) G-quadruplex preferentially forms at the very 3' end of vertebrate telomeric DNA. *Nucleic Acids Res.* **36**, 1200–1208 [CrossRef Medline](#)
24. Zahler, A. M., Williamson, J. R., Cech, T. R., and Prescott, D. M. (1991) Inhibition of telomerase by G-quartet DMA structures. *Nature* **350**, 718–720 [CrossRef Medline](#)
25. Zaug, A. J., Podell, E. R., and Cech, T. R. (2005) Human POT1 disrupts telomeric G-quadruplexes allowing telomerase extension *in vitro*. *Proc. Natl. Acad. Sci. U.S.A.* **102**, 10864–10869 [CrossRef Medline](#)
26. Fry, M., and Loeb, L. A. (1999) Human Werner syndrome DNA helicase unwinds tetrahelical structures of the fragile X syndrome repeat sequence d(CG_nG)_n. *J. Biol. Chem.* **274**, 12797–12802 [CrossRef Medline](#)
27. Sanders, C. M. (2010) Human Pif1 helicase is a G-quadruplex DNA-binding protein with G-quadruplex DNA-unwinding activity. *Biochem. J.* **430**, 119–128 [CrossRef Medline](#)
28. Paeschke, K., Bochman, M. L., Garcia, P. D., Cejka, P., Friedman, K. L., Kowalczykowski, S. C., and Zakian, V. A. (2013) Pif1 family helicases suppress genome instability at G-quadruplex motifs. *Nature* **497**, 458–462 [CrossRef Medline](#)
29. Sun, H., Karow, J. K., Hickson, I. D., and Maizels, N. (1998) The Bloom's syndrome helicase unwinds G4 DNA. *J. Biol. Chem.* **273**, 27587–27592 [CrossRef Medline](#)
30. Sun, H., Bennett, R. J., and Maizels, N. (1999) The *Saccharomyces cerevisiae* Sgs1 helicase efficiently unwinds G-G paired DNAs. *Nucleic Acids Res.* **27**, 1978–1984 [CrossRef Medline](#)
31. Ribeyre, C., Lopes, J., Boulé, J.-B., Piazza, A., Guédin, A., Zakian, V. A., Mergny, J.-L., and Nicolas, A. (2009) The yeast Pif1 helicase prevents genomic instability caused by G-quadruplex-forming CEB1 sequences *in vivo*. *PLoS Genet.* **5**, e1000475 [CrossRef Medline](#)
32. Li, Q.-J., Tong, X.-J., Duan, Y.-M., and Zhou, J.-Q. (2013) Characterization of the intramolecular G-quadruplex promoting activity of Est1. *FEBS Lett.* **587**, 659–665 [CrossRef Medline](#)
33. Zhang, M.-L., Tong, X.-J., Fu, X.-H., Zhou, B. O., Wang, J., Liao, X.-H., Li, Q.-J., Shen, N., Ding, J., and Zhou, J.-Q. (2010) Yeast telomerase subunit Est1p has guanidine quadruplex-promoting activity that is required for telomere elongation. *Nat. Struct. Mol. Biol.* **17**, 202–209 [CrossRef Medline](#)
34. Moye, A. L., Porter, K. C., Cohen, S. B., Phan, T., Zyner, K. G., Sasaki, N., Lovrecz, G. O., Beck, J. L., and Bryan, T. M. (2015) Telomeric G-quadruplexes are a substrate and site of localization for human telomerase. *Nat. Commun.* **6**, 7643 [CrossRef Medline](#)
35. D'Ambrosio, D., Reichenbach, P., Micheli, E., Alvino, A., Franceschin, M., Savino, M., and Lingner, J. (2012) Specific binding of telomeric G-quadruplexes by hydrosoluble perylene derivatives inhibits repeat addition processivity of human telomerase. *Biochimie* **94**, 854–863 [CrossRef Medline](#)
36. Sun, D., Thompson, B., Cathers, B. E., Salazar, M., Kerwin, S. M., Trent, J. O., Jenkins, T. C., Neidle, S., and Hurley, L. H. (1997) Inhibition of human telomerase by a G-quadruplex-interactive compound. *J. Med. Chem.* **40**, 2113–2116 [CrossRef Medline](#)
37. Tauchi, T., Shin-ya, K., Sashida, G., Sumi, M., Okabe, S., Ohyashiki, J. H., and Ohyashiki, K. (2006) Telomerase inhibition with a novel G-quadruplex-interactive agent, telomestatin: *in vitro* and *in vivo* studies in acute leukemia. *Oncogene* **25**, 5719–5725 [CrossRef Medline](#)
38. Yadav, K., Meka, P. N. R., Sadhu, S., Guggilapu, S. D., Kovvuri, J., Kamal, A., Srinivas, R., Devayani, P., Babu, B. N., and Nagesh, N. (2017) Telomerase inhibition and human telomeric G-quadruplex DNA stabilization by a β -carboline-benzimidazole derivative at low concentrations. *Biochemistry* **56**, 4392–4404 [CrossRef Medline](#)
39. Giraldo, R., and Rhodes, D. (1994) The yeast telomere-binding protein RAP1 binds to and promotes the formation of DNA quadruplexes in telomeric DNA. *EMBO J.* **13**, 2411–2420 [CrossRef Medline](#)
40. Giraldo, R., Suzuki, M., Chapman, L., and Rhodes, D. (1994) Promotion of parallel DNA quadruplexes by a yeast telomere binding protein: a circular dichroism study. *Proc. Natl. Acad. Sci. U.S.A.* **91**, 7658–7662 [CrossRef Medline](#)
41. Lin, Y. C., Shih, J. W., Hsu, C. L., and Lin, J. J. (2001) Binding and partial denaturing of G-quartet DNA by Cdc13p of *Saccharomyces cerevisiae*. *J. Biol. Chem.* **276**, 47671–47674 [CrossRef Medline](#)
42. Smith, J. S., Chen, Q., Yatsunyk, L. A., Nicoludis, J. M., Garcia, M. S., Kranaster, R., Balasubramanian, S., Monchaud, D., Teulade-Fichou, M.-P., Abramowitz, L., Schultz, D. C., and Johnson, F. B. (2011) Rudimentary G-quadruplex-based telomere capping in *Saccharomyces cerevisiae*. *Nat. Struct. Mol. Biol.* **18**, 478–485 [CrossRef Medline](#)
43. Makarov, V. L., Hirose, Y., and Langmore, J. P. (1997) Long G tails at both ends of human chromosomes suggest a C strand degradation mechanism for telomere shortening. *Cell* **88**, 657–666 [CrossRef Medline](#)
44. Wright, W. E., Tesmer, V. M., Huffman, K. E., Levene, S. D., and Shay, J. W. (1997) Normal human chromosomes have long G-rich telomeric overhangs at one end. *Genes Dev.* **11**, 2801–2809 [CrossRef Medline](#)
45. Kan, Z., Lin, Y., Wang, F., Zhuang, X., Zhao, Y., Pang, D., Hao, Y., and Tan, Z. (2007) G-quadruplex formation in human telomeric (TTAGGG)₄ sequence with complementary strand in close vicinity under molecularly crowded condition. *Nucleic Acids Res.* **35**, 3646–3653 [CrossRef Medline](#)
46. Larrivé, M., LeBel, C., and Wellinger, R. J. (2004) The generation of proper constitutive G-tails on yeast telomeres is dependent on the MRX complex. *Genes Dev.* **18**, 1391–1396 [CrossRef Medline](#)
47. Wellinger, R. J., Wolf, A. J., and Zakian, V. A. (1993) *Saccharomyces* telomeres acquire single-strand TG_{1–3} tails late in S phase. *Cell* **72**, 51–60 [CrossRef Medline](#)
48. Gajarský, M., Živković, M. L., Stadlbauer, P., Pagano, B., Fiala, R., Amato, J., Tomáška, L., Šponer, J., Plavec, J., and Trantířek, L. (2017) Structure of a stable G-hairpin. *J. Am. Chem. Soc.* **139**, 3591–3594 [CrossRef Medline](#)
49. Bessi, I., Jonker, H. R. A., Richter, C., and Schwalbe, H. (2015) Involvement of long-lived intermediate states in the complex folding pathway of the human telomeric G-quadruplex. *Angew. Chem. Int. Ed. Engl.* **54**, 8444–8448 [CrossRef Medline](#)
50. Chandra, A., Hughes, T. R., Nugent, C. I., and Lundblad, V. (2001) Cdc13 both positively and negatively regulates telomere replication. *Genes Dev.* **15**, 404–414 [CrossRef Medline](#)
51. Garvik, B., Carson, M., and Hartwell, L. (1995) Single-stranded DNA arising at telomeres in cdc13 mutants may constitute a specific signal for the Rad9 checkpoint. *Mol. Cell Biol.* **15**, 6128–6138 [CrossRef Medline](#)
52. Nugent, C. I., Hughes, T. R., Lue, N. F., and Lundblad, V. (1996) Cdc13p: a single-strand telomeric DNA-binding protein with a dual role in yeast telomere maintenance. *Science* **274**, 249–252 [CrossRef Medline](#)
53. Wellinger, R. J., Ethier, K., Labrecque, P., and Zakian, V. A. (1996) Evidence for a new step in telomere maintenance. *Cell* **85**, 423–433 [CrossRef Medline](#)
54. Lewis, K. A., Pfaff, D. A., Earley, J. N., Altschuler, S. E., and Wuttke, D. S. (2014) The tenacious recognition of yeast telomere sequence by Cdc13 is fully exerted by a single OB-fold domain. *Nucleic Acids Res.* **42**, 475–484 [CrossRef Medline](#)
55. Anderson, E. M., Halsey, W. A., and Wuttke, D. S. (2002) Delineation of the high-affinity single-stranded telomeric DNA-binding domain of *Saccharomyces cerevisiae* Cdc13. *Nucleic Acids Res.* **30**, 4305–4313 [CrossRef Medline](#)
56. Hughes, T. R., Weilbaecher, R. G., Walterscheid, M., and Lundblad, V. (2000) Identification of the single-strand telomeric DNA binding domain of the *Saccharomyces cerevisiae* Cdc13 protein. *Proc. Natl. Acad. Sci. U.S.A.* **97**, 6457–6462 [CrossRef Medline](#)
57. Biffi, G., Tannahill, D., McCafferty, J., and Balasubramanian, S. (2013) Quantitative visualization of DNA G-quadruplex structures in human cells. *Nat. Chem.* **5**, 182–186 [CrossRef Medline](#)
58. Piazza, A., Boulé, J.-B., Lopes, J., Mingo, K., Largy, E., Teulade-Fichou, M.-P., and Nicolas, A. (2010) Genetic instability triggered by G-quadruplex interacting Phen-DC compounds in *Saccharomyces cerevisiae*. *Nucleic Acids Res.* **38**, 4337–4348 [CrossRef Medline](#)
59. Grandin, N., Damon, C., and Charbonneau, M. (2001) Ten1 functions in telomere end protection and length regulation in association with Stn1 and Cdc13. *EMBO J.* **20**, 1173–1183 [CrossRef Medline](#)
60. Holstein, E.-M., Clark, K. R. M., and Lydall, D. (2014) Interplay between nonsense-mediated mRNA decay and DNA damage response pathways reveals that Stn1 and Ten1 are the key CST telomere-cap components. *Cell Rep.* **7**, 1259–1269 [CrossRef Medline](#)





61. Lin, J. J., and Zakian, V. A. (1996) The *Saccharomyces* Cdc13 protein is a single-strand TG1-3 telomeric DNA-binding protein *in vitro* that affects telomere behavior *in vivo*. *Proc. Natl. Acad. Sci. U.S.A.* **93**, 13760–13765 [CrossRef Medline](#)
62. Gao, H., Cervantes, R. B., Mandell, E. K., Otero, J. H., and Lundblad, V. (2007) RPA-like proteins mediate yeast telomere function. *Nat. Struct. Mol. Biol.* **14**, 208–214 [CrossRef Medline](#)
63. Sun, J., Yu, E. Y., Yang, Y., Confer, L. A., Sun, S. H., Wan, K., Lue, N. F., and Lei, M. (2009) Stn1-Ten1 is an Rpa2-Rpa3-like complex at telomeres. *Genes Dev.* **23**, 2900–2914 [CrossRef Medline](#)
64. Hang, L. E., Liu, X., Cheung, I., Yang, Y., and Zhao, X. (2011) SUMOylation regulates telomere length homeostasis by targeting Cdc13. *Nat. Struct. Mol. Biol.* **18**, 920–926 [CrossRef Medline](#)
65. Li, S., Makovets, S., Matsuguchi, T., Blethrow, J. D., Shokat, K. M., and Blackburn, E. H. (2009) Cdk1-dependent phosphorylation of Cdc13 coordinates telomere elongation during cell-cycle progression. *Cell* **136**, 50–61 [CrossRef Medline](#)
66. Shen, Z.-J., Hsu, P.-H., Su, Y.-T., Yang, C.-W., Kao, L., Tseng, S.-F., Tsai, M.-D., and Teng, S.-C. (2014) PP2A and Aurora differentially modify Cdc13 to promote telomerase release from telomeres at G₂/M phase. *Nat. Commun.* **5**, 5312 [CrossRef Medline](#)
67. Gopalakrishnan, V., Tan, C. R., and Li, S. (2017) Sequential phosphorylation of CST subunits by different cyclin-Cdk1 complexes orchestrate telomere replication. *Cell Cycle* **16**, 1271–1287 [CrossRef Medline](#)
68. Liu, C.-C., Gopalakrishnan, V., Poon, L.-F., Yan, T., and Li, S. (2014) Cdk1 regulates the temporal recruitment of telomerase and Cdc13-Stn1-Ten1 complex for telomere replication. *Mol. Cell Biol.* **34**, 57–70 [CrossRef Medline](#)
69. Mullins, M. R., Rajavel, M., Hernandez-Sanchez, W., de la Fuente, M., Biendarra, S. M., Harris, M. E., and Taylor, D. J. (2016) POT1-TPP1 binding and unfolding of telomere DNA discriminates against structural polymorphism. *J. Mol. Biol.* **428**, 2695–2708 [CrossRef Medline](#)
70. Traczyk, A., Liew, C. W., Gill, D. J., and Rhodes, D. (2020) Structural basis of G-quadruplex DNA recognition by the yeast telomeric protein Rap1. *Nucleic Acids Res.* **48**, 4562–4571 [CrossRef Medline](#)
71. Rigo, R., Dean, W. L., Gray, R. D., Chaires, J. B., and Sissi, C. (2017) Conformational profiling of a G-rich sequence within the c-KIT promoter. *Nucleic Acids Res.* **45**, 13056–13067 [CrossRef Medline](#)
72. Boulé, J.-B., Vega, L. R., and Zakian, V. A. (2005) The yeast Pif1p helicase removes telomerase from telomeric DNA. *Nature* **438**, 57–61 [CrossRef Medline](#)
73. Qi, H., and Zakian, V. A. (2000) The *Saccharomyces* telomere-binding protein Cdc13p interacts with both the catalytic subunit of DNA polymerase α and the telomerase-associated Est1 protein. *Genes Dev.* **14**, 1777–1788 [Medline](#)
74. Bhattacharjee, A., Wang, Y., Diao, J., and Price, C. M. (2017) Dynamic DNA binding, junction recognition and G4 melting activity underlie the telomeric and genome-wide roles of human CST. *Nucleic Acids Res.* **45**, 12311–12324 [CrossRef Medline](#)
75. Zhang, M., Wang, B., Li, T., Liu, R., Xiao, Y., Geng, X., Li, G., Liu, Q., Price, C. M., Liu, Y., and Wang, F. (2019) Mammalian CST averts replication failure by preventing G-quadruplex accumulation. *Nucleic Acids Res.* **47**, 5243–5259 [CrossRef Medline](#)
76. Bradford, M. (1976) A rapid and sensitive method for the quantitation of microgram quantities of protein utilizing the principle of protein-dye binding. *Anal. Biochem.* **72**, 248–254 [CrossRef Medline](#)
77. Sklenář, V., and Bax, A. (1987) Spin-echo water suppression for the generation of pure-phase two-dimensional NMR spectra. *J. Magn. Reson.* **74**, 469–479 [CrossRef](#)
78. Hänsel-Hertsch, R., Spiegel, J., Marsico, G., Tannahill, D., and Balasubramanian, S. (2018) Genome-wide mapping of endogenous G-quadruplex DNA structures by chromatin immunoprecipitation and high-throughput sequencing. *Nat. Protoc.* **13**, 551–564 [CrossRef Medline](#)
79. De Magis, A., Manzo, S. G., Russo, M., Marinello, J., Morigi, R., Sordet, O., and Capranico, G. (2019) DNA damage and genome instability by G-quadruplex ligands are mediated by R loops in human cancer cells. *Proc. Natl. Acad. Sci. U.S.A.* **116**, 816–825 [CrossRef Medline](#)
80. Graf, M., Bonetti, D., Lockhart, A., Serhal, K., Kellner, V., Maicher, A., Jolivet, P., Teixeira, M. T., and Luke, B. (2017) Telomere length determines TERRA and R-loop regulation through the cell cycle. *Cell* **170**, 72–85.e14 [CrossRef Medline](#)
81. Wanzek, K., Schwindt, E., Capra, J. A., and Paeschke, K. (2017) Mms1 binds to G-rich regions in *Saccharomyces cerevisiae* and influences replication and genome stability. *Nucleic Acids Res.* **45**, 7796–7806 [CrossRef Medline](#)

ARTICLE

<https://doi.org/10.1038/s41467-020-17701-8>

OPEN

Zuo1 supports G4 structure formation and directs repair toward nucleotide excision repair

Alessio De Magis ^{1,4}, Silvia Götz^{2,3,4}, Mona Hajikazemi¹, Enikő Fekete-Szűcs³, Marco Caterino ¹, Stefan Juranek ¹ & Katrin Paeschke ^{1,2,3}✉

Nucleic acids can fold into G-quadruplex (G4) structures that can fine-tune biological processes. Proteins are required to recognize G4 structures and coordinate their function. Here we identify Zuo1 as a novel G4-binding protein *in vitro* and *in vivo*. *In vivo* in the absence of Zuo1 fewer G4 structures form, cell growth slows and cells become UV sensitive. Subsequent experiments reveal that these cellular changes are due to reduced levels of G4 structures. Zuo1 function at G4 structures results in the recruitment of nucleotide excision repair (NER) factors, which has a positive effect on genome stability. Cells lacking functional NER, as well as Zuo1, accumulate G4 structures, which become accessible to translesion synthesis. Our results suggest a model in which Zuo1 supports NER function and regulates the choice of the DNA repair pathway nearby G4 structures.

¹Department of Oncology, Hematology and Rheumatology, University Hospital Bonn, Venusberg-Campus 1, 53127 Bonn, Germany. ²Department of Biochemistry, Biocenter, University of Würzburg, Am Hubland, 97074 Würzburg, Germany. ³European Research Institute for the Biology of Ageing, University of Groningen, A. Deusinglaan 1, 9713 AV Groningen, the Netherlands. ⁴These authors contributed equally: Alessio De Magis, Silvia Götz. ✉email: katrin.paeschke@ukbonn.de

The demonstration that secondary DNA and RNA structures influence biological processes has revolutionized modern biology and brought attention particularly toward G-quadruplex (G4) structures. These are non-canonical secondary arrangements of (at least two) π - π stacking guanine tetrads that form within guanine-rich DNA and RNA sequences^{1,2}. While controversially discussed in the past, there is growing evidence of their formation and biological function in vivo, which is conserved from bacteria to human³. In yeast and human, G4 structure-forming sequences (G4 motifs) are significantly enriched at key functional units like promoters, mitotic and meiotic double-strand breaks (DSBs), and telomeres⁴⁻⁶, pointing to a variety of critical cellular functions including transcription, cell-cycle regulation and telomere maintenance⁷. As G4 structures intervene in such a variety of biological processes they need to be properly regulated and unwound. A large number of proteins, mostly helicases, unfold G4 structures in vitro and in vivo⁸. Changes in G4 structure formation and unfolding can lead to replication fork stalling^{9,10}, accumulation of deletions/mutations¹¹⁻¹³, genomic copy number alterations and a high recombination frequency^{6,14-19}. In model organisms (*Caenorhabditis elegans* and *Saccharomyces cerevisiae*) as well as in human tissue culture it has been shown that changes in G4 structure regulation lead to genome instability^{10,20-23}.

Although the underlying mechanisms have yet to be clarified, the formation of G4 structures is connected to DNA repair as indicated by the findings that many G4 structure-interacting proteins are linked to DNA repair processes²⁴⁻²⁹. BRCA1 and Rad51, as well as Ku80, have been shown to interact with G4 structures and function during either homologous recombination (HR) or non-homologous end-joining (NHEJ), respectively^{25,26}. In addition to these canonical repair pathways, post-replicative repair proteins such as the translesion synthesis (TLS) protein Rev1^{27,29,30} and the polymerase θ ³¹ have also been linked to G4 structure formation. Furthermore, the helicases XPD and XPB, involved in transcription regulation and nucleotide excision repair (NER), have been shown to regulate G4 structures both in vitro and in vivo³². These studies underline the finding that G4 structures are prone to breakage and are a risk for genome stability. Contrarily, G4 structure-induced damage is also beneficial for the cell during class-switch recombination, antigenic variations or the repair of oxidized guanines³³⁻³⁶. These contrary findings demonstrate that there must be a subtle equilibrium between G4 structure-induced genome instability and G4 structure-promoted repair processes. Nevertheless, detailed knowledge on the impact of G4 structures on DNA repair is currently missing.

Based on the here presented data we speculate that G4 structures serve either as loading platforms for proteins involved in DNA repair or as bumps, which are slowing down the replication upstream of a lesion and thereby influencing the choice between different repair systems. We identify more than 100 candidate proteins that bind to G4 structures in *S. cerevisiae*; among these is Zuo1. By in vitro and in vitro experiments we reveal that Zuo1 supports G4 structure formation and contributes to genome stability by recruiting NER factors. Especially after UV damage, when more G4 structures form, Zuo1 function is essential to preserve genome stability. Zuo1 modulates G4 structure levels and acts as a molecular switch for the selection of the appropriate DNA repair pathway.

Results

Zuo1 binds to G-quadruplex structures in vitro. We performed yeast one-hybrid (Y1H) screens with a G4 motif as a bait region to identify proteins that recognize G4 structures in vivo. In detail,

a G4 motif from chromosome IX (G4_{IX}; GGGTACGGTGGG TAATAAGGGAAGGTATCGGG) was used as bait sequence (bait-G4) and was integrated upstream of a reporter gene (*Aureobasidin A* resistance gene) (Fig. 1a). The in vitro folding of G4_{IX} into a parallel quadruplex was confirmed by circular dichroism (CD), with characteristic peaks at 243 and 264 nm, in 100 mM K⁺ (Fig. 1b)³⁷. We identified 157 potential G4 structure-interacting proteins using this approach (Supplementary Data 1). Among the identified proteins was Zuo1, a conserved eukaryote-specific, multifunctional J-protein present in the cytosol and nucleus^{38,39}. Its published function in transcription and DNA repair^{40,41} makes it a prime candidate to further address its biological function at G4 structures in the cell. To validate the specific interaction of Zuo1 with the bait-G4 structure we performed a

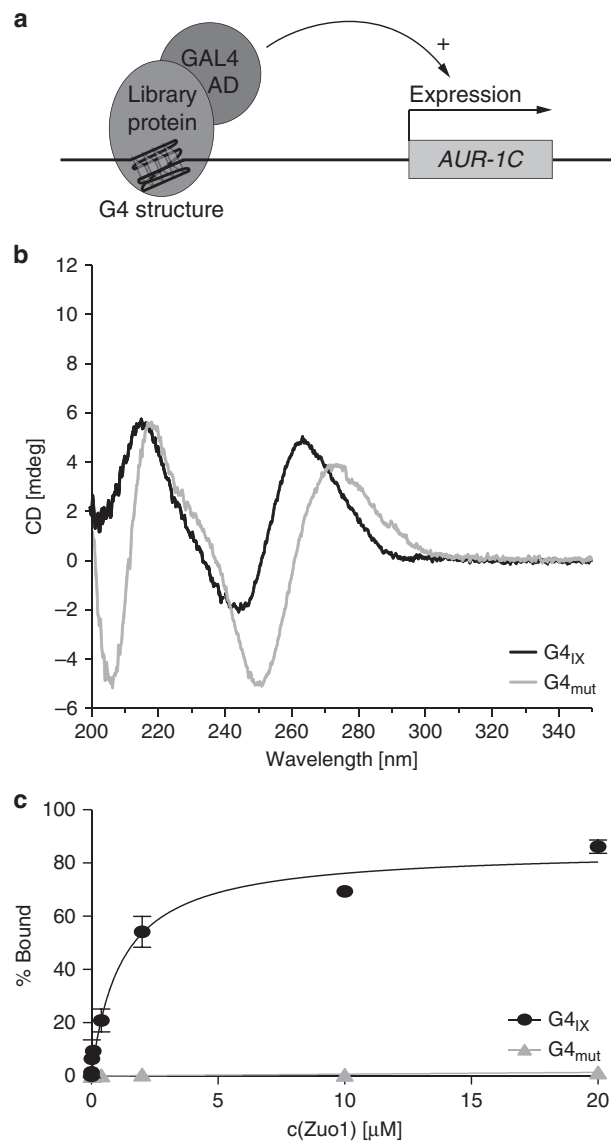


Fig. 1 Zuo1 binds to G-quadruplex structures in vitro. **a** Graphic illustration of the yeast one-hybrid screen (Y1H) system. GAL4 AD, Galactose Activation Domain. *AUR-1C*, Aureobasidin A **b** CD spectra of the folded oligonucleotides G4_{IX} and G4_{mut} in the presence of 100 mM K⁺. **c** Quantification of Zuo1-binding to G4_{IX} and G4_{mut} by filter binding assay. Error bars correspond to one standard deviation of the mean of three independent experiments.

Y1H experiment using a mutated G4 motif ($G4_{mut}$) as a bait construct. CD analysis confirmed that no G4 structure forms within this mutated G4 sequence (Fig. 1b). The lack of growth on selective media when the mutated G4 motif was used as a bait indicated that Zuo1 binds specifically to the G4 sites in the Y1H assay.

There are two limitations in this approach: first, the interaction of Zuo1 with G4 structures can be direct or indirect; second, we cannot reveal whether Zuo1 binds to G4 structures or to unfolded G4 motifs. To overcome these restrictions, we purified Zuo1 from *Escherichia coli* (Supplementary Fig. S1a) and performed in vitro binding analyses (Fig. 1c). Zuo1-binding to G4 structures was determined by double-filter binding assays (Fig. 1c, Supplementary Fig. S1b–e) using four different G4 structures ($G4_{IX}$, $G4_{FDNA}$, $G4_{TP1}$, $G4_{TP2}$) and four non-G4 sequences as controls (dsDNA, $G4_{mut}$, forked and bubbled DNA). Double-filter binding analyses revealed that significant Zuo1 binding to all tested G4 structures (apparent K_d range: 0.67–1.27 μ M) and no binding to any control sequence (Fig. 1c, Supplementary Fig. S1b–e).

Furthermore, CD titration experiments under sub-optimal G4-stabilizing conditions (100 mM Na^+ in place of K^+) served to

prove Zuo1 as able to influence the G4 conformational equilibrium. Under these conditions, $G4_{IX}$ indeed folds into a dominantly hybrid-1 quadruplex as seen by the CD spectrum with an additional distinct positive peak at 295 nm (Supplementary Fig. S1f). Increasing Zuo1: $G4_{IX}$ molar ratio prompted up to 14-fold ellipticity increase at 264 nm, along with the simultaneous decrease of the 295 nm band, proving the Zuo1-induced parallel $G4_{IX}$ stabilization.

Zuo1 binds G4 motif sites genome-wide and supports G4 formation. We performed chromatin immunoprecipitation (ChIP) followed by genome-wide sequencing analysis (ChIP-seq) in asynchronous yeast cultures expressing C-terminal Myc-tagged Zuo1 to test the binding of Zuo1 to G4 motifs in vivo. We obtained 6.1×10^6 reads of which 94% mapped to the *S. cerevisiae* genome (sacCer3). We identified 1594 chromosomal binding sites for Zuo1 using MACS 2.0 (Fig. 2a, Supplementary Data 2). Peaks were compared with genomic features (centromeres, ARS and promoters as annotated by SGD, <https://www.yeastgenome.org>), previously identified protein-binding regions (Pif1, γ -H2AX,

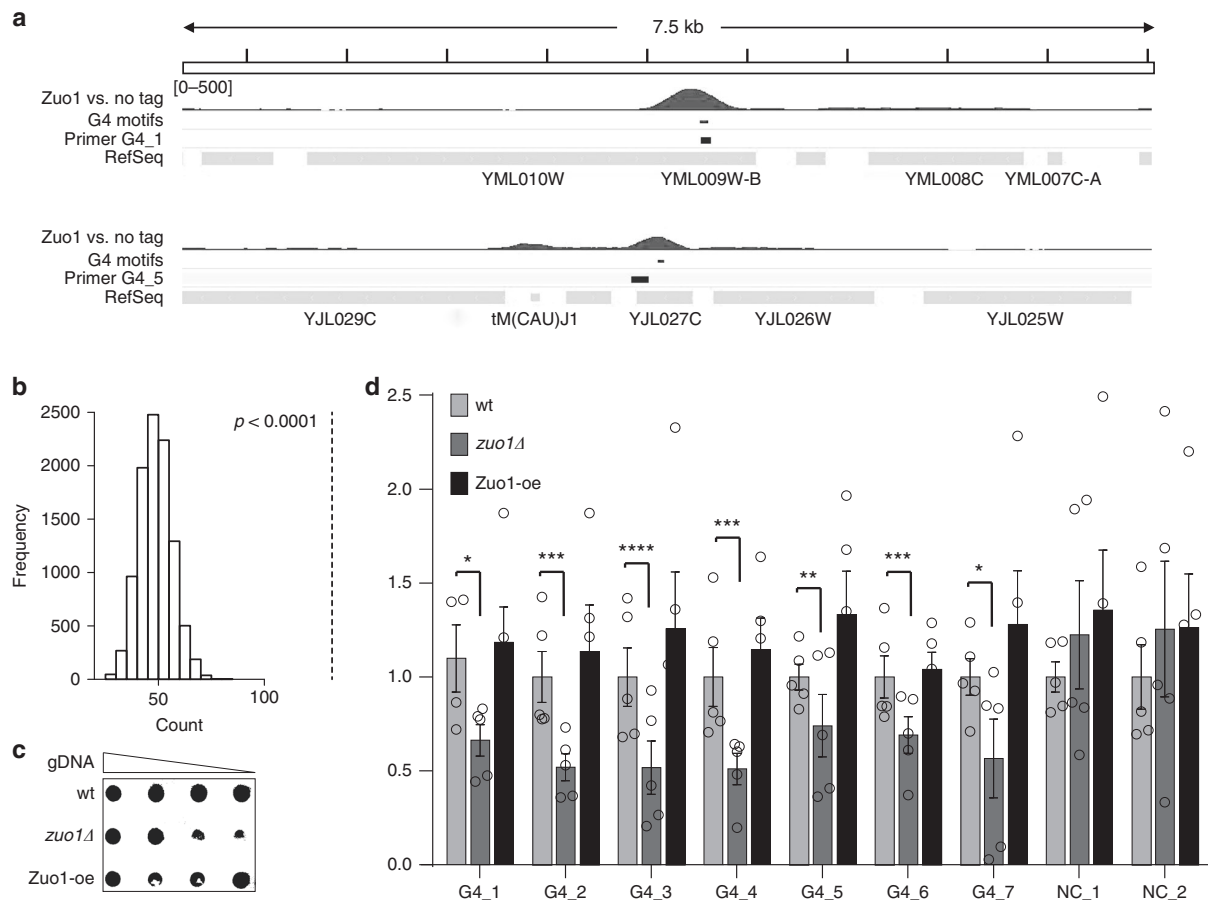


Fig. 2 Zuo1 binds G4 motifs genome-wide and support G4 formation. **a** IGV Genome Browser screenshot. Illustration of two 7.5 kb regions: top Chr XIII location 246,726 to 254,317 ($G4_1$) and bottom Chr X location 388,395 to 395,967 ($G4_5$). Zuo1-binding sites, location of G4 motifs and annotated genes are illustrated below. These regions were also among the regions tested in the qPCR, primers are indicated $G4_1$ and $G4_5$ (black track). **b** Genome-wide overlap of the Zuo1 peaks with G4 motifs as predicted by⁴. The black dotted line indicates a highly significant overlap $p = 0.0001$. **c** Southern-western combination to detect G4 structures in wildtype (wt), *zuo1* Δ and Zuo1-oe cells. Different amounts of genomic DNA were spotted on a membrane (2, 1, 0.5, and 0.25 μ g), incubated with 2 μ g/ml of BG4 antibody and detected by chemiluminescence. **d** BG4-ChIP analysis followed by qPCR of G4 levels in wt, *zuo1* Δ , and Zuo1-oe cells. Plotted are the means of $n = 5$ biologically independent experiments, which were normalized to wildtype. Error bars present \pm SEM. Significance was calculated based on one-sided Student's *t*-test. Asterisks indicate statistical significance in comparison with wildtype. * $p < 0.05$, ** $p < 0.01$, *** $p < 0.001$, **** $p < 0.0001$.

DNA Pol2) and regions harboring putative G4 motifs^{4,9}. Peaks significantly overlapped to G4 motifs (Fig. 2a, b), promoters ($p = 0.007$), replication pausing sites and R-loops ($p = 0.0001$)⁴². No correlation with DNA damage sites marked by phosphorylated H2AX (γ -H2AX)⁴ was observed (Supplementary Fig. S2a–d).

To test, whether Zuo1 changes the G4 structure level in the cell we analyzed the amount of folded G4 structures in Zuo1 deletion (*zuo1Δ*), Zuo1 overexpression (Zuo-oe) and wildtype cells. Genomic DNA was isolated, spotted at four concentrations on a nylon membrane and probed for G4 structures using the G4 structure-specific antibody BG4⁴³. *zuo1Δ* showed ~50% less G4 structures than wildtype cells whereas no change could be determined in Zuo1-oe cells (Fig. 2c, Supplementary Fig. S2e).

Cellular G4 structure levels can also be measured by ChIP. We adapted the published protocol⁴⁴ to yeast and performed ChIP-qPCR. First, to validate the robustness of the method we monitored G4 structure levels in wildtype cells before and after the addition of PhenDC₃, an established G4-stabilizer⁴⁵. We expected an increase of G4 structure levels after treatment with PhenDC₃. The ChIP-qPCR analyses confirmed that G4 structures form in vivo at selected sites (two- to three-fold enriched compared with the no antibody control) and more G4 structures were detectable after PhenDC₃ treatment (four- to eight-fold enriched) (Supplementary Fig. S2f). Here and in all subsequent ChIP and qPCR experiments we used seven Zuo1 target sites (G4_1 to G4_7), which overlap annotated G4 motifs⁴, as well as two negative controls (NC_1, NC_2), which neither fold into G4 structures nor overlap with Zuo1-binding sites (see Supplementary Table S1 for qPCR primer).

We monitored G4 structures by ChIP in wildtype, *zuo1Δ* and Zuo1-oe cells. Similar to the previous experiment, a two-fold decrease in G4 signal was measured at all selected Zuo1 target sites in *zuo1Δ* cells (Fig. 2d). No significant changes in G4 structure levels were detected upon overexpression of Zuo1. We explain this by the finding that Zuo1 binds to a specific subset of G4 regions that do not increase upon Zuo1 overexpression. Meaning increasing amounts of Zuo1 do not increase the G4 targets that are bound by Zuo1. These data showed that Zuo1 binds to G4 structures and supports their formation.

Zuo1 function at G4 has a positive effect on cellular fitness. To understand the cellular role of Zuo1 and the underlying cellular processes, we monitored the cellular consequences of Zuo1 deletion. As the first sign of an unbalanced homeostasis cellular growth is impaired. Changes in cellular growth can be monitored in liquid or on plates. The doubling time of *zuo1Δ* cells increased to 144 min as compared with 90 min in wildtype cells (Fig. 3a, b, $p = 0.0003$). We induced G4 structure formation chemically by adding PhenDC₃ to wildtype and *zuo1Δ* cells (Supplementary Fig. S2f) to assess whether the observed growth defect (Fig. 3a) is due to reduced G4 structures in the cells (Fig. 2c, d). We monitored growth by spotting different concentrations of yeast cells on plates containing 10 μM PhenDC₃. Upon PhenDC₃ addition no changes in colony formation for wildtype cells was detected, but for *zuo1Δ* cells colony formation was increased indicating that G4 structure stabilization rescued the growth defect of *zuo1Δ* (Fig. 3b). In liquid media, we confirmed that PhenDC₃ treatment significantly rescues the growth defects of *zuo1Δ* (without PhenDC₃ 144 min, with PhenDC₃ 112 min doubling time, Supplementary Fig. S3a).

Pif1 and the RecQ helicase Sgs1 have been described to regulate G4 structures in yeast^{5,9,13}. We therefore questioned whether Zuo1 interacts with known G4-unwinding helicases. To test whether Zuo1 functions in the same pathway as either Sgs1 or Pif1, we created *zuo1Δ sgs1Δ* and *zuo1Δ pif1-m2* yeast strains.

Cells with a specific point mutation in the *PIF1* gene (*pif1-m2*) lack the nuclear isoform of Pif1 but express the mitochondrial isoform⁴⁶. Both *sgs1Δ* and *pif1-m2* do not have a growth defect^{46,47}. The double mutants *zuo1Δ sgs1Δ* and *zuo1Δ pif1-m2* exhibited prolonged doubling time compared with *zuo1Δ* (Fig. 3c). Doubling times of 225.6 min for *zuo1Δ sgs1Δ* and 155.4 min for *zuo1Δ pif1-m2* were determined. This hints that Zuo1 does not act in the same pathway as Sgs1 and Pif1 because the double mutant would not increase the initial growth defect otherwise (Supplementary Fig. S3b,c shows the growth rates of single and double mutants). To test whether the growth defects in the double mutants are due reduced G4 structures, we stabilized G4 structures by adding PhenDC₃. The growth defect in *zuo1Δ sgs1Δ* was rescued after the re-stabilization of G4 structures, indicating that Sgs1 and Zuo1 functions are likely connected to G4 structures (Fig. 3d, Supplementary Fig. S3d). No growth changes were observed in *zuo1Δ pif1-m2* cells after PhenDC₃ addition. To test whether either Sgs1 or Pif1 binds to Zuo1 target regions and whether this binding depends on Zuo1, we monitored Pif1 and Sgs1 binding to seven Zuo1 targets and two control regions by ChIP-qPCR (see above). Pif1 did not bind significantly to Zuo1 targets and, consequently, its binding did not change in *zuo1Δ* (Fig. 3f). Sgs1 binding was four-fold reduced in the absence of Zuo1 (Fig. 3e). These results revealed that Zuo1 and Pif1 do not act in the same pathway and targets. However, these data demonstrated that Zuo1 is essential for Sgs1 binding to these G4 sites.

Zuo1 mediates NER pathway recognition at G4 sites. The published function of Zuo1 in transcriptional regulation^{40,41} and the potential function of G4 structures at promoters, prompted us to investigate potential transcriptional changes between wildtype and *zuo1Δ* cells. In a microarray-based screen we identified 80 up- and 142 down-regulated genes in response to Zuo1 deletion. However, no direct correlation to Zuo1 targets could be determined (Supplementary Data 3, Supplementary Fig. S3e).

It has been shown that G4 structure formation can cause DNA damage and drive DNA damage response (DDR) activation^{48,49} in the absence of helicases^{13,50}. DSBs are life-threatening lesions in the genomic DNA repaired by HR or NHEJ⁵¹. To determine whether Zuo1 recruits either NHEJ or HR proteins to target G4 sites, we endogenously tagged yKu70 (NHEJ) and Rad50 (HR) with Myc13. ChIP-qPCR analysis in wildtype and *zuo1Δ* indicated that neither pathway is triggered at these sites nor is altered in a Zuo1-dependent fashion (Fig. 4a, b). Zuo1 binding was also not significantly altered in the absence of either Rad50 or yKu70 (Supplementary Fig. S4a, b). These results agree with the lack of a significant overlap between Zuo1 targets and γ H2ax loci (Supplementary Fig. S2b). Furthermore, rearrangement rates monitored in gross chromosomal rearrangement (GCR) assays at a G4-specific locus, did not show elevated rates in *zuo1Δ* cells either (Supplementary Fig. S4c). These results indicated that the Zuo1 function at G4 structures is not affecting DSB formation and canonical DNA repair.

zuo1Δ cells are sensitive to DNA damage agents such as UV, bleomycin, hydroxyurea (HU), or methyl methanesulfonate (MMS) (Supplementary Fig. S4d). This implies a post-replicative function of Zuo1. TLS, base excision repair (BER) and NER are prominent post-replicative repair pathways. We monitored whether the proteins of these pathways bind to Zuo1 targets and if such interactions depend on the presence of Zuo1. We endogenously tagged for each repair pathway one protein: Rev1 (TLS), Apn1 (BER) and Rad23 (NER). We analyzed the binding of the proteins in wildtype and *zuo1Δ* cells by ChIP-qPCR. ChIP-qPCR data were normalized to *zuo1Δ*/wildtype and fold decrease was plotted. Apn1 and Rev1 showed low levels of binding to Zuo1

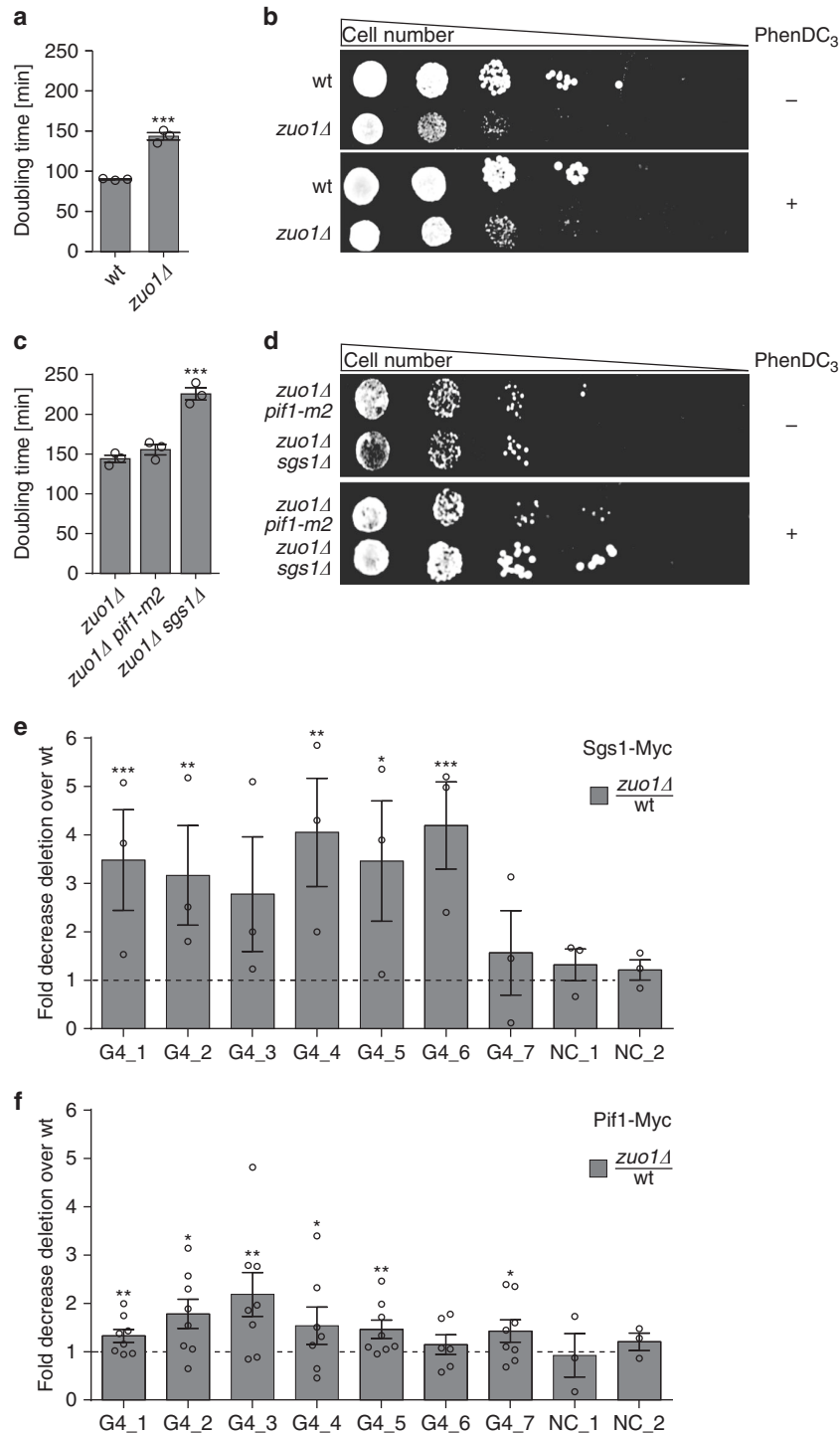


Fig. 3 Zuo1 function at G4 has a positive effect on cellular fitness. **a–d** Monitoring of growth changes in different yeast cells **a, c** Growth curves in liquid media were performed and doubling times (minutes) were calculated using the indicated yeast strains. Plotted are the means of $n = 3$ biologically independent experiments. Error bars present \pm SEM. Significance was calculated based on one-sided Student's t -test. Asterisks indicate statistical significance: * $p < 0.05$, ** $p < 0.01$, *** $p < 0.001$. **b, d** A serial dilution of yeast cells was spotted on rich media with and without $10 \mu\text{M}$ PhenDC₃. Growth changes and sensitivity of $n = 3$ biologically independent experiments were monitored by colonies formation. **e, f** ChIP analysis followed by qPCR that monitored the binding of either Sgs1 (**e**) or Pif1 (**f**) to seven Zuo1 targets (G4_1–7) and two controls (NC_1,2) was monitored after ChIP and qPCR. ChIP was performed in wildtype and *zuo1Δ* cells. Presented data show fold decrease *zuo1Δ*/wt \pm SEM. For all experiments, the means of three biological replicates were plotted. Significance was calculated based on one-sided Student's t -test. Asterisks indicate statistical significance in comparison with wildtype cells. * $p < 0.05$, ** $p < 0.01$, *** $p < 0.001$.

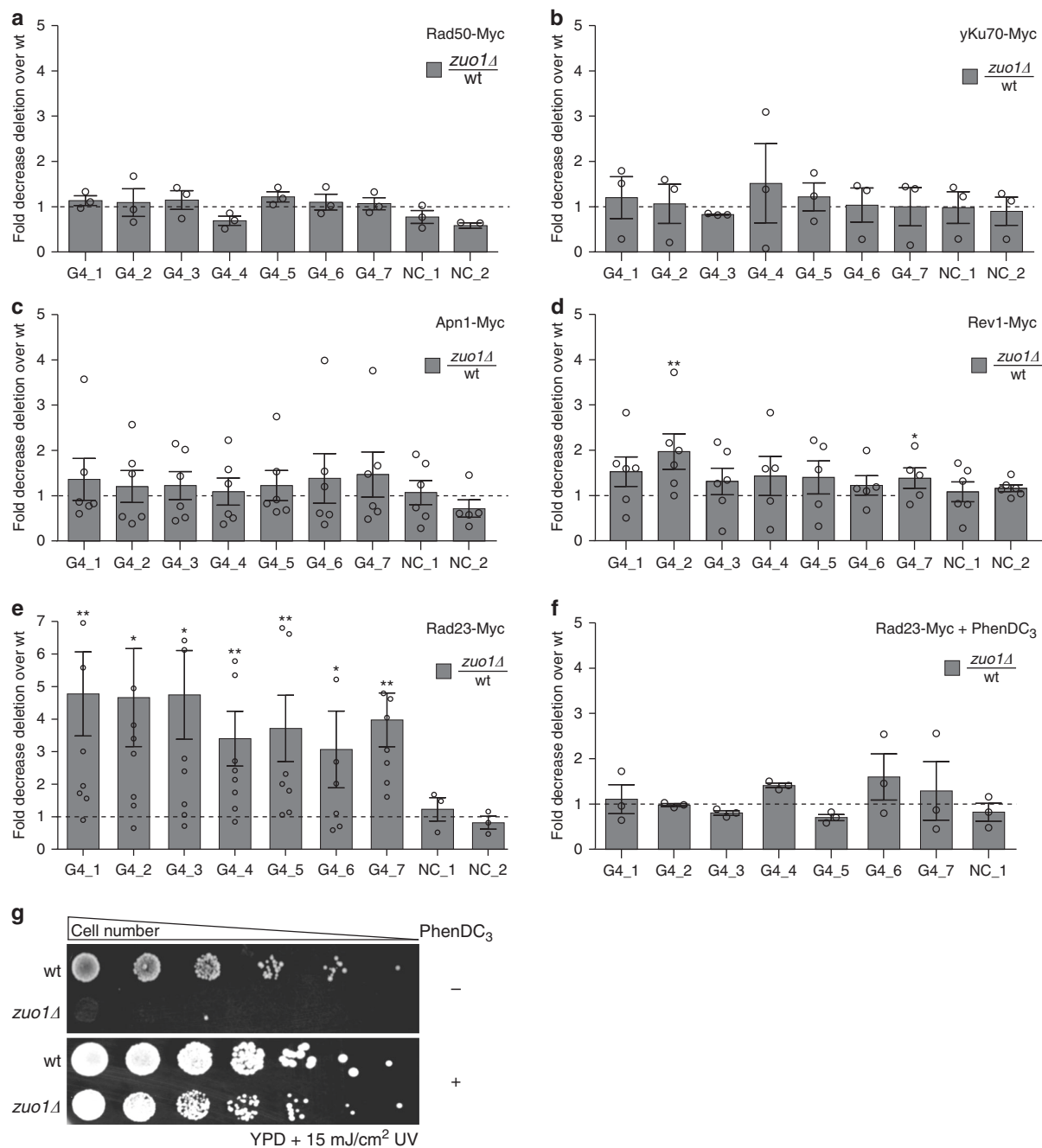


Fig. 4 Zuo1 mediates NER pathway recognition at G4 sites. ChIP and qPCR analysis of different repair proteins in wildtype and *zuo1Δ* cells. All qPCRs were performed at seven Zuo1 targets (G4₁-7) and two controls (NC₁, 2). Presented data show fold decrease *zuo1Δ*/wt ± SEM of *n* = 3 biologically independent experiments. **a** ChIP and qPCR of Rad50-Myc. **b** ChIP and qPCR of Ku70-Myc **c** ChIP and qPCR of Apn1-Myc **d** ChIP and qPCR of Rev1-Myc **e** ChIP and qPCR of Rad23-Myc **f** ChIP and qPCR of Rad23-Myc in the presence of 10 μM of PhenDC₃. All plotted results were based on the average of at least three independent experiments ± SEM. Significance was calculated based on one-sided Student's *t*-test. Asterisks indicate statistical significance in comparison with wildtype cells under the same experimental conditions. **p* < 0.05, ***p* < 0.01. **g** Yeast cells were grown on liquid media in the presence or absence of PhenDC₃, irradiated with 15 J m⁻² UV light (254 nm) and spotted in different concentrations of rich media. Growth changes and sensitivity were monitored by colony formation.

targets and no changes in binding between wildtype and *zuo1Δ* (Fig. 4c, d) indicating that neither BER nor TLS acts at the G4 sites targeted by Zuo1. However, Rad23 (a subunit of the Rad4/Rad23 complex; XPC in human) changed its binding pattern to G4 sites in the absence of Zuo1. Zuo1 deletion resulted in at least a three-fold decrease in the binding of Rad23 to G4 sites (Fig. 4e). These results

indicated that Zuo1 supports the binding of Rad23 to G4 motifs. To exclude that this effect is specific to Rad23, we monitored the binding pattern of additional NER proteins: Rad4, Rad1 (XPF in human) and Rad2 (XPG in human) (reviewed in⁵²). Similar to Rad23 also Rad4, Rad1 and Rad2 exhibit significantly reduced binding to Zuo1 target regions in *zuo1Δ* cells (Supplementary

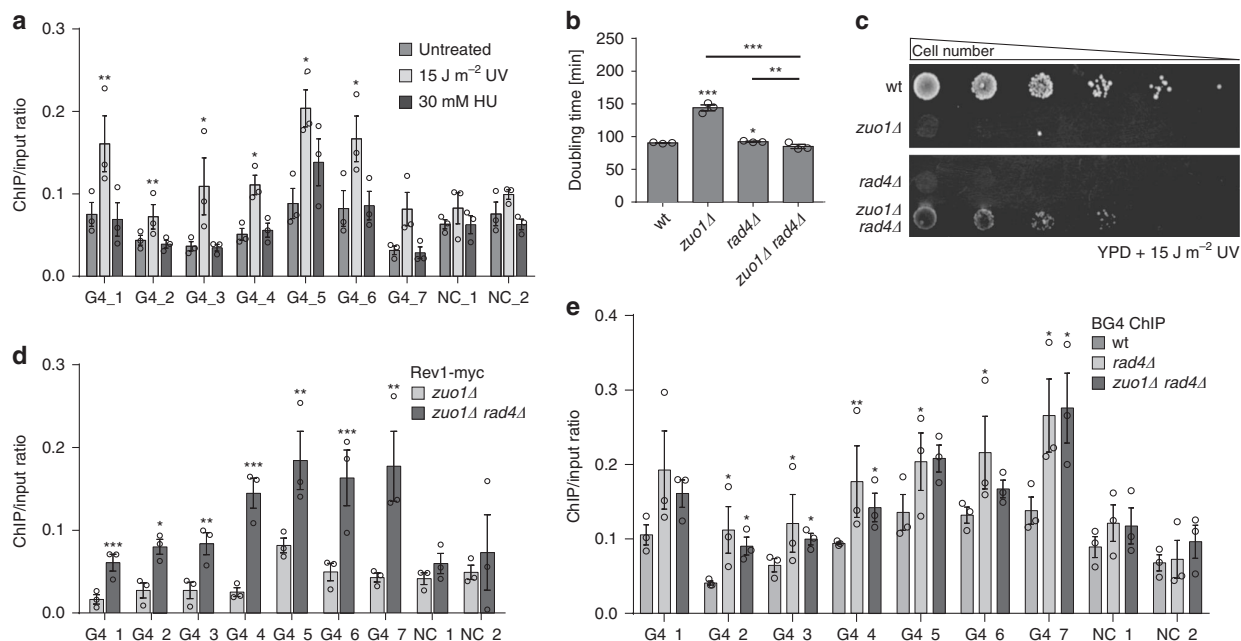


Fig. 5 Zuo1 deficiency and NER impairment increase TLS activity at G4 sites. **a** BG4-ChIP analysis followed by qPCR of G4 levels in untreated wildtype, treated with $J\ m^{-2}$ UV (254 nm) and 30 mM HU strains. Plotted are the means of $n = 3$ biologically independent experiments. Error bars present \pm SEM. Significance was calculated based on one-sided Student's *t*-test. Asterisks indicate statistical significance: * $p < 0.05$, ** $p < 0.01$, *** $p < 0.001$. **b** Growth curves of indicated yeast strains in liquid media. Doubling times (min) were calculated. Plotted are the means of $n = 3$ biologically independent experiments. Error bars present \pm SEM. Significance was calculated based on one-sided Student's *t*-test. Asterisks indicate statistical significance: * $p < 0.05$, ** $p < 0.01$, *** $p < 0.001$. **c** Different concentrations of yeast cells were spotted on rich media, with or without irradiation with $15\ J\ m^{-2}$ UV light (254 nm). Growth changes and sensitivity were monitored by colony formation. **d** Rev1 Myc-ChIP analysis followed by qPCR to test Rev1 binding at nine different loci. The bars show the IP value over the input of the *zuo1Δ* strain as well as the double mutant *zuo1Δ rad4Δ*. Plotted are the means of $n = 3$ biologically independent experiments. Error bars present \pm SEM. Significance was calculated based on one-sided Student's *t*-test. Asterisks indicate statistical significance: * $p < 0.05$, ** $p < 0.01$, *** $p < 0.001$. **e** BG4-ChIP analysis followed by qPCR of G4 levels in wildtype, *rad4Δ* and *zuo1Δ rad4Δ* strains. Plotted results are the means of $n = 3$ biologically independent experiments. Error bars present \pm SEM. Significance was calculated based on one-sided Student's *t*-test. Asterisks indicate statistical significance in comparison with wildtype: * $p < 0.05$, ** $p < 0.01$, *** $p < 0.001$.

Fig. S4e–g). To understand whether reduced G4 structure levels are causing the change in NER binding, we stabilized G4 structures by adding PhenDC₃ and measured the binding of Rad23 in wildtype and *zuo1Δ*. ChIP-qPCR analyses showed that Rad23 binding in *zuo1Δ* cells is rescued after the addition of PhenDC₃ (Fig. 4f). This, as well as the finding that the UV sensitivity of *zuo1Δ* can also be rescued by PhenDC₃ addition (Fig. 4g), suggested that G4 structure stabilization itself recruits NER factors to bind and function at these sites.

Zuo1 deficiency and NER impairment increase TLS activity at G4 sites.

Zuo1 binds and supports G4 structure formation leading to the recruitment of NER factors. Defects in NER^{53–55}, as well as the deletion of Zuo1, resulted in severe UV sensitivity (Fig. 5c, Supplementary Fig. S4d). In order to understand whether the UV sensitivity was due to a delay in the repair of UV lesions, we analyzed the levels of γ H2AX wildtype and *zuo1Δ* cells after UV radiation over time by western blot. Thymine dimers and other photo adducts occurring upon UV irradiation lead to the recruitment of RPA, XPA, and XPC-TFIIH, hence to double-strand break processing⁵⁶. Proteins of wildtype and *zuo1Δ* cells with UV were isolated at 0, 1, and 4 h after UV exposure. Western blot analysis demonstrated that, after 4 h, most DNA damages were cleared in wild type but not in *zuo1Δ*. This data indicated a delay in eliminating UV lesions in *zuo1Δ* cells, which could explain the growth defects in *zuo1Δ* cells after UV treatment. Quantification of these western analyses revealed that without Zuo1 60% less DNA repair after UV damage occurs. We

speculated that G4 structures formed upon UV damage result in Zuo1-binding, which in turn facilitates NER recruitment. To test this hypothesis, we monitored G4 structure levels in wildtype cells upon UV treatment. In line with our assumption, at least two-fold more G4 structures are detectable by ChIP-qPCR upon UV damage compared with no treatment (Fig. 5a). This is specific to UV damage, because treatment with HU (replicative damage) did not increase G4 structure levels in the cells (Fig. 5a).

We monitored the growth in the double deletion *zuo1Δ rad4Δ* with the aim to characterize the relation between Zuo1 and the NER component Rad4. *zuo1Δ* exhibited a growth defect, whereas *rad4Δ* did not. Remarkably, *zuo1Δ rad4Δ* suppressed the growth defect of *zuo1Δ*. The doubling time of *zuo1Δ rad4Δ* was 82 min, which is 57% faster than the single mutant *zuo1Δ* (Fig. 5b, Supplementary Fig. S5a). Both single mutants were UV sensitive ($15\ J\ m^{-2}$), whereas the double mutant was not (Fig. 5c). These results led us to speculate that in the double mutant *zuo1Δ rad4Δ* an alternative repair pathway is recruited to compensate for the loss of the NER activity. To understand which DDR pathway is active in *zuo1Δ rad4Δ*, we examined the binding of Rad50 (HR), Ku70 (NHEJ) and Rev1 (TLS) in *zuo1Δ rad4Δ* cells. ChIP-qPCR analyses were performed with these strains and confirmed that neither HR nor NHEJ compensates for the loss of Zuo1 and Rad4 at Zuo1 target regions (Supplementary Fig. S5b,c). However, Rev1 (TLS) showed at least a twofold increase in binding to Zuo1 target regions in *zuo1Δ rad4Δ* (Fig. 5d) compared with the single mutant *zuo1Δ*. Defects in NER (*rad4Δ*) alone were not sufficient to recruit Rev1 (Supplementary Fig. S5d).

To further examine this change in repair pathway and to connect this to G4 structure formation, we performed BG4 ChIP-qPCR analyses in wildtype, *zuo1Δ*, *rad4Δ*, and *zuo1Δ rad4Δ* cells. Again, less G4 structures were detectable in *zuo1Δ* compared with wildtype (Fig. 2c, d). In *rad4Δ* and *zuo1Δ rad4Δ*, significantly more G4 structures were detected compared with wildtype (Fig. 5e). These results confirmed that Zuo1 supports G4 structure formation, which stimulates the recruitment of NER components. In addition, a functional NER pathway is required for G4 unfolding. G4 structures accumulated and were accessible to TLS in cells lacking both functional Zuo1 and the NER machinery, as indicated by Rev1-binding. The activation of TLS in *zuo1Δ rad4Δ* cells did not make the cells sensitive to UV radiation, unlike the single mutants (Fig. 5c).

Discussion

A number of studies link G4 structure formation to genome instability^{9,12,14,20,22,28–30,50,57–62}. G4 structure formation has also been shown to positively influence biological processes such as telomere maintenance and transcription regulation^{33,63–65}. Proteins that recognize and/or induce the formation of G4 structures are therefore required. Here, we identified 157 G4 structure-binding proteins by a Y1H screen. Among these is Zuo1 and we could show that it supports genome stability by assisting the recruitment of the NER machinery through binding and promoting the formation of G4 structures in *S. cerevisiae*.

zuo1Δ cells are sensitive to all tested DNA damaging agents (Supplementary Fig. S4d), which indicates that Zuo1 functions in post-replicative DNA repair. All post-replicative DNA repair processes (BER, TLS, and NER) are connected to G4 structure formation. During BER, G4 structure formation has been suggested to be stimulated by ROS-mediated oxidation of DNA and APE1 binding, which results in changes in transcription^{33,34}. In eukaryotes, the polymerases Rev1, η , κ , and θ are involved in the replication of G4 motifs during TLS (reviewed in⁶⁶). The helicases XPB and XPD of the NER pathway have been shown to act at G4 sites by ChIP-seq³². However, during post-replicative DNA repair, as well as during canonical DNA repair mechanism, G4 structure formation has been treated as the cause of the activation of the repair machinery^{9,10}. Contrary, our data demonstrated that G4 structures targeted by Zuo1 do not lead to genome instability but rather support genome stability by recruiting repair factors to nearby lesions after UV damage (Figs. 2–5 and Supplementary Figs. S3, S4).

In detail, we showed that Zuo1 binding stimulates G4 structure formation (Fig. 2). However, these Zuo1-bound G4 structures did not lead to the recruitment of proteins of the HR or NHEJ machinery (Fig. 4), caused increased GCR rates (Supplementary Fig. S4c) or changed DNA replication fork progression (data not shown). Contrary, our data indicated that G4 structures formed and bound by Zuo1 positively supported the binding of the proteins of the NER machinery and contributed to NER function (Figs. 4, 5). The binding of Zuo1 to G4 structures was essential for NER function given the severe growth defect and UV sensitivity of *zuo1Δ* cells (Figs. 2, 3 and Supplementary Fig. S4d).

The *zuo1Δ* phenotype could be unambiguously linked to the reduced cellular G4 structure levels because both the cellular doubling time and UV sensitivity could be rescued by treating *zuo1Δ* cells with the G4-stabilizer PhenDC₃ (Figs. 3b, 4g). In addition, PhenDC₃ also rescued the recruitment of NER machinery in *zuo1Δ*, as indicated by Rad23 binding (Fig. 4f). These data demonstrated that Zuo1 and G4 structure formation and function are mechanistically related and positively influence NER.

After UV irradiation, we observed an enrichment in G4 structure formation compared with wildtype (Fig. 5a). We argue that UV-

induced G4 structures are recognized by Zuo1, which stabilizes these structures and facilitates the recruitment of NER proteins. The here presented data indicate that the function of Zuo1 at G4s is direct and not due to Zuo1 blocking the G4 regions against helicase function. Because neither the binding of Pif1 nor Sgs1 helicases are increased in Zuo1 deficient cells (Fig. 3).

These findings are in agreement with recent data showing ZRF1, the human orthologue of Zuo1, directly interacting with the NER machinery^{67,68}. Although the function of ZRF1 is not clear, yet, it is conceivable to expect similarities with Zuo1 in supporting G4 structures and NER recruitment. Indeed, it has been shown that *zuo1Δ* growth defect can be rescued by expressing the human orthologue ZRF1⁶⁹. Interestingly, the NER complex component Mms1 (DDB1 in human) can bind to G4 structures⁵⁸, further underlining the importance of G4 formation for NER function.

In Fig. 3 we showed that not only the *zuo1Δ* growth defect was rescued by the re-stabilization of G4 structures by PhenDC₃, but also that the binding of Sgs1 was again detectable upon G4 structure stabilization. This indicated that also Sgs1 binding to G4 structures is dependent on Zuo1 function at G4 structures. Sgs1 is a multifunctional helicase that belongs to the RecQ helicase family, which function is tightly connected to genome stability (reviewed in⁷⁰). Defects in Sgs1 have been shown to be linked to defects in HR. Recently, it was shown that RecQ helicases also support NER in a so far unknown manner^{71–75}. Sgs1 also interacts with the NER protein Rad16⁷⁶. Combining these findings with our data (Fig. 3) we conclude that Sgs1 is recruited to Zuo1 target regions because of the presence of G4 structures. Without Zuo1, fewer G4 structures form (Fig. 2) and consequently the need for Sgs1-binding and function is reduced. Further analyzes are required to address the question of which function Sgs1 has at G4 sites during NER. A likely scenario is that Sgs1 unfolds G4 structures after NER has repaired the lesion.

In summary, our data lead to a model in which G4 structures have a positive effect on DNA repair (Fig. 6). We propose that, upon UV damage, Zuo1 is recruited at lesion sites by the formation of G4 structures. This results in the stabilization of the G4 structures in the vicinity of this lesion. This G4 stabilization stimulates the binding of the NER machinery, which results in efficient repair. Without Zuo1, less G4 structures form and the binding of NER proteins is reduced (Fig. 4). We draw the conclusion that, in the absence of Zuo1, NER is still acting at such sites but less efficiently, because *zuo1Δ* cells were UV sensitive and no other repair pathway was upregulated in *zuo1Δ*. The binding and function of NER components at G4 sites in *zuo1Δ* was underlined by the finding that without NER more G4 structures formed (Fig. 5), which in turn suggested that the NER machinery itself was involved in G4 structure unwinding. A potential candidate for this unwinding could be Sgs1 (Fig. 3). In the absence of Zuo1 and without an intact NER machinery (double deletion of *zuo1Δ* and *rad4Δ*) cells grew similar to wildtype and were no longer as UV sensitive (Fig. 5). This rescue of UV sensitivity can be explained by our finding that Rev1, the major protein involved in TLS, bound to Zuo1 target regions and compensated for the loss of Zuo1 and Rad4, most likely by repairing the lesion by TLS (Fig. 5). Rev1 bound also to G4 structures because in *zuo1Δ rad4Δ* cells more G4 structures formed in comparison to wildtype and both single mutants (Fig. 5e). This indicated that Zuo1 is not only a signal for NER but also prevents TLS at these sites. Furthermore, our findings demonstrate that G4 structures in the cell are important to assist the choice of DNA repair pathway in the vicinity of G4 structures.

Methods

Strains, constructs, and media. All yeast strains are listed in Supplementary Table S2. All the strains used in this work are derivatives of the *RAD5+* version of

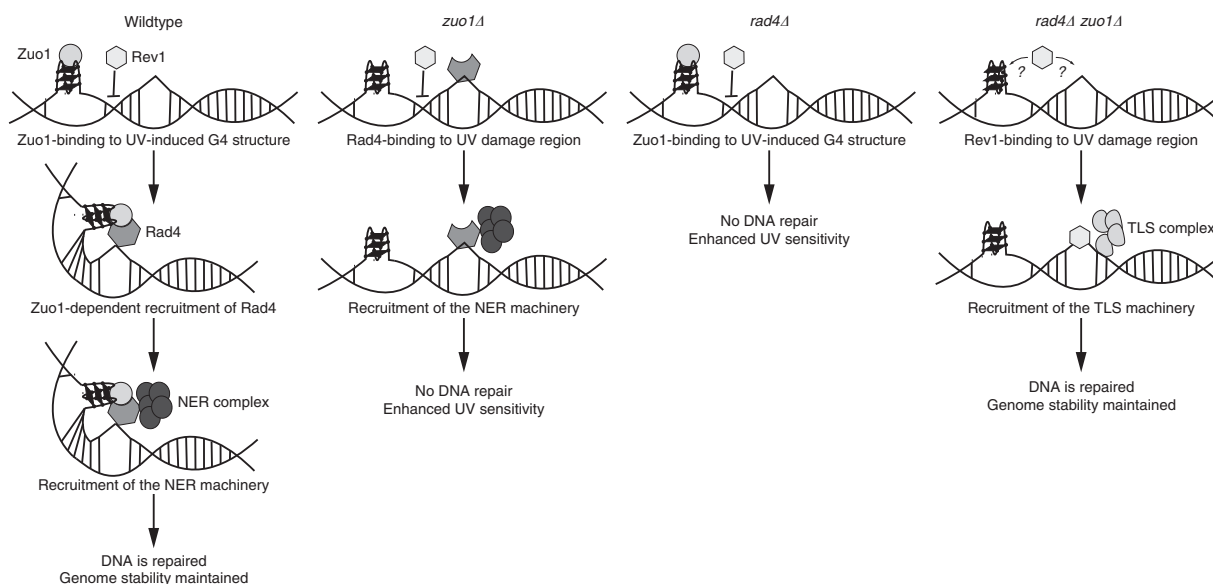


Fig. 6 Illustration of Zuo1 function in G4 structure recognition, stabilization of DNA damage sites and the recruitment of the NER machinery. In detail, UV exposure induces thymine dimer formation in the double helix. As a consequence, more G4 structures are formed that are supported by Zuo1 in the vicinity of the lesion. This stabilization stimulates the binding of the Rad4/23 complex. In the meantime, Zuo1 blocks the binding of Rev1 to those sites. The Rad4/23 complex recruits the NER machinery to repair the lesion and restore the double helix. Without Zuo1, G4 structures are not protected and cells are UV sensitive and the NER machinery is not recruited to the UV lesion. Only in the absence of both Zuo1 and a functional NER machinery an alternative pathway (TLS) is free to bind to these sites and repair the lesion.

W303 (R. Rothstein) or YPH background⁷⁷. Deletions eliminated entire ORFs and were created using the pRS vector system⁷⁷. Tagging at the endogenous locus with 13 Myc epitopes was performed by PCR using the pFA6A vector system⁷⁸. Tagged proteins were expressed from endogenous loci and promoters. The *pif1-m2* point mutation was created by the pop-in/pop-out method using the pRS vector system⁴⁶.

Yeast one-hybrid screen. The yeast one-hybrid screens were performed using the Matchmaker™ Gold Yeast One-Hybrid Library Screening System (Clontech). A G4 motif from chromosome IX ($G4_{IX}$) with short flanking regions was cloned into the *S. cerevisiae* Y1HGold genome as described in the manual to construct the screening bait G4 strain. The control bait $G4_{mut}$ was cloned using the same strategy. After determination of the minimal inhibitory concentration of Aureobasidin A (Aba), screens were performed using the *S. cerevisiae* DUALhybrid cDNA library (Dualsystems Biotech). 7 μ g cDNA library plasmid were transformed into the screening strain bait-G4 according to the manufacturer's protocol. After streaking out each yeast colony twice on selective plates the library plasmids were isolated from overnight cultures. Lysis was performed using DNA lysis buffer (2% (v/v) Triton X-100, 1% (w/v) SDS, 100 mM NaCl, 10 mM Tris HCl pH 8.0, 1 mM EDTA) and glass beads in a FastPrep instrument (MP Biomedicals™ FastPrep-24™) for 1 min at 4 °C, followed by phenol-chloroform extraction and ethanol precipitation. Plasmids were transformed in *E. coli* (XL-1 Blue) and overnight cultures were used to isolate plasmids by alkaline lysis. The obtained library plasmid was sent for sequencing using the primer GAL4ADseq (sequence from Dualsystems Biotech): 5'-ACCACTACAATGGATGATG-3'.

Cloning, expression, and purification of Zuo1. *Zuo1* was amplified by PCR from *S. cerevisiae* genomic DNA using these primers:

SG117 (5'-AAAAAgaattcATGTTTCTTTACCTACCCTAAC-3'),

SG118 (5'-AAAAAagcggcgcTCACACGAAGTAGGACAACAAG-3').

Zuo1 was cloned into the *EcoRI* and *NotI* sites of a pET28a vector (Novagen). The resulting construct was confirmed by sequencing. 6 x His-tagged *Zuo1* was expressed in Rosetta pLysS cells grown in LB medium supplemented with 25 μ g/ml kanamycin (Applichem) and 30 μ g ml⁻¹ chloramphenicol (Applichem), using 1 mM isopropyl β -D-thiogalactoside (IPTG, Applichem) for induction at 18 °C overnight, following the manufacturer's protocol and established protocols⁷⁹.

All purification steps were carried out at 4 °C. Cell lysis was performed in lysis buffer (300 mM NaCl, 20 mM HEPES pH 7.5, 10% (v/v) glycerol, 1 mM DTT, 5 mM imidazole) using an EmulsiFlex-C5 homogenizer (Avestin). The supernatant of centrifuged cell lysate was applied onto a Ni-NTA agarose column (Thermo Scientific) pre-equilibrated with lysis buffer by gravity flow. After three washing steps with 1 column volume wash buffer (300 mM NaCl, 20 mM HEPES pH 7.5, 10% (v/v) glycerol, 1 mM DTT, 15 mM imidazole) bound protein was eluted with elution buffer (300 mM NaCl, 20 mM HEPES pH 7.5, 10% (v/v) glycerol, 1 mM

DTT, 250 mM imidazole). Zuo1-containing fractions were identified by 15% SDS-PAGE and western blotting with an anti-His antibody. Buffer of combined fractions was exchanged to lysis buffer without imidazole and the protein was concentrated using an Amicon Ultra-15 Centrifugal Filter Unit (MWCO 30 kDa). The protein concentration was measured by a Bradford assay and also determined by SDS-PAGE in comparison to known amounts of bovine serum albumin (BSA, Applichem) as a standard protein.

The concentrated Zuo1-containing sample was subjected to a Superdex 200 (GE Healthcare) column and eluted with buffer (300 mM NaCl, 20 mM HEPES pH 7.5, 10% (v/v) glycerol, 1 mM DTT). BSA and aldolase were used as standard proteins for gel filtration.

In vitro folding and analysis of G4 structures. Oligodeoxynucleotides with a G4 motif were dissolved in buffer containing 100 mM KCl. After boiling G4 formation was induced by slowly reducing the temperature to room temperature⁸⁰. G4 structure formation was confirmed by 7% SDS-PAGE and CD measurements. Oligodeoxynucleotides for control DNA structures⁸¹ were treated likewise (Supplementary Table S3). Annealing was performed in annealing buffer (50 mM HEPES, 2 mM magnesium acetate, 100 mM potassium acetate) for 1 min at 98 °C, 60 min at 37 °C and 30 min at 22 °C. G4 structures and annealed control DNA structures for binding studies were desalted using illustra MicroSpin G-25 columns (GE Healthcare).

Binding studies. 20 pmol DNA was 5'-labeled with 25 μ Ci [γ -³²P] ATP using T4 polynucleotide kinase (NEB). G4 and G4mut structures were purified by 7% SDS-PAGE. Control DNA (ds, bubble, fork, 4 fork) was purified using illustra MicroSpin G-25 columns. DNA-protein-binding was analyzed by double-filter binding assays⁸² using a 96-well Bio-Dot SF apparatus (Bio-Rad) and 10 nM DNA in binding buffer (50 mM Tris HCl pH 8.0, 125 mM KCl, 5 mM DTT, 10% (v/v) glycerol)⁸¹. Protein concentrations increased from 0 to 20 μ M Zuo1. After incubation on ice for 30 min the reactions were filtered through a nitrocellulose and a positively charged nylon membrane, followed by three washing steps with binding buffer with no glycerol. The membranes were dried and analyzed by phosphorimaging on a Typhoon FLA 7000 (GE Healthcare). Percentage values of bound Zuo1 were determined using ImageQuant and were used to obtain dissociation equilibrium constants (apparent K_d) by curve fitting using nonlinear regression (Prism, Graphpad). The sequences of oligonucleotides used in these studies are listed in Supplementary Table S3.

Circular dichroism (CD) spectroscopy. CD spectra were recorded on a Jasco J-810 spectropolarimeter at 20 °C and data averaged over three scans⁵⁸. Oligos were dissolved in 100 mM KCl, 10 mM Tris HCl pH 7.0 buffer and annealed overnight after denaturation at 95 °C, 5 min. $G4_{IX}$ for CD titration was dissolved in 100 mM NaCl and 10 mM Tris HCl pH 7.0 buffer, heated at 95 °C for 5 min and quickly annealed on ice. Zuo1 was titrated against 2 μ M DNA at 1, 2.5, and 5 Zuo1:

G4 molar ratios and spectra were recorded after 30 min incubation on ice. Oligonucleotide extinction coefficients were obtained by the nearest-neighbor method and concentration determined at 95 °C. Zuo1 concentration was determined using $\epsilon_{280} = 4.641 \times 10^4 \text{ M}^{-1} \text{ cm}^{-1}$.

Myc-ChIP. Myc-ChIP experiments were performed similar to previous published protocols⁹. Briefly, cells were lysed using glass beads in a Fastprep-24 and the chromatin was sheared to 200–1000 bp using a Bioruptor[®] Pico (Diagenode) with these settings: high intensity, 30 s ON, 30 s OFF, 7 cycles. Shearing quality was assessed on a 1% agarose gel. 8 μg anti-Myc antibody (Takara) was added to the sheared chromatin and incubated for 2 h at 4 °C followed by an incubation with 80 μl Dynabeads-Protein G (Thermo Scientific) for 2 h at 4 °C. After washing three times with washing buffer (100 mM KCl, 0.1% (w/v) Tween-20, 1 mM Tris HCl pH 7.5) the bound DNA was immunoprecipitated and analyzed by quantitative PCR (qPCR) using primers indicated in Supplementary Table S1.

BG4-ChIP. Cells were crosslinked and lysed and DNA was sheared similar to the Myc-ChIP protocol. 0.5 μg of BG4 antibody was added to 1 μg of sheared chromatin (resuspended in ChIP lysis buffer containing 1% (w/v) BSA) and incubated for 2 h at 16 °C followed by incubation with 40 μl FLAG M2 Magnetic Beads (Sigma) for 2 h at 16 °C. Beads were washed three times with washing buffer (100 mM KCl, 0.1% (w/v) Tween-20, 1 mM Tris HCl pH 7.5). Immunoprecipitated DNA was treated with Proteinase K for 1 h at 37 °C and the crosslink was reversed at 65 °C for 2 min followed by overnight incubation at 16 °C.

Immunoprecipitated DNA was purified (PCR purification kit, Qiagen) and used for subsequent qPCR analyses. qPCR was performed using the iTaq Universal SYBR Green Supermix (BioRad). Fold enrichment of binding regions was quantified using the IP/Input method normalized to non-specific binding values. Microsoft Excel was used to plot the graphs and *p* values were calculated using Student's *t*-test.

ChIP-seq analysis. Myc-ChIP experiments were performed as described above. For genome-wide sequencing DNA was treated according to manufacturer's instructions (Next ChIP-seq Library Prep Master Mix Set for Illumina, NEB) and submitted to deep sequencing (HiSeq 2500 sequencer). Obtained sequence reads were aligned to the yeast reference genome (sacCer3) with bowtie⁸³. Binding regions were identified by using MACS 2.0 with default settings for narrow peaks⁸⁴. Supplementary Data 1 contains all obtained Zuo1 peaks. The ChIP input was used as a control data set. Overlap of binding sites with other genomic features and binding regions were determined using a PERL script based on a permutation analysis between the query and subject features.

Growth assay. The strains used for growth assays are listed in Supplementary Table S2. Overnight cultures of *S. cerevisiae* strains were inoculated in YPD media to a starting OD (660 nm) of 0.1. Cultures were grown at 30 °C until an OD (660 nm) ≥ 1 was reached. Measurements were taken at 60 min intervals and doubling times were calculated from log phase OD (660 nm) values. Growth curves were performed in triplicates.

Spot assay. Yeast cultures were inoculated at OD (660 nm) of 0.15 using stationary *S. cerevisiae* culture and grown at 30 °C until OD (660 nm) 0.8 was reached. All yeast cultures were diluted to OD (660 nm) 0.8 and dilution series with six 1:5 dilutions were prepared in a 96-well plate. From each dilution, 3 μl were spotted on a plate and, after drying, incubated at 30 °C. After 2 days the plates were scanned and the growth of strains on different media was compared with estimate the growth defects. 10 μM PhenDC₃, 20 ng/ml Bleomycin (Calbiochem), or 100 mM HU (Sigma) was added to the medium to perform growth assays under G4-stabilizing and DNA damage conditions.

BG4 purification. The plasmid expressing an engineered antibody specific to G4 structures (BG4)⁴³ was kindly provided by S. Balasubramanian (University of Cambridge, UK). The plasmid was transformed into BL21(DE3) competent cells. Competent cells containing the plasmid were grown in 2XTY media (1.6% (w/v) bacto tryptone, 1% (w/v) bacto yeast extract and 0.5% (w/v) NaCl) and 50 $\mu\text{g ml}^{-1}$ kanamycin. Pre-culture was expanded in eight $\times 250 \text{ ml}$ at OD (600 nm) of 0.1. At OD (600 nm) of 0.5 BG4 antibody expression was induced with 0.5 mM IPTG (isopropyl β -D-1-thiogalactopyranoside) at 25 °C for 16 h. The cells were lysed in TES buffer (50 mM Tris-Cl pH 8.0, 1 mM EDTA and 20% sucrose) on ice for 10 min. The lysate was diluted fivefold in water and left on ice for further 10 min prior to centrifugation at 10,000 g at 4 °C for 30 min. The supernatant was filtered (0.2 μm) and purified on a Ni-NTA agarose (Thermo Scientific) column pre-equilibrated with TES buffer by gravity flow. The column was washed with PBS pH 8.0 containing 10 mM imidazole and BG4 antibody was eluted in PBS pH 8.0 containing 250 mM imidazole (pH was adjusted after imidazole addition). Imidazole-containing PBS was exchanged with inner cell salt buffer (25 mM Hepes (pH 7.6), 110 mM KCl, 10.5 mM NaCl, 1 mM MgCl₂). BG4 antibody was concentrated using an Amicon Ultra-15 Centrifugal Filter Unit (Millipore). BG4 antibody was quantified on a NanoDrop spectrophotometer

(Thermo Scientific) and stored at $-80 \text{ }^\circ\text{C}$. Purity of the BG4 preparation was monitored by SDS-PAGE.

BG4 filter binding assay. Asynchronous cultures were grown to OD (660 nm) of 0.6 and crosslinked with 1% (v/v) formaldehyde for 10 min followed by quenching the crosslinking by the addition of 125 mM glycine. Genomic DNA extraction was performed using a MasterPure Yeast DNA Purification Kit (Epicenter). Starting with 2 μg , twofold serial dilution of the gDNA were prepared and spotted on a nylon membrane pre-equilibrated with PBS. After two washes with PBS the membrane was cross-linked in a UV-crosslinker (254 nm) at 120 J m^{-2} for 10–15 s. After blocking (2% (w/v) BSA in PBS) the membrane was incubated with 2 $\mu\text{g/ml}$ BG4 for 2 h at RT in agitation. Three washes with 0.1% (w/v) Tween in PBS were followed by 1 h incubation with 1:800 FLAG-Tag Antibody (Cell Signaling). Three washes with 0.1% (w/v) Tween/PBS were followed by 1 h incubation with 1:5000 Anti-HRP antibody (Santa Cruz). All antibodies were diluted in Blocking Buffer. The membrane was scanned by a ChemiDoc™ Gel Imaging System (BioRad)

Gross chromosomal rearrangement assay. The GCR assay was performed according to a published protocol²². Briefly, seven yeast cultures per GCR strain were grown at 30 °C for 48 h to saturation. 1×10^{-7} cells diluted in water were plated on reference (YPD) or selective plates (drop-out medium lacking uracil and arginine (US Biologicals) supplemented with 1 g l^{-1} 5-FOA and 60 mg l^{-1} canavanine sulfate (FOA + Can)). After incubation for 4 days colony formation was counted. GCR clones are colonies that grew on selective plates. GCR rate was calculated using the FALCOR web server and MMS maximum likelihood method.

γ H2AX western blot. Asynchronous cultures were grown to an OD (660 nm) of 0.6 and collected by centrifugation. Proteins were extracted by standard TCA purification and separated by SDS PAGE and transferred on a membrane. Western Blot analysis was performed with an antibody directed against γ H2AX (Abcam) and Act1 (Santa Cruz Biotechnology). Proteins were detected using an enhanced chemiluminescence system (GE healthcare) and visualized with a Gel Doc XR + system (Bio-Rad). The pictures were quantified using ImageJ.

Statistical analyses. Significance was calculated based on one-sided Student's *t*-test. Asterisks* indicate statistical significance in comparison with wildtype cells: **p* < 0.05, ***p* < 0.01, ****p* < 0.001, *****p* < 0.0001. Plotted results were based on the average of *N* = 3 biologically independent experiments.

Reporting summary. Further information on research design is available in the Nature Research Reporting Summary linked to this article.

Data availability

ChIP-seq data have been deposited in the National Center for Biotechnology Information (NCBI) Sequencing Read Archive under the accession number GSE149502. Additionally, Supplementary Data 2 lists all peaks of the ChIP-seq analysis and Supplementary Data 3 lists all genes that were up- or down-regulated at the microarray analysis. All data is available from the authors upon reasonable request.

Received: 6 November 2019; Accepted: 14 July 2020;

Published online: 06 August 2020

References

- Gellert, M., Lipsett, M. N. & Davies, D. R. Helix formation by guanylic acid. *Proc. Natl Acad. Sci. USA* **48**, 2013–2018 (1962).
- Sen, D. & Gilbert, W. Formation of parallel four-stranded complexes by guanine-rich motifs in DNA and its implications for meiosis. *Nature* **334**, 364–366 (1988).
- Spiegel, J., Adhikari, S. & Balasubramanian, S. The structure and function of DNA G-quadruplexes. *Trends Chem.* **2**, 123–136 (2019).
- Capra, J. A., Paeschke, K., Singh, M., Zakian, V. A. & G-quadruplex, D. N. A. sequences are evolutionarily conserved and associated with distinct genomic features in *Saccharomyces cerevisiae*. *PLoS Comput. Biol.* **6**, 9 (2010).
- Hershman, S. G. et al. Genomic distribution and functional analyses of potential G-quadruplex-forming sequences in *Saccharomyces cerevisiae*. *Nucleic Acids Res.* **36**, 144–156 (2008).
- Chambers, V. S. et al. High-throughput sequencing of DNA G-quadruplex structures in the human genome. *Nat. Biotechnol.* **33**, 877–881 (2015).
- Rhodes, D. & Lipps, H. J. Survey and summary G-quadruplexes and their regulatory roles in biology. *Nucleic Acids Res.* **43**, 8627–8637 (2015).
- Sauer, M. & Paeschke, K. G-quadruplex unwinding helicases and their function in vivo. *Biochem. Soc. Trans.* **45**, 1173–1182 (2017).

9. Paeschke, K., Capra, J. A. & Zakian, V. A. DNA Replication through G-quadruplex motifs is promoted by the *Saccharomyces cerevisiae* Pif1 DNA helicase. *Cell* **145**, 678–691 (2011).
10. Sabouri, N., Capra, J. A. & Zakian, V. A. The essential *Schizosaccharomyces pombe* Pfh1 DNA helicase promotes fork movement past G-quadruplex motifs to prevent DNA damage. *BMC Biol.* **12**, 101 (2014).
11. Müller, S., Kumari, S., Rodriguez, R. & Balasubramanian, S. Small-molecule-mediated G-quadruplex isolation from human cells. *Nat. Chem.* **10**, 1095–1098 (2010).
12. London, T. B. C. et al. FANCF is a structure-specific DNA helicase associated with the maintenance of genomic G/C tracts. *J. Biol. Chem.* **283**, 6132–6139 (2008).
13. Ribeyre, C. et al. The yeast Pif1 helicase prevents genomic instability caused by G-quadruplex-forming CEB1 sequences in vivo. *PLoS Genet.* **e1000475** (2009).
14. Wang, Y. et al. G-quadruplex DNA drives genomic instability and represents a targetable molecular abnormality in ATRX-deficient malignant glioma. *Nat. Commun.* **10**, 943 (2019).
15. Hänsel-Hertsch, R. et al. G-quadruplex structures mark human regulatory chromatin. *Nat. Genet.* **48**, 1267–1272 (2016).
16. De, S. & Michor, F. DNA secondary structures and epigenetic determinants of cancer genome evolution. *Nat. Struct. Mol. Biol.* **18**, 950–955 (2011).
17. Marsico, G. et al. Whole genome experimental maps of DNA G-quadruplexes in multiple species. *Nucleic Acids Res.* **47**, 3862–3874 (2019).
18. Katapadi, V. K., Nambiar, M. & Raghavan, S. C. Potential G-quadruplex formation at breakpoint regions of chromosomal translocations in cancer may explain their fragility. *Genomics.* **100**, 72–80 (2012).
19. Van Wietmarschen, N. et al. BLM helicase suppresses recombination at G-quadruplex motifs in transcribed genes. *Nat. Commun.* **9**, 1–12 (2018).
20. Cheung, I., Schertzer, M., Rose, A. & Lansdorp, P. M. Disruption of dog-1 in *Caenorhabditis elegans* triggers deletions upstream of guanine-rich DNA. *Nat. Genet.* **31**, 405–409 (2002).
21. Kruijselbrink, E. et al. Mutagenic capacity of endogenous G4 DNA underlies genome instability in FANCF-defective *C. elegans*. *Curr. Biol.* **18**, 900–905 (2008).
22. Paeschke, K. et al. Pif1 family helicases suppress genome instability at G-quadruplex motifs. *Nature.* **497**, 458–462 (2013).
23. Piazza, A. et al. Genetic instability triggered by G-quadruplex interacting Phen-DC compounds in *Saccharomyces cerevisiae*. *Nucleic Acids Res.* **38**, 4337–4348 (2010).
24. Wu, Y., Shin-ya, K. & Brosh, R. M. FANCF helicase defective in fanconi anemia and breast cancer unwinds G-quadruplex DNA to defend genomic stability. *Mol. Cell Biol.* **28**, 4116–4128 (2008).
25. Ward, J. D., Barber, L. J., Petalcorin, M. I. R., Yanowitz, J. & Boulton, S. J. Replication blocking lesions present a unique substrate for homologous recombination. *EMBO J.* **26**, 3384–3396 (2007).
26. Zimmer, J. et al. Targeting BRCA1 and BRCA2 deficiencies with G-quadruplex-interacting compounds. *Mol. Cell* **61**, 449–460 (2016).
27. Haracska, L., Prakash, S. & Prakash, L. Yeast Rev1 protein is a G templatespecific DNA polymerase. *J. Biol. Chem.* **277**, 15546–15551 (2002).
28. Sarkies, P., Reams, C., Simpson, L. J. & Sale, J. E. Epigenetic instability due to defective replication of structured DNA. *Mol. Cell.* **40**, 703–713 (2010).
29. Schiavone, D. et al. Determinants of G-quadruplex-induced epigenetic instability in REV1-deficient cells. *EMBO J.* **33**, 2507–2520 (2014).
30. Sarkies, P. et al. FANCF coordinates two pathways that maintain epigenetic stability at G-quadruplex DNA. *Nucleic Acids Res.* **40**, 1485–1498 (2012).
31. Koole, W. et al. A polymerase theta-dependent repair pathway suppresses extensive genomic instability at endogenous G4 DNA sites. *Nat. Commun.* **5**, 3216 (2014).
32. Gray, L. T., Vallur, A. C., Eddy, J. & Maizels, N. G-quadruplexes are genomewide targets of transcriptional helicases XPB and XPD. *Nat. Chem. Biol.* **10**, 313–318 (2014).
33. Fleming, A. M., Ding, Y. & Burrows, C. J. Oxidative DNA damage is epigenetic by regulating gene transcription via base excision repair. *Proc. Natl Acad. Sci. USA* **114**, 2604–2609 (2017).
34. Fleming, A. M., Zhu, J., Ding, Y. & Burrows, C. J. Location dependence of the transcriptional response of a potential G-quadruplex in gene promoters under oxidative stress. *Nucleic Acids Res.* **47**, 5049–5060 (2019).
35. Cahoon, L. A. & Seifert, H. S. An alternative DNA structure is necessary for pilin antigenic variation in *Neisseria gonorrhoeae*. *Science.* **325**, 764–767 (2009).
36. Vink, C., Rudenko, G. & Seifert, H. S. Microbial antigenic variation mediated by homologous DNA recombination. *FEMS Microbiol. Rev.* **36**, 917–948 (2012).
37. Karsisiotis, A. I. et al. Topological characterization of nucleic acid G-quadruplexes by UV absorption and circular dichroism. *Angew. Chem. Int. Ed.* **123**, 10833–10836 (2011).
38. Yan, W. et al. Zuo1, a ribosome-associated DnaJ molecular chaperone. *EMBO J.* **17**, 4809–4817 (1998).
39. Albanese, V., Reissmann, S. & Frydman, J. A ribosome-anchored chaperone network that facilitates eukaryotic ribosome biogenesis. *J. Cell Biol.* **189**, 69–81 (2010).
40. Prunuske, A. J., Waltner, J. K., Kuhn, P., Gu, B. & Craig, E. A. Role for the molecular chaperones Zuo1 and Ssz1 in quorum sensing via activation of the transcription factor Pdr1. *Proc. Natl Acad. Sci. USA* **109**, 472–477 (2012).
41. Ducett, J. K. et al. Unfolding of the C-terminal domain of the J-protein zuo1 releases autoinhibition and activates Pdr1-dependent transcription. *J. Mol. Biol.* **425**, 19–31 (2013).
42. Wahba, L., Amon, J. D., Koshland, D. & Vuica-ross, M. Article RNase H and multiple RNA biogenesis factors cooperate to prevent RNA: DNA hybrids from generating genome instability. *Mol. Cell* **44**, 978–988 (2011).
43. Biffi, G., Tannahill, D., McCafferty, J. & Balasubramanian, S. Quantitative visualization of DNA G-quadruplex structures in human cells. *Nat. Chem.* **5**, 182–186 (2013).
44. Hänsel-Hertsch, R., Spiegel, J., Marsico, G., Tannahill, D. & Balasubramanian, S. Genome-wide mapping of endogenous G-quadruplex DNA structures by chromatin immunoprecipitation and high-throughput sequencing. *Nat. Protoc.* **13**, 551–564 (2018).
45. De Cian, A., DeLemos, E., Mergny, J. L., Teulade-Fichou, M. P. & Monchaud, D. Highly efficient G-quadruplex recognition by bisquinolinium compounds. *J. Am. Chem. Soc.* **129**, 1856–1857 (2007).
46. Schulz, V. P. & Zakian, V. A. The *Saccharomyces PIF1* DNA helicase inhibits telomere elongation and de novo telomere formation. *Cell.* **76**, 145–155 (1994).
47. Watt, P. M., Hickson, I. D., Borts, R. H. & Louis, E. J. Sgs1, a homologue of the Blooms and Werner's syndrome genes, is required for maintenance of genome stability in *Saccharomyces cerevisiae*. *Genetics.* **144**, 935–945 (1996).
48. De Magis, A. et al. DNA damage and genome instability by G-quadruplex ligands are mediated by R loops in human cancer cells. *Proc. Natl Acad. Sci. USA* **116**, 816–825 (2019).
49. Rodriguez, R. et al. Small molecule-induced DNA damage identifies alternative DNA structures in human genes. *Nat. Chem.* **8**, 301–310 (2012).
50. Lopes, J. et al. G-quadruplex-induced instability during leading-strand replication. *EMBO J.* **8**, 301–310 (2011).
51. Ciccia, A. & Elledge, S. J. The DNA damage response: making it safe to play with knives. *Molecular Cell.* **30**, 4033–4046 (2010).
52. Prakash, S. & Prakash, L. Nucleotide excision repair in yeast. *Mutat. Res. - Fundamental and Molecular Mechanisms of Mutagenesis.* **451**, 13–24 (2000).
53. Kang, M. S. et al. Yeast RAD2, a homolog of human XPG, plays a key role in the regulation of the cell cycle and actin dynamics. *Biol. Open.* **3**, 29–41 (2014).
54. Schiestl, R. H. & Prakash, S. RAD1, an excision repair gene of *Saccharomyces cerevisiae*, is also involved in recombination. *Mol. Cell Biol.* **8**, 3619–3626 (1988).
55. Watkins, J. F., Sung, P., Prakash, L. & Prakash, S. The *Saccharomyces cerevisiae* DNA repair gene RAD23 encodes a nuclear protein containing a ubiquitin-like domain required for biological function. *Mol. Cell Biol.* **13**, 7757–7765 (1993).
56. Kemp, M. G. & Sancar, A. DNA excision repair: where do all the dimers go? *Cell Cycle.* **11**, 2997–3002 (2012).
57. Nakken, S., Rognes, T. & Hovig, E. The disruptive positions in human G-quadruplex motifs are less polymorphic and more conserved than their neutral counterparts. *Nucleic Acids Res.* **37**, 5749–5756 (2009).
58. Wanzek, K., Schwindt, E., Capra, J. A. & Paeschke, K. Mms1 binds to G-rich regions in *Saccharomyces cerevisiae* and influences replication and genome stability. *Nucleic Acids Res.* **45**, 7796–7806 (2017).
59. Papadopoulou, C., Guilbaud, G., Schiavone, D. & Sale, J. E. Nucleotide pool depletion induces G-quadruplex-dependent perturbation of gene expression. *Cell Rep.* **13**, 2491–2503 (2015).
60. Lemmens, B., Van Schendel, R. & Tijsterman, M. Mutagenic consequences of a single G-quadruplex demonstrate mitotic inheritance of DNA replication fork barriers. *Nat. Commun.* **6**, 8909 (2015).
61. Ding, H. et al. Regulation of murine telomere length by Rtel: an essential gene encoding a helicase-like protein. *Cell.* **117**, 873–886 (2004).
62. Guilbaud, G. et al. Local epigenetic reprogramming induced by G-quadruplex ligands. *Nat. Chem.* **9**, 1110–1117 (2017).
63. Siddiqui-Jain, A., Grand, C. L., Bearrs, D. J. & Hurley, L. H. Direct evidence for a G-quadruplex in a promoter region and its targeting with a small molecule to repress c-MYC transcription. *Proc. Natl Acad. Sci. USA* **99**, 11593–11598 (2002).
64. Besnard, E. et al. Unraveling cell type-specific and reprogrammable human replication origin signatures associated with G-quadruplex consensus motifs. *Nat. Struct. Mol. Biol.* **19**, 837–844 (2012).
65. Paeschke, K., Simonsson, T., Postberg, J., Rhodes, D. & Lipps, H. J. Telomere end-binding proteins control the formation of G-quadruplex DNA structures in vivo. *Nat. Struct. Mol. Biol.* **12**, 847–854 (2005).

66. Estep, K. N., Butler, T. J., Ding, J. & Brosh, R. M. G4-Interacting D. N. A. helicases and polymerases: potential therapeutic targets. *Curr. Med. Chem.* **26**, 2881–2897 (2017).
67. Gracheva, E. et al. ZRF1 mediates remodeling of E3 ligases at DNA lesion sites during nucleotide excision repair. *J. Cell Biol.* **213**, 185–200 (2016).
68. Chitale, S. & Richly, H. DICER and ZRF1 contribute to chromatin decondensation during nucleotide excision repair. *Nucleic Acids Res.* **45**, 5901–5912 (2017).
69. Shrestha, O. K. et al. Structure and evolution of the 4-helix bundle domain of Zuo1n, a J-domain protein co-chaperone of Hsp70. *PLoS ONE* **14**, 1–21 (2019).
70. Larsen, N. B. & Hickson, I. D. RecQ helicases: conserved guardians of genomic integrity. *Adv. Exp. Med. Biol.* **767**, 161–184 (2013).
71. Fan, W. & Luo, J. RecQ4 facilitates UV light-induced DNA damage repair through interaction with nucleotide excision repair factor xeroderma pigmentosum group A (XPA). *J. Biol. Chem.* **283**, 29037–29044 (2008).
72. Choi, D. H. et al. Hrq1 facilitates nucleotide excision repair of DNA damage induced by 4-nitroquinoline-1-oxide and cisplatin in *Saccharomyces cerevisiae*. *J. Microbiol.* **52**, 292–298 (2014).
73. Li, F., Ball, L. G., Fan, L., Hanna, M. & Xiao, W. Sgs1 helicase is required for efficient PCNA monoubiquitination and translesion DNA synthesis in *Saccharomyces cerevisiae*. *Curr. Genet.* **64**, 459–468 (2018).
74. Manuscript, A. Structures, folding patterns, and functions of intramolecular DNA G-quadruplexes found in eukaryotic promoter regions. *Biochimie* **90**, 1149–1171 (2009).
75. Xu, X. et al. Involvement of budding yeast Rad5 in translesion DNA synthesis through physical interaction with Rev1. *Nucleic Acids Res.* **44**, 5231–5245 (2016).
76. Saffi, J., Feldmann, H., Winnacker, E. L. & Henriques, J. A. P. Interaction of the yeast Pso5/Rad16 and Sgs1 proteins: influences on DNA repair and aging. *Mutat. Res. - DNA Repair.* **486**, 195–206 (2001).
77. Sikorski, R. S. & Hieter, P. A system of shuttle vectors and yeast host strains designed for efficient manipulation of DNA in *Saccharomyces cerevisiae*. *Genetics.* **122**, 19–27 (1989).
78. Van Driessche, B., Tafforeau, L., Hentges, P., Carr, A. M. & Vandenhoute, J. Additional vectors for PCR-based gene tagging in *Saccharomyces cerevisiae* and *Schizosaccharomyces pombe* using nourseothricin resistance. *Yeast.* **22**, 1061–1068 (2005).
79. Sambrook J., E. F. Fritsch, T. M. Molecular cloning: a laboratory manual/J. Sambrook, E. F. Fritsch, T. Maniatis. Version details Trove. (New York: Cold Spring Harbor Laboratory Press, 1989).
80. Giraldo, R. & Rhodes, D. The yeast telomere-binding protein RAP1 binds to and promotes the formation of DNA quadruplexes in telomeric DNA. *EMBO J.* **13**, 2411–2420 (1994).
81. Dempsey, L. A., Sun, H., Hanakahi, L. A. & Maizels, N. G4 DNA binding by LRI and its subunits, nucleolin and hnRNP D, a role for G-G pairing in immunoglobulin switch recombination. *J. Biol. Chem.* **274**, 1066–1071 (1999).
82. Haeusler, A. R. et al. C9orf72 nucleotide repeat structures initiate molecular cascades of disease. *Nature* **507**, 195–200 (2014).
83. Langmead, B., Trapnell, C., Pop, M. & Salzberg, S. L. Ultrafast and memory-efficient alignment of short DNA sequences to the human genome. *Genome Biol.* **10**, R25 (2009).
84. Zhang, Y. et al. Model-based analysis of ChIP-Seq (MACS). *Genome Biol.* **9**, R137 (2008).

Acknowledgements

We thank Wesley Browne (University of Groningen) for his help with circular dichroic measurements; Diana Spierings and Nancy Halsema for support with ChIP-seq analysis; Katharina Wanzek, Theresa Zacheja, and Eike Schwindt for providing strains; Hinke Kazemier and Michaela Limmer for experimental support; Markus Sauer for careful reading of the manuscript. Research in the Paeschke laboratory is funded by an ERC Stg Grant (638988-G4DSB) as well as the Deutsche Forschungsgemeinschaft (DFG, German Research Foundation) under Germany's Excellence Strategy—EXC2151–390873048. Open access funding provided by Projekt DEAL.

Author contributions

Conceptualization, K.P.; Methodology, A.D.M., S.G., E.F.S., S.A.J., M.H.; Data analysis, A.D.M., S.G., S.A.J., M.C., M.H.; Writing—Original draft, S.G., A.D.M., S.A.J., K.P.; Writing—Review and editing, A.D.M., S.A.J., K.P.; Funding acquisition, K.P.; Resources, K.P.; Supervision, K.P.

Competing interests

The authors declare no competing interests.

Additional information

Supplementary information is available for this paper at <https://doi.org/10.1038/s41467-020-17701-8>.

Correspondence and requests for materials should be addressed to K.P.

Peer review information *Nature Communications* thanks Marco Di Antonio and the other anonymous reviewer(s) for their contribution to the peer review of this work. Peer reviewer reports are available.

Reprints and permission information is available at <http://www.nature.com/reprints>

Publisher's note Springer Nature remains neutral with regard to jurisdictional claims in published maps and institutional affiliations.



Open Access This article is licensed under a Creative Commons Attribution 4.0 International License, which permits use, sharing, adaptation, distribution and reproduction in any medium or format, as long as you give appropriate credit to the original author(s) and the source, provide a link to the Creative Commons license, and indicate if changes were made. The images or other third party material in this article are included in the article's Creative Commons license, unless indicated otherwise in a credit line to the material. If material is not included in the article's Creative Commons license and your intended use is not permitted by statutory regulation or exceeds the permitted use, you will need to obtain permission directly from the copyright holder. To view a copy of this license, visit <http://creativecommons.org/licenses/by/4.0/>.


© The Author(s) 2020

RESEARCH ARTICLE

Open Access



Telomerase subunit Est2 marks internal sites that are prone to accumulate DNA damage

Satyaprakash Pandey^{1†}, Mona Hajikazemi^{2†}, Theresa Zacheja², Stephanie Schalbetter³, Matthew J. Neale³, Jonathan Baxter³, Victor Guryev¹, Andreas Hofmann⁴, Dieter W. Heermann⁴, Stefan A. Juranek^{2*} and Katrin Paeschke^{1,2*} 

Abstract

Background: The main function of telomerase is at the telomeres but under adverse conditions telomerase can bind to internal regions causing deleterious effects as observed in cancer cells.

Results: By mapping the global occupancy of the catalytic subunit of telomerase (Est2) in the budding yeast *Saccharomyces cerevisiae*, we reveal that it binds to multiple guanine-rich genomic loci, which we termed “non-telomeric binding sites” (NTBS). We characterize Est2 binding to NTBS. Contrary to telomeres, Est2 binds to NTBS in G1 and G2 phase independently of Est1 and Est3. The absence of Est1 and Est3 renders telomerase inactive at NTBS. However, upon global DNA damage, Est1 and Est3 join Est2 at NTBS and telomere addition can be observed indicating that Est2 occupancy marks NTBS regions as particular risks for genome stability.

Conclusions: Our results provide a novel model of telomerase regulation in the cell cycle using internal regions as “parking spots” of Est2 but marking them as hotspots for telomere addition.

Keywords: DNA damage, Genome stability, Telomerase, Yeast

Background

Telomeres are multi-protein complexes at the ends of eukaryotic chromosomes. A major function of telomeres is to protect the integrity of the genome. The length of the telomeres is critical for survival as shortening of telomeres leads to senescence and eventually cell death [1]. Telomerase, a highly specialized reverse transcriptase, is responsible for maintaining telomere homeostasis using an intrinsic RNA subunit as a template [2]. Telomerase

upregulation is a characteristic signature for cancer cells and genome instability [3]. Telomere structure, function, and maintenance *via* telomerase are conserved throughout eukaryotes [4]. In *Saccharomyces cerevisiae*, telomerase is composed of three proteins, Est1, Est2, Est3, and an RNA subunit, TLC1. The catalytic subunit of telomerase, Est2, is expressed throughout the cell cycle and associates with telomeric regions primarily during late S-phase [5]. Two different pathways recruit telomerase to the telomeres in G1 and S/G2 phase. In G1 phase yKu heterodimer (Ku70, Ku80) interacts with Sir4 and binds to TLC1. This is a prerequisite for the Est2-TLC1 interaction and accumulations of telomerase at telomeres. However, telomerase is devoid of Est1 and Est3 in G1 phase and remains inactive. In S/G2 phase, Cdc13 recruits Est1, which in turns allows the recruitment of

* Correspondence: stefan.juranek@ukbonn.de; katrin.paeschke@ukbonn.de

[†]Satyaprakash Pandey and Mona Hajikazemi contributed equally to this work and shared first authorship.

²Clinic of Internal Medicine III, Oncology, Hematology, Rheumatology and Clinical Immunology, University Hospital Bonn, Bonn, Germany

¹University of Groningen, University Medical Center Groningen, European Research Institute for the Biology of Ageing, 9713 AV Groningen, Netherlands

Full list of author information is available at the end of the article



© The Author(s). 2021 **Open Access** This article is licensed under a Creative Commons Attribution 4.0 International License, which permits use, sharing, adaptation, distribution and reproduction in any medium or format, as long as you give appropriate credit to the original author(s) and the source, provide a link to the Creative Commons licence, and indicate if changes were made. The images or other third party material in this article are included in the article's Creative Commons licence, unless indicated otherwise in a credit line to the material. If material is not included in the article's Creative Commons licence and your intended use is not permitted by statutory regulation or exceeds the permitted use, you will need to obtain permission directly from the copyright holder. To view a copy of this licence, visit <http://creativecommons.org/licenses/by/4.0/>. The Creative Commons Public Domain Dedication waiver (<http://creativecommons.org/publicdomain/zero/1.0/>) applies to the data made available in this article, unless otherwise stated in a credit line to the data.

Est3. Est1 is required for full activation of telomerase [6–10]. Multiple unbiased approaches have yielded a list of proteins involved in regulating telomerase function, but the mechanisms that recruit and activate telomerase are still not completely known [5, 11–13].

Genome stability is constantly challenged and efficient repair mechanisms are essential to maintain genome integrity [14–16]. Defects in the repair pathways result in increased genome instability caused by deletions, mutations, end-to-end fusions, translocation, and de novo telomere addition at internal sites [14]. De novo telomere addition by telomerase at DNA double-strand breaks (DSB) is hazardous for the cell, because all genetic information distal to the DSB is lost [16–19]. Studies in yeast and human suggest that telomerase components are not associated with the telomere throughout the cell cycle and the catalytic subunit of telomerase itself or associated proteins perform a function at internal regions [8, 20–27]. For example, single-molecule image tracking of human telomerase revealed a three-dimensional diffusion model wherein telomerase makes multiple transient and stable contacts with telomeres during different cell cycle phases [8, 27]. Multiple interactions can be observed throughout S phase before telomerase binds to the 3' overhang of the chromosome ends [27]. Microscopic imaging in yeast demonstrated that TLC1 segregates to different cellular locations during different cell cycle stages to prevent de novo telomere addition [24]. Single molecule imaging showed that TLC1 remains in the nucleoplasm in G1/S phase and the nucleolus in G2/M phase. This segregation is lost under DNA damage conditions in *rad52Δ* cells in which TLC1 localizes at DSBs and leads to de novo telomere addition. Multiple proteins such as Pif1, Cdc13, and the SUMO ligase Siz1 are involved in regulating telomerase action at DSBs [24–26, 28–31]. Additionally, genomic sequencing of bleomycin-treated yeast cells revealed additional regions where telomere addition occurs in the genome [24]. Specific subsets of genomic sequences termed as sites of repair-associated telomere addition (SIRTAs) have been identified where de novo telomere addition occurs upon a DSB [25]. Genetic assays using an HO endonuclease system demonstrated that de novo telomere addition at these sites depends on Cdc13 and Rap1 [25]. Although these sites contain a bipartite structure, a global prediction and validation of SIRTAs under different genetic and biochemical conditions is still missing.

Considering these findings, it is essential to reveal whether, when, and where telomerase localizes to specific internal sites and what is the impact of this interaction on genome stability. Here, we provide a comprehensive map of the global occupancy of Est2 within the genome for the first time. Interestingly, Est2

binds to multiple internal genomic loci, termed non-telomere binding sites (NTBS). Using differential cell cycle analysis, we revealed that Est2 binds to NTBS independent of Est1 and Est3 in G1 and G2 phases. In the past, different models have been proposed to explain how telomerase is recruited to the telomeres [25, 27, 29, 32–38]. Using Hi-C analysis, we found that NTBS are in closer proximity to telomeres than expected by random chance, suggesting a potential correlation between chromatin organization and telomerase sequestration in different cell cycle phases. Because Est2 binds independently of other known telomeric factors to NTBS, telomerase is inactive at these sites. However, NTBS regions are prone to DSBs and upon global DNA damage Est2 recruits Est1 and Est3 and active telomerase assembles, resulting in telomere addition at NTBS. We propose a model in which Est2 binds to multiple guanine-rich sites across the genome where it is parked in an inactive form. This renders NTBS a hotspots for telomere addition and genome instability.

Results

Est2 binds to non-telomeric regions within the genome

In order to determine regions of telomerase action within the genome, we monitored the genomic occupancy of Est2 in *S. cerevisiae* using a strain wherein Est2 was internally tagged at its C-terminus with 13 x Myc (Est2-Myc13). Yeast cultures expressing Est2-Myc13 were crosslinked with formaldehyde and subjected to chromatin immunoprecipitation (ChIP). DNA bound to Est2-Myc13 and input DNA were fluorescently labeled and hybridized to a whole-genome DNA microarray (ChIP-chip) (Agilent). The binding sites were identified from the median standardized array values (across biological triplicates) using the ChIPOTle 2.0 program with a significance cut-off of 0.05. The experiment was repeated 5 times and only regions that could be identified in at least three biological replicates were annotated as *bona fide* Est2 targets.

After subtraction of telomeric sequences, Est2 ChIP-chip analysis led to the identification of 978 NTBS (see Additional file 1: Table S1 for a list of NTBS) (Fig. 1A (graphical illustration of regions harboring NTBS) and Additional file 2: Fig. S1A that illustrates Est2 binding peaks of four different regions: NTBS#1-NTBS#4). Bioinformatics analysis revealed that these sequences are significantly more G-rich than the average GC content of the yeast genome (NTBS: 52% GC; yeast genome: 38% GC; p -value < 0.001). MEME motif analysis displayed a characteristic TG-richness, that despite presenting other nucleotides, corresponds the motif of telomeric repeats in yeast (Fig. 1B, E-value = $1.1e^{-69}$). We computationally correlated NTBS peaks to annotated genomic regions (annotated by *S. cerevisiae* genome database (SGD) such

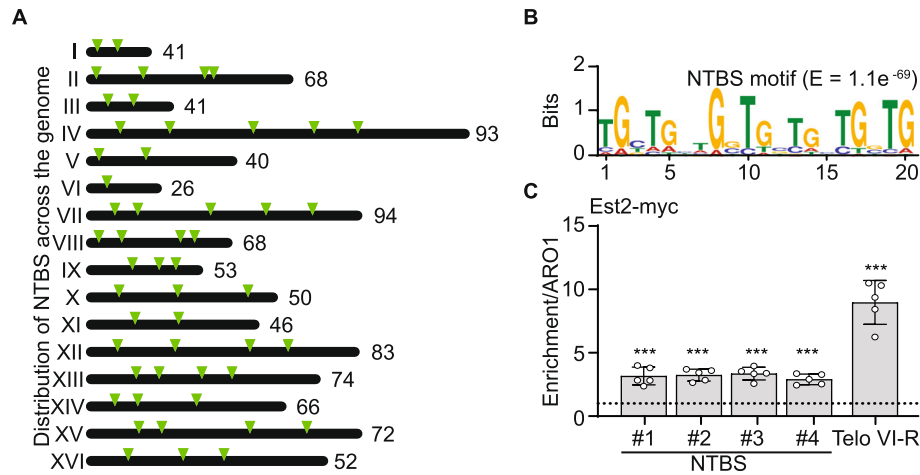


Fig. 1 Global occupancy of Est2 across the yeast genome. **A** The distribution of Est2 occupancy across the *S. cerevisiae* genome. Each triangle represents a non-telomeric binding site (NTBS) of Est2 on a chromosome. All the sites were present in at least 3 out of 5 independent experiments. Note, less triangles are visible on the cartoon because of the resolution of the graphic. Multiple regions that are located at close to each other or as clusters are depicted as one arrow. **B** MEME motif of NTBS regions. The binding sites displayed an enriched TG-richness similar to yeast telomeric regions. (E -value 1.1×10^{-69}) **C** ChIP-qPCR of four different NTBS regions (see Additional file 1: Table S1 for specification of the region). As a positive control, Est2-binding to telomere VI-R was plotted (Telo-VI-R). Reported ChIP values are normalized to input and ARO1 (non-telomeric control). Data are represented as mean \pm standard error mean (SEM) of $n = 5$ biological replicates unless stated otherwise. Statistical significance was compared to ARO1 levels and determined using Student's t -test. ** p -value < 0.01 and *** p -value < 0.001

as autonomously replicating sequence (ARS), promoter) or binding sites of specific proteins. Our analyses showed that NTBS overlap significantly with regions that are also bound by known telomerase regulatory factors: G-quadruplex (G4) regions [39] (35/978 $p < 0.0001$), R-loops [10, 40] (84/978 $p < 0.0001$), and Pif1-binding sites [41] (361/978 $p < 0.0001$). Also these regions are linked to genome instability as indicated that these sites overlap with sites high in DNA polymerase II (DNA Pol II) occupancy—marking regions where DNA replication stalls in wild type [41] (354/978 $p < 0.0001$) and in *pif1-m2* cells (430/978 $p < 0.0001$) [41] as well as sites that are highly linked to DNA damage as indicated by a strong γ -H2A signal [39] (294/978 $p < 0.0001$) (Additional file 2: Fig. S1B-G). In *pif1-m2* no nuclear Pif1 is present, only mitochondrial Pif1 is expressed. Furthermore, correlation analysis revealed that $> 85\%$ of NTBS significantly overlap with open reading frames (ORFs, p -value < 0.001 , of which 56 genes are involved in telomere maintenance and homeostasis (Additional file 3: Table S2). Note, it is not clear to this point if Est2 binding to these ORF is relevant for telomere function or biology.

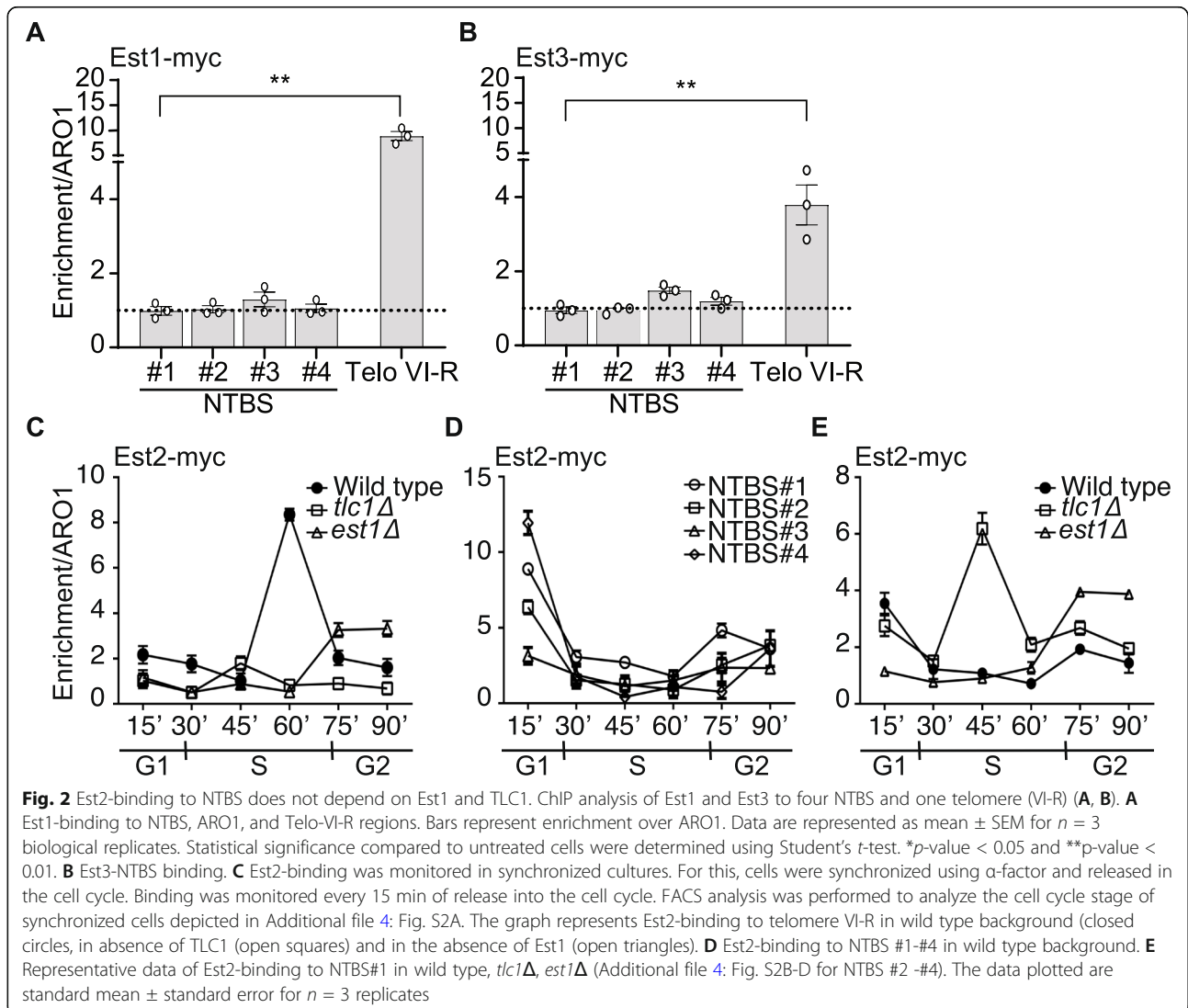
Next, we validated Est2-binding to intrinsic sites by ChIP followed by quantitative PCR (ChIP-qPCR) using primers directed against 4 different NTBS (NTBS#1-NTBS#4). Here, and in all subsequent ChIP experiments, we used the right telomere on chromosome VI (Telo VI-R) as a positive control and *ARO1*, a known region low in telomere-binding proteins, as a negative control [42]. ChIP-qPCR analysis of Est2 revealed a robust and

significant binding to all tested NTBS (Fig. 1C). Est2-binding was 2–3-fold enriched in comparison to the negative control *ARO1*.

Est2-binding to NTBS is regulated throughout the cell cycle

At telomeres Est2 functions in a complex with Est1 and Est3 [5, 43]. In vivo data shows that all components need to be present for an active telomerase holoenzyme [6, 43–46]. To determine whether telomerase is active at NTBS, we asked if only Est2 or the whole telomerase holoenzyme is binding to NTBS. We analyzed the binding of Est1 and Est3 to four different NTBS in asynchronous yeast cells by ChIP-qPCR (Fig. 2A, B). Both, Est1 and Est3, were tagged internally with 13xMyc. After crosslinking, protein binding was monitored by ChIP-qPCR. These analyses revealed that neither Est1 nor Est3 bind significantly to these NTBS, indicating that Est2 binds alone and thus is likely not active at NTBS.

Est2-binding to telomeres changes in a cell cycle-specific manner [5, 7, 42]. We asked whether Est2-binding to NTBS is also cell cycle-dependent. We synchronized yeast cells in G1 with α -factor and released them into S-phase as performed previously [7]. Cell cycle progression was monitored by fluorescence-activated cell sorting (FACS) (Additional file 4: Fig. S2A). Est2-binding in different cell cycle phases was monitored by ChIP-qPCR. Est2-binding peaks at the end of S phase at telomeres, which agrees with published data [7] (Fig. 2C, black circles). On the contrary, Est2-



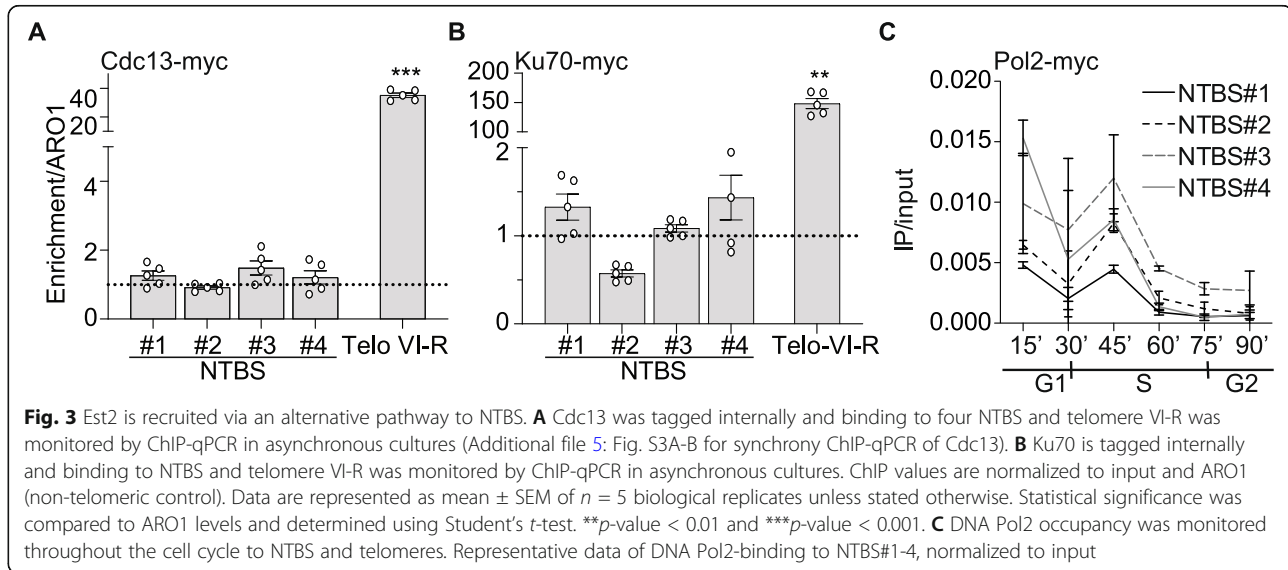
binding to all four NTBS peaked in G1 and late S/G2 phase (Fig. 2D). Note, the Est2-binding to NTBS is less strong as to telomeres.

At telomeres, Est2-binding depends on the presence of Est1, Est3, and TLC1 [6, 7, 9, 42, 45, 46]. To test, if Est2-binding to NTBS changes in the absence of telomerase subunits (Est1, TLC1), we performed cell cycle-dependent ChIP-qPCR in *est1* Δ and *tlc1* Δ backgrounds. At telomeres, Est2-binding is reduced when either TLC1 or Est1 is absent (Fig. 2C, white squares and triangles). This agrees with previously published data [42]. However, at NTBS Est2-binding is enhanced (9.6-fold) in late S/G2 phase in *est1* Δ cells (Fig. 2E, Additional file 4: Fig. S2B-D, white triangles). In *tlc1* Δ cells Est2-binding to NTBS was significantly elevated across all cell cycle stages with a strong peak in mid-S phase (Fig. 2E, Additional file 4: Fig. S2B-D, white squares). We speculate

that without TLC1 Est2 no longer binds to telomeres and consequently more Est2 is “free”, which results in more Est2-binding to NTBS.

Est2 binds to NTBS independently of known telomere-binding proteins

Cdc13, Est1, and the heterodimer yKu70/80 regulate telomerase recruitment to telomeres. They are essential for telomere maintenance [7, 35, 42, 47, 48]. Cdc13 and Est1 recruit Est2 during S/G2 phase, while yKu70/80 is required for Est2-binding at telomeres during G1 and early S phase and significantly contributes to the association of Est2-binding in S/G2 phase at telomeres [7, 35, 42, 47, 48]. Therefore, we aimed to understand if either Cdc13 or yKu heterodimer support Est2-binding to NTBS. We first analyzed Cdc13- and yKu70-binding to NTBS. Both proteins were tagged internally and their



binding to NTBS was measured by ChIP-qPCR (Fig. 3A, B). We observed little to no binding of yKu70 (0.7-1.7-fold binding/ARO1) or Cdc13 (1-3-fold binding/ARO1) to NTBS (Fig. 3A, B). Note, at telomeres, Cdc13 is nearly 30-fold and yKu70 over 100-fold enriched over ARO1 (Fig. 3A, B). Thus, it can be concluded that both proteins do not play a major role in mediating Est2-binding at NTBS. Although Cdc13 binds throughout the cell cycle its binding peaks during S/G2 phase [42]. To rule out that ChIP in asynchronous cells yields false interpretations, we also performed the Cdc13 ChIP experiments in synchronized cells. Nevertheless, similar results were obtained that showed only minor binding of Cdc13 to NTBS (Additional file 5: Fig. S3A-B).

Recruitment of Est2 to NTBS

In addition to Cdc13 and Ku70, other proteins and mechanisms have been postulated to regulate the recruitment of Est2 to telomeres. Among them are Pif1 [28, 29, 31], Mlh1 [49, 50], R-loop formation, and Telomeric repeat-containing RNA (TERRA) [51–53], RNase P components [13], and Rad51-Rad52 [23]. To reveal if one of these potentially regulatory factors contributes to Est2-binding, we monitored Est2-binding by ChIP-seq in the absence of these factors. In summary, no significant changes in Est2-binding were observed in *pif1-m2*, after the deletion of Mlh1 (*mlh1Δ*) or the reduction of R-loops by the overexpression of RNase H1 (Additional file 6: Fig. S4A-C). The yKu70/80 heterodimer binds to telomerase in G1 phase in a Sir4-dependent manner [37, 54, 55]. Sir4 is important for the telomere position effect (TPE), which may also contribute to Est2-binding to NTBS. However, Est2-binding to NTBS was not altered in the absence of Sir4 (Additional file 6: Fig. S4D).

In addition to these factors, it has been shown that the heterochromatic state of telomeres alters the access of telomerase to the telomeres. Sin3 is a component of the histone deacetylase complex that is responsible for the deacetylation of the core histones and effects heterochromatinization [56]. To test if the heterochromatic state of NTBS changes Est2-binding, we analyzed Est2-binding in *sin3Δ* cells by ChIP-qPCR. However, changes in *sin3Δ* had only minor and no-significant effect on Est2-binding to NTBS (Additional file 6: Fig. S4E).

We demonstrated that the recruitment of Est2 did not correlate to known recruitment factors of the telomere. Next, we investigated other published models such as the “replication fork” model. In this model, telomerase co-migrates with the replication fork [20, 36]. NTBS overlap with regions that are marked as replication fork pausing sites and we tested if replication fork pausing correlates with Est2-binding. If replication pauses cause Est2-binding, we assumed that the timing of Est2-binding to NTBS should mimic replication fork progression. We tagged the catalytic subunit of the leading strand polymerase (DNA Pol2) and used its occupancy as a measurement of replication fork pausing [41, 57]. We synchronized yeast cells and measured the binding by ChIP-qPCR. The results indicated that the timing of DNA Pol2-binding and Est2-binding does not correlate with each other (Fig. 3C). Our data indicate that replication fork pausing is not the cause for Est2-binding to NTBS.

Telomerase-binding to telomeres follows a three-dimensional model wherein telomerase makes multiple contacts with the chromosomes before binding to the telomeric regions [27]. To assess whether the three-dimensional organization of chromosomes has a role in the binding of Est2 to NTBS we performed chromosome

conformation capture using the Hi-C technique. Wild type cells were subjected to Hi-C as described [58] and the resulting libraries were sequenced to determine the interactions between NTBS-NTBS and NTBS-telomeric regions (Fig. 4A). We analyzed whether for a given NTBS the other binding sites are on average (mean Hi-C contact probability) closer to another NTBS or to telomeric regions (max Hi-C contact probability). Our bioinformatics analyses revealed the mean Hi-C contact probability of NTBS-NTBS interactions is 841/978 (86%) (Fig. 4B). 137/978 (14%) NTBS regions are closer to telomeric regions. Importantly, an iteration analysis showed that the NTBS are significantly closer to telomeres than randomized control regions (p -value $2.2e^{-16}$) (Fig. 4C). These data suggest that the chromatin organization dictates Est2-binding to NTBS.

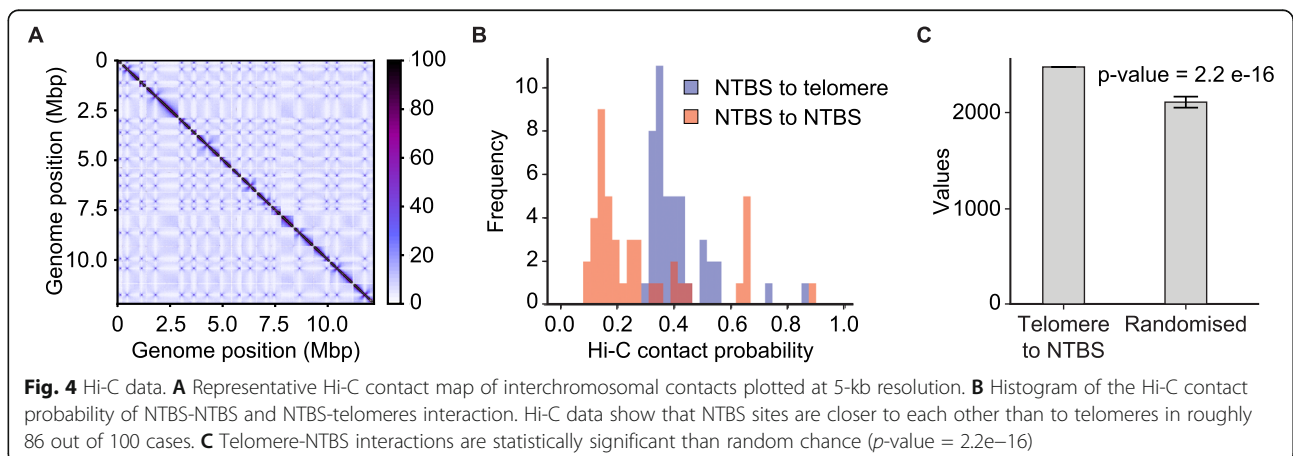
DNA damage repair is not supporting Est2-binding to NTBS

Telomerase can act at DSBs under specific conditions [25, 26, 29, 30, 59–61]. In many cancers, telomerase is reactivated at telomeres as well as at internal sites and these events cause genome instability and can drive tumorigenesis [62–67]. In addition, telomeres are known to be hotspots to accumulate DNA damage, as indicated by high levels of γ -H2A. γ -H2A is a histone modification (phosphorylation) that occurs in response to DNA breaks [68]. We speculated that NTBS, which show similarities to telomeric G-rich repeats, are also DNA damage prone. We performed bioinformatic analyses that revealed a significant overlap between a DNA damage marker (phosphorylated histone H2A, γ -H2A) with NTBS sites (Additional file 2: Fig. S1G). NTBS, like telomeres, are significantly enriched in regions that accumulate high levels of γ -H2A (294/978) [$p < 0.0001$] (Additional file 2: Fig. S1G). ChIP-qPCR using an anti- γ -

H2A antibody was performed to confirm these results. We observed a 5–12-fold higher binding of γ -H2A to NTBS in comparison to a H2A S129A mutant, which cannot be phosphorylated (Fig. 5A) [69].

Due to high levels of γ -H2A, we conclude that NTBS regions are vulnerable to accumulate DNA damage. In yeast, DNA damage is mainly repaired by homologous recombination (HR). However also telomerase can act at DSB, which should be avoided to preserve genome stability. Rad52 is a critical protein for HR in yeast [23, 70]. We examined whether the enrichment of Est2 is altered in the absence of Rad52. At telomeres, Est2-binding was 2-fold reduced in *rad52 Δ* . However, at NTBS, we did not detect significant changes in Est2-binding in *rad52 Δ* , suggesting that Est2-binding to NTBS is not HR dependent (Additional file 7: Fig. S5A).

To further address whether Est2-binding to NTBS causes telomere addition, we quantified telomere addition using a telomere healing assay [26, 60] (Fig. 5B, Additional file 7: Fig. S5B). We speculated that telomerase is not active at this site, because Est1 and Est3 are not present (Fig. 2). A lack of de novo telomere addition would further support that telomerase is not active at NTBS. Telomere addition was observed if telomeric repeats (TG80) were added next to an HO endonuclease cut site. If a random sequence (called N80) was near the HO cut site no telomere addition occurred (Fig. 5B, D, Additional file 7: Fig. S5B). To address if NTBS act like telomeric sequences and enhance telomere addition, we cloned four different NTBS at the same position adjacent to an HO cut site (see Additional file 8: Table S3 for list of the NTBS). Addition of galactose led to the induction of the HO endonuclease and subsequent processing at the HO cut site. In dependency to the repair at the HO cut site, the cell either loses or retains the adjacent marker (*LYS2*). If the break is repaired by



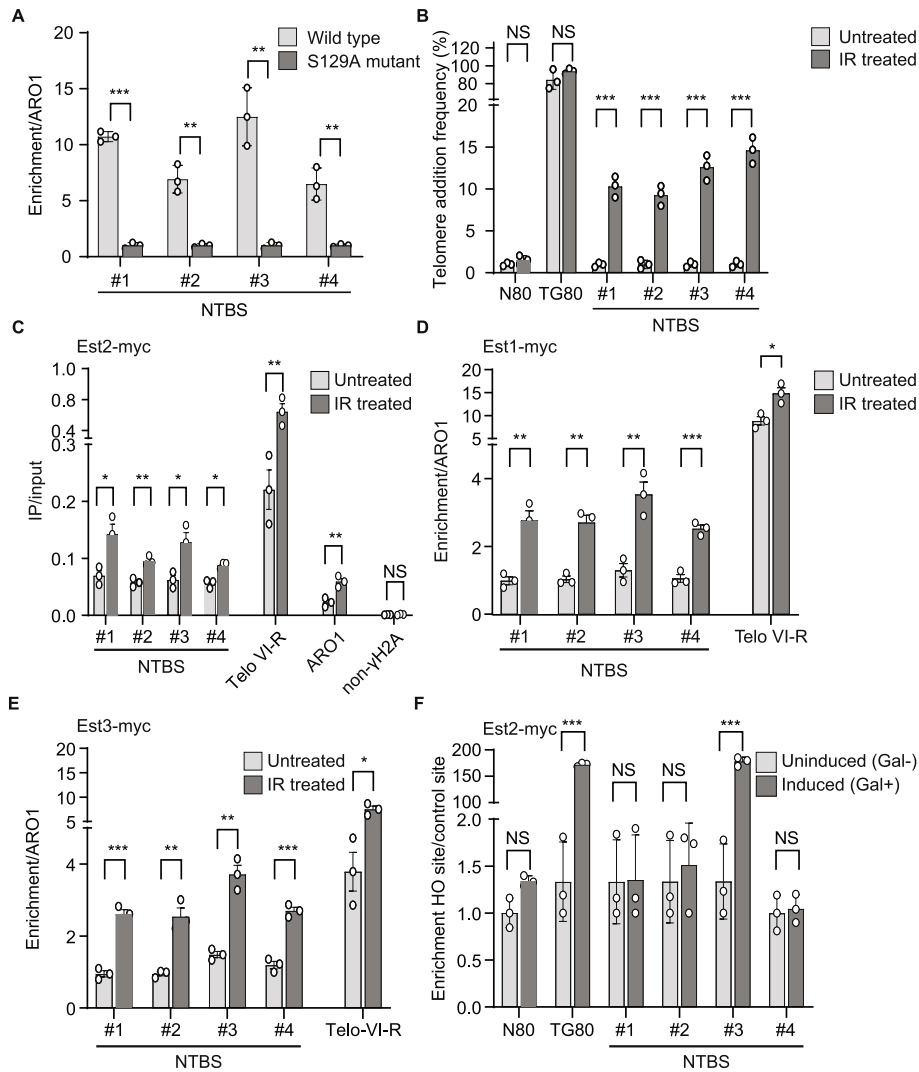


Fig. 5 Est2 binding is affected by DNA damage. **A** ChIP-qPCR of γ -H2A-binding to NTBS regions demonstrating their DNA damage prone nature. H2A-binding to four NTBS (#1-#4) and compared to S129A mutant (no γ -H2A phosphorylation). Data plotted are mean \pm SEM for $n = 3$ biological replicates with wild type (light grey bars) and S129 mutant (dark grey bars) conditions. Statistical significance compared to S129 mutant conditions were determined using Student's *t*-test. ***p*-value < 0.01. **B** Telomere addition frequency was determined in undamaged (light grey bars) and in damage (IR, dark grey bars) and was calculated as described before [26]. For IR treatment, cells were irradiated at 20 Gy before crosslinking and immunoprecipitated using the standard procedures mentioned in the methods. Telomere addition frequency was measured using a genetic assay based on loss of distal *LYS2* gene (resistance to α -amino adipate). TG80 and N80 were used as positive and negative control. TG80 contains 80 bp TG₁₋₃; N80 contains 80 bp lambda DNA. **C-E** ChIP analysis of Est2, Est1, and Est3 to four NTBS and one telomere (VI-R) in undamaged (light grey bars) and damaging (IR, dark grey bars) conditions. For IR treatment, cells were irradiated at 20 Gy before crosslinking and immunoprecipitated using the standard procedures mentioned in the methods. **C** Est2-binding to NTBS, *ARO1* and non- γ -H2A regions. Data plotted are IP/Input values represented as mean \pm SEM of $n = 3$ biological replicates. Statistical significance compared to untreated cells were determined using Student's *t*-test. **p*-value < 0.05 and ***p*-value < 0.01. **D** Est1-NTBS-binding. ChIP is normalized to *ARO1* and represented as mean \pm SEM. **E** Est3-NTBS-binding in undamaged (light grey bars) and damaging (IR, dark grey bars) conditions. Bars represent enrichment over *ARO1*. Data are represented as mean \pm SEM for $n = 3$ biological replicates. Statistical significance compared to untreated cells were determined using Student's *t*-test. **p*-value < 0.05 and ***p*-value < 0.01. **F** Quantification of Est2-binding upon induction of cleavage at the HO site. Est2-binding by ChIP to NTBS near HO cut sites was monitored before (light grey bars) and after induction (dark grey bars) of HO endonuclease. Data were plotted as mean \pm SEM of $n = 3$ biological replicates. Statistical tests were performed by comparing induced to uninduced conditions and were determined using Student's *t*-test. ** *p*-value < 0.01

telomere addition, the *LYS2* marker is lost. If the break is repaired via non-homologous end joining, the *LYS2* marker is retained (Fig. 5B, Additional file 7: Fig. S5B).

After the break induction colony formation was monitored. Colony counting revealed that no telomere addition was monitored at 4/4 NTBS regions whereas 100%

telomere addition was observed at TG80 controls (Fig. 5B). These data confirm binding of inactive Est2 to NTBS.

NTBS are hotspot for genome instability

Cancer is connected to increased telomerase activity and genome instability [71]. In multiple cancers, telomerase is activated and telomere addition can be observed at many internal sites, which drives genome instability, aneuploidy, and polyploidy [72–76]. To test if increased genome instability leads to telomerase activation at these sites, we treated cells with ionizing gamma radiation (IR) to increase overall DNA damage in cells. Following treatment, we monitored Est2-binding by ChIP-qPCR to NTBS and controls. We selected 20 Gy, which causes global DNA damage but leaves 80–90% of the cells viable [77]. Upon IR treatment Est2-binding to NTBS was significantly enhanced (1.5–3-fold) compared to untreated control cells (Fig. 5C). However, Est2-binding to *ARO1* also increased 2-fold but binding remained the same to a region devoid of γ -H2A-binding previously identified by genome-wide approaches [39] (Fig. 5C). We concluded that although NTBS have high levels of γ -H2A, enhanced global DNA damage stimulates Est2-binding to NTBS and leads to Est2-binding to additional internal sites (for example, *ARO1*).

NTBS are prone for DNA damage (Fig. 5A, B, Additional file 7: Fig. S5A-B) and Est2-binding is stimulated upon IR (Fig. 5C). To test if an active telomerase complex assembles during DNA damage at NTBS, we performed ChIP analyses with Est1 and Est3 after IR treatment. Interestingly, both proteins bind to NTBS upon IR treatment 2–4-fold more compared to untreated control cells, supporting the conclusion that in untreated cells telomerase enzyme is inactive, but upon damage the holoenzyme assembles (Fig. 5D, E, gray bars). To check if elevated binding of Est1 and Est3 are mediated via enriched binding of Cdc13 or Ku70 after IR treatment, we performed ChIP-qPCR after IR treatment. Asynchronous cells were treated with IR and binding of Cdc13 and Ku70 was monitored by ChIP-qPCR. Analysis revealed that upon IR treatment, no significant binding was observed for neither Cdc13 and Ku70 to NTBS (Additional file 5: Fig. S3C-D). These data indicate that upon damage, Est1 and Est3 are recruited to NTBS because of the presence of Est2. Because we can exclude that Est1 and Est3 are recruited by similar mechanisms as to telomeres, it is not clear how they are recruited to NTBS-Est2.

We next wanted to determine if a specific break at the NTBS stimulates Est2-binding similar to IR treatment. We performed ChIP-qPCR after HO induction to quantify Est2-binding to NTBS [60]. HO induction resulted in a specific cleavage near the NTBS as opposed to IR treatment wherein global DNA damage occurs. ChIP-

qPCR quantification revealed that Est2 associates to NTBS near the HO sites but binding of Est2 is not stimulated upon HO induction apart from one NTBS site (Fig. 5F). This indicated that a threshold of global damage is required for Est1- and Est3-binding to NTBS regions (Fig. 5D, E). Next, we investigated if increased global DNA damage not only results in more Est1-, Est2-, and Est3-binding, but also leads to telomerase activation. To monitor telomere addition, we used the previously described telomere addition assay where we inserted NTBS near HO sites after IR treatment (see Additional file 7: Fig. S5B). Colony formation showed that upon increased global DNA damage telomere addition can be monitored at 4/4 NTBS sites (Fig. 5B). We could demonstrate that NTBS are parking spots for Est2 in normal conditions, but hotspots for telomere addition if overall DNA damage increases in these cells. We predict that these sites are marked for telomere addition due to the presence of Est2.

Discussion

We identified internal DNA binding sites of Est2 and addressed the questions: how Est2 is recruited and localized to NTBS. Multiple studies have focused in the past on telomerase recruitment [5], and its activity and regulation at telomeres vs. DSB [16, 29, 78]. The here determined internal binding regions of Est2 binding leads to the hypothesis that internal Est2 binding sites are prone for telomere addition and cause genome instability.

Our data demonstrates that Est2 binds to over 900 NTBS. These sites are TG-rich and which has similarities to telomeric repeats in *S. cerevisiae* (Fig. 1). The cell cycle specific binding pattern of Est2 either to telomeres (S phase) or to NTBS (G1/G2 phase) suggests a cell cycle specific recruitment process. Therefore, we investigated if Est2 is recruited to NTBS via similar mechanisms as to telomeres. We observed that Est2 is not recruited to NTBS via similar mechanisms than it is to telomeres (Cdc13, Ku70/80, R-loops, Pif1, Mlh1) (Fig. 3, Additional files 5, 6: Fig. S3, S4). Furthermore, neither HR (Additional file 7: Fig. S5B), heterochromatin formation, or replication pausing [20, 36] (Additional file 6: Fig. S4) is the cause of Est2-binding to NTBS. Est2-binding to NTBS is also TLC1-independent (Fig. 2E). But we observed enhanced binding of Est2 to NTBS when TLC1 is missing in the cells (Fig. 2E). We anticipate that without TLC1, Est2 is no longer efficiently recruited and anchored to telomeres and therefore “free” to bind to other (internal) G-rich regions. Our data suggest that the three dimension organization of the chromatin dictates and supports Est2 localization to NTBS, which we indeed could show in Hi-C analysis (Fig. 4). Telomere looping maintains the telomere position effect (TPE), leading to the repression of transcription of telomere-adjacent genes [34]. How

telomere looping is mediated, if its function is only to maintain the TPE, and whether Est2 is involved in this process are not clear, yet. It is likely that other DNA structures support this looping and sequestering of Est2 to NTBS. We speculate that G4-G4 interaction might support this looping, because telomeres as well as NTBS are regions prone for G4 formation. NTBS overlap to published G4 regions ($p < 0.0001$) [39] (Additional file 2: Fig. S1B). In addition, G4 formation has also been discussed to promote long-range DNA interactions [79–81], which makes it tempting to speculate that G4 might support Est2-binding to NTBS. The function and relevance of G4 structures for telomere maintenance is a long ongoing discussion. Multiple data show how G4 formation can alter different aspects of telomere maintenance [82, 83], such as binding of telomere binding proteins [84], altering telomerase function [83–87], or the telomere organization within the nucleus [84, 85, 88].

Telomere addition at DSB contributes to genome instability and should be always prevented. Our finding that Est2 binds under normal wildtype conditions to internal sites is counterintuitive and raises the question of telomere addition at NTBS and their impact on genome stability. In unchallenged yeast cells Est2 binds to NTBS without the telomerase subunits Est1 and Est3 (Fig. 2), which are required in vivo for full telomerase function [5]. Consequently, no telomere addition can be monitored (Fig. 5B). But the binding of Est2 to NTBS increased upon

IR treatment and under these conditions even Est1 and Est3 bind to NTBS (Fig. 5C–E). Interestingly, one single break induced by a HO endonuclease is not sufficient to enhance Est2-binding and no telomere addition was detectable (Fig. 5B, F). However, after IR treatment NTBS show telomere addition at 10–15% whereas no telomere addition is monitored at the N80 control region (Fig. 5B). Our data agree with studies in which multiple novel telomere addition sites were identified after DNA damage [24, 25]. In the first study, internal regions in the yeast genome were identified as the site of repair-associated telomere addition (SiRTA). In the second study, deep sequencing of yeast cells with an overload of DNA damage revealed novel sites of telomere addition. In general, uncontrolled telomere addition is regulated by the Pif1 helicase in yeast [28, 29, 31, 86]. Without Pif1 multiple telomere additions sites can be detected within internal regions [28]. NTBS sites overlap significantly with Pif1-binding sites (Additional file 2: Fig. S1D), but Est2-binding is not restricted by the presence of Pif1 (Additional file 6: Fig. S4A). We speculated that only 10–15% telomere addition were measured at NTBS in the telomere addition assay, because cells still have a functional Pif1 helicase, which prevents telomerase action to a certain extent.

Our study provides a comprehensive global occupancy map of yeast telomerase and presents a panel of sites at which telomere addition is prone to occur upon DNA damage (Fig. 6). Our data suggest a model in which

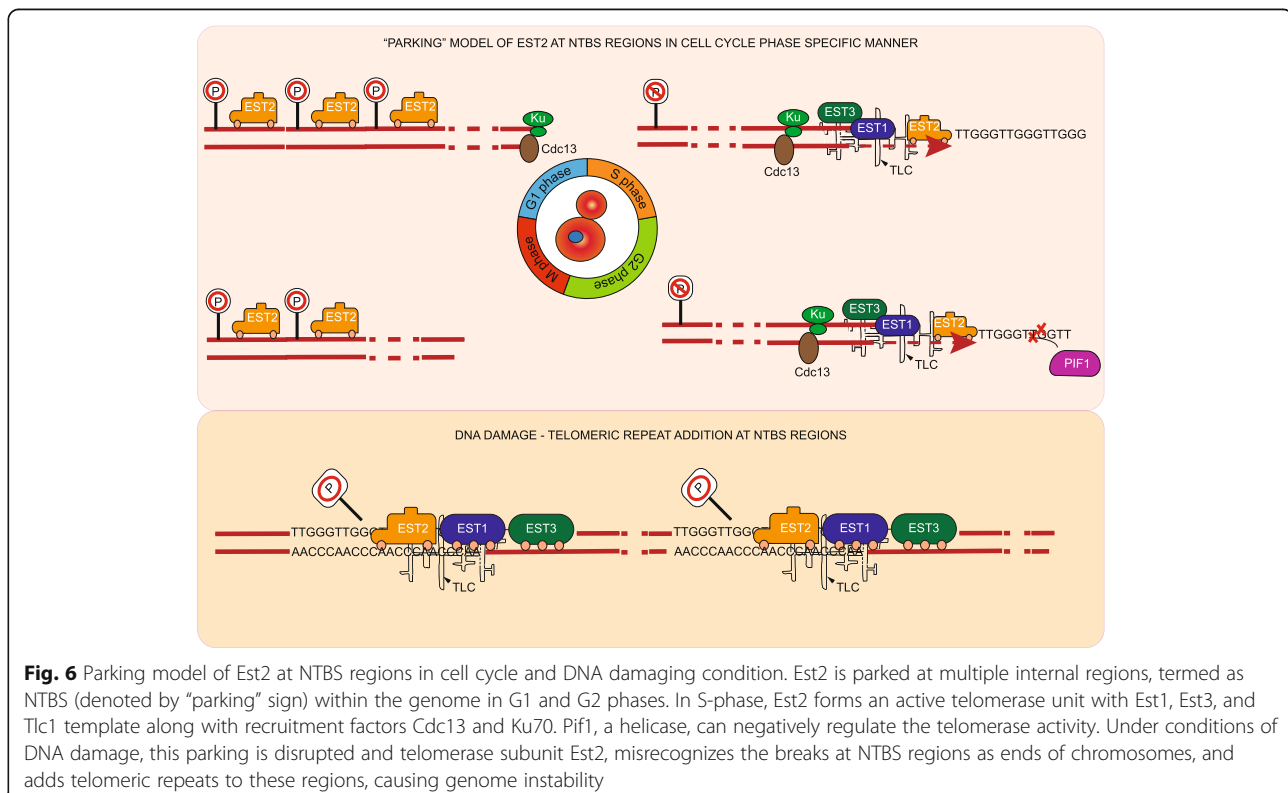


Fig. 6 Parking model of Est2 at NTBS regions in cell cycle and DNA damaging condition. Est2 is parked at multiple internal regions, termed as NTBS (denoted by “parking” sign) within the genome in G1 and G2 phases. In S-phase, Est2 forms an active telomerase unit with Est1, Est3, and Tlc1 template along with recruitment factors Cdc13 and Ku70. Pif1, a helicase, can negatively regulate the telomerase activity. Under conditions of DNA damage, this parking is disrupted and telomerase subunit Est2, misrecognizes the breaks at NTBS regions as ends of chromosomes, and adds telomeric repeats to these regions, causing genome instability

under normal conditions Est2 binds to telomeres in S phase and to NTBS during G1 and G2 phase. Est2 binding to NTBS is supported by the 3D organization of the chromatin. Under unchallenging conditions, Est2 is inactive (parked) and no telomere addition occurs at internal sites (Fig. 6). Upon global DNA damage, Est1 and Est3 joint Est2 at NTBS and telomere addition occurs, and genome instability is enhanced.

Conclusions

Telomere addition within the genome is observed in human cancer and congenital disorders [18, 89–91]. Telomerase-associated signatures in cancer and subtypes reveal that telomerase is not limited to ends of chromosomes but has additional functions [62–65, 67, 92–94]. Our work provides a genomic map of potentially vulnerable internal sites where telomerase subunits can bind. We reveal a novel mechanism of how telomerase is regulated in a 3D context and distinguishes between internal telomeric regions and chromosome ends. Further, the here-presented data give new insights related to genome stability and indicates certain internal regions that are more prone for telomere addition than other sites. The observation that the three-dimensional organization of telomeres alters during the cell cycle and that this organization is distorted in cancer cells [95–97], leads to the speculation that a similar mechanism also exists in higher eukaryotes.

Methods

Strains, plasmids, and media

All yeast strains, primers, and plasmids used in the study are listed in Additional files 8, 9, 10: Table S3, S4, and S5, respectively. Proteins were epitope-tagged at their internal loci using TRP as a marker with thirteen Myc epitopes unless stated otherwise [98]. All the strains were grown in standard YPD media under standard conditions. The epitope tagging and deletions were confirmed using PCR and sequencing before performing subsequent experiments. The strains with Est2-G8-myc in *tlc1Δ*, *est1Δ*, *est3Δ* were a generous gift from the Zakian lab. All these diploid strains were sporulated and freshly dissected spores of desired genotypes were used for ChIP analyses. RNH1 plasmid for overexpression of RNase H1 was a kind gift from Brian Luke lab.

Chromatin immunoprecipitation (ChIP) and qPCR

ChIP experiments were performed as described previously [7]. Briefly, yeast strains were grown to OD of 0.4–0.6 and crosslinked with 1% (v/v) formaldehyde for 5 min followed by quenching of the crosslinker with the addition of 125 mM glycine. Cells were centrifuged and washed once with HBS buffer and with ChIP lysis buffer. The pellet was resuspended in ChIP lysis buffer and

snap-chilled in liquid nitrogen and stored in -80°C . Frozen cell pellets were thawed, and cells were lysed using glass beads in a FastPrep (MP Biomedicals) in two rounds (60 s followed by 30 s with incubation on ice for 4 min). Chromatin was sheared to 200–1000 bp using Bioruptor Pico (Diagenode) with these settings: high intensity, 30 s ON, 30 s OFF, 7 cycles. Shearing quality was estimated on an agarose gel. Eight-microgram c-Myc antibody (Clontech) was added to the sheared chromatin and incubated at 4°C for 1 h followed by incubation with 80 μl Dynabeads protein G (Invitrogen) for 2 h. Beads were washed sequentially with SDS buffer, high-salt buffer, Tris-Lithium buffer, and Tris-EDTA buffer to remove non-specific bound DNA. Immunoprecipitated DNA was eluted using Tris-EDTA +1% SDS followed by incubation at 65°C to reverse the crosslink. Immunoprecipitated DNA was purified using Qiagen PCR purification kit and used for subsequent analyses. qPCR was performed using SyBr Green (Roche) and fold enrichment of binding regions was quantified using IP/Input method normalized to ARO1 (non-specific binder) values. Prism7 (GraphPad) was used to plot the graphs and the *p*-value was calculated using Student's *t*-test. For IR treatments, the cells were subjected to 20 Gy of IR and allowed to recover for 30 min at 30°C before being subjected to crosslinking and ChIP.

Telomere healing assay

Telomere addition events were quantified as described previously [26, 30]. Yeast cultures were grown overnight in XY media (10 g l^{-1} yeast extract, 20 g l^{-1} bacto-peptone, 0.1 g l^{-1} adenine, 0.2 g l^{-1} tryptophan) + 2% glucose to log phase and subcultured into XY + raffinose (2%) for overnight growth. Fifteen micrograms per milliliter nocodazole was added to the cells to a density of $5\text{--}7.5 \times 10^6$ cells ml^{-1} for 2 h to synchronize cells in the G2/M phase. 3% galactose was added to induce HO endonuclease expression in the strains and samples were collected after 4 h of galactose induction. Cells were plated on XY+glucose plates before and after induction of HO endonuclease and grown for 2–3 days. The total number of colonies were counted, and colonies were replica-plated to media without lysine and media with α -amino adipic acid (α -AA) to identify the cells which have lost the distal *LYS2* gene on chromosome VII. The frequency of telomere addition was calculated as the percentage of colonies that were α -AA-resistant after HO induction. For IR experiments, the cells were exposed to 20 Gy after galactose induction and recovered for 2 h.

Cell cycle analysis and chromatin immunoprecipitation (ChIP)

Cell synchrony experiments were performed as described previously [41]. Briefly, 320-ml yeast culture at

an OD of 0.15 was arrested in G1 phase using alpha factor at a concentration of $5 \mu\text{g ml}^{-1}$ for 3–4 h. The cells were examined microscopically for shmoo. Cells were filtered and resuspended in fresh YPD media and released into YPD+pronase at 24°C. Samples were collected after every 15 min for FACS analysis and cross-linking was performed using the conditions mentioned above. FACS samples were spun down and fixed in 70% (v/v) ethanol overnight at 4°C. Cells were washed with 50 mM Tris buffer (pH 7.8) followed by RNase digestion for 5 h at 37°C and proteinase K digestion for 60 min at 50°C. Cells were sonicated with low intensity (30 s on, 30 s off, 3 cycles) to break clumps and incubated with SYTOX Green before being subjected to FACS analysis. FACS data was analyzed with FlowJo (BD).

ChIP-chip

ChIP was performed as described above and for genome-wide analysis, immunoprecipitated DNA was amplified, labeled with minor modifications of Agilent Yeast ChIP on chip protocol v9.2. Binding sites were identified using ChIPOTle 2.0 [99] and corrections were applied to control for the false discovery rate as described in [41]. The identified sites and their location within the genome are listed in Additional file 1: Table S1.

Hi-C methods

The Hi-C protocol used here was amended from the Hi-C 2.0 [100] to yeast cells. Briefly, *S. cerevisiae* diploid cells were grown in YPD (1% yeast extract, 2% peptone, 2% glucose) to exponential phase, and 100 ml of cells (50–80 OD, sufficient for 1 Hi-C library) was fixed with formaldehyde at 3% final concentration for 20 min at 30°C, 250 rpm, and quenched by incubating with a final concentration of 0.35 M glycine (2× the volume of formaldehyde added) for an additional 5 min. Cells were washed with water and pellets were snap frozen and stored at –80°C. Cells were thawed, washed in spheroplasting buffer (SB, 1 M sorbitol, 50 mM Tris pH 7.5), and digested with $10 \mu\text{g ml}^{-1}$ Zymolyase 100T in SB containing 0.5% beta-mercaptoethanol for 10 min at 35°C. Cells were washed in restriction enzyme buffer (NEB3.1) and chromatin was solubilized by adding SDS to 0.01% and incubating at 65°C for 5 min. Excess SDS was quenched by addition of Triton X100 to 1%. Chromatin was incubated with 400 U of DpnII overnight at 37°C and 400 rpm. DpnII was inactivated by incubation at 65°C for 20 min and DNA ends were filled-in with nucleotides substituting dCTP for biotin-14-dCTP using Klenow fragment DNA polymerase I at 23°C for 4 h in a thermomixer (900 rpm mixing for 10 s every 5 min). The sample volume was diluted 2-fold and crosslinked DNA ends ligated at 16°C for 4 h using 50 U of T4

DNA ligase in 1x T4 ligation buffer (Invitrogen), 1% Triton and 0.1 mg ml^{-1} BSA.

Crosslinks were reversed overnight at 65°C in the presence of proteinase K ($400 \mu\text{g ml}^{-1}$) and an additional 2 h with another addition of proteinase K ($400 \mu\text{g ml}^{-1}$). DNA was purified by phenol:chloroform:isoamylalcohol (25:24:1) extraction and precipitated with 2.5 vol ethanol, dissolved in TE (10 mM Tris pH 8.0, 0.1 mM EDTA) and washed and concentrated with an Amicon 30 kDa column, before treating with $10 \mu\text{g/ml}$ of RNase A at 37°C for 30 min. Biotin was removed from unligated ends by incubation with $0.3 \text{ U } \mu\text{l}^{-1}$ T4 DNA polymerase and low abundance of dATP and dGTP (25 μM each) at 20°C for 4 h and at 75°C for 20 min for inactivation of the enzyme. DNA was washed on an Amicon 30 kDa column and subsequently fragmented using a Covaris M220 ultrasonicator (duty factor 20%, 200 cycles/burst, 240 s, 20°C). DNA ends were repaired using T4 DNA polymerase, T4 polynucleotide kinase, and Klenow fragment DNA polymerase I. Biotinylated fragments were enriched using Streptavidin C1 magnetic beads (Invitrogen). DNA ends were A-tailed and NextFlex (Bio Scientific) barcoded adapters were ligated while the DNA was on the beads. Resulting libraries were minimally amplified by PCR and sequenced using paired end 75 bp reads on a NextSeq550 (Illumina).

Hi-C bioinformatic analyses

We performed iteration analyses to quantify the overlap between NTBS sites and genomic features such as ORFs, Pif1-binding sites and DNA damage sites. We then mapped the sequencing reads to the yeast genome using the HiCUP pipeline [101]. Statistical analysis of the telomere proximal ends was performed using custom R scripts and significance of the results was determined by non-parametric Wilcoxon-rank tests.

Generation of Hi-C contact maps

Paired-end sequencing reads were mapped independently to the genome of *S. cerevisiae* S288C (NCBI Primary Assembly: GCF_000146055.2) using Bowtie 2.3.5 [102] and an algorithm which iteratively increases truncation length to maximize yield of valid Hi-C interactions. Only read pairs with both reads uniquely aligned to the genome were considered for subsequent steps. The *S. cerevisiae* genome was then divided into restriction fragments produced by the restriction enzyme DpnII. Each read of a read pair was sorted into its corresponding restriction fragment. Read pairs were classified as valid Hi-C products, non-ligation or self-ligation products; only valid Hi-C products were considered below.

To create interaction matrices, the *S. cerevisiae* genome was first divided into bins of length 10 kbp. We

then assigned valid Hi-C products to the bins proportional to their overlap, i.e., each read contributes a count of one to the contact map, but it can be split between bins. As raw Hi-C contact frequency maps are biased due to the uneven distribution of restriction enzyme sites, differences in GC content, and the mappability of individual reads, we normalized raw contact maps using the Sinkhorn-Knopp balancing algorithm. Resulting matrices were normalized so that Hi-C scores for each row and column sum to 1. Subsequent analysis and visualization were done using Python and R scripts. (<http://projecteuclid.org/euclid.pjm/1102992505>).

To quantify NTBS-NTBS vs. NTBS-telomeres interactions, we assigned NTBS sites and telomeres to the respective bin of the Hi-C contact matrix of wild-type *S. cerevisiae* and collected the respective Hi-C contact probabilities. We then checked for each NTBS site whether its contact probability with one of the two telomeres is higher than the mean contact probability with all the other NTBS sites. This analysis yielded that NTBS sites are closer to each other (86%) than to telomeres (14%).

Abbreviations

ARS: Autonomously replicating sequence; ChIP: Chromatin immunoprecipitation; DNA: Deoxyribonucleic acid; DSB: Double-strand break; FACS: Fluorescence-activated cell sorting; G4: G-quadruplex; GCR: Gross chromosomal rearrangement; HR: Homologous recombination; IR: Ionizing gamma radiation; MRX: Mre11-Rad50-Xrs2; NTBS: Non-telomeric binding sites; ORF: Open reading frames; RNA: Ribonucleic acid; SGD: *S. cerevisiae* genome database; SiRTAs: Sites of repair-associated telomere addition; TERRA: Telomeric repeat-containing RNA; TPE: Telomere position effect

Supplementary Information

The online version contains supplementary material available at <https://doi.org/10.1186/s12915-021-01167-1>.

Additional file 1: Supplementary Table S1. Genomic coordinates of NTBS regions discovered in at least three out of five independent ChIP-chip experiments.

Additional file 2: Supplementary Figure S1. A Snapshots of IGV browser showing the presence of NTBS #1-4 in the yeast genome. **B-F** Bioinformatics' analyses demonstrating the overlap of genomic features with the NTBS regions. P-value denotes statistical significance of their enrichment in the NTBS set between the features and NTBS regions. In **B** NTBS vs. G4s, **C** NTBS vs R-loops, **D** NTBS vs. Pif1-binding sites, **E** NTBS vs. DNA Pol2 sites in *pif1-m2* cells, **F** NTBS vs. DNA Pol2 sites and **G** NTBS vs. γ -H2A-binding sites significantly overlapped with NTBS regions.

Additional file 3: Supplementary Table S2. Table defining the NTBS overlap with gene bodies, percentage overlap of NTBS region and the gene and gene function description.

Additional file 4: Supplementary Figure S2. Est2-binding to NTBS regions in absence of telomerase components TLC1 and Est1. **A** Cell cycle progression was monitored with flow cytometry and FACS analysis demonstrated the cell cycle stage of synchronized cells in wild type, *tlc1Δ* and *est1Δ*. **B-D** Est2-binding to NTBS #2-#4 in wild type (closed circles), *tlc1Δ* (open squares) and *est1Δ* (open triangles). A reproducible increase of Est2-NTBS-binding was observed in absence of *tlc1* and *est1* in independent replicates. The data plotted are standard mean \pm SEM for n = 3 replicates.

Additional file 5: Supplementary Figure S3. Canonical telomerase recruitment factors, Cdc13 and Ku70, do not bind to NTBS. **A** Cdc13-binding to four NTBS (#1-#4) and telomere VI-R was monitored by ChIP-qPCR in synchronous cultures. ChIP analysis of Cdc13 in different cell cycle stages did not show enrichment to NTBS regions. Data plotted are mean \pm SEM normalized to ARO1 levels at respective timepoints. **B** Cell cycle analysis was determined using flow cytometry. Representative graphs demonstrating different cell cycle stages after release from α -factor. **C** Cdc13 and **D** Ku70-binding to NTBS regions in undamaged (light grey bars) and damaging conditions (IR, dark grey bars). No statistically significant enrichment of Cdc13 and Ku70 was observed to NTBS regions. Data represented are mean \pm standard error for n = 3 biological replicates. Statistical significance compared to untreated cells were determined using Student's t-test. * p-value < 0.05.

Additional file 6: Supplementary Figure S4. Est-NTBS interaction is independent of regulatory factors, Pif1, Mlh1, R-loops, heterochromatin stage and Sir4. Est2-binding to NTBS regions (NTBS#1-#4) in wild type (grey bars) and absence of regulatory factors (white bars) **A** Est2-NTBS-binding was evaluated using ChIP-qPCR in *pif1-m2* cells that express reduced nuclear Pif1, negative regulator of telomerase. No significant change was observed in *pif1-m2* cells (dark grey bars) compared to wild type condition (light grey bars). **B** R-Loops were resolved using overexpression of RNaseH1 plasmid (RNH1) (dark grey bars) compared to wild type condition (light grey bars). **C** ChIP-qPCR of Est2-NTBS-binding in *mlh1Δ* (suppressor of genomic telomere insertions) cells (dark grey bars) compared to wild type condition (light grey bars). **D** Est2-NTBS interaction in *sir4Δ* cells (dark grey bars) compared to wild type condition (light grey bars). No statistically significant enrichment to NTBS sites were observed for all the tested conditions. **E** Est2-NTBS interaction in *sin3Δ* (component of histone deacetylase complexes) cells (dark grey bars) compared to wild type condition (light grey bars). No statistically significant enrichment to NTBS sites were observed for all the tested conditions. Data represented are mean \pm SEM. Statistical significance was calculated in comparison to ARO1 levels for n = 3 biological replicates and determined using Student's t-test. No statistically significant enrichment to NTBS sites were observed for all the tested conditions.

Additional file 7: Supplementary Figure S5. HR connection to Est2-NTBS interaction and schematic of telomere healing assay. **A** Est2-binding to NTBS regions in wild type (light grey bars) and in absence of Rad52 (dark grey bars). Bars represent mean \pm standard error mean for n = 3 biological replicates. The significance was calculated between wild type and *rad52Δ* cells using Student's t-test. * p-value < 0.05. **B** Telomere healing assay description. NTBS regions cloned adjacent to HO site were subjected to HO cleavage to create a double stranded break. Lysine (LYS2) marker was lost upon telomere addition and retained if the break was repaired.

Additional file 8: Supplementary Table 3. List of bacterial strains used in this study.

Additional file 9: Supplementary Table 4. List of yeast strains used in this study.

Additional file 10: Supplementary Table 5. List of primers used in this study.

Acknowledgements

We thank Virginia Zakian for strains and initial ChIP-chip experiments (grant number NIH grant 1R35GM118279). We thank Brian Luke for a plasmid to overexpress RNase H. We thank Michael Chang and Liesbeth Veenhoff for discussion and advice during the project.

Authors' contributions

SP and KP conceived the project. SP, TZ, MH, SAS, MJN, JB and SJ performed the experiments. SP, SJ, SAS, MJN, AH, and VG analyzed the data. SP, SJ, MH, and KP wrote the original draft. Funding and resource acquisition was done by KP and MJN. Supervision was done by MJN, JB, DH, and KP. All authors read and approved the final manuscript.

Funding

This study was supported by a DFG Emmy Noether Programme and by a starting grant from the European Research Council (ERC Stg. Grant: 638988-

G4DSB). Open Access funding enabled and organized by Projekt DEAL. ERC starting grant 311336 and Wellcome Trust Investigator Award 200843/Z/16/Z.

Availability of data and materials

The datasets generated during this study are available at Gene Expression Omnibus (GEO) GSE143187 [103].

Declarations

Ethics approval and consent to participate

Not applicable.

Consent for publication

Not applicable.

Competing interests

The authors declare that they have no competing interests.

Author details

¹University of Groningen, University Medical Center Groningen, European Research Institute for the Biology of Ageing, 9713 AV Groningen, Netherlands. ²Clinic of Internal Medicine III, Oncology, Hematology, Rheumatology and Clinical Immunology, University Hospital Bonn, Bonn, Germany. ³Department of Life Science, University of Sussex, Brighton, UK. ⁴Institute for Theoretical Physics, University of Heidelberg, Philosophenweg 12, 69120 Heidelberg, Germany.

Received: 23 July 2021 Accepted: 15 October 2021

Published online: 20 November 2021

References

- Greider CW, Blackburn EH. A telomeric sequence in the RNA of Tetrahymena telomerase required for telomere repeat synthesis. *Nature*. 1989;337(6205):331–7. <https://doi.org/10.1038/337331a0>.
- Blackburn EH, Collins K. Telomerase: an RNP enzyme synthesizes DNA. *Cold Spring Harb Perspect Biol*. 2011;3(5). <https://doi.org/10.1101/cshperspect.a003558>.
- Shay JW. Role of telomeres and telomerase in aging and cancer. *Cancer Discov*. 2016;6(6):584–93. <https://doi.org/10.1158/2159-8290.CD-16-0062>.
- Nakamura TM, Morin GB, Chapman KB, Weinrich SL, Andrews WH, Lingner J, et al. Telomerase catalytic subunit homologs from fission yeast and human. *Science*. 1997;277(5328):955–9. <https://doi.org/10.1126/science.277.5328.955>.
- Wellinger RJ, Zakian VA. Everything you ever wanted to know about Saccharomyces cerevisiae telomeres: beginning to end. *Genetics*. 2012; 191(4):1073–105. <https://doi.org/10.1534/genetics.111.137851>.
- Taggart AK, Teng SC, Zakian VA. Est1p as a cell cycle-regulated activator of telomere-bound telomerase. *Science*. 2002;297(5583):1023–6. <https://doi.org/10.1126/science.1074968>.
- Fisher TS, Taggart AK, Zakian VA. Cell cycle-dependent regulation of yeast telomerase by Ku. *Nat Struct Mol Biol*. 2004;11(12):1198–205. <https://doi.org/10.1038/nsmb854>.
- Gallardo F, Olivier C, Dandjinou AT, Wellinger RJ, Chartrand P. TLC1 RNA nucleocytoplasmic trafficking links telomerase biogenesis to its recruitment to telomeres. *EMBO J*. 2008;27(5):748–57. <https://doi.org/10.1038/emboj2008.21>.
- Tuzon CT, Wu Y, Chan A, Zakian VA. The Saccharomyces cerevisiae telomerase subunit Est3 binds telomeres in a cell cycle- and Est1-dependent manner and interacts directly with Est1 in vitro. *PLoS Genet*. 2011;7(5):e1002060. <https://doi.org/10.1371/journal.pgen.1002060>.
- Chan YA, Aristizabal MJ, Lu PY, Luo Z, Hamza A, Kobor MS, et al. Genome-wide profiling of yeast DNA:RNA hybrid prone sites with DRIP-chip. *PLoS Genet*. 2014;10(4):e1004288. <https://doi.org/10.1371/journal.pgen.1004288>.
- Lemieux B, Laterreur N, Perederina A, Noel JF, Dubois ML, Krasilnikov AS, et al. Active yeast telomerase shares subunits with ribonucleoproteins RNase P and RNase MRP. *Cell*. 2016;165(5):1171–81. <https://doi.org/10.1016/j.cell.2016.04.018>.
- Lin KW, McDonald KR, Guise AJ, Chan A, Cristea IM, Zakian VA. Proteomics of yeast telomerase identified Cdc48-Npl4-Ufd1 and Ufd4 as regulators of Est1 and telomere length. *Nat Commun*. 2015;6(1):8290. <https://doi.org/10.1038/ncomms9290>.
- García PD, Leach RW, Wadsworth GM, Choudhary K, Li H, Aviran S, et al. Stability and nuclear localization of yeast telomerase depend on protein components of RNase P/MRP. *Nat Commun*. 2020;11(1):2173. <https://doi.org/10.1038/s41467-020-15875-9>.
- Myung K, Chen C, Kolodner RD. Multiple pathways cooperate in the suppression of genome instability in Saccharomyces cerevisiae. *Nature*. 2001;411(6841):1073–6. <https://doi.org/10.1038/35082608>.
- Paques F, Haber JE. Multiple pathways of recombination induced by double-strand breaks in Saccharomyces cerevisiae. *Microbiol Mol Biol Rev*. 1999;63(2):349–404. <https://doi.org/10.1128/MMBR.63.2.349-404.1999>.
- Pennaneach V, Putnam CD, Kolodner RD. Chromosome healing by de novo telomere addition in Saccharomyces cerevisiae. *Mol Microbiol*. 2006;59(5): 1357–68. <https://doi.org/10.1111/j.1365-2958.2006.05026.x>.
- Putnam CD, Pennaneach V, Kolodner RD. Chromosome healing through terminal deletions generated by de novo telomere additions in Saccharomyces cerevisiae. *Proc Natl Acad Sci U S A*. 2004;101(36):13262–7. <https://doi.org/10.1073/pnas.0405443101>.
- Bonaglia MC, Giorda R, Beri S, De Agostini C, Novara F, Fichera M, et al. Molecular mechanisms generating and stabilizing terminal 22q13 deletions in 44 subjects with Phelan/McDermid syndrome. *PLoS Genet*. 2011;7(7): e1002173. <https://doi.org/10.1371/journal.pgen.1002173>.
- Wilkie AO, Lamb J, Harris PC, Finney RD, Higgs DR. A truncated human chromosome 16 associated with alpha thalassaemia is stabilized by addition of telomeric repeat (TTAGGG)_n. *Nature*. 1990;346(6287):868–71. <https://doi.org/10.1038/346868a0>.
- Matmati S, Lambert S, Geli V, Coulon S. Telomerase repairs collapsed replication forks at telomeres. *Cell Rep*. 2020;30(10):3312–22 e3313. <https://doi.org/10.1016/j.celrep.2020.02.065>.
- Dave A, Pai CC, Durlay SC, Hulme L, Sarkar S, Wee BY, et al. Homologous recombination repair intermediates promote efficient de novo telomere addition at DNA double-strand breaks. *Nucleic Acids Res*. 2020;48(3):1271–84. <https://doi.org/10.1093/nar/gkz1109>.
- Appanah R, Jones D, Falquet B, Rass U. Limiting homologous recombination at stalled replication forks is essential for cell viability: DNA2 to the rescue. *Curr Genet*. 2020;66(6):1085–92. <https://doi.org/10.1007/s00294-020-01106-7>.
- Epum EA, Mohan MJ, Ruppe NP, Friedman KL. Interaction of yeast Rad51 and Rad52 relieves Rad52-mediated inhibition of de novo telomere addition. *PLoS Genet*. 2020;16(2):e1008608. <https://doi.org/10.1371/journal.pgen.1008608>.
- Ouenzar F, Lalonde M, Laprade H, Morin G, Gallardo F, Tremblay-Belzile S, et al. Cell cycle-dependent spatial segregation of telomerase from sites of DNA damage. *J Cell Biol*. 2017;216(8):2355–71. <https://doi.org/10.1083/jcb.201610071>.
- Obodo UC, Epum EA, Platts MH, Seloff J, Dahlsøn NA, Velkovsky SM, et al. Endogenous hot spots of de novo telomere addition in the yeast genome contain proximal enhancers that bind Cdc13. *Mol Cell Biol*. 2016;36(12): 1750–63. <https://doi.org/10.1128/MCB.00095-16>.
- Strecker J, Stinus S, Caballero MP, Szilard RK, Chang M, Durocher D. A sharp Pif1-dependent threshold separates DNA double-strand breaks from critically short telomeres. *eLife*. 2017;6. <https://doi.org/10.7554/eLife.23783>.
- Schmidt JC, Zaug AJ, Cech TR. Live cell imaging reveals the dynamics of telomerase recruitment to telomeres. *Cell*. 2016;166(5):1188–97 e1189. <https://doi.org/10.1016/j.cell.2016.07.033>.
- Boule JB, Vega LR, Zakian VA. The yeast Pif1p helicase removes telomerase from telomeric DNA. *Nature*. 2005;438(7064):57–61. <https://doi.org/10.1038/nature04091>.
- Phillips JA, Chan A, Paeschke K, Zakian VA. The pif1 helicase, a negative regulator of telomerase, acts preferentially at long telomeres. *PLoS Genet*. 2015;11(4):e1005186. <https://doi.org/10.1371/journal.pgen.1005186>.
- Zhang W, Durocher D. De novo telomere formation is suppressed by the Mec1-dependent inhibition of Cdc13 accumulation at DNA breaks. *Genes Dev*. 2010;24(5):502–15. <https://doi.org/10.1101/gad.1869110>.
- Zhou J, Monson EK, Teng SC, Schulz VP, Zakian VA. Pif1p helicase, a catalytic inhibitor of telomerase in yeast. *Science*. 2000;289(5480):771–4. <https://doi.org/10.1126/science.289.5480.771>.
- Bourns BD, Alexander MK, Smith AM, Zakian VA. Sir proteins, Rif proteins, and Cdc13p bind Saccharomyces telomeres in vivo. *Mol Cell Biol*. 1998; 18(9):5600–8. <https://doi.org/10.1128/MCB.18.9.5600>.

33. Baumann P, Cech TR. Protection of telomeres by the Ku protein in fission yeast. *Mol Biol Cell*. 2000;11(10):3265–75. <https://doi.org/10.1091/mbc.11.10.3265>.
34. de Bruin D, Kantrow SM, Liberatore RA, Zakian VA. Telomere folding is required for the stable maintenance of telomere position effects in yeast. *Mol Cell Biol*. 2000;20(21):7991–8000. <https://doi.org/10.1128/MCB.20.21.7991-8000.2000>.
35. Qi H, Zakian VA. The *Saccharomyces* telomere-binding protein Cdc13p interacts with both the catalytic subunit of DNA polymerase alpha and the telomerase-associated est1 protein. *Genes Dev*. 2000;14(14):1777–88.
36. Greider CW. Regulating telomere length from the inside out: the replication fork model. *Genes Dev*. 2016;30(13):1483–91. <https://doi.org/10.1101/gad.280578.116>.
37. Chen H, Xue J, Churikov D, Hass EP, Shi S, Lemon LD, et al. Structural insights into yeast telomerase recruitment to telomeres. *Cell*. 2018;172(1-2):331–43 e313. <https://doi.org/10.1016/j.cell.2017.12.008>.
38. Margalef P, Kotsantis P, Borel V, Bellelli R, Panier S, Boulton SJ. Stabilization of reversed replication forks by telomerase drives telomere catastrophe. *Cell*. 2018;172(3):439–53 e414. <https://doi.org/10.1016/j.cell.2017.11.047>.
39. Capra JA, Paeschke K, Singh M, Zakian VA. G-quadruplex DNA sequences are evolutionarily conserved and associated with distinct genomic features in *Saccharomyces cerevisiae*. *PLoS Comput Biol*. 2010;6(7):e1000861. <https://doi.org/10.1371/journal.pcbi.1000861>.
40. Wahba L, Costantino L, Tan FJ, Zimmer A, Koshland D. S1-DRIP-seq identifies high expression and polyA tracts as major contributors to R-loop formation. *Genes Dev*. 2016;30(11):1327–38. <https://doi.org/10.1101/gad.280834.116>.
41. Paeschke K, Capra JA, Zakian VA. DNA replication through G-quadruplex motifs is promoted by the *Saccharomyces cerevisiae* Pif1 DNA helicase. *Cell*. 2011;145(5):678–91. <https://doi.org/10.1016/j.cell.2011.04.015>.
42. Chan A, Boule JB, Zakian VA. Two pathways recruit telomerase to *Saccharomyces cerevisiae* telomeres. *PLoS Genet*. 2008;4(10):e1000236. <https://doi.org/10.1371/journal.pgen.1000236>.
43. Lendvay TS, Morris DK, Sah J, Balasubramanian B, Lundblad V. Senescence mutants of *Saccharomyces cerevisiae* with a defect in telomere replication identify three additional EST genes. *Genetics*. 1996;144(4):1399–412. <https://doi.org/10.1093/genetics/144.4.1399>.
44. Lundblad V, Szostak JW. A mutant with a defect in telomere elongation leads to senescence in yeast. *Cell*. 1989;57(4):633–43. [https://doi.org/10.1016/0092-8674\(89\)90132-3](https://doi.org/10.1016/0092-8674(89)90132-3).
45. Hughes TR, Evans SK, Weillbaeher RG, Lundblad V. The Est3 protein is a subunit of yeast telomerase. *Curr Biol*. 2000;10(13):809–12. [https://doi.org/10.1016/S0960-9822\(00\)00562-5](https://doi.org/10.1016/S0960-9822(00)00562-5).
46. Evans SK, Lundblad V. Est1 and Cdc13 as comediators of telomerase access. *Science*. 1999;286(5437):117–20. <https://doi.org/10.1126/science.286.5437.117>.
47. Lin JJ, Zakian VA. The *Saccharomyces* CDC13 protein is a single-strand TG1-3 telomeric DNA-binding protein in vitro that affects telomere behavior in vivo. *Proc Natl Acad Sci U S A*. 1996;93(24):13760–5. <https://doi.org/10.1073/pnas.93.24.13760>.
48. Nugent CI, Hughes TR, Lue NF, Lundblad V. Cdc13p: a single-strand telomeric DNA-binding protein with a dual role in yeast telomere maintenance. *Science*. 1996;274(5285):249–52. <https://doi.org/10.1126/science.274.5285.249>.
49. Jia P, Chai W. The MLH1 ATPase domain is needed for suppressing aberrant formation of interstitial telomeric sequences. *DNA Repair (Amst)*. 2018;65:20–5. <https://doi.org/10.1016/j.dnarep.2018.03.002>.
50. Jia P, Chastain M, Zou Y, Her C, Chai W. Human MLH1 suppresses the insertion of telomeric sequences at intra-chromosomal sites in telomerase-expressing cells. *Nucleic Acids Res*. 2017;45(3):1219–32. <https://doi.org/10.1093/nar/gkw1170>.
51. Balk B, Maicher A, Dees M, Klermund J, Luke-Glaser S, Bender K, et al. Telomeric RNA-DNA hybrids affect telomere-length dynamics and senescence. *Nat Struct Mol Biol*. 2013;20(10):1199–205. <https://doi.org/10.1038/nsmb.2662>.
52. Cerritelli SM, Crouch RJ. Ribonuclease H: the enzymes in eukaryotes. *FEBS J*. 2009;276(6):1494–505. <https://doi.org/10.1111/j.1742-4658.2009.06908.x>.
53. Graf M, Bonetti D, Lockhart A, Serhal K, Kellner V, Maicher A, et al. Telomere length determines TERRA and R-loop regulation through the cell cycle. *Cell*. 2017;170(1):72–85 e14. <https://doi.org/10.1016/j.cell.2017.06.006>.
54. Hass EP, Zappulla DC. The Ku subunit of telomerase binds Sir4 to recruit telomerase to lengthen telomeres in *S. cerevisiae*. *eLife*. 2015;4:e07750.
55. Palladino F, Laroche T, Gilson E, Axelrod A, Pillus L, Gasser SM. SIR3 and SIR4 proteins are required for the positioning and integrity of yeast telomeres. *Cell*. 1993;75(3):543–55. [https://doi.org/10.1016/0092-8674\(93\)90388-7](https://doi.org/10.1016/0092-8674(93)90388-7).
56. Bernstein BE, Tong JK, Schreiber SL. Genomewide studies of histone deacetylase function in yeast. *Proc Natl Acad Sci U S A*. 2000;97(25):13708–13. <https://doi.org/10.1073/pnas.250477697>.
57. Azvolinsky A, Giresi PG, Lieb JD, Zakian VA. Highly transcribed RNA polymerase II genes are impediments to replication fork progression in *Saccharomyces cerevisiae*. *Mol Cell*. 2009;34(6):722–34. <https://doi.org/10.1016/j.molcel.2009.05.022>.
58. Schalbetter SA, Fudenberg G, Baxter J, Pollard KS, Neale MJ. Principles of meiotic chromosome assembly revealed in *S. cerevisiae*. *Nat Commun*. 2019;10(1):4795.
59. Flint J, Craddock CF, Villegas A, Bentley DP, Williams HJ, Galanello R, et al. Healing of broken human chromosomes by the addition of telomeric repeats. *Am J Hum Genet*. 1994;55(3):505–12.
60. Bianchi A, Negrini S, Shore D. Delivery of yeast telomerase to a DNA break depends on the recruitment functions of Cdc13 and Est1. *Mol Cell*. 2004;16(1):139–46. <https://doi.org/10.1016/j.molcel.2004.09.009>.
61. Makovets S, Blackburn EH. DNA damage signalling prevents deleterious telomere addition at DNA breaks. *Nat Cell Biol*. 2009;11(11):1383–6. <https://doi.org/10.1038/ncb1985>.
62. Shay JW, Bacchetti S. A survey of telomerase activity in human cancer. *Eur J Cancer*. 1997;33(5):787–91. [https://doi.org/10.1016/S0959-8049\(97\)00062-2](https://doi.org/10.1016/S0959-8049(97)00062-2).
63. Broccoli D, Young JW, de Lange T. Telomerase activity in normal and malignant hematopoietic cells. *Proc Natl Acad Sci U S A*. 1995;92(20):9082–6. <https://doi.org/10.1073/pnas.92.20.9082>.
64. Luo Z, Wang W, Li F, Songyang Z, Feng X, Xin C, et al. Pan-cancer analysis identifies telomerase-associated signatures and cancer subtypes. *Mol Cancer*. 2019;18(1):106. <https://doi.org/10.1186/s12943-019-1035-x>.
65. Shay JW, Wright WE. Telomeres and telomerase: three decades of progress. *Nat Rev Genet*. 2019;20(5):299–309. <https://doi.org/10.1038/s41576-019-0099-1>.
66. Roake CM, Artandi SE. Regulation of human telomerase in homeostasis and disease. *Nat Rev Mol Cell Biol*. 2020;21(7):384–97. <https://doi.org/10.1038/s41580-020-0234-z>.
67. Low KC, Tergaonkar V. Telomerase: central regulator of all of the hallmarks of cancer. *Trends Biochem Sci*. 2013;38(9):426–34. <https://doi.org/10.1016/j.tibs.2013.07.001>.
68. Mah LJ, El-Osta A, Karagiannis TC. GammaH2AX: a sensitive molecular marker of DNA damage and repair. *Leukemia*. 2010;24(4):679–86. <https://doi.org/10.1038/leu.2010.6>.
69. Redon C, Pilch DR, Rogakou EP, Orr AH, Lowndes NF, Bonner WM. Yeast histone 2A serine 129 is essential for the efficient repair of checkpoint-blind DNA damage. *EMBO Rep*. 2003;4(7):678–84. <https://doi.org/10.1038/sj.embor.embor871>.
70. Symington LS, Rothstein R, Lisby M. Mechanisms and regulation of mitotic recombination in *Saccharomyces cerevisiae*. *Genetics*. 2014;198(3):795–835. <https://doi.org/10.1534/genetics.114.166140>.
71. Maciejowski J, de Lange T. Telomeres in cancer: tumour suppression and genome instability. *Nat Rev Mol Cell Biol*. 2017;18(3):175–86. <https://doi.org/10.1038/nrm.2016.171>.
72. Davoli T, de Lange T. Telomere-driven tetraploidization occurs in human cells undergoing crisis and promotes transformation of mouse cells. *Cancer Cell*. 2012;21(6):765–76. <https://doi.org/10.1016/j.ccr.2012.03.044>.
73. O'Hagan RC, Chang S, Maser RS, Mohan R, Artandi SE, Chin L, et al. Telomere dysfunction provokes regional amplification and deletion in cancer genomes. *Cancer Cell*. 2002;2(2):149–55. [https://doi.org/10.1016/S1535-6108\(02\)00094-6](https://doi.org/10.1016/S1535-6108(02)00094-6).
74. Maciejowski J, Li Y, Bosco N, Campbell PJ, de Lange T. Chromothripsis and kataegis induced by telomere crisis. *Cell*. 2015;163(7):1641–54. <https://doi.org/10.1016/j.cell.2015.11.054>.
75. Artandi SE, DePinho RA. Telomeres and telomerase in cancer. *Carcinogenesis*. 2010;31(1):9–18. <https://doi.org/10.1093/carcin/bgp268>.
76. Tubbs A, Nussenzweig A. Endogenous DNA damage as a source of genomic instability in cancer. *Cell*. 2017;168(4):644–56. <https://doi.org/10.1016/j.cell.2017.01.002>.
77. Novarina D, Mavrova SN, Janssens GE, Rempel IL, Veenhoff LM, Chang M. Increased genome instability is not accompanied by sensitivity to DNA damaging agents in aged yeast cells. *DNA Repair (Amst)*. 2017;54:1–7. <https://doi.org/10.1016/j.dnarep.2017.03.005>.

78. Schulz VP, Zakian VA. The *Saccharomyces* Pif1 DNA helicase inhibits telomere elongation and de novo telomere formation. *Cell*. 1994;76(1):145–55. [https://doi.org/10.1016/0092-8674\(94\)90179-1](https://doi.org/10.1016/0092-8674(94)90179-1).
79. Li L, Williams P, Ren W, Wang MY, Gao Z, Miao W, et al. YY1 interacts with guanine quadruplexes to regulate DNA looping and gene expression. *Nat Chem Biol*. 2021;17(2):161–8. <https://doi.org/10.1038/s41589-020-00695-1>.
80. Hou Y, Li F, Zhang R, Li S, Liu H, Qin ZS, et al. Integrative characterization of G-Quadruplexes in the three-dimensional chromatin structure. *Epigenetics*. 2019;14(9):894–911. <https://doi.org/10.1080/15592294.2019.1621140>.
81. Selvam S, Yu Z, Mao H. Exploded view of higher order G-quadruplex structures through click-chemistry assisted single-molecule mechanical unfolding. *Nucleic Acids Res*. 2016;44(1):45–55. <https://doi.org/10.1093/nar/gkv1326>.
82. Zhang ML, Tong XJ, Fu XH, Zhou BO, Wang J, Liao XH, et al. Yeast telomerase subunit Est1p has guanine quadruplex-promoting activity that is required for telomere elongation. *Nat Struct Mol Biol*. 2010;17(2):202–9. <https://doi.org/10.1038/nsmb.1760>.
83. Smith JS, Chen Q, Yatsunyk LA, Nicoludis JM, Garcia MS, Kranaster R, et al. Rudimentary G-quadruplex-based telomere capping in *Saccharomyces cerevisiae*. *Nat Struct Mol Biol*. 2011;18(4):478–85. <https://doi.org/10.1038/nsmb.2033>.
84. Paeschke K, Simonsson T, Postberg J, Rhodes D, Lipps HJ. Telomere end-binding proteins control the formation of G-quadruplex DNA structures in vivo. *Nat Struct Mol Biol*. 2005;12(10):847–54. <https://doi.org/10.1038/nsmb982>.
85. Oganessian L, Karlseder J. Telomeric armor: the layers of end protection. *J Cell Sci*. 2009;122(Pt 22):4013–25. <https://doi.org/10.1242/jcs.050567>.
86. Ribeyre C, Lopes J, Boule JB, Piazza A, Guedin A, Zakian VA, et al. The yeast Pif1 helicase prevents genomic instability caused by G-quadruplex-forming CEB1 sequences in vivo. *PLoS Genet*. 2009;5(5):e1000475. <https://doi.org/10.1371/journal.pgen.1000475>.
87. Zahler AM, Williamson JR, Cech TR, Prescott DM. Inhibition of telomerase by G-quartet DNA structures. *Nature*. 1991;350(6320):718–20. <https://doi.org/10.1038/350718a0>.
88. Traczyk A, Liew CW, Gill DJ, Rhodes D. Structural basis of G-quadruplex DNA recognition by the yeast telomeric protein Rap1. *Nucleic Acids Res*. 2020; 48(8):4562–71. <https://doi.org/10.1093/nar/gkaa171>.
89. Fouladi B, Sabatier L, Miller D, Pottier G, Murnane JP. The relationship between spontaneous telomere loss and chromosome instability in a human tumor cell line. *Neoplasia*. 2000;2(6):540–54. <https://doi.org/10.1038/sj.neo.7900107>.
90. Kostiner DR, Nguyen H, Cox VA, Cotter PD. Stabilization of a terminal inversion duplication of 8p by telomere capture from 18q. *Cytogenet Genome Res*. 2002;98(1):9–12. <https://doi.org/10.1159/000068536>.
91. Fortin F, Beaulieu Bergeron M, Fetni R, Lemieux N. Frequency of chromosome healing and interstitial telomeres in 40 cases of constitutional abnormalities. *Cytogenet Genome Res*. 2009;125(3):176–85. <https://doi.org/10.1159/000230002>.
92. Martinez P, Blasco MA. Telomeric and extra-telomeric roles for telomerase and the telomere-binding proteins. *Nat Rev Cancer*. 2011;11(3):161–76. <https://doi.org/10.1038/nrc3025>.
93. Jafri MA, Ansari SA, Alqahtani MH, Shay JW. Roles of telomeres and telomerase in cancer, and advances in telomerase-targeted therapies. *Genome Med*. 2016;8(1):69. <https://doi.org/10.1186/s13073-016-0324-x>.
94. Li Y, Tergaonkar V. Noncanonical functions of telomerase: implications in telomerase-targeted cancer therapies. *Cancer Res*. 2014;74(6):1639–44. <https://doi.org/10.1158/0008-5472.CAN-13-3568>.
95. Rutledge MT, Russo M, Belton JM, Dekker J, Broach JR. The yeast genome undergoes significant topological reorganization in quiescence. *Nucleic Acids Res*. 2015;43(17):8299–313. <https://doi.org/10.1093/nar/gkv723>.
96. Chuang TC, Moshir S, Garini Y, Chuang AY, Young IT, Vermolen B, et al. The three-dimensional organization of telomeres in the nucleus of mammalian cells. *BMC Biol*. 2004;2(1):12. <https://doi.org/10.1186/1741-7007-2-12>.
97. Schalbetter SA, Goloborodko A, Fudenberg G, Belton JM, Miles C, Yu M, et al. SMC complexes differentially compact mitotic chromosomes according to genomic context. *Nat Cell Biol*. 2017;19(9):1071–80. <https://doi.org/10.1038/ncb3594>.
98. Longtine MS, McKenzie A 3rd, Demarini DJ, Shah NG, Wach A, Brachat A, et al. Additional modules for versatile and economical PCR-based gene deletion and modification in *Saccharomyces cerevisiae*. *Yeast*. 1998;14(10): 953–61. [https://doi.org/10.1002/\(SICI\)1097-0061\(199807\)14:10<953::AID-YEA293>3.0.CO;2-U](https://doi.org/10.1002/(SICI)1097-0061(199807)14:10<953::AID-YEA293>3.0.CO;2-U).
99. Buck MJ, Nobel AB, Lieb JD. ChIPOTle: a user-friendly tool for the analysis of ChIP-chip data. *Genome Biol*. 2005;6(11):R97. <https://doi.org/10.1186/gb-2005-6-11-r97>.
100. Belaghal H, Dekker J, Gibcus JH. Hi-C 2.0: An optimized Hi-C procedure for high-resolution genome-wide mapping of chromosome conformation. *Methods*. 2017;123:56–65. <https://doi.org/10.1016/j.jmeth.2017.04.004>.
101. Wingett S, Ewels P, Furlan-Magaril M, Nagano T, Schoenfelder S, Fraser P, et al. HiCUP: pipeline for mapping and processing Hi-C data. *F1000Res*. 2015;4:1310.
102. Langmead B, Salzberg SL. Fast gapped-read alignment with Bowtie 2. *Nat Methods*. 2012;9(4):357–9. <https://doi.org/10.1038/nmeth.1923>.
103. Pandey SS, Baxter J, Juranek SA, Guryev V, Schmitz T, Hofmann A, Heermann DW, Paeschke K. Telomerase subunit Est2 marks internal sites that are prone to accumulate DNA damage. *NCBI GEO*. 2020. <https://www.ncbi.nlm.nih.gov/geo/query/acc.cgi?acc=GSE143187>. Accessed Jan 2020.

Publisher's Note

Springer Nature remains neutral with regard to jurisdictional claims in published maps and institutional affiliations.

Ready to submit your research? Choose BMC and benefit from:

- fast, convenient online submission
- thorough peer review by experienced researchers in your field
- rapid publication on acceptance
- support for research data, including large and complex data types
- gold Open Access which fosters wider collaboration and increased citations
- maximum visibility for your research: over 100M website views per year

At BMC, research is always in progress.

Learn more biomedcentral.com/submissions

